



David Publishing Company
www.davidpublishing.com

ISSN 1934-8932 (Print)
ISSN 1934-8940 (Online)

Journal of **Environmental Science** and **Engineering**

Volume 5, Number 11, November 2011



From Knowledge to Wisdom

Journal of Environmental Science and Engineering

Volume 5, Number 11, November 2011 (Serial Number 48)



David Publishing Company
www.davidpublishing.com

Publication Information:

Journal of Environmental Science and Engineering is published monthly in hard copy (ISSN 1934-8932) and online (ISSN 1934-8940) by David Publishing Company located at 1840 Industrial Drive, Suite 160, Libertyville, Illinois 60048, USA.

Aims and Scope:

Journal of Environmental Science and Engineering, a monthly professional academic journal, covers all sorts of researches on environmental management and assessment, environmental monitoring, atmospheric environment, aquatic environment and municipal solid waste, etc..

Editorial Board Members:

Dr. Bishnu Rajupreti (Nepal), Prof. Jianhua Wang (China), Prof. Mankolli Hysen (Albania), Dr. Jungkon Kim (South Korea), Prof. Samira Ibrahim Korfali (Lebanon), Prof. Pradeep K. Naik (Bahrain), Dr. Ricardo García Mira (Spain), Dr. Leucci Giovanni (Italy), Prof. Konstantinos C. Makris (Gonia Athinon & Nikou Xiouta), Prof. Kihong Park (South Korea), Prof. Mukesh Sharma (India), Dr. Hesham Gehad Mohamed Ibrahim (Palestine), Dr. Jyoti Prakash Maity (India), Dr. Giuseppe Mascolo (Italy), Dr. Satinder Kaur Brar (Canada), Dr. Jo-Ming Tseng (Taiwan).

Manuscripts and correspondence are invited for publication. You can submit your papers via Web Submission, or E-mail to environmental@davidpublishing.com or info@davidpublishing.com. Submission guidelines and Web Submission system are available at <http://www.davidpublishing.com>.

Editorial Office:

1840 Industrial Drive, Suite 160, Libertyville, Illinois 60048
Tel: 1-847-281-9862
Fax: 1-847-281-9855
E-mail: environmental@davidpublishing.com; info@davidpublishing.com

Copyright©2011 by David Publishing Company and individual contributors. All rights reserved. David Publishing Company holds the exclusive copyright of all the contents of this journal. In accordance with the international convention, no part of this journal may be reproduced or transmitted by any media or publishing organs (including various websites) without the written permission of the copyright holder. Otherwise, any conduct would be considered as the violation of the copyright. The contents of this journal are available for any citation. However, all the citations should be clearly indicated with the title of this journal, serial number and the name of the author.

Abstracted / Indexed in:

CAS (Chemical Abstracts Service)
Database of EBSCO, Massachusetts, USA
Chinese Database of CEPS, Airiti Inc. & OCLC
Cambridge Science Abstracts (CSA)
Ulrich's Periodicals Directory
Chinese Scientific Journals Database, VIP Corporation, Chongqing, China
Summon Serials Solutions

Subscription Information:

Price (per year):
Print \$520, Online \$360
Print and Online \$680

David Publishing Company
1840 Industrial Drive, Suite 160, Libertyville, Illinois 60048
Tel: 1-847-281-9862. Fax: 1-847-281-9855
E-mail: order@davidpublishing.com



David Publishing Company
www.davidpublishing.com

Journal of Environmental Science and Engineering

Volume 5, Number 11, November 2011 (Serial Number 48)

Contents

Aquatic Environment

- 1389 **Competitive Adsorption of Phenol and Lead from Synthetic Wastewater onto Granular Activated Carbon**

A.H. Sulaymon, D.W. Abbood and A.H. Ali

- 1400 **Cascaded Simultaneous Nitrification and Denitrification Process for Nitrogen and Phosphorus Reduction from RO Reject Wastewater: A Bench-Scale Study**

A.B. Shahalam, A. Abusam, A. Matouk and M. Khaja

Environmental Monitoring

- 1407 **Energy Efficiency, Indoor Air Quality and Thermal Comfort Studies at the Faculty of Engineering and Built Environment, University Kebangsaan Malaysia**

N.L. Teng, S.M. Zain, N.E.A. Basri and S. Mat

- 1414 **Olkaria Geothermal Power Plants, Kenya: Preliminary Evaluation of Mercury Emission to the Atmosphere**

G.N. Wetang'ula

Environmental Chemistry

- 1427 **Optimization of Wax Esters Production from Palm Fatty Acid Distillate and Oleyl Alcohol over Amberlyst 15**

M. Tapanwong and V. Punsuvon

Environmental Ecology

- 1435 **Territorial Repartition and Ecological Importance of Wetlands in Moldova (Romania)**

G. Romanescu, C. Stoleriu and C. Zaharia

- 1445 **Test Bench for the Mechanical Distribution of Predators to Control Insect Pests**

M. Khelifi, F. Paré and M. Aider

Environmental Economics

- 1454 **Economic Analysis of CO₂ Emission Abatement Applying a Dynamic CGE Model with Endogenous Technological Change: Impacts of the Time Horizon**

K. Matsumoto

Environmental Management and Assessment

- 1464 **Effect of Percolation Pattern on Yields and Accumulation of Copper and Cadmium in the Rice Plants with Soil Dressing Models**

S.K. Paul, C. Sasaki, N. Matsuyama and K. Kato

- 1474 **Comparative Study of the Impact of Climate Variability on Prevalence of Urinary Schistosomiasis: Cases at Sunyani Regional Hospital and among School Children in Atronie, Sunyani**

S.C.K. Tay, L.K. Amekudzi and G. Tagoe

- 1483 **Effect of Soil and Water Conservation Measures on Selected Soil Physical and Chemical Properties and Barley (*Hordeum spp.*) Yield**

Tadele Amdemariam, Yihenew G. Selassie, Mitiku Haile and C. Yamoh

- 1496 **Beta Diversity of Mbuna in Lake Malawi**

L.G. Kanyumba, W.J. Changadeya, A.J.D. Ambali, L.A. Kamwanja and E.K.W. Kaunda

- 1507 **Counteracting the Effects of Sea Level Rise in Southeast Florida**

F. Bloetscher, B.N. Heimlich and T. Romah

- 1526 **A “Trojan” in Climatic Change: The Urban Effect**

J. Quereda Sala, E. Montón Chiva and J. Escrig Barberá

- 1537 **Seasonal Effect on Atmospheric Refractivity in Diverse Terrains**

Y.O. Olasoji and M.O. Kolawole

- 1542 **Review Article of Landscape Metrics Based on Remote Sensing Data**

A.F. Petrosyan and V. Karathanassi

Competitive Adsorption of Phenol and Lead from Synthetic Wastewater onto Granular Activated Carbon

A.H. Sulaymon¹, D.W. Abbood² and A.H. Ali²

1. Environmental Engineering Department, College of Engineering, University of Baghdad, Baghdad 10001, Iraq

2. Environmental Engineering Department, College of Engineering, University of Al-Mustansiriyah, Baghdad 10001, Iraq

Received: May 16, 2011 / Accepted: June 22, 2011 / Published: November 20, 2011.

Abstract: The equilibrium uptake of phenol and lead(II) ions, both singly and in combination, by granular activated carbon was studied in a batch system. The initial pH, temperature, mixing speed and contact time were fixed at 4, 30 °C, 250 rpm and 6 hrs respectively. Adsorption isotherms were developed for both the single and binary component systems and expressed by ten models for single and four models for binary systems and model parameters were estimated by the non-linear regression method using STATISTICA version-6 and EXCEEL-2007 software. The maximum loading capacity (q_m) of the phenol was 66.8234, 60.4823 mg/g and 37.0370, 13.0988 mg/g for lead in single and binary systems respectively. Desorption experiments indicate that the desorption efficiency with 0.1 M NaOH, 0.1 M HCl solution reaches 97.35%, 98% for phenol and lead respectively. There was only 3.58%, 4.93% decrease in removal efficiency for phenol and lead respectively when used regenerated GAC for one cycle.

Key words: Adsorption, GAC, phenol, lead, adsorption isotherms.

Nomenclature

A_R	Redlich-Peterson model parameter, L/mg	E_{ad}	Adsorption efficiency, %
Å	Angstrom, 1×10^{-10} m	F_{RP}	Radke-Praunzitz model parameter
a_t	Toth model constant	HCl	Hydrochloric acid
B	Constant indicating the energy of interaction between the solute and the adsorbent surface, L/mg	H_2SO_4	Sulphoric acid
B_R	Redlich-Peterson model parameter, $(L/mg)^{m_R}$	K_F	Freundlich adsorption constant, related to adsorption intensity, $(mg/g)(mg/L)^{1/n_F}$
B_1	Temkin isotherm constant, L/mg	K_T	Equilibrium binding constant in Temkin model, L/mg
B	Langmuir adsorption constant related to the affinity to binding sites, L/mg	K_{RP}	Radke-Praunzitz model parameter, L/mg
b_{RK}	Redlich-Peterson model parameter derived from the corresponding individual isotherm equations, $(L/mg)^{m_R}$	K_t	Toth model constant, mg/g
b_K	Khan model constant, L/mg	K_{Fi}	Individual Freundlich adsorption constant of each component, $(mg/g)(mg/L)^{1/n_F}$
B_i	Individual Langmuir adsorption constant of each component, L/mg	K_{Ri}	Individual Redlich-Peterson adsorption constant of each component, L/mg
C_o	Initial phenol/lead concentration, mg/L	m_{Ri}	Redlich-Peterson model parameter
C_e	Equilibrium concentration, mg/L	n_F	Freundlich adsorption constant, related to the affinity to binding sites
C_s	Saturation concentration of the adsorbed component, mg/L	n_{Fi}	Individual Freundlich adsorption constant of each component
C_d	Desorbed equilibrium concentration, mg/L	N_{RP}	Radke-Praunzitz model parameter
DDW	Deionized distilled water	NaOH	Sodium hydroxide
EDTA	Ethylene diamine tetra acetic acid	Na_2CO_3	Sodium carbonate
		q_{eq}	Adsorbed phenol/lead quantity per gram of GAC at equilibrium, mg/g
		q_m	Langmuir adsorption constant of the pollutants shows the maximum amount of pollutants bound to the GAC, mg/g
		Q_{max}	Khan model constant, mg/g
		Q	Constant indicating the amount of solute adsorbed forming a complete monolayer, mg/g

Corresponding author: A.H. Ali, assistant lecturer, Ph.D., main research fields: wastewater technologies, air pollution, environmental impact assessment. E-mail: ahmedhassoon_2021@yahoo.com.

q_{ei}	Amount of adsorbate adsorbed per mass of adsorbent of component i, mg/g
q_{mi}	Individual Langmuir adsorption constant of each component, mg/g
R	Universal gas constant (= 8.314), kJ/mol·K
t	Toth model constant
T	Absolute temperature, K
V_L	Volume of solution, L
V_e	Volume of eluant solution, L
W_A	Mass of activated carbon, gm

1. Introduction

The removal of toxic contaminants such as heavy metal ions and organic pollutants from industrial wastewaters is one of the most important environmental issues to be solved today. Lead(II) has been found together with a variety of aromatic compounds including phenol, naphthalene, and trichloroethylene (TCE) at high concentrations in a number of contaminated sites. Lead(II) and its organic co-pollutants often originate from industrial sources such as the iron-steel, cook, petroleum, pesticides, paints, solvent, pharmacuities, wood preserving chemicals. Phenol containing water, when chlorinated during disinfection of water, results in the formation of chlorophenol [1-3].

A number of treatment methods for removing heavy metals and organics from domestic and industrial wastewater include chemical precipitation, ion exchange, filtration, membrane separation and adsorption. Among them adsorption was found to be the most effective method for removing dissolved metals and organics from wastes. A typical activated carbon particle, whether in a powdered or granular form, has a porous structure consisting of a network of interconnected macropores, mesopores, and micropores that provide a good capacity for the adsorption of organic molecules and heavy metals due to high surface area. The surface chemistry of activated carbon and the chemical characteristics of adsorbate, such as polarity, ionic nature, functional groups, and solubility, determine the nature of bonding mechanisms as well as the extent and

strength of adsorption. A variety of physicochemical mechanisms/forces, such as van der Waals, H-binding, dipole-dipole interactions, ion exchange, covalent bonding, cation bridging, and water bridging, can be responsible for the adsorption of organic compounds in activated carbon [4-10].

While much research has been carried out on the uptake of single species of metal ions and organic species by activated carbon, little attention seems to have been given to the study of organic-metal ion mixtures. Despite the fact that not only single toxic metallic species but organic components also exist in wastewaters and the presence of a multiplicity of metals and organics often gives rise to interactive effects, insufficient attention seems to have been paid to this problem. The examination of the effects of metal ions and organics in various combinations is more representative, of the actual environmental problems faced by treatment technologies, than are single metal or organic studies [11].

2. Experimental Materials and Procedure

2.1 Adsorbate

50 mg/L standard stock solution of phenol and lead(II) were prepared by dissolving Ph and $Pb(NO_3)_2$ in distilled water. The salts were bought from local market with the specifications in Table 1 [12].

2.2 Adsorbent

Commercial granulated activated carbon (GAC) was used as an adsorbent in the present work. It was supplied by (Unicarbo, Italians) and was bought from the Iraqi markets. The physical and chemical properties were measured at the laboratories of the Ministry of Industry and Minerals (Ibn Sina State Company), Ministry of Oil (Petroleum Development and Research Center), Al-Mustansiriya University (College of Engineering, Environmental Department) and according to the data from the supplier. The physical and chemical properties of GAC are listed in Table 2.

Table 1 Main properties of phenol and lead nitrate [12].

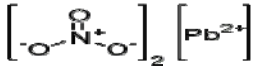
Symbol	Ph	Pb ²⁺
Formula	C ₆ H ₅ OH	Pb(NO ₃) ₂
Structure		
Appearance	White crystalline solid	White colorless crystals
Molecular weight (g/mole)	94.11	331.2
Solubility in water (at 20 °C) (mg/L)	86000	520000
Octanol-Water, Log (K _{ow})	1.5	-
Molar volume (cm ³ /mole)	93.7	-
Specific gravity	1.058	4.53
Melting point (°C)	40.5	270
Boiling point (°C)	181.7	-
Molecular cross-sectional area (Å ²)	30.49	21.40
Manufacturing company	MERCK	MERCK

Table 2 Physical and chemical properties of GAC.

Property	GAC
Actual density (kg/cm ³)	1544
Apparent density (kg/cm ³)	641
BET surface area (m ² /g)	751.965
Particle porosity	0.584
Bed porosity	0.64
Average particle diameter (mm)	0.775
Pore volume (cm ³ /g)	0.422
Iodine number (mg/g)	1100-1130
pH	10.2-10.6
Ash content (%)	3-5

2.3 Procedure

The initial pH of phenol and lead solutions were measured by pH meter (ORION 3 STAR, Thermo, US) and it's found to be 5.45 and 4.40 respectively. The adsorption of metals and organics decrease at low pH values because of competition for binding sites between cations and protons, while at pH higher than 5.5, solubility of metal complexes decreases sufficiently allowing precipitation, which may complicate the sorption process and do not bind to the adsorption sites on the surface of the GAC. Therefore, the optimum pH was found around 4 [13, 14]. So, pH was adjusted with the range of 4 for all single and binary systems by adding the 0.1 N HNO₃ and 0.1 N NaOH for acidic and basic pH respectively. A sample of 100 mL of each solution was placed in bottles of 250

mL in volume, containing 0.05, 0.1, 0.15, to 0.6 g of GAC. The bottles were then placed on a shaker and agitated continuously at 250 rpm for 6 hours at 30 °C to achieve equilibrium concentrations. Then the solution was filtrated using filter paper type (Wattmann No. 4) and a sample of 20 mL from each bottles was taken for analysis using Gas Chromatograph (GC 1000, Italia) and/or Atomic Absorption Spectrometric (AAS, Buck, Accusys 211, USA) for phenol and lead measuring concentration respectively. The adsorbed amount was calculated using Eq. (1) [15]:

$$q_e = \frac{V_L(C_o - C_e)}{W_A} \quad (1)$$

The adsorption efficiency was calculated by the difference in the initial and equilibrium concentration of each pollutant by the following relationship:

$$E_{ad} = \frac{(C_o - C_e)}{C_o} \times 100 \quad (2)$$

3. Adsorption Isotherm Models

A porous solid material of large surface area per unit mass in which adsorption of liquids or gases occurs on its surface is known as “adsorbent”. The material to be adsorbed on the adsorbent is known as “adsorbate”. Adsorption is usually described through isotherm, which is the equilibrium relationship between the adsorbate concentration in the fluid phase and the adsorbate concentration in the adsorbent particles at a

given temperature. It is a plot of the amount of adsorbate per unit weight of adsorbent (q_e) against the equilibrium concentration of the adsorbate remaining in solution (C_e) [16].

3.1 Single Component Isotherm Models

Ten models for single system have been tested in the present study and they are:

3.1.1 Freundlich Model (Freundlich, 1907)

The first mathematical fit to an isotherm was published by Freundlich and Kuster in 1907. Freundlich showed that adsorption from solution could be expressed by empirical formula [17]:

$$q_e = k_F C_e^{1/n_F} \quad (3)$$

3.1.2 Langmuir Model (Langmuir, 1916)

In 1916, Irving Langmuir published a new model isotherm for gas or liquid adsorbed on solid, which retained his name. The Langmuir adsorption model is valid for single-layer adsorption. It is based on the assumption that maximum adsorption corresponds to a saturated monolayer of solute molecules on the adsorbent surface, that the energy of adsorption is constant, and that there is no transmigration of adsorbate in the plane of the surface. The Langmuir isotherm equation is [18]:

$$q_e = \frac{q_m b C_e}{1 + b C_e} \quad (4)$$

The essential characteristics of a Langmuir isotherm equation could be expressed in terms of a dimensionless constant separation factor or equilibrium parameter, " R_s ", which is defined by the following equation:

$$R_s = \frac{1}{1 + b C_o} \quad (5)$$

This separation factor yields the type of isotherm which was described by Weber and Chakravorti (1974) as shown in Table 3 [19].

3.1.3 Temkin Model (Temkin, 1934)

Temkin isotherm takes into account the adsorbing species adsorbent interaction and the adsorption isotherm expressed as [20]:

$$q_e = \frac{RT}{B_1} \ln(K_T C_e) \quad (6)$$

Table 3 Values of separation factor and type of isotherm.

Values of R_s	Type of isotherm
$R_s > 1$	Unfavorable
$R_s = 0$	Linear
$0 < R_s < 1$	Favorable
$R_s < 0$	Irreversible

3.1.4 BET Model (BET, 1938)

Often adsorbate molecules do form multilayer, that is, some are adsorbed on already adsorbed molecules and the Langmuir isotherm is not valid. In 1938 Stephan Brunaur, Paul Emmett and Edward Teller developed a model isotherm that takes this possibility into account, their model is called BET isotherm model. This model extends the Langmuir model from a monolayer to several molecular layer. Above the monolayer, each additional layer of adsorbate molecules is assumed to equilibrate with the layer below it and layers of different thickness are allowed to coexist, it takes the following form [21]:

$$q_e = \frac{BQC_e}{(C_s - C_e)[1 + (B - 1)(C_e/C_s)]} \quad (7)$$

3.1.5 Harkins-Henderson Model (Harkins and Peterson, 1952)

This model explains multilayer adsorption and the existence of heterogeneous pore distribution in the adsorbent expressed as [22]:

$$q_e = \frac{K^{1/n}}{C_e^{1/n}} \quad (8)$$

3.1.6 Redlich-Peterson Model (Redlich and Peterson, 1959)

The Redlich-Peterson model is expressed by Eq. (9) [23]:

$$q_e = \frac{A_R C_e}{1 + B_R C_e^{m_R}} \quad (9)$$

This model expresses the adsorption process when dealing with a certain pollutants at high concentration.

3.1.7 Toth Model (Toth, 1971)

This model is derived from potential theory and is used in heterogeneous system. It assumes a quasi-gaussian energy distribution. Most sites have an adsorption energy lower than the peak of maximum

adsorption energy. The model is expressed as [24]:

$$q_e = \frac{K_t C_e}{(a_t + C_e)^{1/t}} \quad (10)$$

3.1.8 Radke-Praunzitz Model (Radke and Praunzitz, 1972)

The Radke-Praunzitz model is expressed empirically by the following equation [25]:

$$q_e = \frac{K_{RP} C_e}{1 + \left(\frac{K_{RP}}{F_{RP}}\right) C_e^{1-N_{RP}}} \quad (11)$$

The Radke-Praunzitz equation has several important properties, which make it suitable for use in many adsorption processes. At low concentration it reduces to a linear isotherm. At high concentration it becomes Freundlich isotherm and for the special case of $N_{PR} = 0$ it becomes Langmuir isotherm.

3.1.9 Combination of Langmuir-Freundlich Model (Sips, 1984)

This model referred as Sips model is widely used for a single component adsorption. This model is applied when a single component adsorption process obeys Langmuir isotherm in some condition and turned to obey Freundlich isotherm or vice-versa. The Sips model can be expressed as [26]:

$$q_e = \frac{b q_m C_e^{1/n}}{1 + b C_e^{1/n}} \quad (12)$$

3.1.10 Khan Model (Khan, 1997)

This model is derived by Khan (1997) to represent the adsorption isotherm of phenol onto activated carbon. This model is expressed by Eq. (13) [27]:

$$q_e = \frac{Q_{\max} b_k C_e}{(1 + b_k C_e)^{a_k}} \quad (13)$$

3.2 Multi-Component Isotherm Models

The experimental measurement of multicomponent adsorption isotherm is time consuming because of large number of variables involved. Thus, the problem of predicting multicomponent adsorption isotherm from single component adsorption data has attracted a lot of attention. Several isotherms have been proposed to describe the competitive adsorption. Most of these isotherms are based on single component isotherm

parameters and correction factors extracted from the experimental competitive data [28]. Four of these models are:

3.2.1 Extended Langmuir Model

The Langmuir isotherm can be extended for multicomponent system to give the following form:

$$q_{e,i} = \frac{q_{m,i} b_i C_{e,i}}{1 + \sum_{k=1}^N b_k C_{e,k}} \quad (14)$$

This model is applicable when each single component obeys the Langmuir model in a single component system [28].

3.2.2 Combination of Langmuir-Freundlich Model

The competitive Sips model related to the individual isotherm parameters are expressed in Eq. (15) [29]:

$$q_{e,i} = \frac{q_{m,i} b_i C_{e,i}^{1/n_i}}{1 + \sum_{i=1}^N b_i C_{e,i}^{1/n_i}} \quad (15)$$

3.2.3 Extended Freundlich Model

The empirical extended form of the Freundlich model restricted to binary mixtures can be given by Eq. (16) [30]:

$$q_{e,i} = \frac{K_{Fi} C_{e,i}^{ni+1}}{C_{e,i}^{n1} + \sum_{j=1}^N b_j C_{e,j}^{nj}} \quad (16)$$

3.2.4 Redlich-Peterson Model

The competitive Redlich-Peterson model related to the individual isotherm parameters is given by Eq. (17) [29]:

$$q_{e,i} = \frac{K_{Ri} (b_{Ri}) C_{e,i}}{1 + \sum_{k=1}^N b_{R,k} (C_{e,k})^{m_{R,k}}} \quad (17)$$

4. Phenol and Lead Desorption and GAC Regeneration

Desorption experiments were performed in order to demonstrate the ability of exhausted GAC for regeneration and reuse. Desorption experiments were performed by adding 0.6 gm of GAC to six glass bottles. The desorption procedure was the same as that previously described for adsorption experiments. The

Ph and Pb^{2+} -loaded GAC was washed with deionized water and dried at 110 °C for 24 h after equilibrium adsorption experiments. Then, the GAC is contacted with 50 mL of 0.1 M eluant for 6 h to allow Ph/ Pb^{2+} to be released from the GAC. Six eluants have been examined (EDTA, Na_2CO_3 , NaOH, H_2SO_4 , HCl and DDW) as listed in Table 4.

Thereafter, the desorbed Ph/ Pb^{2+} was analyzed and the eluting efficiencies of the desorbents E_d are expressed as follows:

$$E_d(\%) = \frac{m_{ad.} \cdot C_{d.} \times V_e}{m_d \cdot C_{ads.} \times V_L} \quad (18)$$

The most efficient eluant was then used in consecutive adsorption-cycle. The experimental setup for the adsorption-desorption-regeneration cycle is depicted in Fig. 1.

5. Results and Discussion

5.1 Adsorption Isotherms Constants for Single Component System

The adsorption isotherms for single component system of Ph and Pb^{2+} onto GAC are shown in Figs. 2 and 3 respectively. The obtained data for single component system were correlated with the ten models illustrated previously. The parameters for each model were estimated by non liner regression using STATITICA version-6 and EXCEL-2007 software. All parameters with correlation coefficient are summarized in Table 5.

From the figures and tables for single component systems for phenol and lead adsorption one can conclude the following:

(1) The equilibrium isotherm for each solute is of favorable type since $R_S < 1$ ($R_S = 0.2532, 0.1372$ for Ph and Pb^{2+} respectively). Relatively high adsorbent loading was obtained at low concentrations of solute in water;

(2) For phenol, Langmuir and combination of Langmuir-Freundlich models gives the best fit of the experimental data with high correlation coefficients (0.9959). While the experimental data for lead were described successfully with Langmuir, Toth and Khan models with correlation coefficient (0.9922);

(3) It was found that at a batch condition for each single component, the maximum amount of adsorbate adsorbed per mass of activated carbon (q_m) for Ph is greater than that for Pb^{2+} ($q_{m, Ph} = 66.8234$ mg/g; $q_{m, Pb^{2+}} = 37.0370$ mg/g). At the same time, the adsorption efficiency for phenol is greater than for lead ($E_{ad, Ph} = 97.340$; $E_{ad, Pb^{2+}} = 96.926$). This can be explained by:

- Phenol has less solubility (86000 mg/L) in water in comparison with lead nitrate (520000 mg/L) and consequently with lead;
- Molecular cross-sectional area (molecular volume) for phenol is greater than lead (21.40 Å² for lead; 30.49 Å² for phenol);
- Phenol can be adsorbed by means of electrostatic attraction between negatively charge phenols and positively charged binding sites. Physical adsorption by means of Vander Waals, H-bonding, dipole-dipole and dipole-induced dipole has been the main way to adsorb organics such as phenol. However, lead adsorption depended mainly only on the activity and availability of functional groups onto GAC (electrostatic attraction). This depended on type and treating of activated carbon with heat, acids or biases to increased these groups.

5.2 Adsorption Isotherms Constants for Binary Component System

The adsorption isotherms for binary component systems of Ph and Pb^{2+} onto GAC is shown in Fig. 4, whereas Table 6 represents the parameters of each used model and their correlation coefficient (R^2).

Table 4 Eluents used in desorption of Ph and Pb^{2+} from GAC.

	Acid eluants			Alkaline eluants		
	HCl	H_2SO_4	Mineral salt eluant	NaOH	Na_2CO_3	Other eluant
pH	1.956	2.180	5.241	12.798	11.282	7

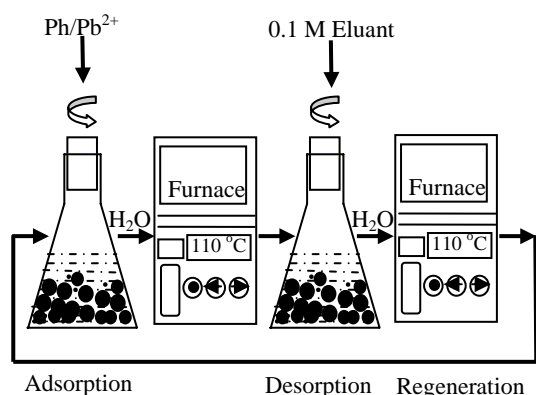


Fig. 1 Experimental setup for the phenol/lead (adsorption-desorption-regeneration) cycle onto GAC.

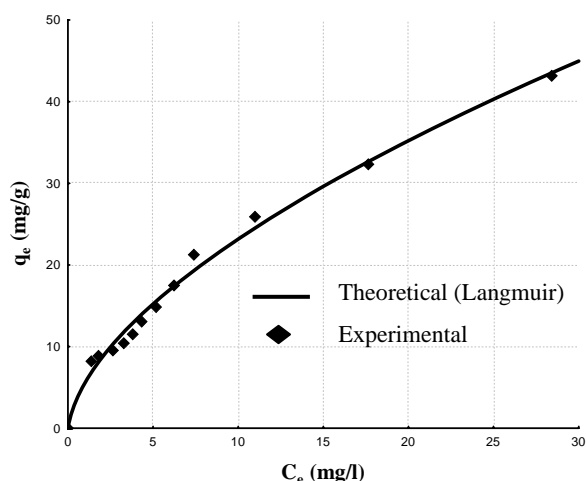


Fig. 2 Adsorption isotherm for Ph onto GAC.

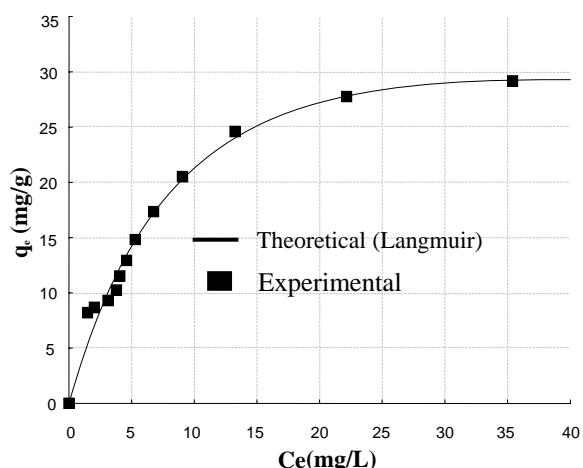


Fig. 3 Adsorption isotherm for Pb²⁺ onto GAC.

From the figure and table for binary component systems, it is clear that:

- The extended Langmuir and Redlich-Peterson

models seems to give the best fitting for the experimental data ($R^2 = 0.9987$; 0.9963) for phenol adsorption. While for lead adsorption, the extended Langmuir model give highest value of R^2 ;

- The behavior of the equilibrium isotherms for the binary systems is of a favorable type;

- The q_m values and the adsorption efficiency for the binary systems were less than those in single systems due to competition between the solutes;

There is a weak competition in binary systems in the adsorption capacity of phenol, whereas the uptake of lead is very much reduced by the presence of phenol solute due to high affinity between phenol and GAC.

5.3 Desorption and Regeneration Studies

The desorption efficiencies of desorbing eluants under batch experimental conditions for GAC are shown in Table 7 and Figs. 5 and 6. The equilibrium concentration (C_e) was found to be 1.362 and 1.723 mg/L for phenol and lead respectively.

It is clear from the previous figures and table that the elution tendency as a percentage recovery of phenol followed the sequence as:

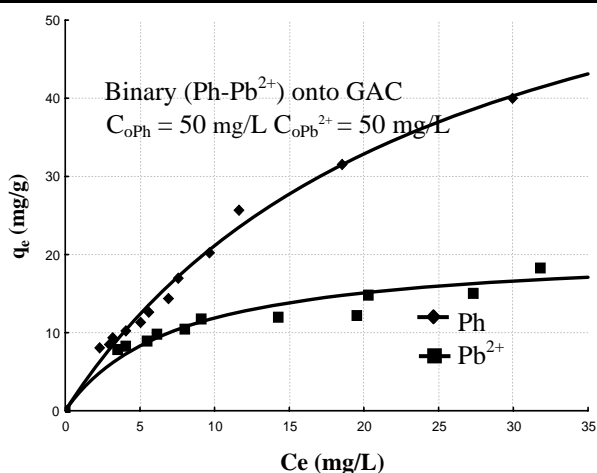


This observed trend may be due to formation of ions. Phenoxide ions have more energy than phenol itself due to no charge separation in the canonical structures as well as having negative charge on the more electronegative element, oxygen. Thus, the ion is more stable in water.

Therefore, it is expected that the adsorbed phenol should be eluated more easily with alkaline eluants than with acidic and DDW eluants. Acidic eluants can protonate the oxygen of phenol but the ion formed is less stable due to charge separation in the canonical structures and positive charge on the electronegative element (oxygen). A similar conclusions was given by Qadeer and Rehan (1998) in desorption of phenol from activated carbon. The eluation of adsorbed phenol was carried out by DW, NaOH and HCl with the following efficiency [31]:

Table 5 Parameters of single solute isotherm for Ph and Pb²⁺ onto GAC.

Model	Parameters	Ph	Pb ²⁺
Freundlich model	K_F (mg/g)(L/mg) ^{1/n_F}	5.7184	7.0332
	n_F	1.6483	2.3448
	R^2	0.9956	0.9750
Langmuir model	q_m (mg/g)	66.8234	37.0370
	b (L/mg)	0.0590	0.1258
	R^2	0.9959	0.9922
	R_s	0.2532	0.1372
	$E_{ad.}$ (%)	97.340	96.926
Temkin model	$B1$ (KJ/mole)	11.5900	7.9170
	K_T (L/mg)	0.8995	12.5218
	R^2	0.9150	0.9520
BET model	B (L/mg)	17.4328	189.1539
	Q (mg/g)	20.9017	11.4879
	R^2	0.9826	0.79110
Harkins-Henderson model	K	0.1771	5.7052
	n	0.6131	-0.5225
	R^2	0.9730	0.9360
Reddlich-Peterson model	A_R (L/mg)	12.2271	3.9387
	B_R (L/mg) ^{m_R}	1.3667	0.0585
	m_R	0.4895	1.1649
	R^2	0.9958	0.99180
Toth model	K_t (mg/g)	5.8241	282.5796
	a_t	0.1068	18.0189
	t	2.5086	0.6818
	R^2	0.9956	0.9922
Radke-Praunsitz model	K_{RP} (L/mg)	12.0239	3.9203
	F_{RP}	9.0270	68.6567
	N_{RP}	0.5085	-0.1704
	R^2	0.9958	0.9918
Combination of Langmuir-Freundlich model	q_m (mg/g)	123.3115	36.5002
	b (L/mg) ^{1/n}	0.0417	0.1243
	n	1.3182	0.9776
	R^2	0.9959	0.9907
Khan model	Q_{max} (mg/g)	2.0343	72.4579
	b_K (L/mg)	5.9081	0.0563
	a_K	0.4018	1.45587
	R^2	0.9956	0.9922

Fig. 4 Adsorption isotherm for (Ph-Pb²⁺) onto GAC.

0.5 M NaOH (99%) > 0.1 M HCl (12%) > DW (6%)

However, for lead the process is reverse and followed the following sequence:

HCl > EDTA > Na₂CO₃ > H₂SO₄ > NaOH > DDW

Therefore, NaOH and HCl were selected as an effective desorbing eluants for phenol and lead respectively and used in adsorption-desorption-regeneration for on one cycle. The adsorption isotherm for single component system of phenol and lead onto regenerated GAC using Langmuir model is listed in Table 8.

From Table 7 and Figs. 7 and 8, it is clear that there

Table 6 Parameters of a binary solute isotherm for Ph and Pb²⁺ onto GAC.

Model	Parameters	Ph	Pb ²⁺
Extended Langmuir model	q _m (mg/g)	60.4823	13.0988
	B (L/mg)	0.0467	0.2167
	R ²	0.9987	0.9963
	R _s	0.2999	0.0845
	E _{ad.} (%)	95.356	93.084
Combination of Langmuir-Freundlich model	q _m (mg/g)	58.5867	1.3622 × 10 ¹⁵
	b (L/mg) ^{1/n}	0.0590	4.4887
	n	6.2120 × 10 ¹⁵	2.6794
	R ²	0.9958	0.9832
Extended Freundlich model	K _F (mg/g)(L/mg) ^{1/n}	23.2068	9.7838
	n	0.0539	0.1000
	b	-0.9923	0.1543
	R ²	0.9923	0.9775
Reddlich-Peterson model	B (L/mg)	17.4328	189.1539
	Q (mg/g)	20.9017	11.4879
	R ²	0.9826	0.79110

Table 7 Desorption efficiency of the different eluants.

Eluant	Desorption of Ph from GAC V _e = 50 mL C _{ads.} = 48.638 mg/L		Desorption of Pb ²⁺ from GAC V _e = 50 mL C _{ads.} = 48.277 mg/L	
	C _{d.} (mg/L)	E _d (%)	C _{d.} (mg/L)	E _d (%)
HCl	7.724	7.940	94.622	98
H ₂ SO ₄	10.068	10.349	29.614	30.671
NaOH	94.698	97.350	27.596	28.581
Na ₂ CO ₃	93.608	96.229	44.107	45.681
EDTA	86.534	88.957	91.960	95.242
DDW	7.192	7.393	5.031	5.211

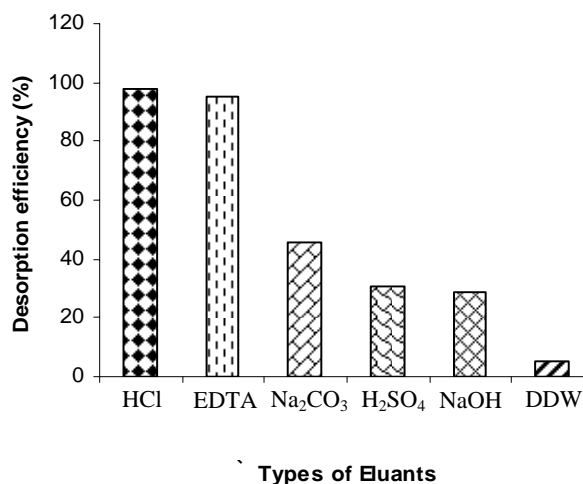
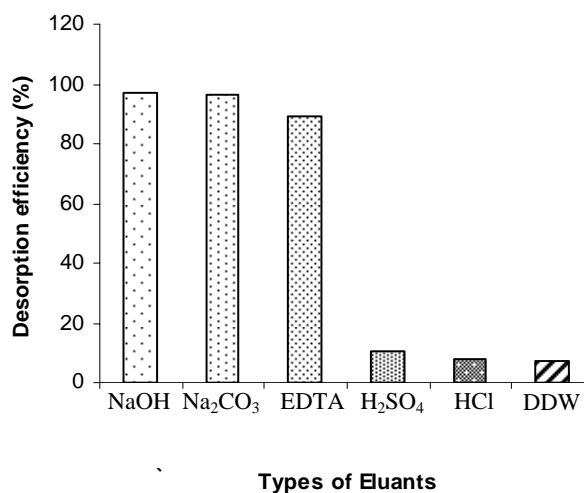
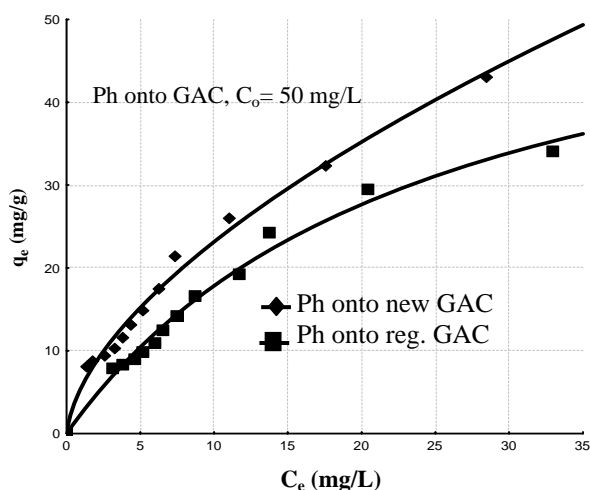
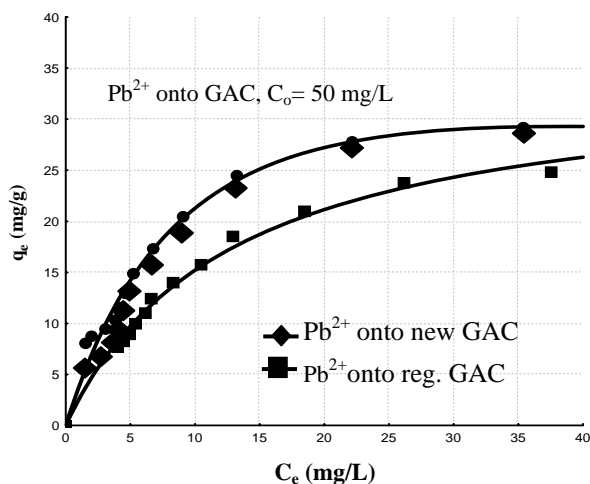


Fig. 5 Desorption efficiency of Ph from GAC.

Fig. 6 Desorption efficiency of Pb²⁺ from GAC.

Table 8 Parameters of single solute isotherm for Ph and Pb^{2+} onto regenerated GAC.

Model	Parameters	Ph	Pb^{2+}
Langmuir model	q_m (mg/g)	61.4931	34.6920
	B (L/mg)	0.0409	0.0781
	R^2	0.9939	0.9962
	R_s	0.3284	0.2039
	$E_{ad.}$	93.760	0.920

**Fig. 7** Adsorption isotherm for Ph onto new and regenerated (reg.) GAC.**Fig. 8** Adsorption isotherm for Pb^{2+} onto new and regenerated GAC.

is only 3.58%, 4.93% decrease in removal efficiency for phenol and lead onto regenerated GAC. This proved the suitability of using NaOH and HCl in desorption process.

6. Conclusions

Based on experimental results the following

conclusions can be drawn:

- Phenol can be removed more efficient than lead. GAC has more affinity to organics than inorganic pollutants;
- The equilibrium isotherm for each solute is of favorable type both in single and binary systems;
- Langmuir, combination of Langmuir-Freundlich, Toth and Khan models give the best fit of the experimental data in single component system;
- The extended Langmuir and Redlich-Peterson models seem to give the best fitting for the experimental data for binary component system;
- Alkaline (NaOH) was found an effective desorbing eluant for positive ions (Pb^{2+}). On contract, acids (HCl) was the suitable eluant for negative ions or component (Ph);
- The different model parameters obtained in this work can be used to estimate reactor volume, required adsorbent quantity for desired separation, purification degree, etc. from mass balance in a batch single component or binary system with satisfactory agreement with experimental results. Moreover, using these data multi-stage continuous systems can be also designed and stage number can be found for desired purification.

References

- [1] J.W. Patterson, Industrial Wastewater Treatment Technology, Butterworth Publishers, 1985, pp. 53-393.
- [2] E.N. Chirwa, Y.T. Wang, Determination of lead biosorption properties by experimental and modeling simulation study, Water Res. 34 (2000) 2376.
- [3] Z. Aksu, D. Akpinar, Modeling of simultaneous biosorption of phenol and nickel(II) onto dried activated sludge, Biochem. Eng. 12 (2001) 183.
- [4] J.W. Hassler, Purification with Activated Carbon, Chemical Publishing Co., New York, 1974.
- [5] J.R. Perrich, Activated Carbon Adsorption for Waste Water Treatment, CRC Press, Boca Raton, Fla., 1981.
- [6] G. Callega, J. Serna, J. Rodriguez, Kinetics of adsorption of phenolic compounds from wastewater onto activated carbon, Carbon 31 (1993) 691-697.
- [7] M. Streat, J.W. Patrick, M.J. Camporro, Sorption of phenol and p-chlorophenol from water using conventional and novel activated carbons, Water Sci. Res.

- 29 (1995) 467-473.
- [8] M.A. Ferro-Garcia, J. Rivera-Utrilla, I. Bautista-Toledo, C.M. Moreno-Castilla, Chemical and thermal regeneration of an activated carbon saturated with chlorophenols, *J. Chem. Technol. Biotechnol.* 67 (1996) 183-189.
- [9] J.H. Lee, D.I. Song, W.Y. Jeon, Adsorption of organic phenols onto dual organic cation montmorillonite from water, *Sci. Technol.* 32 (1997) 1975-1992.
- [10] R.U. Edgehill, G.Q. Lu, Adsorption characteristics of carbonized bark for phenol and pentachlorophenol, *J. Chem. Technol. Biotechnol.* 71 (1998) 27-35.
- [11] Z. Aksu, F. Gonen, Binary biosorption of phenol and chromium(VI) onto immobilized activated sludge in a packed bed: Prediction of kinetic parameters and breakthrough curves, *Separation and Purification Technology* 49 (2005) 205-216.
- [12] ATSDR (Agency for Toxic Substances and Disease Registry), Toxicological Profile for Dichlorophenol, Atlanta, Georgia: US Department of Health and Human Services, DHHS, Publication, No.TP-91/14, 1992.
- [13] Z. Aksu, D. Akpınar, Modelling of simultaneous biosorption of phenol and nickel(II) onto dried aerobic activated sludge, *Purif. Technol.* 21 (2000) 87-99.
- [14] A. Esposito, F. Pagnanelli, F. Vegliò, pH-related equilibria models for biosorption in single metal systems, *Chem. Eng. Sci.* 57 (2002) 307-313.
- [15] J.C. Crittenden, Evaluating multi-component competitive adsorption in fixed-bed, *J. Environmental Engineering* 113 (1987) 1363-1375.
- [16] S.C. Bhatia, *Environmental Pollution and Control in Chemical Process Industries*, Khana Publisher, 2001, pp. 250-260.
- [17] J.Y. Farah, N.S. El-Gendy, L.A. Farahat, Biosorption of Astrazone blue basic dye from anaqueous solution using dried biomass of baker's yeast, *J. Hazard Mater* 148 (2007) 402-408.
- [18] I. Langmuir, The adsorption of gases on plane surfaces of glass, mica and platinum, *J. Am. Chem. Soc.* 40 (1918) 1361-1403.
- [19] T.W. Weber, P. Chakravorti, Pore and solid diffusion models for fixed-bed adsorbers, *AIChEj* 20 (1974) 228.
- [20] M. Temkin, Die gas adsorption under constant pressure, *Acta Physicochim URSS* 1 (1934) 36-52.
- [21] W.J. Weber, *Adsorption in Physicochemical Processes for Water Quality Control*, New York, Wiley, 1972, pp. 206-211.
- [22] A.J. Garden, Application of Harkins model in adsorption, *International Association of Hydrogeologists J.* 7 (2006) 11-14.
- [23] O. Redlich, D.L. Peterson, A useful adsorption isotherm, *J. Phys. Chem.* 63 (1959) 1024.
- [24] J. Toth, State equations of the solid gas interface layer, *Acta. Chem. Acad. Hung.* 69 (1971) 311-317.
- [25] C.J. Radke, J.M. Prausnitz, Adsorption of organic solutions from dilute aqueous solutions on activated carbon, *Ind. Eng. Chem. Fundam.* 11 (1972) 445-451.
- [26] R. Sips, On the structure of a catalyst surface, *J. Chem. Phys.* 16 (1948) 490-495.
- [27] A.R. Khan, T.A. Al-Bahri, A. Al-Haddad, Adsorption of phenol based organic pollutants on activated carbon from multi component dilute aqueous solutions, *Water Res.* 31 (1997) 2102-2112.
- [28] W.J. Weber, P.M. McGinley, L.E. Katz, Sorption phenomena in subsurface systems: Concepts, models, and effects on contaminant fate and transport, *Wat. Res.* 25 (1991) 499-528.
- [29] A. Fahmi, K. Munther, Competitive adsorption of Nickel and cadmium on sheep manure waste, experimental and prediction studies, *Separation Science and Technology* 38 (2003) 483-497.
- [30] Ch. Katarzyna, *Biosorption and Bioaccumulation in Practice*, Nova Science Publishers Inc., New York, 2009.
- [31] R. Qadeer, A. Rehan, A study of the adsorption of phenol y activated carbon from aqueous solutions, *Turk J. Chem.* 26 (1998) 357-361.

Cascaded Simultaneous Nitrification and Denitrification Process for Nitrogen and Phosphorus Reduction from RO Reject Wastewater: A Bench-Scale Study

A.B. Shahalam, A. Abusam, A. Matouk and M. Khaja

Kuwait Institute for Scientific Research, Safat 13109, Kuwait

Received: April 21, 2011 / Accepted: May 25, 2011 / Published: November 20, 2011.

Abstract: The use of the reverse osmosis (RO) process, for refining secondary or tertiary effluent from plants treating domestic wastewater, is rapidly increasing. However, the disposal of the RO reject water poses a problem due to the presence of very high concentrations of salts, metals, and nutrients in it. This paper contains results of a bench-scale study aimed at reducing nutrients from RO-discarded streams utilizing a sequential bioreactors system, under partial aerobic and anoxic conditions. The tests were performed on synthetic wastewater resembling RO-reject water of an operating treatment plant, with glucose, methanol or acetate added to the water as sources of carbon. Study results indicate that the RO process removed about 50-60% of the total nitrogen and 50% of the phosphate; it reduced chemical oxygen demand (COD) by 79 to 82%, and affected no change in the metal concentrations. A clear cut removal preference for any one of the external carbon sources was not observed, although a slight advantage of glucose and methanol was recorded. The process maintained about 20% of the reactor volume in the anoxic environment.

Key words: Brine, wastewater treatment, biological nutrient removal, sequential aerobic-anoxic reactors.

1. Introduction

Water shortage is a critical problem throughout the world particularly in arid and semiarid regions. In many of these water-stressed regions, ambitious programs of water conservation and reuse of once-used water to augment the amount of water available were taken up by concerned organizations. Such water augmentation programs are under way in almost all Middle Eastern Countries. One main component of such programs is to treat and reuse it as an irrigant or for other safe uses. In the process, some countries started using reverse osmosis (RO) to reduce residual metal, chemical oxygen demand (COD) and bacterial concentrations even in tertiary effluent. This specific refinement of wastewater effluent produces ultra-clean

water; however, it produces about 15% of RO influent as reject wastewater which has very high concentrations of nitrogen, phosphorus, metals, COD, and salts, and very low concentration of organics. Based on salt concentration, this water can be graded as brine. The disposal and/or reuse of this water pose another new problem. The nutrient level in this water, in particular, needs to be reduced for its safe disposal or reuse.

A biological nitrification and denitrification process of a cascaded aerator system under partial anaerobic conditions with a spiked organic level was tested at bench scale to determine the process performance in reducing nitrogen and phosphorus. The process was tested on with synthetic RO brine-wastewater for the convenience of testing the effects of varying concentrations of pollutants on the process performance.

Corresponding author: A.B. Shahalam, senior research scientist, Ph.D., main research fields: water resources, wastewater treatment, systems, environmental engineering. E-mail: salam@kisir.edu.kw.

2. Background

2.1 Nutrient Removal in Wastewater

In wastewater treatment, biological processes for nutrient reduction are preferred due to process economy and simplicity in operation. The processes are known as BNR (biological nutrient removal). Chemical processes of coagulation/flocculation is also used widely particularly for phosphorus removal for small flow of wastewater. However, it has limited use due to production of hard-to-handle sludge by-products. Biologically total nitrogen removal is accomplished in two-stage process of nitrification and denitrification. In this treatment, phosphorus is simultaneously removed due to bio-cell use of phosphorus for cell build-up. The combined process is termed as SND (simultaneous nitrification and denitrification process).

Barnard [1] indicated that three principal factors predominantly influence the SND and accomplishments in phosphorus reduction. These are carbon supply, oxygen concentrations, and sludge floc-size. His study found that in most domestic wastewaters, complete denitrification could be achieved with a TCOD (total chemical oxygen demand):TKN (total Kjeldahl nitrogen) ratio of 7. Generally, a minimum value of 9 is required for achieving both biological N and P reduction [2]. Isaacs and Henze [3] proposed that 1.5-2.5 g COD/g P is used for the phosphate reduction whereas the COD:N ratio for denitrification is in the range of 3.5-4.5 g COD/g N. This is close to the theoretical requirement for denitrification without COD loss due to aerobic processes in domestic wastewater. Henze [4] compared the denitrification rates using several organic components and found that the rate with domestic wastewater was about one third of the value obtained with acetic acid or methanol. In comparing acetate, methanol, and glucose, in carbon source evaluation, Tam et al. [5] and Gerber et al. [6] found acetate to give the highest denitrification rate. Painter [7] indicated that dissolved oxygen (DO) concentration for

nitrification should be higher than 2 mg O₂/L, otherwise DO can be the limiting factor. At the same time, a value of 0.2 mg O₂/L is considered as a critical value, at which nitrification no longer occurs [8]. However, it has also been found that a DO concentration of around 0.5 mg/L is suitable to achieve a nitrification rate equal to the denitrification rate which would, therefore, lead to complete SND [9]. The physical explanation for bio-floc effect is that a substantial anoxic mass fraction exists in the center of biomass flocs and it enhances denitrification activity.

2.2 Nitrogen and Phosphorus Reduction in Saline/Brackish/Brine Wastewater

The utilization of biological processes for nitrogen and phosphorus removal from saline wastewater is a special problem mainly due to the adverse effect of salinity on biomass growth. Saline wastewater with high contents of nitrogen and phosphorus is generated in seafood industries, aquaculture farms, coastal tourist spots, fishing ports, and discarded streams of processes such as RO, membrane filtration and ion-exchange applied to refine secondary or tertiary effluent of conventional wastewater treatment plants.

Elevated salinity impedes biological activity due to presence of Na⁺ and Cl⁻ ions in water. Previous studies indicated that high salinity adversely effects the reduction of chemical oxygen demand (COD) in normal wastewater plants of activated sludge [10, 11]. However, the adaptation of biomass to saline wastewater improved COD reduction [12, 13]. Another study indicated that nitrogen reduction is insignificantly effected up to a salt level of 4000 mg/L just little above 10% of salt concentration in normal seawater. Even at this low level of salt however, phosphorus reduction dropped from normal reduction of 82% to only 25% showing severe interference of salt [14]. Concerning nitrogen, a similar study reported that in low salt concentration, ammonia reduction can be achieved within the range of 20 to 50% [15].

Past records of studies with highly saline wastewater

from seafood industry and RO or other membrane processes treating wastewater effluent are inadequate to draw any conclusive inference on the treat-ability of saline wastewater. In such water, high levels of nutrients (nitrogen ranging of 50-60 mg/L and phosphorus ranging 10-12 mg/L) are common features.

A recent sequential batch reactor (SBR) study [16] concentrated on nutrient reduction from saline wastewater (artificial seafood processing wastewater). A synthetic wastewater was utilized. The wastewater was prepared to have the approximate concentrations of total COD 1000 mg/L, soluble COD 500 mg/L, TKN 120 mg/L, PO₄-P 20 mg/L. Intrasungkha [16] reported 80-92% organics and nitrogen reduction. The author reported nutrient reduction efficiency in sequential bio-reactors with variable hydraulic retention time. Best removal rate was recorded at 24 h hydraulic retention and 12 days sludge age. The author reported that better result is accomplished from the acclimatization of bacteria at higher salinity as reported by others [12, 13]. Intrasungkha' study [16] also found that after the influent was modified with acetate addition, satisfactory phosphorus reduction was also achieved within 2-3 d.

3. Present Study with Synthetic RO Reject Wastewater

3.1 Test Unit

The background search indicated that the biological system with sequential aerobic and anoxic reactors [17, 18] appeared to have great potential for treating of treating RO rejected brine wastewater for reducing high concentrations of nutrients. Fig. 1 depicts the schematic diagram of the system that was tested on synthetic wastewater resembling RO-reject wastewater resulting from the application of the RO process for refining tertiary effluent of a biological treatment plant, treating mainly municipal wastewater.

3.2 Methodology

The bench-scale system was designed for a flow

range of 20 to 50 mL/m. For tank assembly, plexi-glass materials were used. Design features of the unit are shown in Table 1. Five identical small tanks connected in series provided total reactor volume. All laboratory determinations followed the outlined Standard Method for Water and Wastewater analysis [19].

3.2.1 Feed

The unit was operated with synthetic wastewater resembling the RO reject water produced in an operating RO system in Kuwait. Initial seeding of bacterial mass in reactors was done by using settled sludge obtained from an operating sludge thickener. The preparation of the synthetic RO-reject wastewater closely followed the quality of the real RO-reject wastewater production (Table 2). For basic chemical ingredients of synthetic wastewater, media preparation of Intrasungkha et al. [16] was followed (Table 3).

Chemicals NaNO₃ and KH₂PO₄ were used to spike the concentrations of nitrate and phosphate to reach target concentrations in the synthetic wastewater. For 1

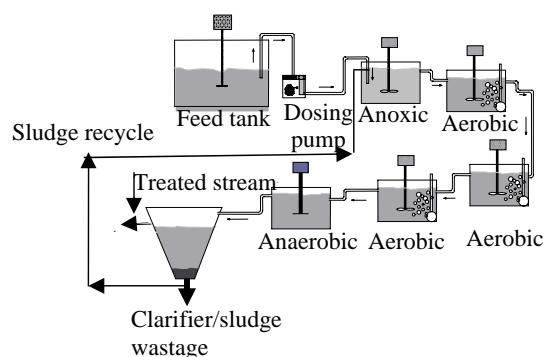


Fig. 1 Cascaded aerator process.

Table 1 Physical properties of bench-scale cascaded reactor system.

Item	Quantity/Dimension
Number of reactor tanks	5 (Equal volume each)
Number of anoxic reactor tanks	Variable
Depth	0.2 (m)
Volume of each reactor tank	0.00756 (0.27 × 0.14 × 0.2) (m ³)
Total volume of reactor tanks	0.0378 (m ³)
Number of clarifier	1 (conical)
Surface area of clarifier	0.051 (m ²)
Volume of clarifier	0.008 (m ³)
Depth	0.3 (m)

Table 2 Quality of RO reject water from Sulaibiya treatment plant (Kuwait).

Parameter	Average monthly value for February, 2007
pH	7.29
Conductivity ($\mu\text{S}/\text{cm}$)	9,201
TSS (mg/L)	7
COD (mg/L)	183
TDS (mg/L)	4,600
N-NO ₃ (mg/L)	29
TN (mg/L)	73.7
TP (mg/L)	20.6
TPO ₄ (mg/L)	63.1
Cl (mg/L)	1,580
SO ₄ (mg/L)	2,272

COD: chemical oxygen demand; TDS: total dissolved solids; TN: total nitrogen; TP: total phosphorous; TPO₄: total phosphate as PO₄; Cl: free chlorine; SO₄: sulfate.

Table 3 Basic chemical ingredients in synthetic waste (Source: Intrasungkha [16]).

Ingredient	Concentration of synthetic wastewater (g/L)
(NH ₄) ₂ SO ₄	0.235
K ₂ HPO ₄	0.084
NaHCO ₃	0.5
MgSO ₄ ·7H ₂ O	0.1
CaCl ₂	0.05
KCl	0.02
FeSO ₄ ·7H ₂ O	0.001
NaCl	0.3
MnSO ₄ ·7H ₂ O	0.001
KH ₂ PO ₄	0.001
Na ₂ MoO	0.0005

mg/L N-NO₃, the carbon sources of methanol (CH₃OH), acetate (CH₃COONa), or glucose (C₆H₁₂O₆) were added by amounts of 0.08, 0.07, or 0.09 mg/L, respectively. For 1 mg/L P-PO₄, the carbon sources of methanol (CH₃OH), acetate (CH₃COONa), or glucose (C₆H₁₂O₆) were added by amounts of 0.05, 0.04 or 0.06 mg/L respectively [16, 18]. NaCl was added in the solution to achieve the desired level of conductance, within the range of 6000-9000 $\mu\text{S}/\text{cm}$ [16] and the required amount of salinity.

4. Process Operation

Twenty six (carbon source: 10 glucose, 10 methanol, and 6 acetate) steady state cases based on effluent

quality were recorded. Average hydraulic-detention time in the total system (combined aerobic and anoxic) was 24 h with a standard deviation of 1.5 h. Sludge wastage was performed daily by discarding sludge from the bottom of the clarifier, manually. Wastage solid mass was calculated on the basis of average solid-mass in all tanks with targeted average sludge-age of 15 d. Sludge age varied within the range of 13 to 16.5 d. Average inflow rate in the system was 26 mL/min while average return sludge flow was 25 mL/m. First tank receiving inflow and return sludge was mixed very gently to add to floc formation in the absence of any air supply. The oxygen level in this tank remained around 1 mg/L. The last tank was maintained at anoxic conditions and its contents received constant gentle mixing to keep the solids suspended. The oxygen level in the fifth tank mostly remained below 1 mg/L. Oxygen level in the three aerated tanks was maintained at an average of 2.5 mg/L. The water temperature and pH were within the range of 22 to 23 °C and 6.3 to 8.7, respectively. Table 4 shows the range of values of the main quality parameters in inflow in the 26 test cases.

5. Results and Discussion

During the one-year study, 26 distinct steady states (glucose carbon source 10, methanol carbon source 10, and acetate carbon source 6) were identified. Quality parameters such as conductance, chemical oxygen demand COD, total nitrogen (TN), phosphate as P-PO₄,

Table 4 Average, maximum, minimum, and standard deviation of influent (synthetic RO reject wastewater) quality parameters.

Parameters	Units	Average	Maximum	Minimum
Temperature	°C	25.7	28.5	24.4
pH	-	7.5	8.4	7
Conductivity	$\mu\text{S}/\text{cm}$	6,155.0	7,110	5,410
COD	mg/L	324.2	665	169
N-NO ₃	mg/L	23.0	28	17
TN	mg/L	57.5	76	43
Total PO ₄	mg/L	73.7	89.6	58
BOD ₅	mg/L	6.0	9.5	4

COD: chemical oxygen demand; TN: total nitrogen; BOD: biochemical oxygen demand.

and several metals were measured in inflow and effluent of the system.

Conductance in inflow remained within the range of 8000 to 9500 $\mu\text{S}/\text{cm}$ which is within the brine range. Through the process it did not change considerably. In average, a three-percent reduction in conductance in the process was observed.

COD in inflow varied from 535 to 620 mg/L. An average COD removal of 80% was recorded which is significant, and it appeared that most of degradable carbon was utilized by the bacterial mass.

Fig. 2 shows the average TN and P- PO_4 reduction in the process. The three different sources of carbon (glucose, methanol, and acetate) did not indicate significant differences in TN reduction. The lowest nitrogen removal was observed with acetate (56.20%), while maximum reduction (64.75%) was observed with glucose. This observation did not go along with the findings elsewhere [5, 6] where it was found that acetate is more effective. However, a direct comparison is not valid as those findings were with normal domestic wastewater. Phosphate-reduction difference among glucose, methanol, and acetate was insignificant. Reduction percentage varied from a minimum 47.3 with acetate, to a maximum 51.0 with glucose. Phosphate reduction with glucose and methanol were almost the same.

Inflow and effluent TN and P- PO_4 in two carbon sources of glucose and methanol are shown in Figs. 3-6 in 10 steady state cases of each source. The figures indicated the effect of inflow concentrations of TN and P- PO_4 on their reduction efficiency. It is observed in Figs. 3 and 4 that when inflow nitrogen level is high, the reduction of TN is high (steady states 1, 2, 3 and 9 with glucose and steady states 1, 3, 4, and 5 with methanol).

At high concentrations of TN in inflow, overall reduction of TN with carbon sources glucose and methanol remained high in all cases. TN reduction increased as inflow TN increased. It indicates that biomass uptake and conversion of N responded with

amount of TN presence. The observation also indicated that the process of nitrification and denitrification was effectively working in the system. The maximum reduction that could be achieved was around 50%. Unlike TN, the amount of P- PO_4 reduction appeared to be independent of P- PO_4 concentration in the inflow. The basic need of phosphorus for physiological build up of bacterial cell probably was the main factor in the P- PO_4 reduction in the process.

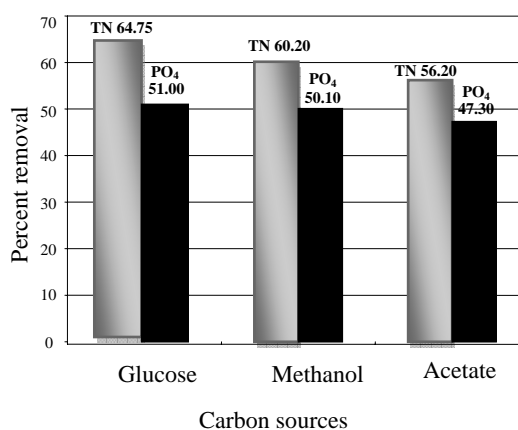


Fig. 2 Average removal of TN and PO_4 in tested cases.

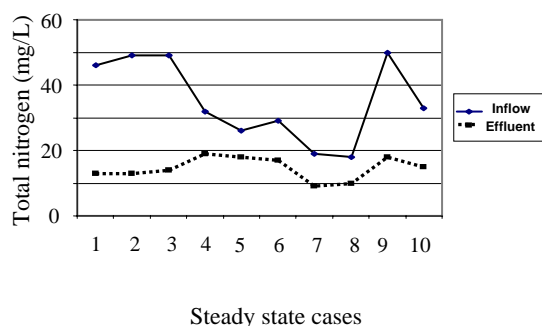


Fig. 3 Total nitrogen (TN) with glucose as carbon source.

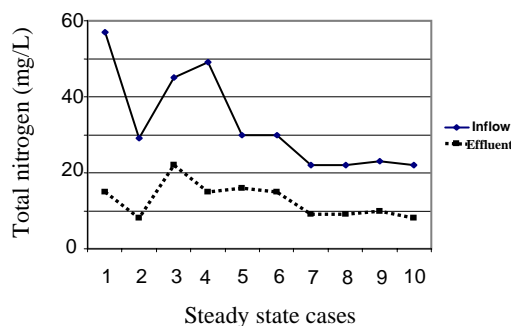


Fig. 4 Total nitrogen (TN) with methanol as carbon source.

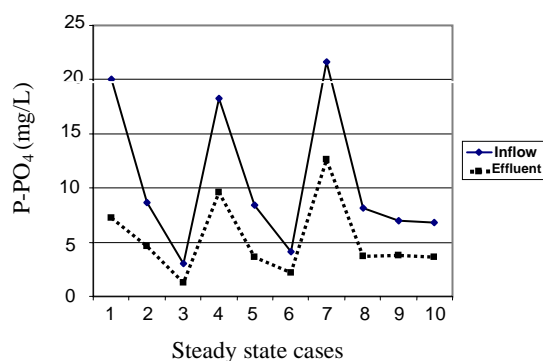


Fig. 5 P as P-PO₄ with glucose as carbon source.

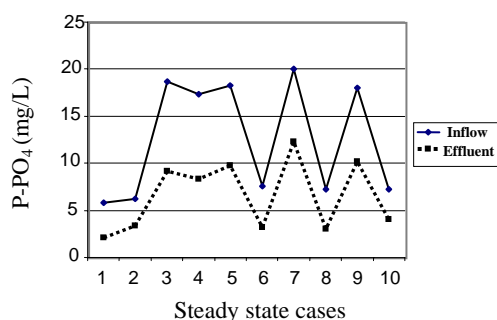


Fig. 6 P as P-PO₄ with methanol as carbon source.

Table 5 Average metal concentrations in process inflow and effluent.

Parameter	Average concentration	
	Inflow	Effluent
Cd	0.11	0.11
Cu	0.018	0.02
Pb	0.025	0.025
Hg	0.057	0.051
Ca	0.775	0.752
Mg	8.259	8.148
Zn	0.136	0.123

Selected metal concentrations in process inflow and effluent were determined for all steady-state cases. Average concentrations of some trace metals are shown in Table 5. Overall metal concentrations did not change appreciably in the process. The reduction of metals remained within three percent.

6. Conclusion

Cascaded nitrification and denitrification process appeared to be working in brine RO reject wastewater and is capable of reducing in average 55-60% of TN and about 50% of P-PO₄. As this type of wastewater has very low BOD₅ (<10 mg/L), an external carbon

source is needed to sustain biological activity. The performances of both glucose and methanol as carbon sources have similar outcomes in TN and P-PO₄ reduction.

Through the process the brine-salt concentration did not change appreciably. Only three to four percent of its reduction was achieved. The COD level reduced significantly within the range of 79-82% indicating efficient bacterial utilization of degradable carbons.

Acknowledgments

The authors would like to extend thanks to the Kuwait Foundation for Advancement of Sciences and the Kuwait Institute for Scientific Research for financing the study.

References

- [1] J.L. Barnard, Design and Retrofit of Wastewater Treatment Plants for Biological Nutrient Removal, Technomic Publishing, Pennsylvania, 1992.
- [2] M.C. Goronszy, Course Notes on Intermittently Operated Activated Sludge Plants, Department of Chemical Engineering, University of Queensland Press, Australia, 1992.
- [3] S.H. Isaacs, M. Henze, Controlled carbon source addition to an alternating nitrification-denitrification wastewater treatment process including biological P removal, *Wat. Res.* 29 (1995) 77-89.
- [4] M. Henze, Carbon sources for denitrification of wastewater, in: Seminar on Nutrients Removal from Municipal Wastewater, Tampere University, Tampere, Finland, Sept. 4-6, 1989.
- [5] N.F.Y. Tam, Y.S. Wong, G. Leung, Significance of external carbon sources on simultaneous removal of nutrients from wastewater, *Wat. Sci. Tech.* 26 (1992) 1047-1055.
- [6] A. Gerber, E.S. Mostert, C.T. Winter, R.H. de Villiers, The effect of acetate and other short-chain carbon compounds on the kinetics of biological nutrient removal, *Wat. S.A.* 12 (1986) 7-12.
- [7] H.A. Painter, Microbial transformations of inorganic nitrogen, *Proc. Wat. Tech.* 8 (1977) 3-29.
- [8] P. Bliss, D. Barnes, Modeling nitrification in plant scale activated sludge, *Wat. Sci. Tech.* 18 (1986) 139-148.
- [9] E.V. Munch, P.A. Lant, J. Keller, Simultaneous nitrification and denitrification in bench-scale sequencing batch reactors, *Wat. Res.* 30 (1996) 277-284.
- [10] A. Li, G. Guowei, The treatment of saline wastewater

- using a two-stage contact oxidation method, *Wat. Sci. Tech.* 28 (1996) 31-37.
- [11] F. Omil, R.J. Mendez, J.M. Lema, Characterization of biomass from a pilot plant digester treating saline wastewater, *J. Chem. Tech. Biotech.* 63 (1995) 384-392.
- [12] M.F. Hamoda, I. Alattar, Effects of high sodium chloride concentrations on activate sludge treatment, *Wat. Sci. Tech.* 31 (1995) 61-72.
- [13] F. Kargi, A.R. Dincer, Biological treatment of saline wastewater in an aerated percolator unit utilizing halophilic bacteria, *Environ. Tech.* 19 (1996) 529-537.
- [14] Z.H. Abu-Gharah, J.H. Sherrard, Biological nutrient removal in high salinity wastewater, *J. Environ. Sci. Health A28* (1993) 599-613.
- [15] S.L. Klemetson, M.E. Lang, Treatment of saline wastewaters using a rotating biological contractor, *JWPCF.* 56 (1984) 1254-1259.
- [16] N. Intrasungkha, J. Keller, L. Blackall, Biological nutrient removal efficiency in treatment of saline wastewater, *J. Wat. Sci. Technology* 39 (1999) 180-190.
- [17] O. Nowak, V. Kuhn, V. Muller, A comparison of different concepts of the running-in of nitrification and denitrification in activated sludge plants, *J. Wat. Sci. Tech.* 39 (1999) 53-60.
- [18] I.M. Sudiana, T. Mino, H. Sato, K. Nakamura, T. Matsua, Metabolism of enhanced biological phosphorus removal and non-enhanced biological phosphorus removal sludge with acetate and glucose as carbon source, *J. Wat. Sci. Technology* 39 (1999) 29-35.
- [19] APHA (American Public Health Association), *Standard Methods for Examination of Water and Wastewater*, Washington, D.C., USA, 1998.

Energy Efficiency, Indoor Air Quality and Thermal Comfort Studies at the Faculty of Engineering and Built Environment, University Kebangsaan Malaysia

N.L. Teng¹, S.M. Zain¹, N.E.A. Basri¹ and S. Mat²

1. Department of Civil and Structural Engineering, Faculty of Engineering and Built Environment, University Kebangsaan Malaysia, Bangi, Selangor 43600, Malaysia

2. Solar Energy Research Institute, University Kebangsaan Malaysia, Bangi, Selangor 43600, Malaysia

Received: February 10, 2011 / Accepted: April 13, 2011 / Published: November 20, 2011.

Abstract: The study was conducted to identify indoor air quality and the level of thermal comfort in various selected locations in Faculty of Engineering and Built Environment (FKAB), University Kebangsaan Malaysia (UKM) with built-up area of 250,936 ft². The indoor air quality and thermal comfort were measured at various selected locations by using indoor air quality equipment (Thermal Comfort SERI). The thermal comfort assessments are based on Malaysian Code of Practice Indoor Air Quality 2005 and Moderate Thermal Environments-Determination of the PMV and PPD indices specification of the condition for thermal comfort (ISO7730:1994). From the data analysis, the FKAB building is considered inadequately vented space. The concentration of CO₂ for all sampling area evaluated exceeds the recommended concentration (> 1000 ppm). The ventilation system used in FKAB building is designed by delivering fix amount of fresh air into building from external building without consideration on the number of occupants. This common ventilation design will increase the amount of CO₂ dramatically all day long and these reflect the inefficiency of energy used. The faculty needs to be equipped with a comprehensive energy management system that can allow detailed documentation of continuous performance of all energy system and consumption in the building.

Key words: Energy efficiency, indoor air quality, comfort survey, FKAB UKM.

1. Introduction

The commercial and residential buildings in Malaysia account for about 13% of total energy consumption and 48% of the country's electricity consumption [1]. Due to environmental factors and inconsistent of oil price at international market, the Malaysian government stressed on the low energy consumption building concept. Energy crisis in 1970s brought engineers and building managers design and maintain indoor environment more efficiently by sealing up the building and thus cause less ventilation rate to save the electricity [2]. Carbon dioxide (CO₂) concentration is a key parameter for assessing indoor

air quality and ventilation efficiency. Inadequate ventilation and elevated indoor pollutants concentrations can affect occupant's health. CO₂ contributes to 55% of the greenhouse effect. Therefore, increase in atmospheric concentrations of CO₂ may indirectly increase the rate of global climate change.

The amount of air conditioning load required and air conditioning energy used depend on the air temperature maintained in the building. Some buildings maintain indoor temperatures as low as 18 °C to 20 °C whereas the comfortable temperature should be at 24 °C. Thus, increasing the temperature to the comfort level can make a significant difference in the consumption of energy in the building. Improving energy efficiency not only decreases electricity usage

Corresponding author: N.L. Teng, bachelor, research field: low energy building. E-mail: eveneoh@hotmail.com.

in a building, it helps to improve indoor air quality and thermal comfort occupants as well.

Energy saving measures implemented in building envelope systems and also their associated environmental control systems such as lighting, heating, and cooling systems can be categorised into two groups: “passive systems” and “active systems”. Passive systems is a combination of building features to make use of energy, natural sources such as sun, wind, and others to illuminate, heat, ventilate and thus reduce the need for mechanical cooling, heating and daytime artificial lighting. Passive design includes building shape and orientation, utilize natural daylighting and natural ventilation, whereas active design is the common modern design relying on technology of Heating, Ventilation, and Air Conditional System (HVAC).

The intensity of building occupancy will affect energy use in building. The amount of energy used will generally be directly proportional to the intensity of building occupancy. The level of physical activities such as clothing worn, duration of occupancy, age, size and background of the occupant will also affect the cooling/heating requirements. These factors affect cooling requirements by influencing the preferred air temperature. Different type of wearing will have different thermal comfort level. For example a person wearing light clothes and doing light desk work seated will feel comfortable at 25 °C while he will only feel comfortable at 21 °C with a light business suit. This 4 degrees difference can mean a 100% difference in the air conditioning energy requirement of a room. The attitude of the occupants towards energy use and building management in terms of operation and maintenance will reflect on its efficiency and thus the energy.

2. Methodology

2.1 Indoor Air Quality (IAQ) Sampling

Indoor air conditions were measured at various selected sampling locations in Faculty of Engineering

and Built Environment (FKAB), UKM. The indoor air quality (IAQ) was measured using indoor air quality equipment “Thermal Comfort SERI” from “Solar Energy Research Institute, UKM”. Parameters measured includes carbon dioxide (CO₂), relative humidity (% RH), wind speed (m/s), room temperature (°C), radiant temperature, pressure, sound and light intensity. There are two types of selected sampling locations: air-conditioned room and open spaces area. Air conditioned room are lecture hall (DK3), dean’s office (PD) and library (PS) whereas open space area are geotechnical laboratory (Geo) and foyer (RL). A period of four consecutive sampling was conducted from 9 am to 5 pm representing the IAQ status of sampling area for the whole day and the average data were calculated.

2.2 Thermal Comfort Questionnaire

Concurrently during IAQ sampling, thermal comfort questionnaires were distributed at different time of the day randomly to respondents express their thermal response to the room conditions. This comfort questionnaire is divided into two sections. The first section is on personal informations such as gender, age, height, weight, activity, types of cloths respondent wore on the day of survey.

In the second part of the questionnaire, common questions were asked about thermal sensation in response to the room conditions. The ASHRAE thermal sensation scale (Table 1) was used for instance: (-3 = cold, -2 = cool, -1 = slightly cool, 0 = neutral, 1 = slightly warm, 2 = warm, 3 = hot). The lighting sensation and overall comfort level of respondent at the sampling area were also included in the questionnaire. Each respondent were required to make only one choice from the scale for each question.

2.3 Assessment

IAQ assessment and thermal comfort evaluation were conducted according to Malaysian Code of Practice Indoor Air Quality Malaysia [3] and Moderate

Table 1 Sensation scale questionnaire.

Scale	-3	-2	-1	0	1	2	3
Temperature	Cold	Cool	Slightly cool	Neutral	Slightly warm	Warm	Hot
Humidity	Very humid	Humid	Slightly humid	Neutral	Slightly dry	Dry	Very dry
Brightness	Too dark	Inadequate	Slightly	Neutral	Slightly	Adequate	Too bright
Overall	Poor	→					Excellent

Thermal Environments-Determination of the PMV and PPD indices and specification of the conditions for thermal comfort [4] respectively. List of indoor air contaminants and the maximum limits is shown in Table 2.

Fanger’s Predicted Mean Vote (PMV) model was developed for the evaluation of generic comfort conditions and predicts its limits. The PMV scale is constituted by seven thermal sensation points based on ASHRAE thermal sensation scale. Fanger [5] also developed a related index, called the Predicted Percentage Dissatisfied (PPD). PPD index is calculated from PMV, and predicts the percentage of people who are likely to be dissatisfied with a given thermal environment [2-4]. The PMV and PPD form a U-shaped relationship (Fig. 1), where percentage dissatisfied increases for PMV values above and below zero (thermally neutral).

ASHRAE proposed reference values between the PMV and PPD by outlining the assumptions on the rates

Table 2 List of indoor air contaminants and the maximum limits.

Indoor air contaminants	Eight-hour time-weighted	
	Average airborne concentration	
	ppm	mg/m ³
Carbon dioxide	C1000	
Carbon monoxide	10	
Formaldehyde	0.1	
Respirable particulates		0.15
Total volatile organic compounds	3	

Source: Malaysia Code of Practice Indoor Air Quality, 2005 [3].

Where:

-C is the ceiling limit;

-mg/m³ is milligrams per cubic meter of air at 25° Celsius and one atmosphere pressure;

-ppm is parts of vapour or gas per million parts of contaminated air by volume.

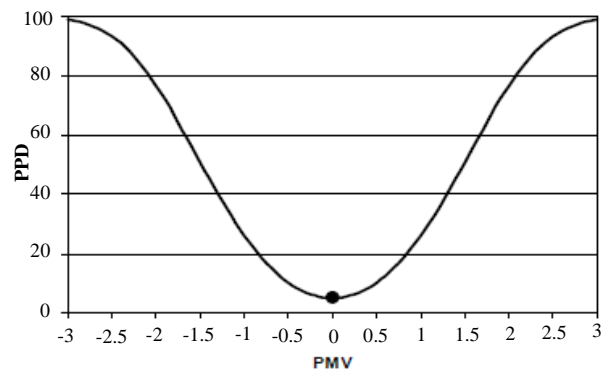


Fig. 1 Evolution of PPD on the basis of PMV.

Source: Moderate Thermal Environments (ISO7730:1994) [4].

of Fanger’s PMV and PPD. This would indicate that for a PMV value between -0.5 and +0.5, the percentage of dissatisfied (PPD) is below 10%. This research of thermal comfort and indoor air quality therefore can be used to judge the quality of the thermal environment. Consequently, it also reflects the efficiency of the HVAC systems and thus the energy used.

3. Result and Discussion

3.1 Indoor Air Quality (IAQ) Sampling

Fig. 2 shows carbon dioxide (CO₂) concentration at various selected sampling area. Code of Practice on IAQ recommends a maximum concentration of CO₂ of 1000 ppm (0.1%) for airborne concentration of a contaminant that is not to be exceeded at any time during the work shift. Most of the measured data show that the mean carbon dioxide for all sampling areas evaluated exceeds the recommended concentration and it can be considered as an inadequately vented space. Exceeding recommended levels of carbon dioxide indicate that an insufficient amount of fresh outdoor air is being delivered to the occupied areas of the building. This also indicates that other pollutants in the building

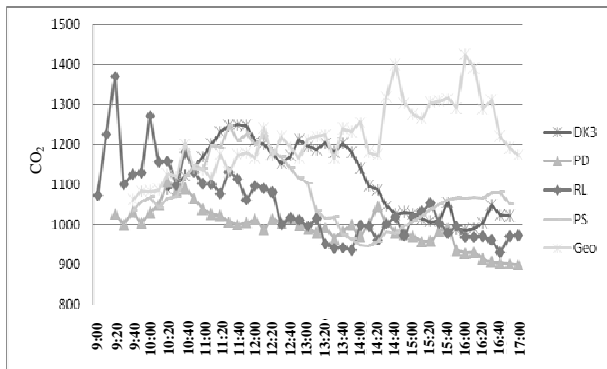


Fig. 2 Carbon dioxide (CO₂) concentration at various selected sampling area.

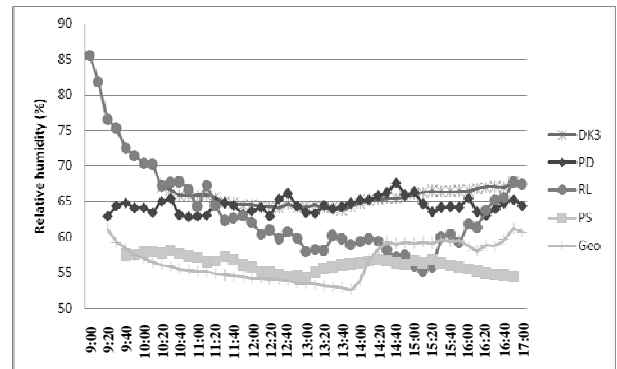


Fig. 3 Percentage of relative humidity at various selected sampling area.

may exist at elevated levels since there is not enough fresh air to dilute them. Study by Aizat et al. [6] on sick building syndrome (SBS) in Malaysia shows that the level of CO₂ concentration was the major factor contributing to the SBS complain among office workers.

Fig. 3 shows the percentage of relative humidity at various selected sampling areas for all human comfort level. Relative humidity is the percentage of water vapour in the air at a specific temperature, as compared to the amount of water vapour the air is capable of holding at that temperature. The human body is comfortable when relative humidity range between 20 and 60 percent. Fig. 4 shows the surrounding temperature at various selected sampling area. In tropical countries such as Malaysia, the recommended design temperature for typical air-conditioned room is 24 °C while acceptable temperature for an open space with mechanical ventilation is between 27.1 °C and 29.3 °C.

From the result obtained, PMV and PPD are calculated (Figs. 5-9) to predict the percentage of occupants who are likely to be dissatisfied with the surrounding thermal environment. Majority of respondents in the dean’s office and library felt uncomfortable with the cold environment while respondents in geotechnical laboratory and foyer felt hot. The negative responds of the PMV from the dean’s office and library clearly shows that most of the air-conditioned sampling area is over cooled.

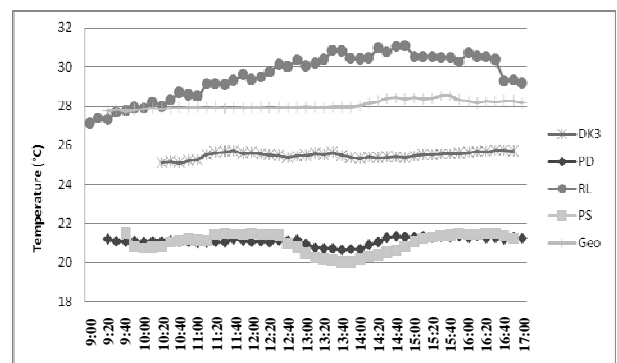


Fig. 4 Surrounding temperature at various selected sampling area.

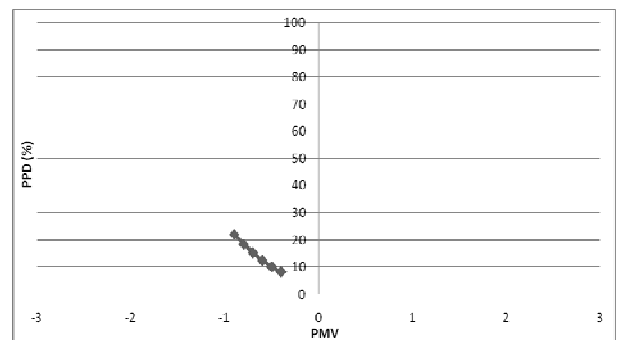


Fig. 5 Evolution of PPD on the basis of PMV at lecturer hall, DK3.

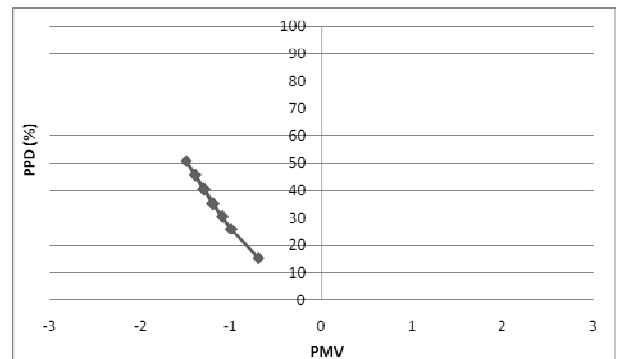


Fig. 6 Evolution of PPD on the basis of PMV at dean office, PD.

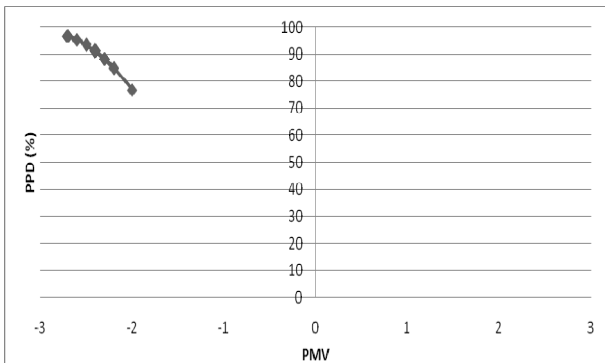


Fig. 7 Evolution of PPD on the basis of PMV at library, PS.

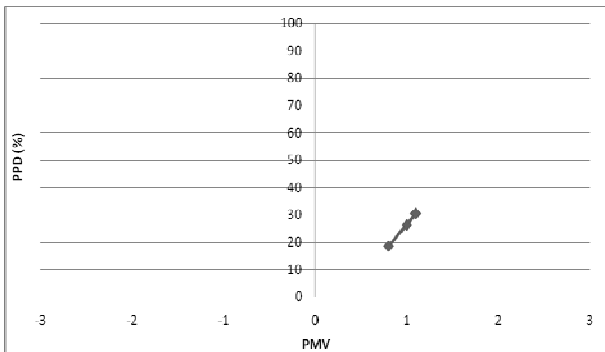


Fig. 8 Evolution of PPD on the basis of PMV at geotechnique laboratory, Geo.

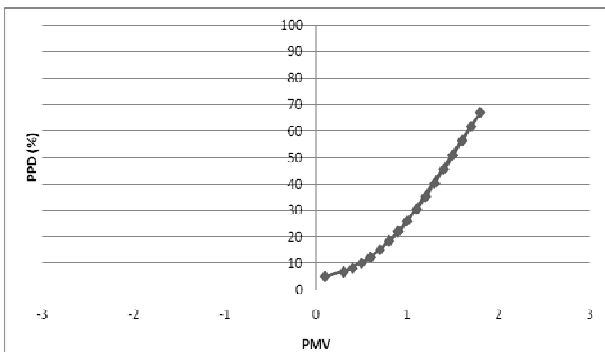


Fig. 9 Evolution of PPD on the basis of PMV at foyer, RL.

3.2 Thermal Comfort Questionnaire

The total respondents surveyed were 105 persons: 55 male and 50 female. The ages of the respondents ranged from 20-50 years old and the average was 24 years old. The average weight and height were 48.5 kg and 163.2 cm respectively. Clothing insulation and metabolic rates was quoted following recommended procedure in Moderate Thermal Environments [4]. Clothing insulation varied between 0.25 and 1.29 clo and the weighted mean in various zones was 0.50 clo.

Respondents were involved in various types of activities at difference locations, for example students in DK3 do light activity such as writing and moving their parts of body like hand and feet (light activity level or office work was about 1.2 met). Thermal acceptability of the respondents towards room climate is mostly considered, which is defined by the respondents who selected the three central thermal sensations namely, slightly cool, neutral, and slightly warm, in all of which the room occupants can normally stay and work. Figs. 10-13 show the sensation vote of respondent at lecturer hall (DK3), library (PS), dean office (PD) and geotechnique laboratory (Geo) respectively.

The reason for not considering the respondents who select for “neutral” is that each person has different thermal comfort sensation towards the room climate and it is difficult to set a room temperature which makes everybody feel “neutral”. Therefore, the acceptable way is to set the temperature of air conditioning so that approximately 80% of the occupants have thermal sensations between slightly cool and slightly warm.

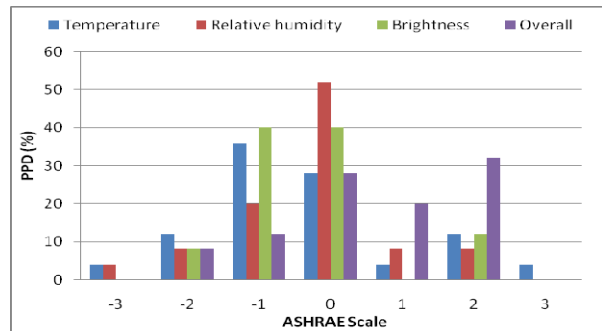


Fig. 10 Sensation vote of respondent at DK3.

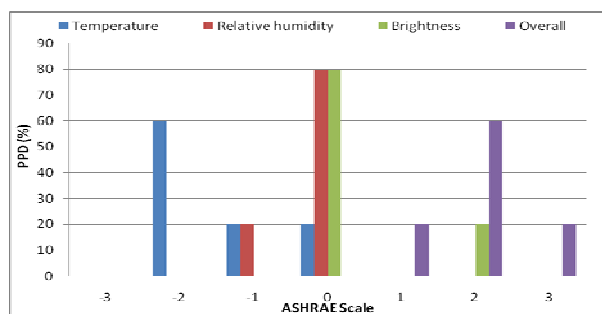


Fig. 11 Sensation vote of respondent at PS.

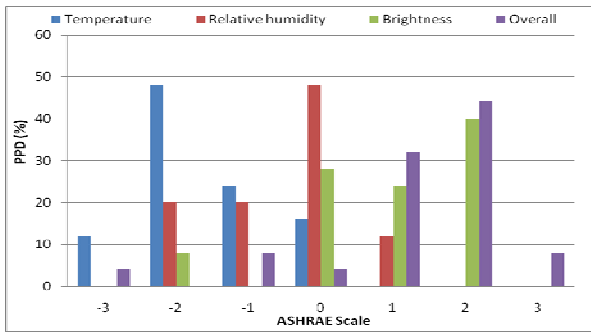


Fig. 12 Sensation vote of respondent at PD.

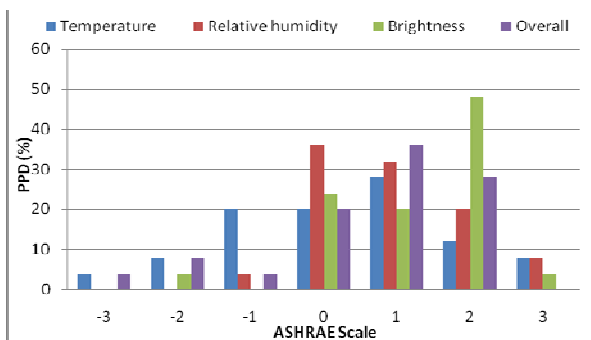


Fig. 13 Sensation vote of respondent at Geo.

3.3 Recommendation

There are some recommendations for environment improvement, reducing maintenance and operation cost of the FKAB, based on the results and analysis of sampling data. The FKAB needs to be equipping with a comprehensive energy management system that can allow detailed documentation of continuous performance for all energy system and consumption in the building. At minimum, it is required to install utility sub-metering for energy monitoring. Moreover, the utility sub-metering is also able to store electricity consumption separately for lighting, task lighting, office equipment and cooling load delivered to the building.

Planting trees is one of the easiest ways to reduce carbon dioxide level in foyer. Trees absorb carbon dioxide emitted by occupants in the foyer and produce oxygen, thus suitable for the purpose of carbon balancing. From the data analysis, it is shown that the mean temperature for the dean’s office and library is only 21.5 °C and 20.5 °C respectively. On the other hand, thermal sensation selection from the respondents proves that most of the respondents are not satisfied

with the cold environment in the respective areas. The recommended temperature is at 24 °C. By increasing the room temperature set point to 24 °C, it will reduce the cooling load and therefore be able to save more energy. It is estimated that 10% of energy cooling can be reduced by increasing the room temperature by 1 °C.

The ventilation system used in FKAB building (DK3) is designed by delivering fixed amount of fresh air into the building without considering the number of occupants. This common ventilation design will increase the amount of CO₂ dramatically all day long. CO₂ demand control ventilation is a real time, occupancy-based ventilation approach that can offer significant energy saving over traditional fixed ventilation approaches by controlling the amount of outside air brought into the building. Thus, firstly it saves energy by not heating or cooling unnecessary quantities of outside air. Secondly, it can provide assurance that sufficient outside air is being supplied to the occupants. DCV is able to save energy by lowering the ventilation rate to the actual occupancy in the space area.

Strategy to install electric lighting by sensor is one basic element to increase energy efficiency indoor. Lighting sensor automatically can help to turn on the lights when there is sign of insufficient condition of light or to switch-off the lights when the area is not occupied. Two types of sensors are proposed which are:

(1) Control with light sensor, put off electric lighting automatically when daylight is sufficient. Light sensors were proposed at the foyer, multipurpose space in the lecturer building, perimeter building, corridor and place which obtained enough daily light.

(2) Control with occupancy sensor, off electrical lighting when a room or a zone is vacant. These control sensors are suitable for lecture room and lecture theatre.

The type of fluorescent light used in FKAB is Philips LIFEMAX (T8). T5 fluorescent energy saving lights

Table 3 Total energy and cost saving of T5 fluorescent light replacement.

Type	T5 fluorescent light with length			
	600 mm		1200 mm	
	4285		2907	
	(Watt)	RM/KW	(Watt)	RM/KW
Energy saving for each T5	13		15	
Total energy save per day (peak hour)	668,460	192.51648	523,260	150.69888
Total energy save per day (non peak hour)	334,230	59.16	261,630	46.31
Total energy save per month	28,075,320	8,085.69	21,976,920	6,329.35
Total energy save per year	336,903,840	97,028.31	263,723,040	75,952.24

Table 4 Total T5 installation cost and return of investment.

	T5 fluorescent light with length	
	600 mm	1200 mm
Total installation cost (RM)	192,825.00	130,815.00
Return of investment (Year)	1.99	1.72

have higher system efficiency and miniaturization compared with conventional T8. The 28 W T5 luminaire consumed only 25 W circuit power and achieved a saving of 40% to 50% as compared with conventional electromagnetic ballast. By using T5 fluorescent light, it also minimizes fossil fuels use and thus directly reduces CO₂ emissions. Tables 3 and 4 show the total energy and cost saving of T5 fluorescent light replacement and T5 installation cost and return of investment respectively. Based on usage, the return of investment for high efficiency T5 fluorescent light replacement is between 20 to 25 months.

4. Conclusion

The FKAB building is considered as inadequately vented space. The concentrations of CO₂ at all sampling area evaluated exceed the recommended concentration (> 1000 ppm). From the PMV and PPD analysis, it predicted that the percentage of respondent dissatisfied with the surrounding. There are numerous methods that can be implemented in order to improve the energy efficiency, thermal comfort and the indoor air quality in the FKAB. Through energy efficiency

and conservation measures, it can dramatically reduce energy use and utility bills, thus helping to limit greenhouse gas emission and preserve the environment.

References

- [1] Malaysia Energy Centre, Energy Smart: Energy Efficient Building-A Strategic Resource, Quater 1 Issue 00017 KDN:PP11456/4/2005, 2005.
- [2] World Health Organization, Indoor air pollutants: Exposure and health effects, EURO Reports and Studies No. 78, WHO Regional Office for Europe, Copenhagen, 1986.
- [3] Department of Safety and Health, Code of Practice on Indoor Air Quality, JKKP GP(1)05/2005, Ministry of Human Resources Malaysia, 2005.
- [4] ISO, Moderate Thermal Environments—Determination of the PMV and PPD Indices and Specification of the Conditions for Thermal Comfort (ISO7730), Geneva International Organization for Standardization, 1994.
- [5] K.E. Charles, Fanger’s Thermal Comfort and Draught Models, Canada IRC Research Report RR-162, Institute for Research in Construction National Research Council of Canada, K1A0R6, Ottawa, Oct. 10, 2003.
- [6] S.I. Aizat, J. Juliana, O. Norhafizalina, Z.A. Azman, J. Kamaruzaman, Indoor air quality and sick building syndrome in Malaysian building, Global Journal of Health Science 2 (2009) 126-135.

Olkaria Geothermal Power Plants, Kenya: Preliminary Evaluation of Mercury Emission to the Atmosphere

G.N. Wetang'ula^{1,2,3}

1. Geothermal Development Company, Nakuru 17700-20100, Kenya

2. United Nations University-Geothermal Training Programme, Grensasvegur 9, 108 Reykjavik, Iceland

3. Faculty of Life and Environmental Science, University of Iceland, Sturlugata 7, 107 Reykjavik, Iceland

Received: April 20, 2011 / Accepted: June 27, 2011 / Published: November 20, 2011.

Abstract: At Olkaria (Kenya) geothermal energy has been used since 1981, to generate electricity and now there are currently 3 plants with a nominal capacity of 205 MW. Preliminary measurement and evaluation of possible mercury (Hg) emission from two plants has been investigated. Potential atmospheric Hg emission has been determined based on an existing model for estimating the transport of mercury along geothermal fluid flow streams as pertains to energy recovery and conversion from liquid dominated geothermal reservoirs. Hg concentrations, addition, retention and release rates were calculated at a number of locations in the geothermal power plants based on the plant operating parameters and steam flow process (turbine, condenser, non-condensable gas ejector, and cooling tower). Potential Hg emission rates through plume range from 0.455 g/h to 2.17 g/h, or 10-30 mg/h per MWe. The emission per hour per MWe is 130-300 times lower compared to Hg levels reported for 88 MWe five operating geothermal power plants around Mt. Amiata area in Italy. These emissions are coupled with a release of 1.07 kg/h per MW of hydrogen sulphide (H₂S). The potential Hg release rates to the environment will depend greatly on the concentration of H₂S in the system. Any higher H₂S contents may reduce solubility of Hg in the brine hence making it to be available in the steam. The volatile Hg may travel with the non-condensable gases as Hg vapour.

Key words: Olkaria, geothermal steam, mercury, cooling system, atmospheric emission, oxidation.

1. Introduction

Power production by geothermal steam started in Olkaria (Naivasha, Kenya) in 1981. The installed geothermal electrical capacity in Kenya is, at present, about 210 MW, with an annual energy production slightly over 1032.594 GWh [1]. All the power plants are located in the Olkaria geothermal field. The Olkaria geothermal field is located in a multi-centered volcanic complex comprising of at least 80 small centres covering an area of approximately 240 km². It is located in the eastern branch of the African rift system in Kenya about 120 km to the northwest of the capital city of Nairobi. The geothermal field currently supports

four geothermal power plants (Olkaria I plant-45 MWe, Olkaria II plant-105 MWe, Olkaria III plant-55 MWe and Oserian Plant-5 MWe) and proposed two units Olkaria I Unit 4 & 5-140 MWe and Olkaria IV-140 MWe (Fig. 1).

The Olkaria I geothermal power plant, which was the first geothermal power plant in Africa, has been operating in the Olkaria east geothermal field for 30 years. In the Olkaria northeast field, there is the Olkaria II power plant commissioned in 2003. The Olkaria I and II power plants are owned and operated by Kenya Electricity Generating Company (KenGen). In the Olkaria west and central fields, there are Olkaria III and Oserian binary power plants operated by OrPower4 Inc. and Oserian Development Company, which are Independent Power Producers, respectively.

The environmental impact of geothermal power

Corresponding author: G.N. Wetang'ula, chief scientist, Ph.D. candidate, main research fields: environmental fluids transport processes (ecotoxicology, air quality modeling, environmental impacts & risk assessment). E-mail: gwetangula@gmail.com or gwetangula@gdc.co.ke.

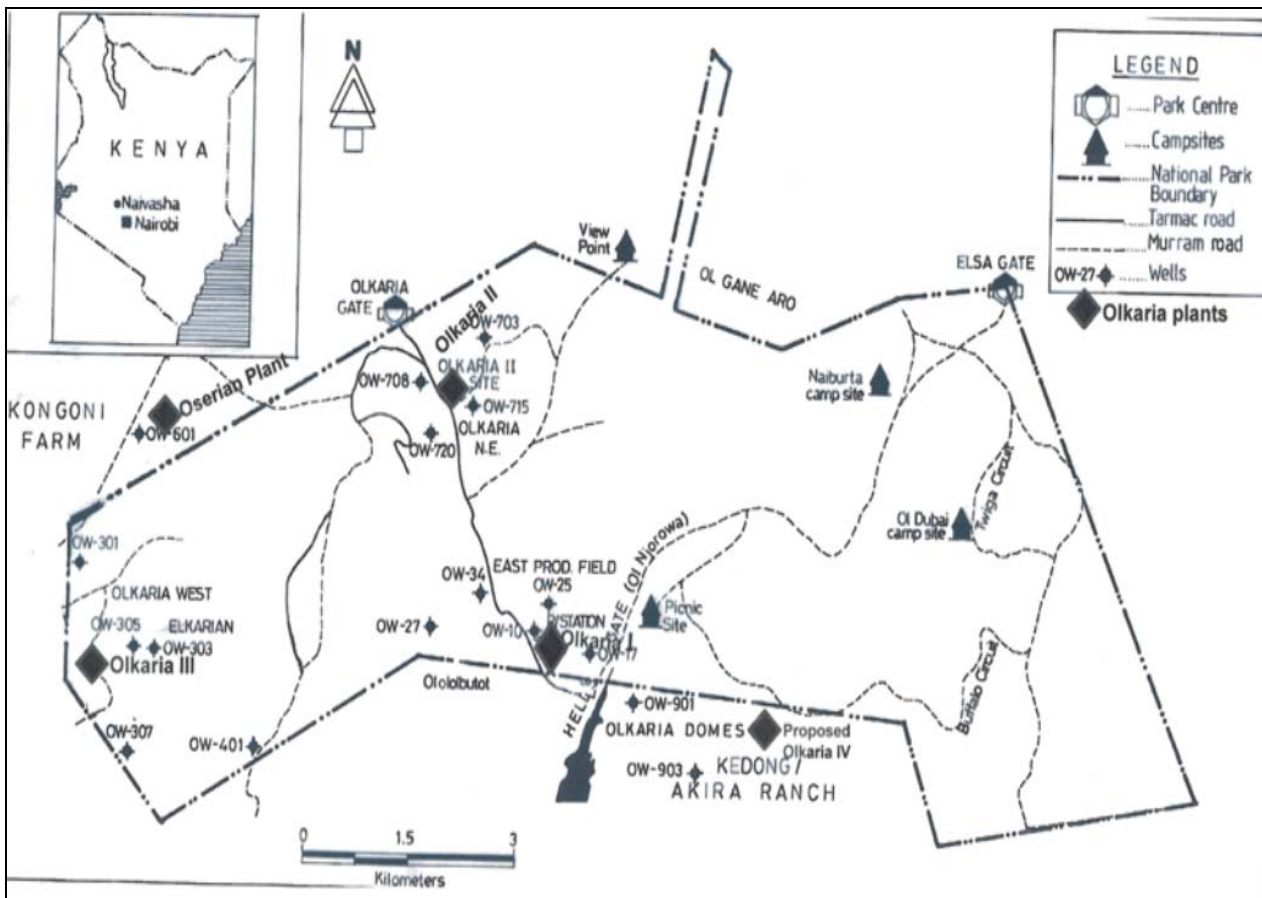


Fig. 1 Map of Hells Gate National Park showing the location of existing and proposed Olkaria geothermal power plants (modified from Ref. [2]).

stations is partly related to the atmospheric emission of a significant amount of non-condensable greenhouse gases (NCGs) as well as elements and compounds of toxicological significance which may be dangerous to environment [3]. Geothermal power plants are thus receiving increasing attention as regards the mobilisation of mercury to the environment. Mercury is a trace element that may be present in the geothermal fluid, and is transferred mainly into the vapour phase. Due to its high volatility, it may be discharged to the atmosphere with the non-condensable gases. Since the non-condensable gases present in the geothermal fluid are generally characterised by a reducing behaviour, mercury is prevalently emitted as elemental mercury (Hg) [4, 5]. It has also been observed that in reservoirs containing hydrogen sulphide and hydrogen, the important

chemical species of mercury in the geothermal fluid will be elemental mercury (Hg) and gaseous mercuric sulphide (HgS). Mercuric sulphide along with elemental gaseous mercury make up a substantial amount of the mercury transported from the separator through the plant to the cooling tower [6]. This will be released to the atmosphere as mercury vapour.

Mercury is discharged as elemental mercury (Hg) gaseous species and reaches the atmosphere with the non-condensable gas fraction. In the Olkaria geothermal field, the Non Condensable Gas (NCG) composition in geothermal steam in the Olkaria I power station steam is 0.025% w/w and the percentage of CO₂ in the NCGs is 90.48% w/w. These average values are based on the 2000-2004 biannual reservoir monitoring results for the Olkaria east production field when most of the geothermal wells were monitored [7, 8]. The

specific steam consumption of the Olkaria I power plant is 2.55 kg/s/MWe (or 9180 kg/hr/MWe) according to Board of Geothermal Consultants Report to KenGen, 23rd April 2004. In the Olkaria II power plant, the NCG concentration in the geothermal steam is 0.3-0.75% w/w and the average percentage of CO₂ in the NCG is 88.45% w/w. These values are obtained from the Turbine Performance Test Results for Unit 1 at 90% load condition. The specific steam consumption of Olkaria II is 2.087 kg/s per MWe (or 7513.2 kg/hr per MWe) according to the Design Report for the Olkaria II plant Unit 3 Extension [9].

The aim of the present study is to estimate atmospheric mercury emission from Olkaria I and II power plants. This has been achieved through steam quality analysis of condensed steam Hg concentration levels to be used in calculating the average levels of mercury released to the atmosphere through the cooling and gas ejection or extraction system. Due to the relatively well known plant operation parameters such as steam consumption, amount of steam condensed after power generation, cooling system water flow rates, cooling tower water loss through carryover and drift, and emission rates of gaseous contaminants (H₂S, CO₂ etc.), mercury emission into the atmosphere can be calculated to quantify atmospheric mercury input.

1.1 Emission of Mercury from Geothermal Sources

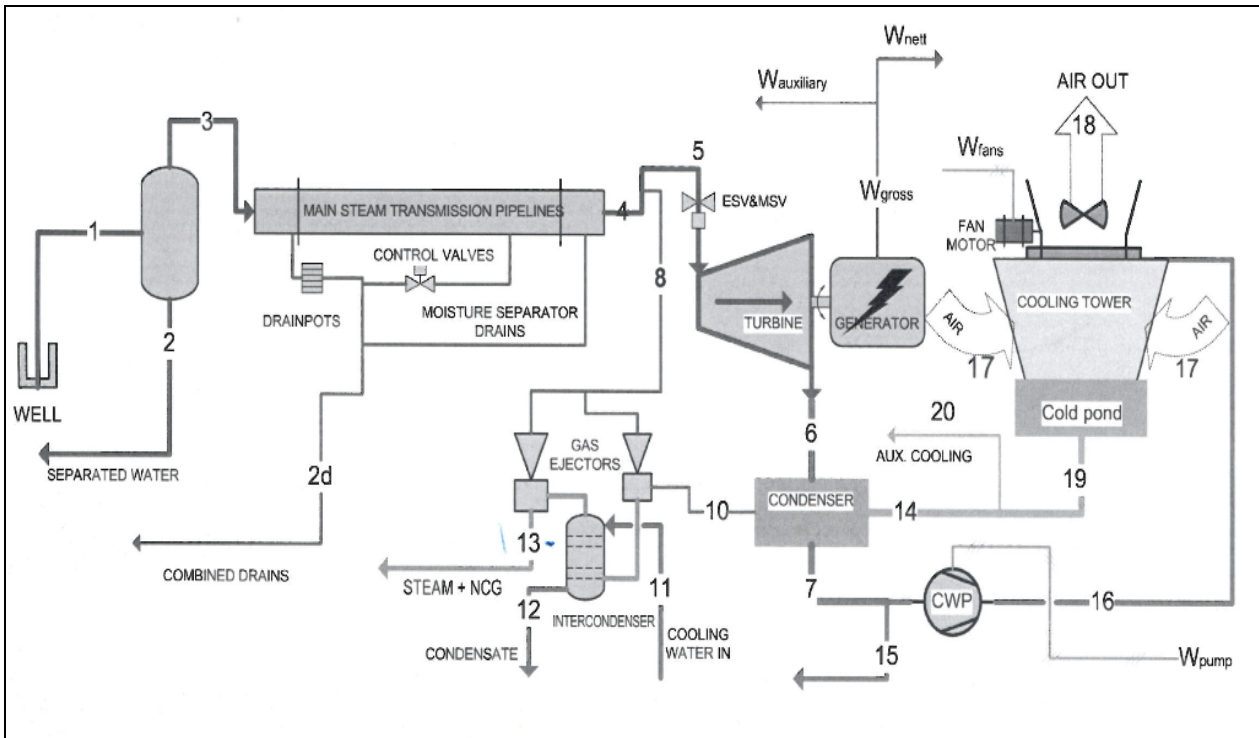
Various values for mercury concentrations in spent geothermal fluids in Olkaria (Kenya) have been reported in previous studies. The mercury concentrations have ranged from 0.0301 to 9.31 µg/L in geothermal fluids of selected discharging and shut-in wells in the Olkaria east field [10-13]. Were et al. [11] also reported a 0.97 µg/L mercury concentration for Lake Naivasha water which was higher than mercury concentrations in fluids from some from Olkaria east field geothermal wells.

In Italy, the increasing production of electricity from geothermal sources around Mt. Amiata (100 km SE from Larderello, Italy) caused growing concern among

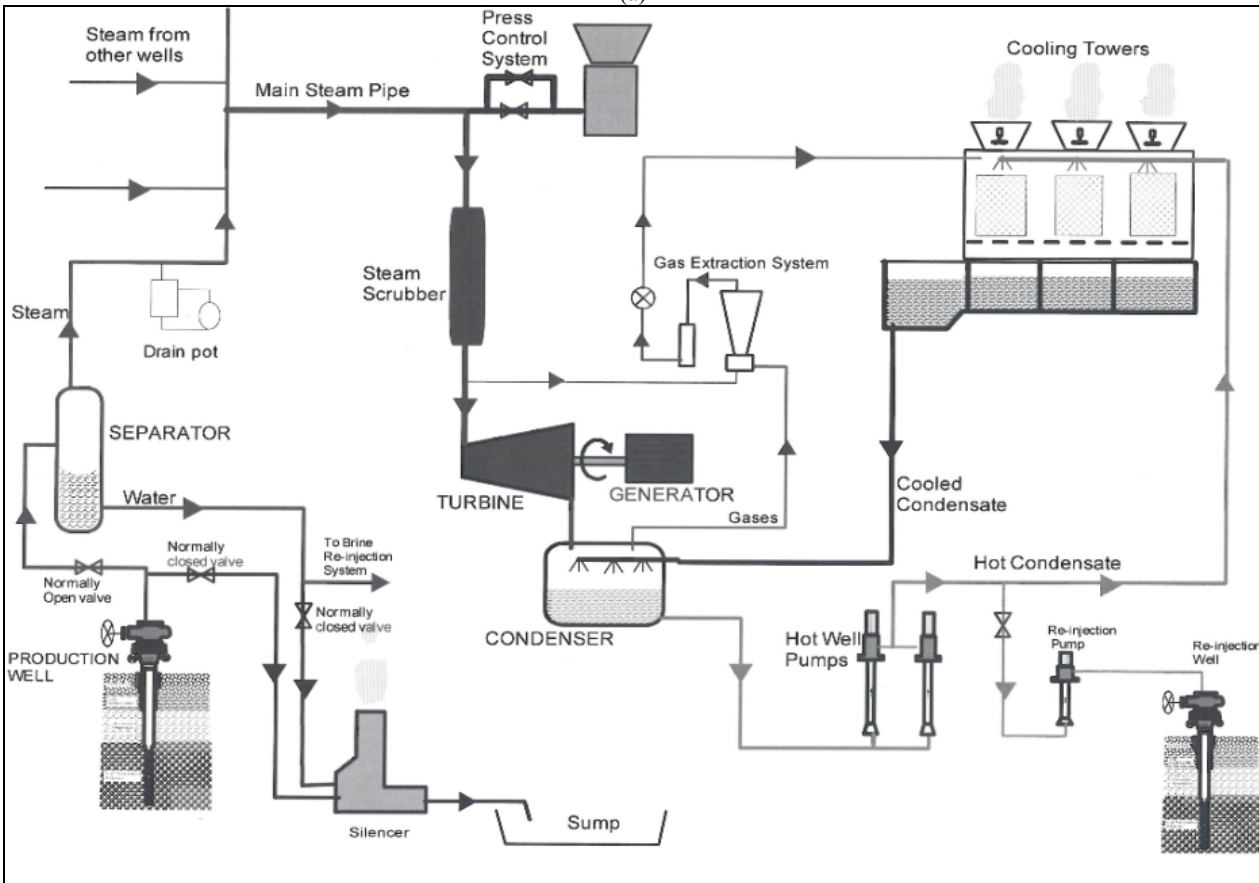
the inhabitants leading to a lot of investigations into the biological hazards of geothermal emissions [14-16]. Studies focused on Piancastagnaio close to Mt. Amiata where geothermal energy has been used since 1969 to generate electricity in five geothermal plants with a nominal capacity of 88 MW (4×20 and 1×8 MW operating plants). In this geothermal area, Bacci et al. [16] estimated mercury emission rates ranging from 300 to 400 g/h, or 3-4 g/h per MW installed electrical capacity. These emissions were coupled with a release of 7-8 kg/h/MW of hydrogen sulphide (H₂S) due to the high gas concentration (off-gas) in these geothermal fluids. Mercury was discharged as the Hg gaseous species and reached the atmosphere with the non-condensable gas fraction. In this fraction CO₂ was the major component (94-98%), H₂S was around 1% and mercury concentration was as high as 1-10 mg/m³. Direct measurements of mercury and hydrogen sulphide vapours in atmospheric air reached by power plant emissions showed a ratio of about 1-2000 corresponding to typical concentrations of mercury and hydrogen sulphide of the order of 10-20 ng/m³ and 20-40 µg/m³, respectively [16]. In the Bagnore geothermal area around Mt. Amiata, evaluation of the environmental distribution of mercury and other trace elements revealed that after a new geothermal power plant went into operation, the concentration of Hg in lichen showed a 50% increase from 0.22 to 0.32 µg/g dry weight. This value was however in line with those found in lichens from non-producing areas with hot springs and fumaroles [17].

1.2 Plant and Steam Transmission Process Diagram Considered in the Study

Figs. 2a and 2b show steam process flow diagrams for the Olkaria I and II power plants respectively. The steam flow processes have been simplified to a geothermal well, steam separation, steam transmission, steam expansion-energy conversion, steam condensing and cooling water systems. For this paper the Olkaria I plant flow diagram (Fig. 2a) has been used to illustrate the steam flow process in the system which is slightly



(a)



(b)

Fig. 2 (a) Steam flow diagram for the Olkaria I plant [8]; (b) Steam flow diagram for the Olkaria II plant.

different from that of the Olkaria II plant in terms of non condensable gas ejection. The steam from the connected (3) wells is fed into steam gathering pipes which feed into three steam transmission pipes. Auxiliary steam (8) is tapped from the main steam pipe after the orifice flow meters but before the steam enters the turbines. The steam enters the turbine (5) with properties characterised by inlet conditions. The design inlet pressure is 5.0 bar absolute (bar-a) dry steam and the exhaust pressure is 0.127 bar-a.

Steam leaving the turbine (6) is exhausted into the condenser where it is mixed with a spray of cold water (14) from the cooling towers. The steam condenses on the water droplets and the condensate at 50°C drains through a barometric leg (7) into a seal pit tank located 9 m below the bottom of the condenser to overcome atmospheric pressure. Non-condensable gases (NCG) are sucked from the condenser (10) by gas ejectors. In the Olkaria II power plant, disposal is achieved by pumping the gases to the cooling tower and releasing them at high upward velocity below the cooling tower fans where the gases mix with the rising hot plume.

Motive steam is tapped from the main steam line (8) and delivered to the gas extraction system (GES). The high-velocity steam creates suction by passing through a convergent-divergent nozzle. The low-pressure point of the first stage ejector nozzle is connected to the gas cooler section of the condenser. The non-condensable gases (NCG) with some water vapour flow into the ejector nozzle (10) as a result of the low-pressure suction. The NCG together with the motive steam are condensed in the intercondenser by cold water (11) from the cooling tower. The NCG is sucked again from the inter-condenser by the second stage ejector nozzle and are discharged into the atmosphere (13) for dispersal. The condensate from the inter-condenser drains into the seal pit (12).

This cooling system covers the seal pit and the cooling towers. The condensate leaves the condenser and enters the seal pit (7). Excess condensate

overflows at the seal pit (15). The circulating condensate (16) is pumped by a circulating water pump (CWP) to the top of the cooling towers. Water reaches the top of the cooling towers and is poured onto hot water basins where it falls down through spray nozzles. The hot water falls through a splash bar grid and the water droplets are split into very fine droplets by the grid. As the water droplets fall down and break up into fine droplets, a stream of air (17) flows across the water droplets thus creating cooling by evaporation and convection-conduction mechanisms. The stream of air is created by suction of air fans (W_{fans}) located at the top of the cooling towers. The water droplets eventually fall into the cold pond from where it is siphoned into the condenser inlet pipeline at 20 °C (19). Some water goes to the auxiliary cooling (20) and the rest into the condenser (14). Warm moist air leaves the cooling tower (18) driven out by air fans (W_{fans}). Some condensate is lost to the air. Carryover and drift losses are 5% of the condensate entering the cooling towers.

The geothermal power plant operating parameters that have been incorporated into the calculation of Hg from the plants are as indicated in Table 1.

2. Methods and Data

2.1 Sampling Locations

Eighteen sampling locations were established within the Olkaria east and northeast geothermal fields to assess the Hg concentration levels in condensed steam. The locations were categorized as: (1) geothermal wells—OW-2, OW-5, OW-10, OW-15, OW-19, OW-20, OW-22, OW-23, OW-26, OW-701, OW-709, OW-716, and OW-725; (2) geothermal plants: Olkaria I power plant-Condensers for Units 1, 2 and 3, and Olkaria II power plant-Condensers for Units 1 and 2. Two geothermal power plant namely 55 MW Olkaria III plant and 2 MW Oserian Plant were not accessed for mercury sampling as they are privately owned hence restrictions unlike Olkaria I & II Plants publicly

Table 1 Plant operating parameters of Olkaria I and II geothermal plants [8] and current Olkaria II plant data.

Parameter and units	Olkaria I plant (45 MWe)	Olkaria II plant (105 MWe)
NCGs in steam (% w/w)	0.25	0.3-0.75
CO ₂ in NCGs (% w/w)	90.48	90-95
Specific steam consumption (kg/s/MWe)	2.55	2.087
Specific steam consumption (kg/hr/MWe)	9180	7513.2
Yearly MWh generated	394,200	613,200
Yearly steam consumption (tonnes)	3,618,756	4,607,094.24
Yearly MWh generated (98% availability)	386,316	601,961.039
Yearly steam consumption (tonnes) 98% availability	3,546,380.88	4,514,952.36
Turbine exhaust temperature (°C)	56	40.3
Condenser inlet water temperature (°C)	24	21.3
Condenser outlet water temperature (°C)	51	37.3
Gas ejector steam pressure (bar-a)	5.26	4.8
Gas ejector exit temperature (°C)	64.3	35
Mass flow rate of steam into turbine (kg/h)	413,670	525,924
Mass flow rate of motive steam into NCGs extraction system (kg/h)		6,140
Mass flow rate of motive steam + NCGs from extraction system to cooling tower (kg/h)		1,966
Mass flow rate of steam into gas ejector system1 (kg/h)	4,140	
Mass flow rate of steam into gas ejector system2 (kg/h)	4,740	
Flow rate of water in GES condenser (m ³ /h)	42	
Flow rate of water into condenser (m ³ /h)	6900	7,900
Flow rate of water into cooling tower (m ³ /h)	7,860	8,644
Flow rate of water out of cooling tower (m ³ /h)	7,026	8,445

owned by the Government of Kenya.

2.2 Steam Sampling and Analysis

The procedures for sampling geothermal steam for Hg analysis were adopted from those used by Mroczek and Graham [18]. Good results require competent sampling techniques. It has been recognized that much of the error present in mercury analysis is due to contamination and loss of mercury during sample collection and analysis [18]. All equipment after the stainless steel Webre separator or main pipeline fitting were cleaned. Glassware and inert Teflon fittings were cleaned with chromic acid. The glassware was rinsed/soaked in cold chromic acid for overnight.

Steam samples from geothermal wells were collected (via a T piece venting to atmosphere to reduce pressure) and condensed into 350 mL Erlenmeyer/conical flasks containing 10 mL of concentrated sulphuric acid. At the laboratory 10 mL of 4% potassium permanganate is subsequently added to

the flask and the samples transferred into PET plastic bottles. The samples were then shipped to the contracting laboratory (ALS Scandinavia Ltd Lulea, Sweden) where they were analysed for total mercury by Atomic Fluorescence Spectrometry (AFS) carried out according to Swedish Standard-European Norm (SS-EN) 17852:2008. At the power plants, steam samples were collected at the condenser units. The flask train was placed in a shallow tray of ice water mixture and steam collected at a slow rate, typically 1-2 mL of condensate per minute to a total volume of 350 mL in the flask.

3. Calculations

3.1 Background

Mercury distribution in a geothermal power plant may be derived based on the methodology described in Ref. [6] for determining mercury distribution in a geothermal system (from the well to the power plant

and the atmosphere). The key locations and plant operation characteristics which have been utilized during this study for the Olkaria geothermal plants are shown in Fig. 2 and Table 1 respectively.

When mercury is added to the cooling system from the turbine, the amount of mercury remaining in the cooling system, B , after t hours is given by:

$$B = \frac{a}{b^*} (e^{b^*t} - 1) \quad (1)$$

where, a is the rate at which mercury is being added to the cooling system from the turbine exhaust in $\mu\text{g/hr}$. The value of b^{*j} is the combined loss rates of mercury releases through vapour and spray emissions from the cooling tower (drift) and blowdown, in μg per hour.

The integrated amount of mercury lost from the cooling system in μg , R is given by:

$$R = at \left[\frac{a}{b^*} (e^{b^*t} - 1) \right] \quad (2)$$

The integrated amounts of mercury lost from the cooling system by plume, in μg is given by $R \times F$, where, F is the fraction of mercury either in the spray or the vapour in the plume to the total (plume plus blowdown).

The steady state amount of mercury (S), in μg , in the cooling system is given by:

$$S = \frac{a}{b^*} \quad (3)$$

3.2 Calculation Guidelines and Assumptions during This Study

A minimal number of assumptions were made in order to use the analytical results in Table 2 to determine the mercury transport rates within the geothermal power plant. They include:

- Thermodynamic equilibrium is assumed in all locations in the system;
- The potential for mercury deposition along the system have not been evaluated. However, in the actual mercury transport calculations, any mercury precipitates will be assumed to be carried along the

steam to the next location in the system;

- The annual plant availability was assumed to be approximately 98%.

The mercury emission from the Olkaria geothermal power plants calculation guide was as follows:

The total annual megawatthours (MWh) of electricity generated from the Olkaria geothermal power plants was used to calculate the annual steam consumption based on the specific steam consumption for each plant as per the plant operation parameters in Table 1.

The steam was analysed for mercury to determine the mercury concentration of the steam being exhausted from the turbine into the condenser (condensate). When steam from the turbine is exhausted into the condenser, it condenses which leads to an increase in the flow rate of water flowing from the condenser to the cooling tower compared to water entering the condenser from the cooling tower. The specific steam consumption ($\text{kg}\cdot\text{hr}^{-1}$ plant capacity in $\text{M}\cdot\text{We}^{-1}$) is thus equivalent to the difference in flow rates (m^3/h) of water entering the condenser from the cooling tower and water flowing from the condenser (condensed steam) to the cooling tower after condensation. Mercury emitted to the atmosphere due to the full oxidation process in the cooling tower will be derived from this volume difference.

The water loss in the cooling system can be calculated based on the amount of water that enters and leaves the cooling tower. This water loss accounts for cooling tower carryover/drift and blowdown. ReInjection of cooling tower blowdown (excess water) is very minimal for Olkaria I plant (1981) as compared to Olkaria II Plant (2003) due to the time difference in technological advancement when the two plants were commissioned. The water loss to the atmosphere by cooling tower carryover and drift has been established to be 5% [19]. Mercury emitted to the atmosphere through carryover and drift loss if no oxidation reactions are occurring in the cooling towers is derived from this figure. Blowdown water flow rate (m^3/h) is

1. b^* is a negative number.

Table 2 Flow characteristics [7, 8] and mercury concentrations in steam (current study) from selected wells in the Olkaria east and northeast fields and Olkaria power plants.

Well No./Plant	Stable bottom temp (°C)	Total (ton/hr)	mass Enthalpy (kJ/kg)	MWe	Steam flow (ton/hr)	Steam Hg conc. (µg/kg)
Selected Olkaria east field wells						
OW-2	282		2400	2.9	16.3	0.0621
OW-5	256		2627	5.4	51	0.0937
OW-10	274	13	2000	2.5	15.5	0.342
OW-15	230	40.6	1950	2.2	24.1	0.544
OW-19	275	69.7	2200	1.6	18.6	0.496
OW-20	243	34	2400	2.8	17	0.0576
OW-22	269	24	2400	2.2	14	0.0931
OW-23	200	23	1900	1.6	11.8	0.667
OW-26	212	25	1900	3.3	34.6	0.388
Selected Olkaria northeast field wells						
OW-701	309		1085	4		0.499
OW-709	296	71	1988	9		1.31
OW-716	318	72	2524	5		6.64
OW-725	313	50	2180	3		1.45
Olkaria power plants						
Olkaria I Unit 1				15	137.7	0.111
Olkaria I Unit 2				15	137.7	0.0902
Olkaria I Unit 3				15	137.7	0.283
Olkaria II Unit 1				35	262.96	0.681
Olkaria II Unit 2				35	262.96	2.32

calculated less 5% of the water lost to the atmosphere by cooling tower carryover and drift.

Mercury emission to the atmosphere has also been calculated for the motive steam that is tapped from the main steam line and delivered to the gas ejectors for Olkaria I plant and gas extraction system (GES) for the Olkaria II plant. The motive steam is important in removing NCGs. The steam flow rate in the gas ejectors and the GES are as indicated in the plant parameters (Table 1) and is less 0.25% and 0.75% NCGs for the Olkaria I and II plants respectively. The annual mercury emission from the Olkaria I and II power plants was calculated as discussed in subsequent sections based on the mercury concentration in the hourly specific steam consumption for 8760 hours of generation annually.

3.3 Calculation of Mercury Addition, Release and Retention

Concentration of mercury in the Olkaria I and II

plant steam were determined to be 0.4842 µg/kg and 3.0 µg/kg respectively.

The specific steam consumption per hour per MWe and mass flow rate of steam (kg/h) in the turbine for the 45 MWe Olkaria I plant and the 70 MWe Olkaria II plant is 413,100 kg/h and 507,500 kg/h respectively. This steam condenses to give a net of 960 m³/h and 744 m³/h of condensate for Olkaria I and II plants respectively. From the mercury concentration in the condensate analyzed, mercury in specific steam consumption per hour per plant capacity (MWe) is given by the amount of condensate (m³/h) /hour/plant capacity (MWe) × mercury content per kg of steam. This gives 0.46 g and 2.23 g of mercury being added to the cooling system per hour in the Olkaria I and II plants respectively. The annual mercury output from turbine steam added to the cooling system (condenser) is calculated based on 8760 hours annually and the hourly mercury input from the turbine steam into the condenser.

The annual mercury emissions from the Olkaria I plant through gas ejectors and Olkaria II plant gas extraction system (GES) to the atmosphere less 0.25% (Olkaria I) and 0.75% (Olkaria II) NCGs content has also been determined. Annual mercury output in cooling water blow-down (excess cooling water) was also determined. Approximately 6.24 m³/h and 115.124 m³/h of Olkaria I and II plant cooling tower blow-down is reinjected respectively.

Atmospheric mercury emission through cooling tower carryover and drift loss has also been determined. The condensate loss through cooling tower carryover and drift has been established to be 5% of the amount of condensate/water entering the cooling tower from the condenser [6, 8, 19].

4. Results and Discussion

4.1 Mercury Concentrations in Steam of Olkaria Plants and Wells

Mercury was analysed in the steam from selected wells in the Olkaria east and northeast fields and the condensers (i.e. steam leaving the turbine) of the Olkaria I and II power plants. The mercury concentration in steam from selected wells and the Olkaria power plants is shown in Table 2. In the Olkaria I power plant, the mercury concentration range in steam in three condensers was 0.09 to 0.283 µg/kg

while in the Olkaria II plant it was 0.681 and 2.32 µg/kg for Units 1 and 2 respectively. However, the mercury concentration in condensed steam from selected wells sampled in the Olkaria east and northeast fields ranged from 0.0621 µg/kg to 6.64 µg/kg.

4.2 Atmospheric Mercury Release without Oxidation

The mercury levels and releases from the Olkaria I and II geothermal power plants are detailed in Tables 3 and 4 at no and full oxidation. Calculation steps have also been summarized in the previous sections.

4.3 Atmospheric Mercury Release by Oxidation

The hot condensate is pumped to the cooling tower where it is cooled and re-circulated back to the condenser to condense the steam exhausting from the turbine. Non-condensable gases (hydrogen sulphide, H₂S; carbon dioxide, CO₂) carried over to the condenser by steam remain in a gaseous state in the condenser. These gases are extracted to maintain the condenser vacuum and disposed of to the atmosphere through gas ejectors in the Olkaria I plant and a gas extraction system via the cooling tower in the Olkaria II plant. It has been observed that the condensate is very acidic (pH about 3) due to oxidation taking place in the cooling towers. The geothermal blowdown (excess condensate) is quite acidic with a pH of 3 due

Table 3 Mercury additions, releases and retentions with no oxidation (grams).

No oxidation	45 MWe Olkaria I plant	70 MWe Olkaria II plant
Annual mercury added to the cooling system	3,990.49	19,161.27
Annual mercury loss through cooling tower blowdown	3,360.6	5,229.72
Annual mercury retained in the cooling system	456.59	13,625.04
Annual mercury emitted through gas ejectors	36.82	-
Annual mercury emitted through gas extraction system	-	50.25
Annual mercury emitted through cooling tower carry over and drift	173.3	256.26
Annual mercury emitted through cooling tower and gas extraction system/ejectors	210.16	306.51
Hourly mercury in cooling tower blowdown	0.384	0.597
Hourly mercury release (blowdown+emissions)	0.408	0.631
Hourly mercury emission	0.024	0.034
Hourly mercury release per MWe	9.0×10^{-3}	9.0×10^{-3}
Hourly mercury emission per MWe	5.3×10^{-4}	4.9×10^{-4}

Table 4 Mercury addition, release and retention at full oxidation (grams).

Full oxidation	45 MWe Olkaria I plant	70 MWe Olkaria II plant
Annual mercury added to the cooling system	3,990.49	19,161.27
Annual mercury emitted through gas ejectors	36.82	
Annual mercury emitted through gas extraction system		51.28
Annual mercury emitted through cooling tower and gas extraction system/ejectors	4,027.31	19,211.53
Hourly mercury emitted	0.455	2.17
Hourly mercury emitted per MWe	0.01	0.03
Annual mercury in the cooling tower sludge	40.27	192.12

to oxidation of the dissolved H₂S and CO₂ in the cooling tower causing the formation of sulphurous and carbonic acids respectively. Each of the Olkaria power plants possesses a chemical dosing plant to control the acidity. One of the tasks of this plant is to dose the cooling water system (including blow down) with alkali to raise the pH to between 4.5 and 5.5 upstream of the cooling tower. Approximately 300 kg of soda ash/sodium carbonate (Na₂CO₃) is used daily to dose the condensate produced to attain a near neutral to alkaline pH.

Approximately 99% of mercury will be released as a plume in the form of elemental mercury, while 1% will be retained in the cooling tower sludge, assuming that oxidation reactions are taking place and due to the low pH of the cooling system water, according to Ref. [6] model experiment which also holds true for this study. Annual mercury additions, retention, releases into the plume due to oxidation in the cooling system and emission from gas ejectors and GES are as indicated in Table 4. This has been determined to be 4,027.31 g and 19,211.53 g of mercury for Olkaria I and II plant respectively. This mercury emission translates to 0.455 g/h and 2.17 g/h or 0.01 g/h/MWe and 0.03 g/h/MWe of mercury for Olkaria I and II plant respectively. The difference in mercury emission between the two plants could be due to difference in nominal installed capacity and steam consumption. Olkaria I and Olkaria II has installed capacity of 45 MW and 105 MW respectively. Build up and release of mercury at the cooling tower is a function of time and possible conversion of mercuric sulphide (HgS) into mercury (Hg) and sulphur by air

oxidation process. The annual mercury retained in the cooling tower sludge is 40.27 g and 192.12 g in the Olkaria I and II plants respectively. During sampling done in September 2004 when the performance test of Olkaria II power plant's Unit I was being evaluated by the Consultants, Wetang'ula et al. [20] reported mercury concentrations of 0.00045 mg/L and 0.4-0.71 mg/kg in the Olkaria II plant cooling tower water and sludge respectively.

4.4 Comparison of Atmospheric Mercury Release at No and Full Oxidation

Mercury emissions from the Olkaria I and II power plants through a plume without oxidation are 0.024 g/h and 0.034 g/h respectively. Taking the mercury emission rates from these plants based on no oxidation is an underestimate of mercury releases into the atmosphere because of oxidation taking place in the cooling tower that is confirmed by the low pH (pH 3) of the cooling tower water, blow-down and condensate. With oxidation in the cooling tower, mercury atmospheric release has been determined to be 0.455 g/h and 2.17 g/h from the Olkaria I and II plants respectively.

These atmospheric mercury emissions are low when compared to mercury emission rates of 300-400 g/h or 3-4 g/h/MWe from five geothermal power plants with a nominal installed capacity of 88 MWe around Mt. Amiata in Italy [16]. Annual mercury release by the plume from the Olkaria I power plant with no and full oxidation were 210.16 g and 3,987.04 g respectively. The mercury releases with and without

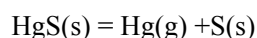
oxidation differ by a factor of 18.97. However, in Ref. [6], it was observed that it differs by a factor of 18 under the steady-state conditions, which is in the same range.

The mercury levels and releases from the Olkaria geothermal power plants as indicated in Tables 3 and 4 have been determined based on the 148.6-292.8 ppm H₂S reservoir concentrations from selected Olkaria East field wells [21, 22]. Compared to arsenic and boron concentrations, knowledge of the magnitude of H₂S in the geothermal fluid is important in determining the flow and distribution of the mercury in the geothermal system. H₂S concentration is not a crucial factor for near neutral or acidic geothermal fluids as its level is usually higher than those of other trace elements [6]. For Olkaria geothermal fluids in which the fluid pH has been determined to be in the range of 8.57-9.93 [21, 22], H₂S may be an important factor in mercury distribution. With a measured H₂S concentration range of 148.6 to 292.8 ppm, the precipitation of mercuric sulphide (HgS) and other metallic sulphides that would have been occasioned by a lower H₂S concentration (< 30 ppm) will not take place.

It has been assumed that there is insufficient hydrogen (0.3-9.8 ppm in Ref. [21]) after the NCG ejection to maintain any appreciable levels of elemental mercury (Hg), and thus mercury from the turbine is precipitated in the condenser as mercuric sulphide (HgS) dust which mixes with cooling water [6]. Some mercury is released by blow-down and some by mechanical entrapment in the cooling tower spray. Alternatively some is collected as sludge at the bottom of the cooling tower. The mercury released by the cooling tower plume would be expected to be solid mercuric sulphide (non volatile) particles suspended into water vapour. However, plant experience according to Ref. [5] suggests that a considerable percentage, if not all, is present as mercury vapour.

The transformation of mercuric sulphide to mercury

vapour can be explained only by other chemical reactions taking place in the cooling tower. For example, introduction of oxygen into the cooling system may make a substantial difference due to reactions which will both oxidize the sulphur in mercuric sulphide as well as reduce the mercury as indicated below:



and



An alternative explanation for the observation of mercury vapour releases from the cooling tower might be that there is much more hydrogen present than expected from the previous assumptions. While oxygen can oxidize the sulphur in the mercuric sulphide to release elemental mercury, hydrogen can reduce the mercury in HgS to give elemental mercury too. To support this last idea, hydrogen analysis of fluids from the cooling system would be useful as such analysis was not carried out during this study. However, the level of hydrogen and oxygen in the geothermal steam has been determined to be in the range 0.001-0.089 and 0.001-0.013 mmoles/mole of steam. Hydrogen sulphide concentration range of 0.019-0.168 mmoles/mole of steam have also been measured. With measured hydrogen sulphide as opposed to sulphur dioxide at the cooling towers, it can be postulated that reactions leading Eq. (5) is more preferential than Eq. (4).



5. Conclusions

In this study it has been shown that mercury releases from the Olkaria geothermal power plants through plumes are in the range 0.455 g/h to 2.17 g/h or 10 mg/h/MWe to 30 mg/h/MWe assuming complete oxidation to take place in the cooling system. This translates into an annual amount of mercury atmospheric emissions of 4,027.31 g and 19,211.53 g from the Olkaria I and II geothermal plants respectively. With pronounced oxidation in the cooling tower, more

mercury will be released through the cooling tower than if there was no oxidation. The mercury release was only through cooling tower carryover/drift, gas ejectors and the gas extraction system. It is worth noting that cooling tower mercury emission rates will vary depending on the H₂S and hydrogen concentrations, and whether air in the cooling system reacts with mercuric sulphide (HgS) to give elemental mercury and oxidize sulphur compounds, too. If mercuric sulphide is not oxidized, much of the mercury will be retained in cooling tower sludge and blow-down water. Proper disposal of blow-down water through reinjection therefore becomes critical because of the mercury that could contaminate the environment with surface disposal. The same applies to disposal of cooling tower sludge, which should be dried, encased in concrete and buried because improper disposal may lead to soil contamination. Due to oxidation in the cooling system mercury release will mainly be elemental mercury released as mercury vapour. With mercury emitted in this form, ambient monitoring of mercury vapour and mercury in precipitation around these plants has been recommended.

Acknowledgments

This study was funded by United Nations University-Geothermal Training Programme. Sincere thanks go to geochemistry laboratory technicians, Kenya Electricity Generating Company, Olkaria Geothermal Power Project for helping in the geochemical sampling of the wells and power plants. My sincere thanks to all other persons who provided essential plant operation data.

References

- [1] CDM Executive Board, Clean Development Mechanism, Project Design Document, Olkaria II Geothermal Expansion Project, Version 06, 2010, available online at: <http://www.cdm.unfccc.int/>.
- [2] G.N. Wetang'ula, Wildlife population dynamics in Hell's Gate National Park, Olkaria Kenya, in: Proceedings of 25th PNOC-EDC Geothermal Conference, Manila, Philippines, 2004, pp. 191-199.
- [3] H. Armannsson, H. Kristmannsdottir, Geothermal environmental impact, *Geothermics* 21 (1992) 869-880.
- [4] S. Vitolo, M. Seggiani, Mercury removal from geothermal exhaust gas by sulfur impregnated and virgin activated carbons, *Geothermics* 31 (2002) 431-442.
- [5] D.E. Robertson, E.A. Crecelius, J.S. Fruchter, J.D. Ludwick, Mercury emissions from geothermal power plants, *Science* 196 (1977) 1094-1097.
- [6] J.W. Cobble, A theory on mercury in geothermal fluids, Report prepared for Electric Power Research Institute (EPRI) AP-5111 Project 1525-6, Final Report, 1987, p. 72.
- [7] M. Kariuki, J. Wambugu, Status report on steam production, Olkaria east field 2002/2003, KenGen Co. Ltd., Internal Report, 2002.
- [8] C.B. Kwambai, Exergy analysis of Olkaria I power plant, Kenya, Report 5 in Geothermal Training in Iceland, UNU-GTP, 2005, p. 37.
- [9] CDM Executive Board, Clean Development Mechanism, Project Design Document, Olkaria II Geothermal Expansion Project, Version 03, 2006, available online at: <http://www.cdm.unfccc.int/> (accessed on July 28, 2010).
- [10] G. Simiyu, M. Tole, Concentrations of trace elements in waters, soils and plants of Olkaria geothermal field, Kenya, in: Proceedings of World Geothermal Congress, Kyushu-Tohoku, Japan, 2000, pp. 681-688.
- [11] J.O. Were, The speciation of trace elements in spent geothermal fluids and implications for environmental health around Olkaria, Kenya, MSc. Thesis, Department of Earth Sciences, Faculty of Science, University of Iceland, UNU-GTP, 2007, p. 73.
- [12] G.N. Wetang'ula, Assessment of geothermal wastewater disposal effects, case studies: Nesjavellir (Iceland) and Olkaria (Kenya) fields, M.Sc. Thesis, Department of Biology, University of Iceland, 2004, p. 175.
- [13] G.N. Wetang'ula, S.S. Snorrason, Evaluation of trace element levels and their ecotoxicological relevance in geothermal wastewater of Olkaria East Field, Kenya, in: Proceedings of World Geothermal Congress, Antalya, 2005, p. 15.
- [14] S. Loppi, Monitoring of arsenic, boron and mercury by lichen and soil analysis in the Mt Amiata geothermal area (Central Italy), *Geothermal Resources Council Trans.* 21 (1997) 137-140.
- [15] S. Loppi, J. Nascimbene, Lichen bioindication of air quality in the Mt Amiata geothermal area (Central Italy), *Geothermics* 27 (1997) 295-304.
- [16] E. Bacci, C. Gaggi, E. Lanzillotti, S. Ferrozzi, L. Valli, Geothermal power plants at Mt. Amiata (Tuscany-Italy): Mercury and hydrogen sulphide deposition revealed by vegetation, *Chemosphere* 40 (2000) 907-911.
- [17] S. Loppi, Environmental distribution of mercury and other trace elements in the geothermal area of Bagnore (Mt. Amiata, Italy), *Chemosphere* 45 (2001) 991-995.

- [18] E. Mroczek, D. Graham, Sampling and analysis for mercury in steam collected from geothermal wells and fumaroles, in: Proceedings of World Geothermal Congress, Antalya, Turkey, 2005, p. 7.
- [19] C.B. Kwambai, Exergy analysis of Olkaria I power plant, Kenya, in: Proceedings of World Geothermal Congress, Bali, Indonesia, 2010, p. 12.
- [20] G.N. Wetang'ula, Olkaria II Power Station wastewater and sludge analysis, KenGen Internal Brief Report, 2004, p. 2.
- [21] C.W. Karingithi, Geochemical characteristics of the greater Olkaria geothermal field, Kenya, Report 9 UNU-GTP, 2000, pp. 165-188.
- [22] C. Karingithi, Hydrothermal mineral buffers controlling reactive gases concentration in the greater Olkaria geothermal system, Kenya, MSc. Thesis, University of Iceland, UNU-GTP, 2002, p. 51.

Optimization of Wax Esters Production from Palm Fatty Acid Distillate and Oleyl Alcohol over Amberlyst 15

M. Tapanwong^{1,2} and V. Punsuvon^{1,2,3}

1. Department of Chemistry, Faculty of Science, Kasetsart University, Bangkok 10900, Thailand

2. Center of Excellence-Oil Palm, Kasetsart University, Bangkok 10900, Thailand

3. Center for Advanced Studies in Tropical Natural Resources, NRU-ku, Kasetsart University, Bangkok 10900, Thailand

Received: May 26, 2011 / Accepted: June 20, 2011 / Published: November 20, 2011.

Abstract: Wax esters were derived from long chain fatty acids and long chain alcohols with chain length of 12 carbons or more. These compounds have many potential applications in cosmetics, pharmaceuticals and food industries. The present work focuses on the synthesis of wax esters using palm fatty acid distillate and oleyl alcohol catalyzed by Amberlyst 15. Response surface methodology (RSM) based on a five-level, three-variable central composite design (CCD) was used to evaluate the interactive effects of synthesis, of amount of Amberlyst 15 catalyst (21.6-38.4% w/w), reaction time (18-102 min) and molar ratio (palm fatty acid distillate to oleyl alcohol, 1:1.16-1:2.84) on the percentage conversion of palm fatty acid distillate. The optimum conditions derived via RSM were: amount of catalyst 33% w/w, reaction time 95 minute and palm fatty acid to oleyl alcohol molar ratio 1:2.7. The actual experimental conversion was 81.52% under optimum condition, which compared well to the maximum predicted value of 80.50%. Analysis of the yield showed that at optimum condition, 80.54% wax esters were produced.

Key words: Palm fatty acid distillate, wax esters, response surface methodology, esterification.

1. Introduction

Palm fatty acid distillate (PFAD) is the byproduct from crude palm oil refinery industry. The main component of PFAD is free fatty acid and also has glyceride, squalene, sterols, vitamin E and other substance [1]. At room temperature, PFAD is a light brown solid and melting to brown liquid on heating. Mostly, PFAD is used as raw material in oleochemical industry such as laundry soap industry, biodiesel and animal feed. But, the best way to increase value added of PFAD is to synthesize wax esters products.

Wax esters are long chain esters that are including of fatty acids and long chain alcohols with more than 12 carbons atom of chain lengths. These compounds have been used in many applications due to their

potential such as excellent wetting behavior at interface [2] and non greasy feeling when applied on skin surface. The wax esters are one of many ingredients in cosmetics, pharmaceuticals, lubricants, plasticizers and other chemical industries [3].

Animal, vegetables and mineral can be generated natural waxes such as beeswax, however, the main obstacle is its cost and availability. Thus, the synthesized wax esters from cheap raw materials such as PFAD have become interesting. Chemical and enzymatic method can be used to synthesize wax esters from various raw material such as palm olein, palm stearin, palm kernel, oleic acid with oleyl alcohol, over different catalyst. The homogenous chemical catalyst may lead to several problem such as corrosion of equipment, handle hazards of corrosive acids or base and high energy consumption. The enzymatic reaction performs under mild condition, but it is more expensive. So, the heterogeneous catalyst

Corresponding author: V. Punsuvon, associate professor, Ph.D., main research fields: biodiesel, green chemistry. E-mail: fscivit@ku.ac.th.

specificly Amberlyst 15 was selected in this work [4].

Amberlyst 15 is a acidic styrenedivinylbenzene sulfonated ion-exchange resin. It is usually used as heterogeneous solid acid catalyst to replace homogeneous acid catalyst such as sulfuric acid for esterification reaction of biodiesel that produces toxic waste water and difficulties in recovery after the reaction. So, in the view of green chemistry esterification by solid acid catalyst, it has the advantage of being easily recovered and reused as well as being compatible with environmental consideration. Response surface methodology (RSM) is a useful statistical technique which has been applied in research into complex variable process. It employs multiple regression and correlation analyses as tools to assess the effect of two or more independent factors on the dependent variables. Its principle advantage is the reduced number of experimental runs required to generate sufficient information for a statistically acceptable results. RSM has successfully been applied to optimize the wax esters. The objective of this research was to study esterification reaction of PFAD and oleyl alcohol over solid acid catalyst by using response surface methodology to optimize the reaction and to search for relationship between the percentage conversion of PFAD and the operation variables. The variables studied were amount of catalyst, reaction time and molar ratio of oleyl alcohol to PFAD. In addition, wax esters yield and biodiesel synthesis were also studied on RSM to optimize conditions by Gunawan [5] and Vicente [6].

2. Methods

2.1 Materials

Palm fatty acid distillate is obtained from Patum vegetable oil Co., Ltd (Thailand). Table 1 shows the fatty acid composition of PFAD. Reference standards of fatty acid methyl esters with > 99% purity were purchased from sigma chemical Co., Ltd (St. Louis, MO, USA). Amberlyst 15 produced from Rohm and Haas was purchased from Aldrich Co., Ltd (USA). Oleyl alcohol, oleyl palmitate, oleyl oleate, oleyl linoleate, methyl laurate and all other chemicals were of analytical grade.

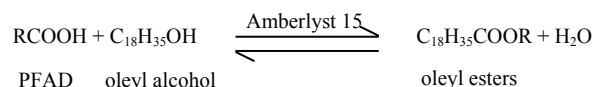
2.2 Apparatus and Esterification Reaction Procedures

The esterification reactions were conducted in 50 mL three necked flask equipped with a reflux condenser, a thermometer. The flask was heated and stirred with magnetic stirrer on agitator heater. Temperature and rate of agitation were set constant at 60 °C and 500 rpm, respectively, of all experiment. For esterification experiment, the flask was charged with 2 g of palm fatty acid distillate (PFAD) and heated to the setting temperature with agitation. After achieving the setting temperature of the reactant, a certain quantity of Amberlyst 15 catalyst and oleyl alcohol were added to the flask. The reaction parameters were designed as shown in Table 2. Wax esters obtained from esterification reaction were determined by acid value for percentage conversion of PFAD. In addition, wax esters obtained at the optimization condition were further characterized by

Table 1 Fatty acid composition of palm fatty acid distillate.

Fatty acid	Formula	Structure	wt%
Lauric acid	C ₁₂ H ₂₂ O ₂	12:0	0.25
Myristic acid	C ₁₄ H ₂₈ O ₂	14:0	0.86
Palmitic acid	C ₁₆ H ₃₂ O ₂	16:0	42.49
Stearic acid	C ₁₈ H ₃₆ O ₂	18:0	3.35
Oleic acid	C ₁₈ H ₃₄ O ₂	18:1	34.77
Linoleic acid	C ₁₈ H ₃₂ O ₂	18:2	8.25
Others	-	-	10.03

gas chromatograph (GC) for percentage yield of wax esters and their physical, chemical properties. The reaction of PFAD and oleyl alcohol is given below.



2.3 Experimental Design for Reaction

A five-level-three-factor central composite design (CCD) was employed in this optimization study, requiring 20 experiments. Molar ratio of oleyl alcohol-to-PFAD (O), Amberlyst 15 catalyst concentration (C) and reaction time (T) were the independent variables to optimize the percentage conversion of wax esters. The coded and uncoded levels of the independent variables are showed in Table 2. The central values (zero level) chosen for experimental design were 2 mole of oleyl alcohol-to-PFAD molar ratio, 30% (w/w) of Amberlyst 15 catalyst concentration and 60 min of reaction time. Table 2 showed the coded and uncoded independent factor, level and experimental design.

2.4 Statistical Analysis

The experimental data was analyzed by response surface methodology of SPSS software to fit the following second-order polynomial as showed in Eq. (1)

$$y = b_0 + \sum_{i=1}^3 b_i x_i + \sum_{i=1}^3 b_{ii} x_i^2 + \sum_{i < j=1}^3 \sum_{j=1}^3 b_{ij} x_{ij} \quad (1)$$

where, y is the response (percentage conversion, %), b_0 is constant, b_i is linear term coefficients, b_{ii} is quadratic team coefficients, b_{ij} is cross-product term coefficients. SPSS package was used for regression analysis of variance (ANOVA) and response surface

methodology was performed using STATISCA. Response surface plots were developed using the fitted second-order polynomial equation obtain from regression analysis holding one of the independent variables at a constant value corresponding to the stationary point and changing the other two variables. Confirmatory experiments were carried out to validate the equation, using combinations of independent variables which were not part of the original experimental design but within the experimental region [7].

2.5 Analytical Methods

2.5.1 Determination of the Percentage Conversion of PFAD

The percentage conversion (%) of PFAD was measured by determining the remaining unreacted fatty acids in the reaction mixture by titration with 0.1 M potassium hydroxide solution following AOCS Ca 5a-40 standard method. All the samples were assayed in duplicate. The percentage conversion of PFAD was calculated in accordance with the following Eq. (2)

$$\text{conversion of PFAD (\%)} = \left(\frac{S_i - S_t}{S_i} \right) \times 100\% \quad (2)$$

in which S_i was initial acid value in PFAD and S_t was final acid value in wax esters product.

2.5.2 Determination of Percentage Yield of Wax Esters by Gas Chromatograph (GC)

The percentage yield of wax esters was analyzed by a gas chromatograph (Agilent Technique, 6890 N, USA) using DB-5HT capillary column (30 m × 0.32 mm i.d.; film thickness 0.1 μm) with a flame-ionization detector. Injector and detector temperature were set at 250 and 300 °C respectively. The oven temperature

Table 2 Independent variables and level used for central composite design (CCD) for esterification reaction.

Variables	Symbols	Levels				
		-1.68 (-α)	-1	0	1	1.68 (α)
Amberlyst 15 concentration (%w/w)	C	21.6	25	30	35	38.40
Oleyl alcohol-to-PFAD molar ratio (mole)	O	1.16	1.50	2	2.50	2.84
Reaction time (min)	T	18	35	60	85	102

was maintained at 150 °C for 2 min, increased to 270 °C with a ramping rate 3 °C/min and held for 16 min at 290 °C. Helium was used as a carrier gas with the flow rate of 0.8 mL/min. The wax esters compositions were quantitated by an internal standard method with methyl laurate as the internal standard. The concentration of ester was calculate by equation:

$$C_x = (A_x/A_{is}) \times (C_{is} \times D_{Rf is} / D_{Rf x})$$

where C is amount of component x or internal standard, A is area of component x or standard and D_{Rf} is detector response factor for component x or internal standard ($D_{Rf x} = A_x/C_x$ and $D_{Rf is} = A_{is}/C_{is}$). The percentage yield of wax esters was calculated by equation:

$$Yield (\%) = \frac{\text{weight of wax esters}}{\text{weight of PFAD}} \times 100 \% \quad (3)$$

2.6 Characterization of Wax Esters Properties

Wax esters were characterized by determining their flash point, refractive index, saponification value, specific gravity, iodine value and acid value. The following test methods were used: flash point (AOCS Cc 9c-95), refractive index (AOCS Cc 7-25), saponification value (AOCS Cd 3-25), specific gravity (AOCS Cc 10b-25), iodine value (AOCS Cd 1-25) and acid value (AOCS Cd 3d-63).

3. Results and Discussion

3.1 Properties of PFAD

The physical and chemical properties of PFAD are shown in Table 3. It indicates that the PFAD has initial acid value 170 mg KOH/g or 85% on free fatty

acid content. The rest content (about 15%) is triglycerides, diglycerides, monoglycerides, and traces of impurities. The high free fatty acid content in PFAD makes this material a cheap low-cost non-food feedstock for oleochemical industries.

3.2 Model Development

The percentage conversion of PFAD for esterification reaction at the design point was given in Table 4. Fig. 1 showed the high correlation coefficient ($R^2 = 0.980$) determined from the regression model of esterification reaction of PFAD. Statistical analysis of the model was performed by analysis of variance (ANOVA) in Table 5.

The model characteristics and the coefficients were presented in Tables 4 and 5, which indicated that the predictability of the model is at 95% confidence level. The model has high correlation coefficient, a significant F-value, an insignificant lack-of-fit F-value. From the analysis of variance (ANOVA), the model F-value of 54.765 implied the model was significant. The high correlation coefficient ($R^2 = 0.980$) indicated that the model was suitable to represent the real relationship among the variables studied [8, 9].

The insignificant lack-of-fit which was relative to the pure error of the experiment also indicated that the model was suitable to represent the experimental data [10]. Coefficients of full model equation were evaluated by regression analysis and tested for their significance. The final reduced models to predict the percentage conversion of PFAD in esterification reaction was followed Eq. (4).

Table 3 Physical and chemical properties of PFAD.

Properties	Unit	Amount
Density@ 40 °C	g/cm ³	0.87
Kinematic viscosity @ 40 °C	cSt	10.75
Acid value	mg KOH/g	170
Water content	%wt	0.05
Saponification value	mg KOH/g	200.57
Iodine value	g I ₂ /100g	57.57
Free fatty acid	%	85

Table 4 Central composite design (CCD) arrangement and response for esterification reaction.

Treatment	C	O	T	C (%w/w)	O (mole)	T (min)	Conversion(%)	
							Experimental	Predicted
1	-1	-1	-1	25.0	1.50	35.00	63.19	62.97
2	-1	-1	1	25.0	1.50	85.00	73.03	72.12
3	-1	1	-1	25.0	2.50	35.00	73.74	73.57
4	-1	1	1	25.0	2.50	85.00	79.71	78.02
5	1	-1	-1	35.0	1.50	35.00	63.69	64.89
6	1	-1	1	35.0	1.50	85.00	73.81	73.54
7	1	1	-1	35.0	2.50	35.00	75.63	76.07
8	1	1	1	35.0	2.50	85.00	80.26	80.02
9	-1.68	0	0	21.6	2.00	60.00	71.37	72.24
10	1.68	0	0	38.4	2.00	60.00	75.75	75.53
11	0	-1.68	0	30.0	1.16	60.00	63.67	63.57
12	0	1.68	0	30.0	2.84	60.00	77.25	77.92
13	0	0	-1.68	30.0	2.00	18.00	67.63	67.96
14	0	0	1.68	30.0	2.00	102.00	79.21	78.96
15	0	0	0	30.0	2.00	60.00	74.46	73.46
16	0	0	0	30.0	2.00	60.00	74.45	73.46
17	0	0	0	30.0	2.00	60.00	73.15	73.46
18	0	0	0	30.0	2.00	60.00	74.00	73.46
19	0	0	0	30.0	2.00	60.00	72.59	73.46
20	0	0	0	30.0	2.00	60.00	72.04	73.46

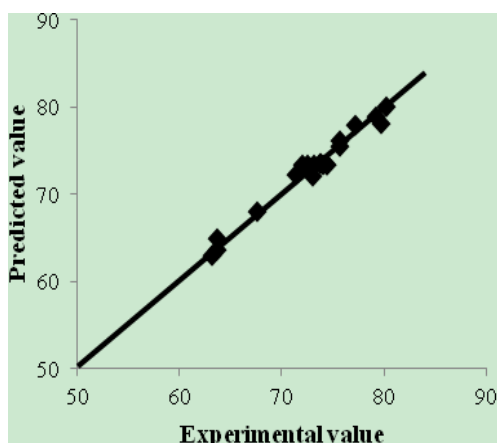


Fig. 1 Correlation coefficient (R^2) determined from the regression of esterification reaction of PFAD and oleyl alcohol.

$$Y = 23.068 - 0.220 C + 27.812 O + 0.349 T + 0.006 C^2 - 3.843 O^2 + 0.058 CO - 0.001 CT - 0.094 OT \quad (4)$$

where C is the amount of Amberlyst 15 catalyst, O is the molar ratio of oleyl alcohol-to-PFAD and T is the reaction time.

3.3 Response Surface Plot

The optimized level of variables was determined by constructing three-dimensional surface plots according

to Eq. (4). Two variables were plotted at any one time on the x_1 , and x_2 axes, respectively, with the other remaining variables set at their centre point values (coded level: 0). Fig. 2(a) shows the effect of oleyl alcohol-to-PFAD molar ratio (O), Amberlyst 15 catalyst amount (C). Fig. 2(b) shows the effect of oleyl alcohol-to-PFAD molar ratio (O), reaction time (T) and Fig. 2(c) shows the effect of Amberlyst 15 catalyst amount (C), reaction time and their mutual interaction of the percentage conversion of PFAD.

The result from Figs. 2(a), 2(b) and 2(c) indicates the optimum value of Amberlyst 15 catalyst amount, oleyl alcohol-to-PFAD molar ratio and reaction time in the range 30-36%, 2.6-2.8 mole and 90-102 min respectively that have percentage conversion of PFAD more than 80%.

3.4 Optimization of Esterification Reaction

The optimum conditions for esterification reaction from PFAD were predicted using the optimization function of the SPSS software. These are presented in Table 6 along with their predicted and experimental values. Among the various optimum conditions, the highest % conversion (81.52%) from experiment 2 was

Table 5 Analysis of variance (ANOVA) for the quadratic polynomial model of esterification reaction.

Model	Sum of squares	df	Mean square	F	Sig.
Regression	468.249	9	52.028	54.765	0.000
Residual	9.500	10	0.950		
Total	477.750	19			

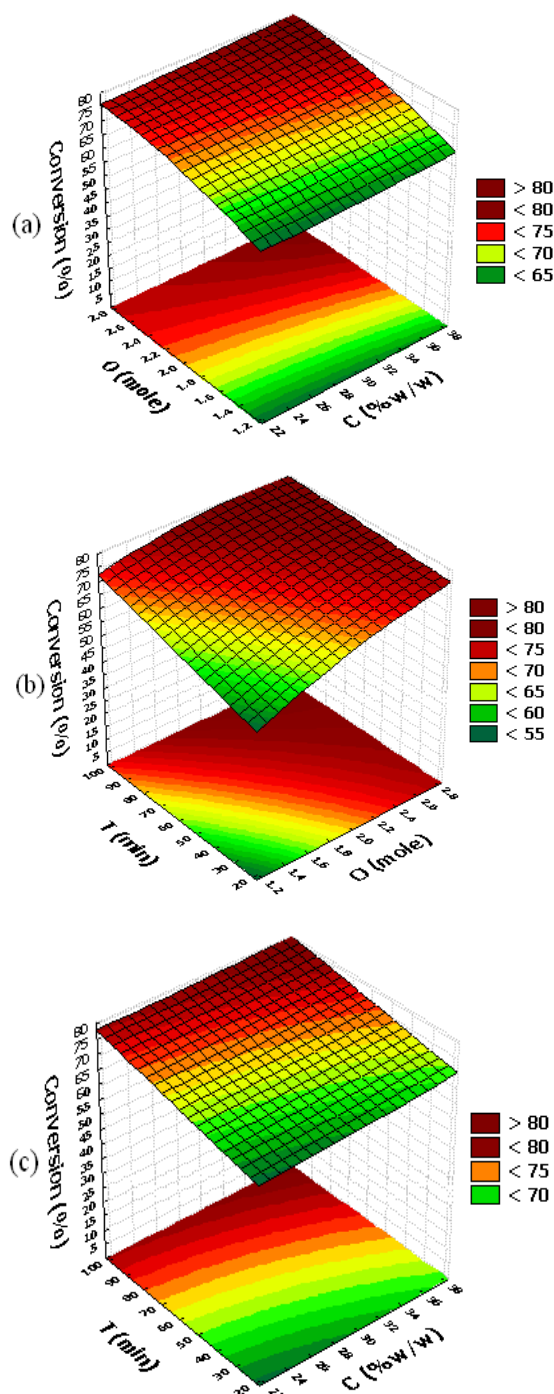


Fig. 2 Response surface plot representing the effect of factor on percentage conversion of 3.5 PFAD from the model.

chosen as the optimum condition because this condition used less amount of catalyst, oleyl alcohol and short time in PFAD conversion than other experiments. This optimum condition was 95 min of reaction time, 33% of amount of Amberlyst 15 catalyst and 2.70:1 of molar ratio of oleyl alcohol-to-PFAD.

3.5 Percentage Yield of Wax Esters at the Optimum Condition by GC

The amounts of three oleyl esters (oleyl palmitate, oleyl oleate, oleyl linoleate) were calculated at the optimum condition. The percentage yield was calculated by dividing the amount of each oleyl esters with the initial weight of PFAD and multiple with one hundred. The result of chromatogram and the percentage yield of wax esters were shown in Fig. 3 and Table 7.

The analysis of chromatogram in Fig. 3 was carried out by comparing the retention time of each peak with the authentic oleyl esters standard. Methyl laurate with retention time 4.071 minute was used as internal standard for quantitative of three oleyl esters in wax esters product. The retention times of oleyl palmitate, oleyl oleate and oleyl linoleate were 14.888, 16.794 and 16.907 minute, respectively. The result of percentage yield from Table 7 showed that oleyl palmitate had the highest percentage yield (49.34%) followed by oleyl oleate (25.59%) and oleyl linoleate (4.6%). The total percentage yield of three oleyl esters in wax esters product was 80.54%.

3.6 Properties of Wax Esters

The properties characterization of wax esters: flash point, refractive index, saponification value, specific gravity, iodine value, water content and acid value

Table 6 Optimized condition of esterification reaction by RSM.

Experiments No.	Optimized condition			Conversion (%)	
	O (mole)	C (%w/w)	T (min)	Experimental	Predicted
1	32	2.8	100	77.65	80.49
2	33	2.7	95	81.52	80.50
3	34	2.6	95	78.88	80.69
4	35	2.7	90	79.37	80.69
5	36	2.6	90	79.40	80.86

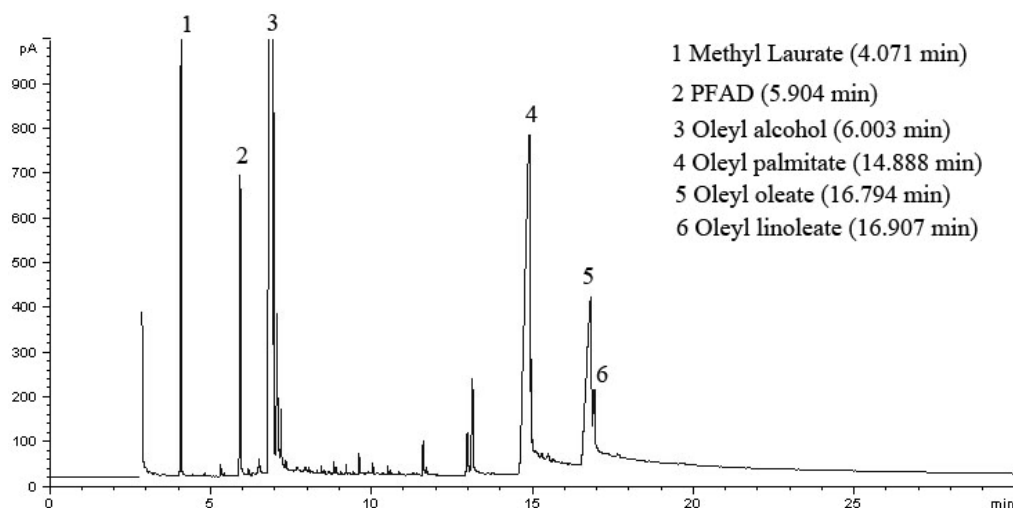

Fig. 3 Chromatogram of wax esters at the optimum condition of esterification reaction.

Table 7 Percentage yield of oleyl esters in wax ester at the optimum condition.

Oleyl esters	Retention time (min)	Amount (mg)	Yield (%)
Methyl laurate (IS)*	4.071	-	-
Oleyl palmitate	14.888	5.9878	49.34
Oleyl oleate	16.794	3.2266	26.59
Oleyl linoleate	16.907	0.5597	4.61
Total oleyl esters	-	-	80.54

* Internal standard.

Table 8 Properties of wax esters.

Properties	Wax esters product		
	From PFAD	From palm stearin	From palm olein
Acid value (mg KOH/g)	0.87	0.70	0.80
Kinematic viscosity at 60 °C (cSt)	16.49	N.D	N.D
Saponification value (mg KOH/g)	69.36	96.50	84.00
Iodine value (g I ₂ /100g)	83.18	62.10	71.60
Water content (%)	0.05	-	-
Refractive index	1.460	1.453	1.457
Density (g/cm ³)	0.856	0.841	0.838
Flash point (°C)	228	N.D	N.D

were shown in Table 8. These properties were compared with the result of Keng et al. [11] who used palm olein and palm stearin as raw material for wax

esters synthesis and Rahman et al. [12].

The result from Table 8 showed that the properties of wax esters from PFAD were nearly similar with the

properties of wax esters from palm stearin and palm olein especially acid value, refractive index, and density. This result indicated that PFAD can be used as raw material for replacing palm olein and palm stearin in wax esters synthesis.

4. Conclusion

PFAD, by-product from palm oil refinery industry, could be used as a cheap raw material for wax esters production. The percentage conversion of PFAD could be converted to more than 80% by using the central composite design and response surface methodology in esterification reaction. The optimum condition of esterification reaction was obtained at 2.70:1 of molar ratio of oleyl alcohol-to-PFAD, 33% of Amberlyst 15 catalyst amount and 95 min of reaction time. After the optimum condition was accepted, GC was applied to determine the percentage yield of wax esters product. The total percentage yield of wax esters was 80.15% and it had almost the same properties as another wax esters which prepared from different types of palm oil.

In addition, utilization of by-product such as PFAD will lead not only to a value-added application, but also to a zero-waste strategy in palm oil refinery industry.

Acknowledgments

The authors gratefully acknowledge the financial support of this work from the Graduate School Kasetsart University.

References

- [1] A.G.M. Top, Production and utilization of palm fatty acid distillate, *Lipid Technology* 22 (2010) 11-13.
- [2] N.M. Hadzir, M. Basri, M.B.A. Rahman, C.N.A. Razak, R.N.Z.A. Rahman, A.B. Salleh, Enzymatic alcoholysis of triolein to produce wax ester, *J. Chem. Technol. Biotechnol.* 76 (2001) 511-515.
- [3] M.L. Hallberg, D. Wang, M. Harrod, Enzymatic synthesis of wax esters from rapeseed fatty acid methyl esters and fatty alcohol, *J. Am. Oil Chem. Soc.* 76 (1999) 20-22.
- [4] K.P. Sin, M. Basri, M.B.A. Rshman, A.B. Sallenh, R.N.Z.A. Rahman, A. Ariff, Optimization of palm-based wax esters production using statistical experimental design, *Journal of Oleo Science* 54 (2005) 519-528.
- [5] E.R. Gunawan, M. Basri, M.B.A. Rahman, A.B. Salleh, R.N.Z.A. Rahman, Study on response surface methodology (RSM) of lipase-catalyzed synthesis of palm-based wax ester, *Enzyme and Microbial Technology* 37 (2005) 739-744.
- [6] G. Vicente, A. Coteron, M. Martinea, J. Aracil, Application of the factorial design of experiments and response surface methodology to optimize biodiesel production, *Industrial Crops and Products* 8 (1998) 29-35.
- [7] S.V. Ghadge, H. Raheman, Process optimization for biodiesel production from mahua (*Madhuca indica*) oil using response surface methodology, *Bioresource Technology* 97 (2006) 379-384.
- [8] H. Bidin, M. Basri, S.M. Hadzi, A. Ariff, R.N.Z.R.A. Rahman, A.B. Salleh, Optimization of lipase-catalyzed synthesis of palm amino acid surfactant using response surface methodology (RSM), *Industrial Crops and Products* 30 (2009) 206-211.
- [9] H.C. Chen, Y.K. Twu, C.J. Chang, Y.C. Lui, C.J. Shieh, Optimized synthesis of lipase-catalyzed octyl caffeate by Novozym 435, *Industrial Crops and Products* 32 (2010) 522-526.
- [10] W.N.N.W. Omar, N.A.S. Amin, Optimization of heterogeneous biodiesel production from waste cooking palm oil via response surface methodology, *Biomass and Bioenergy* 35 (2011) 1329-1338.
- [11] P.S. Keng, M. Basri, M.R.S. Zakaria, M.B.A. Rahman, A.B. Ariff, R.N.Z.A. Rahman, et al., Newly synthesized palm esters for cosmetics industry, *Industrial Crops and Products* 29 (2009) 37-44.
- [12] N.F.A. Rahman, M. Basri, M.B.A. Rahman, R.N.Z.R.A. Rahman, A.B. Salleh, High yield lipase-catalyzed synthesis of Engkabang fat esters for the cosmetic industry, *Bioresource Technology* 102 (2011) 2168-2176.

Territorial Repartition and Ecological Importance of Wetlands in Moldova (Romania)

G. Romanescu, C. Stoleriu and C. Zaharia

Department of Geography, Faculty of Geography and Geology, University of Iasi, Iasi 700505, Romania

Received: February 18, 2011 / Accepted: May 20, 2011 / Published: November 20, 2011.

Abstract: The present paper is the first study conducted in Romania on the inventory of wetlands of a large surface of the country. The focus of this study is the Moldavian Plateau, located in the east of Romania. It is delimited by the Eastern Carpathians on the west, the Romanian Plain on the south, the Ukrainian border on the north and the Prut Valley (border with the Republic of Moldavia) on the east. Although the Moldavian Plateau is situated in the driest region of Romania, the majority of the wetlands and of the low discharge rivers is found in this region. The existence of numerous wetlands, respectively small ponds, is influenced by the human activities and the scarcity of water resources. The impermeable clayey substratum favored the occurrence and survival of a large number of wetlands. Most of them are found in the northern Moldavian Plain, and the fewest to the south, in the Covurlui Plateau. The most important wetlands are those developed along the two main rivers draining this territory: Prut and Siret. Unfortunately, Siret River floodplain has been in most of its part protected by means of flood prevention dikes. Consequently, many of the wetlands entered agricultural use.

Key words: Aridization, deep waters, inventory, typology, wetlands.

1. Introduction

Comprehensive studies on large areas wetlands inventories are inexistent in Romania. Punctual studies on wetlands have been conducted; however, they are all missing the aspect of inventorying and classification.

The first studies regarding the typology and inventory of wetlands have been conducted during the period of 2000 to 2008, and were finalized for the Moldavian Plateau only in 2008 [1].

The detailed research of wetlands in eastern Romania has only focused on the inventory and classification of wetlands as well as their spatial distribution for each landscape units or administrative segments (counties). The study also dealt with the differences in wetland inventory between the northern and southern parts of the region, and between the Romanian territory and that of the Republic of

Moldova (even if in the same landscape unit, that of the Moldavian Plateau).

In preparation of the studies dealing with the wetland inventory of the Moldavian Plateau an extensive literature review was carried out in order to consider the adequate methodology that could be adapted to the local conditions of the region considered in the present study.

The authors consulted several studies of high interest in terms of the methodology for conducting inventory of the wetlands [1-15]. A number of researchers investigated the geomorphology of wetlands [16-23].

The complex hydrology of wetlands has been investigated over the past two decades [19, 24-32]. Another important component of the wetlands is represented by their extremely rich biodiversity. Studies were conducted on this particular topic as the conservation of the biodiversity of one of the key components of the wetlands [33-35]. Other studies on the wetlands delta with pedological studies of such areas are Refs. [17, 36, 37]. Finally, the management

Corresponding author: G. Romanescu, professor, research fields: hydrology, wetlands, littoral geomorphology. E-mail: geluromanescu@yahoo.com.

and conservation of wetlands, maybe one of the most acute issues confronting these areas, is under intense scrutiny and several researchers have proposed various approaches for this issue [38-40]. Several other researchers worked on more general aspects of wetlands [41-43].

2. Regional Characteristics and Setting

The Moldavian Plateau is the largest and most representative tableland in Romania. It occupies the eastern part of the country, being surrounded by Obcinele Bucovinei, the Moldavian Sub-Carpathians, the north-east of Romanian Plain, Prut and Danube Valley [1] as shown in Fig. 1.

This unit is a part of the large hilly area included in the Carpathian-Danube region and had a total surface of 25,000 km², which represents approximately 10% of the Romanian territory. From a morphostructural aspect, the largest part of the plateau is identified within the Moldavian Platform, while the southern sector corresponds to the Bârlad Depression [44].

The geologic composition consists of a complex of clays and marls with alternations of sands, in which thin horizons of sandstones, limestone, conglomerates, gravels, andesitic cinerites can also be found. At their upper part, along the valleys or in the lacustrine areas, thin Quaternary loess-like deposits and loamy-sandy-

clayey alluvial deposits are deposited [45].

The present landscape bears the imprint of the monocline structure, and of the lithological and external modeling factors represented by the hydrographic network and the slope degradation processes. The higher peaks of the Moldavian Plateau and its extended sub-plateaus can be found in several large areas, with altitudes of 350 to 500 meters in the central and western sector and of 200 to 300 meters towards east and south [44].

The most extended landforms are those conditioned by the monocline structure: hills and valleys oriented mainly NW-SE, cuesta alignments, structural plateaus, etc.. The frequency and development of landslides, as well as of other slope degradation processes, represent a characteristic feature of almost the entire Moldavian Plateau.

Due to its extra-Carpathian position, the climate of the Moldavian Plateau is temperate-continental, with excessive nuances. Towards west and north-west, the climate interferes with the temperate continental climate characteristic to the continental western part of Romania. The most characteristic features are the East European influences, induced by the domination of the cold air masses during winter and of the hot and dry ones in the summer [46].

The mean annual temperature is between 7.5 and

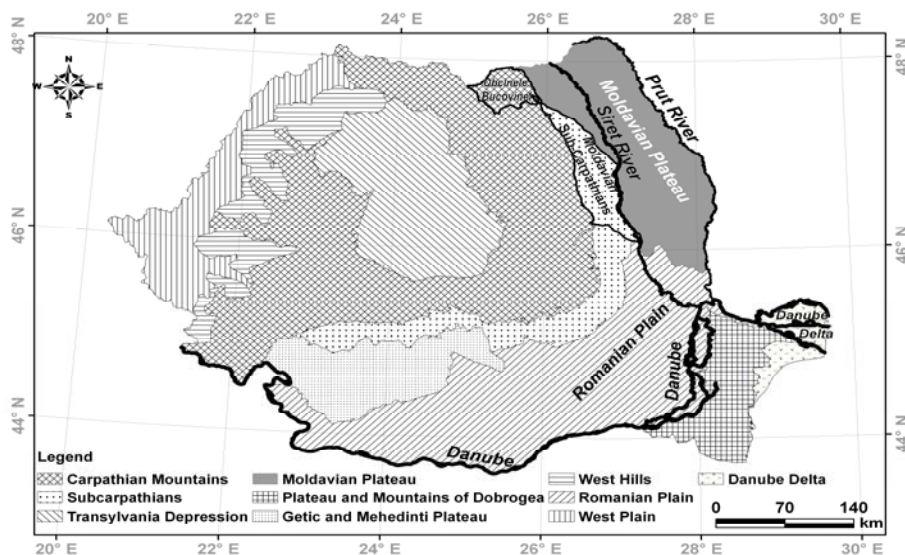


Fig. 1 Geographical position of Moldavian Plateau on Romania's territory.

10 °C, with increasing variations in the north-south direction. Rainfall quantities are of the order of 500 to 700 mm, with lower values in the low-lying or southern sectors.

The hydrographic characteristics are strongly related to the climatic and geomorphologic conditions. Surface waters have generally a weak density and they originate from the Carpathian Mountains. The main river is Siret, with its right-side tributaries and Prut River. Allochthonous rivers are numerous, but they are relatively small and with small discharge rates. They often have an intermittent character in terms of flow rate and duration. However, lakes are relatively numerous, but many of them have anthropic origin, especially in the Moldavian Plain [29, 47].

In this context, one can delimitate a Moldavian province, with variable or deficient humidity, drained by rivers with moderate rainfall supply in the higher areas of the central and north-western part and rainfall-snow melt supply in the lower altitude sectors. A moderate underground alimentation is also contributing to the general rivers' discharge in this province [48].

The vegetation, fauna and soils are specific to the decreasing altitude of the Carpathian unit towards east and, by some interference of the central and east European elements, to the local differences according to the climatic and geomorphologic conditions. Human activity has radically influenced the occurrence of the biotic and soil cover elements.

3. Methodology

For the wetland inventory from the Moldavian Plateau the authors used the analysis of satellite images. The interpretation of satellite images, a method that comes to complete and complement field investigations, represents a modern instrument modern of terrain study. Satellite interpretation is relatively new for the Romanian scientific community and this is one of the first such studies.

Satellite images are obtained with the aid of sensors

which are sensitive to the reflectance of the organisms and systems from the Earth surface.

Following the delineation of the wetlands on these images, several expeditionary field surveys have been conducted to collect data needed for the classification of wetlands to their respective typology. These field surveys were conducted during summer, and the samples have been taken during noon.

For the creation of the wetland map the authors used both Landsat TM 7 satellite images taken between 2000 and 2005 [49], as well as a series of topographic maps scaled at between 1:25.000 and 1:50.000 [50, 51].

The applied methodological norms are found in the technical guide of the Corine Land Cover 2000 program (elaborated by the European Environment Agency experts). These methodological norms establish a series of polygon identification, delineation, aggregation, inclusion etc..

The combination of the spectral bands used in the current photo-interpretation is TM4, TM5, and TM6. This is in fact the combination recommended in the CLC 2000 technical guide, which is useful in the identification of the hygrophyte and hydrophile vegetation. The wetness index (Fig. 2) was used to refine the results obtained during satellite images interpretation. The operation, known as Kauth's

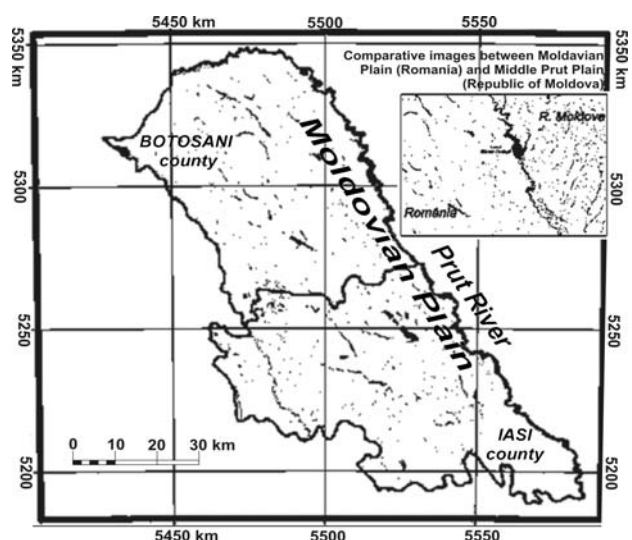


Fig. 2 Kauth's tasseled cap wetness index applied to identify wetlands in the Moldavian Plateau.

Tasseled Cap, calculates three Kauth biophysical indices (greenness, brightness and wetness) departing from Landsat images, and uses six spectral bands: TM1, TM2, TM3, TM4, TM5, TM7.

The wetness is calculated using the following formula: $Wetness = 0.13929 \times TM1 + 0.22490 \times TM2 + 0.40359 \times TM3 + 0.25178 \times TM4 - 0.70133 \times TM5 - 0.45732 \times TM7$. This index identifies wetlands by including also the water included in the vegetal biomass. This is the reason for which the forested surfaces represent sources of mapping errors. The wetland map was obtained in vector format, using the TNTMips 6.9 GIS software. The authors have chosen the most important sectors which comprise typical and diverse wetlands, as well as those for which satellite images could not provide a clear classification.

A special scheme was used for obtaining the wetland typology of the Moldavian Plateau. This scheme was specially adapted to the Romanian context, which uses a classification based on the system, sub-system, class, subclass, water regime, chemistry, pH, soil type, evolution of the protection level, and perspectives. The authors considered for the wetland typology of the following tests: analysis of the water chemistry, the analysis of the content of organic and inorganic matter, drilling boreholes for the determination of the thickness of the moist-affected strata, analysis of the grain size distribution and of the type of solid materials, the mapping of the indicator plant species and the survey of the floristic associations [1, 12].

The observations and analyses conducted in the Moldavian Plateau were performed during the summers of 2000 through 2008. During those tests, water samples were sampled during daytime, between 10:00 and 18:00.

4. Results and Discussion

Although on the territory of the Moldavian Plateau, covering the Iasi and Botoşani Counties, climatic conditions (temperature, evapotranspiration, rainfall, etc.) do not favor the occurrence of large wetlands, they

appear to be in quite high number and occupy an important percentage in the area investigated as shown in Figs. 3 and 4.

The number and area covered by wetlands in the analyzed region are due relatively low altitude relief, characterized by large and fine textured (clayey) floodplains. Consequently, the geology and terrain morphology have favored the extension of these wetlands over a relatively important area. The majority of wetlands and deepwater basins can be found in the floodplains of the local rivers (Jijia, Başeu, Bahlui, Bahlueţ, Miletin, Bodeasca, etc.) and rarely on structural surfaces (very rare in the Moldavian Plain).

The most extended wetlands and deep waters can be found in the northern part of the Moldavian Plateau, especially in the Counties of Botoşani and Iaşi. This is favored firstly by the presence of lakes (mention since

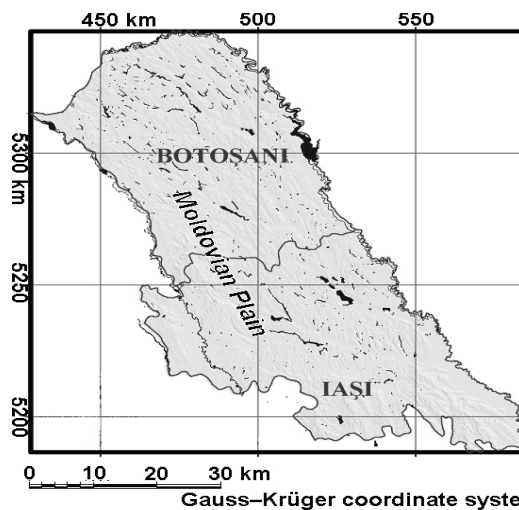


Fig. 3 Distribution of wetlands and deep waters in the Iasi and Botoşani Counties.

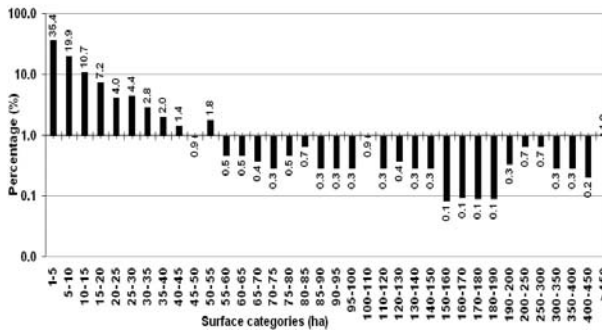


Fig. 4 Distribution of wetlands and deep waters on surface categories in the Iasi and Botoşani Counties.

the 14th and 15th centuries AD) and secondly, the presence of the clayey soil that prevent the rapid infiltration of precipitations [52]. Significantly fewer wetlands and deep waters are present in the southern part of the Moldavian Tableland, mainly in the Tutova hills and Covurlui Plateau.

Most of the water courses from these areas (e.g., Berheci, Tutova, Geru, Drăgușeni, Perișani, Jeravăț, Horincea, etc.) are small and often dry. The forest cover is almost inexistent, and erosion, in all types, including wind erosion, manifests itself intensely. Moreover, the regional aridization phenomenon is accentuated by the global climatic changes.

The disappearance of wetlands from the southern Moldavian Plateau is also caused by accelerated erosion due to human activities in the form of deforestations and tillage. This anthropic activity induced an intense alluvial transport with severe repercussions on the most of the valleys' floor aggradation. Most of the torrential formations and hydrographic basins suffer strong aggradation along their downstream sectors, where sedimentation is intense during floods. Some water courses do not have regular floodplain delineation along their downstream sectors, so that the rest of the river is over-elevated and does not intersect the phreatic water level anymore. Due to alluvial material deposition directly in the major floodplain, rill erosion cannot outrun the aggradation and the water course remains simply isolated from the phreatic water level. Thus, the river becomes temporary rather than permanent, as shown in Fig. 5.

Unfortunately, such phenomena do not represent isolated cases, but are quite frequent in the Covurlui Plateau. River water drying is accentuated also by the high permeability of the high thicknesses loess-like layers, present on most of the main valleys.

As a consequence of the fact that agricultural activities developed rapidly and are expected to continue, and since especially during the last few years tillage is performed incorrectly, that is, perpendicular on the elevation curves, it is certain that a large part of

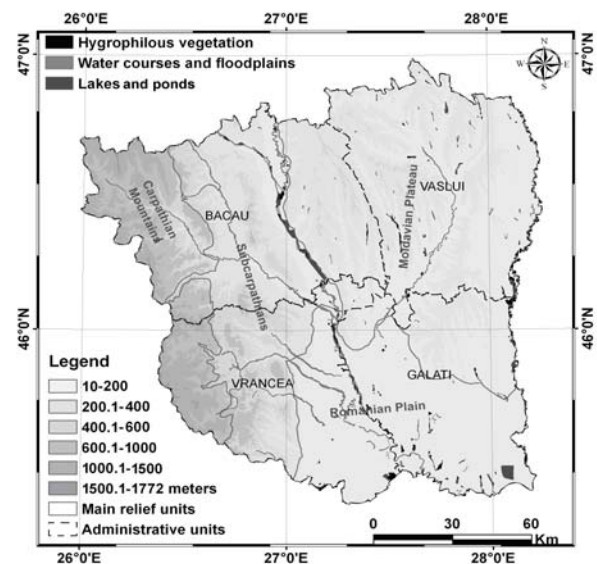


Fig. 5 Wetlands distribution in the southern part of the Moldavian Plateau.

the wetlands, especially the small ones, may disappear in the near future.

Significant river engineering works have been performed on the majority of the water courses which are presently well protected against flooding. Flood protection artificial reservoirs (lakes) have already been created on most of the rivers in the Moldavian Plateau. Only a few of these creeks and rivers have a torrential character and hence, that does not affect wetland evolution.

Climate aridization in the eastern part of Romania, as well as the anthropic activities and the natural riverine evolution will lead to reduced wetlands surfaces, and consequently, there is an acute need for an aggressive wetland protection policy.

The authors would like to stress that the areas identified with the help of satellite images as wetlands, according to the vegetation indices, water surface and floodplain geomorphologic conditions, do not meet all criteria to be classified as such. One could observe hydrophile vegetation that does not enter the wetland because the floodplain has been dammed and the link with the water source was interrupted or limited. Aspen, willow or alder forests all fit this pattern for this particular area. These species adapted the new conditions of relative draught and can be observed

along the dammed floodplains.

The same aspect can be found in the case of the floodplains. Not all floodplains can be classified as wetlands. In the region of Moldavia, main water courses have been encroached by flood protection dikes, and a part of the major floodplains were thus taken out of the natural flow conditions. Some floodplains are no longer supplied by the groundwater aquifers since the minor floodplains have deepened and the influence of the aquifer strata on the river flow disappeared.

There are major discrepancies in the wetland repartition in the two distinct areas of northern and southern Moldavia. If in the northern part the clayey substratum which favors the local occurrence of wetlands is present, in the southern part sandy deposits dominate. Consequently, the strong infiltration does not favor the development of wetlands. The southern hydrographic network is better represented since the soil is more friable. However, the majority of rivers have either only maintained their minor floodplain while the major floodplain strongly aggraded and no longer interacts with the aquifer layer. In this last case, these areas became alluvial plains suitable for intensive grazing (Fig. 6).

At the same time, the sandy-loamy substratum and the reduced river discharge did not favor the creation of artificial ponds, typical only for northern Moldavia.

The most important wetland in southern Moldavia is represented by Prut River floodplain and the Lower Siret Plain, mostly encroached by flood protection dikes.

Unfortunately, the lower floodplain of Prut has been radically modified by engineering and flood protection works during the past three decades, and most of the wetlands have been eliminated (Fig. 7). Following the 2005 catastrophic floods, when the discharge of Siret River reached historical levels of 5.000 to 5.500 m³/s (discharge flow rate reconstructed at Cosmești and Movileni hydrological stations by Romanescu [29]), the attitude towards wetlands importance may be

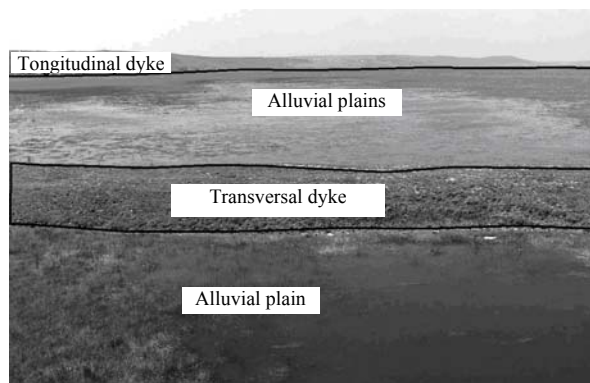


Fig. 6 Dikes in the floodplain of Jijia River and the penetration of phreatic water in the floodplain area.



Fig. 7 Prut's floodplain with abandoned arms (downstream of Oancea).

revised and may become part of a concerted action of the government to render them in their natural state.

At the same time, a strong differentiation in wetland development was observed between the two dominant relief units in the studied region: the Moldavian plateau and Moldavian plain. In the Moldavian Plateau area, due to the development of a rich hydrographic network and of higher rainfalls, a larger surface is occupied by wetlands. For the Moldavian Plain, wetlands are mostly lacking. One of the reasons is also the fact that the terrain is use for agriculture (mainly cereal crops).

The relief of the Moldavian Plateau allowed the preservation of water surfaces, which are of interest also for the local economy. However, the lakes in the Moldavian Plain, except for the floodplain ones, have almost completely disappeared because the need for agricultural fields has been extremely high and the lakes were consequently drained.

The Moldavian Plateau, especially its southern part, has a relatively limited floodplain development in

comparison to the alluvial units specific to the subsidence plains (Lower Siret Plain), as shown in Fig. 8. Although wetland vegetation should be more developed in the plains, it has disappeared after the land started being used for agriculture. In the plateau areas, wetland vegetations are better represented, especially in the areas affected by landslides or in places where clayey rocks, local observed, are dominant.

After preparing the vector wetland and the hydrographic network strata (orders 4, 5, 6, and 7 in Horton system), the authors proceeded to database interrogation, further obtaining a series of statistical data on wetlands, presented based on categories and regions as shown in Table 1.

The relief unit that holds the largest areal of wetlands is the Moldavian Plain, which, as mentioned, is part of the Moldavian Plateau. The presence of these areas is favored by the relatively low altitudes, the existence of a clayey substratum and the tradition of artificial pond creation as shown in Figs. 9 and 10.

Using this database, statistical data regarding wetlands were obtained. 745 polygons that represent wetlands and deep water surfaces, occupying a total surface of 27.582 ha, have been identified. Their

average area is of 37 hectares and varies between 1 hectare (the minimum surface taken into consideration) and 4.315 hectares. Most wetlands and deep water surfaces are small, between 1 and 5 hectares. Considering these areas, one can identify a clear trend of disappearance due to natural or human intervention. If this trend continues, most of these surfaces will probably become agricultural land.

In the Moldavian Plain (Iasi and Botoşani Counties) wetland and open water surfaces have surfaces between 1 and 55 hectares. Thus, they are of small dimensions, and most of them are in the form of lakes and ponds (Fig. 11).

The comparison between the wetlands of the Romanian sectors and those present on the territory of the Republic of Moldova is interesting. In the later case, the wetlands and open waters density is much higher. The drainage of this territory has been weak and the relief morphology allowed the occurrence and existence of a large number of wetlands (Fig. 2).

5. Conclusion

The inventory and classification of the wetlands and deep waters from Romania and especially of those of the Moldavian Plateau is the first detailed study for wetlands in this region of Romania. The methodology used in the present study follows the trends and methodology proposed by several North-American and European universities.

Although the Moldavian Plateau is situated in the eastern part of Romania in a region with a continental climate with excessive features, some of the most interesting and the largest wetlands in Romania can be found here, with the exception of the wetlands of the Danube Delta. This is due to the existence of an impermeable clayey substratum and to the artificial pond creation traditions. Hence, most of the wetlands and open waters are anthropic in nature, because the local population had to construct such ponds in this semiarid climate.

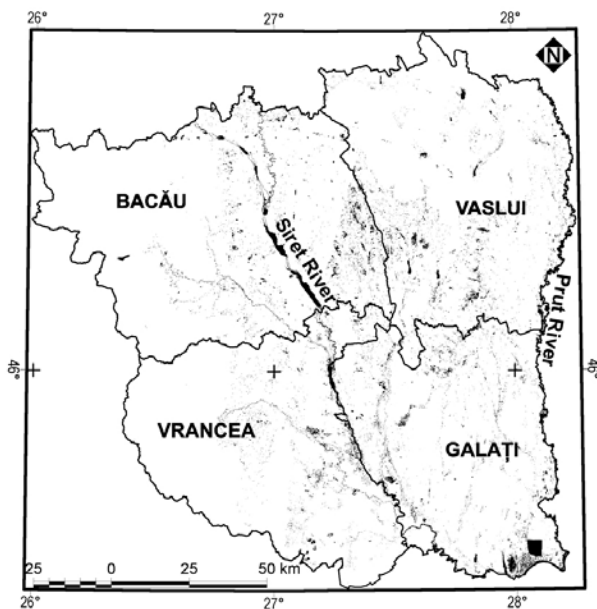


Fig. 8 Wetland repartition in the southern part of the Moldavia.

Table 1 Wetland presence for various types on relief units.

Wetland type	Administrative Moldavia		Romanian plain		Moldavian plateau	
	Polygon number	Surface (km ²)	Polygon number	Surface (km ²)	Polygon number	Surface (km ²)
Wetland vegetation	339	313.81	42	32.32	109	106.01
Floodplains	486	384.53	36	74.31	198	46.31
Lakes	189	301.79	12	16.85	51	127.12
-	Administrative Moldavia		Romanian plain		Moldavian plateau	
Length of water courses (km)	5,246		589.71		1,466.21	

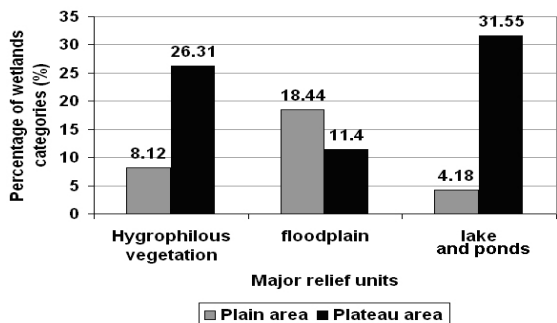


Fig. 9 The percentage distribution of wetlands in relation to the major relief units (Vaslui, Bacău, Vrancea and Galați Counties).



Fig. 11 An example of an wetland area of the pond situated in upstream Ciric reservoir, Iasi County.

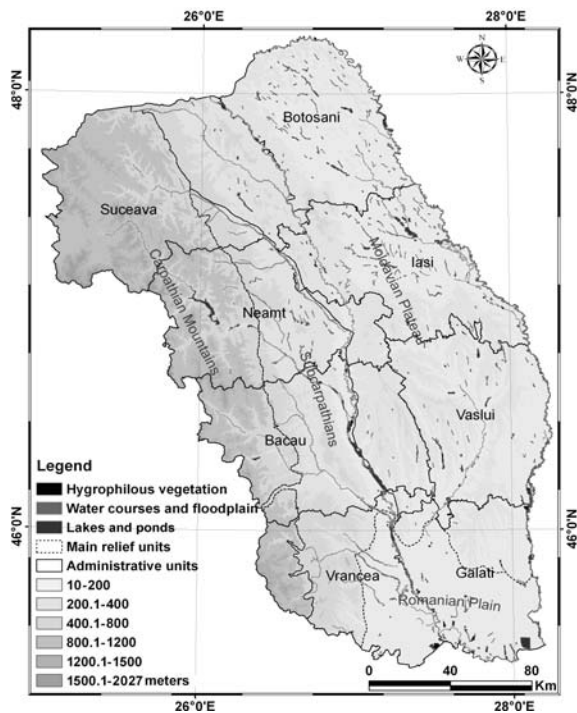


Fig. 10 Wetland distribution in the Moldavian Plateau and neighboring mountainous regions.

Wetland typology outlined the existence of numerous features specific to the relief units of medium and low altitudes [53]. Unfortunately, the largest part of the lacustrine wetlands is under the

presently negative influence of the human factor. The global climatic changes that lead to aridization, or even desertification, also have the potential to natural reduced the surface of the wetlands which are dependent of the aquifer strata and of the river floods. Valley aggrading, especially in the southern part of the plateau, presently leads to a rapid disappearance of the wetlands from the main floodplains.

The most rapid and economically effective way to restore wetlands that the authors recommend would be the return of the wetlands to their natural state. For this purpose, several controversial measures such as the removal of the flood protection dikes and water transfers from other watersheds may be required for the restoration of the biological fund.

Acknowledgments

The authors would like to acknowledge the support of the CNCIS Department, Romanian Ministry of Education, through a research grant (No. 145 and 426) and of the Geoarchaeology Laboratory of the “Alexandru Ioan Cuza” University of Iasi, Romania. The authors would also like to thank Dr. Petre Plaru

from the Water Direction Siret and Ursu Adrian from the Department of Geography of the “Alexandru Ioan Cuza” University of Iasi, Romania for their logistic support. This manuscript greatly benefited from suggestions provided by two anonymous reviewers.

References

- [1] G. Romanescu, C.C. Stoleriu, A. Ursu, Inventory and Typology of Wetlands and Deep Waters from Moldavian Plateau, Publisher Terra Nostra, Iasi, Romania, 2008, pp. 42-72. (in Romanian)
- [2] L.M. Cowardin, V. Carter, F.C. Golet, E.T. LaRoe, Classification of wetlands and deepwater habitats of the United States, U.S. Fish and Wildlife Science Report FWS/OBS-79/31, 1979, pp.1-79.
- [3] P.R. Adamus, E.J.Jr. Clairain, R.D. Smith, R.E. Young, Wetland Evaluation Technique (WET), Volume II: Methodology, Operational Draft, US Army Engineer Waterways Experiment Station, Vicksburg, MS, 1987, pp. 1-968.
- [4] Environmental Laboratory, Corps of Engineers Wetlands Delineation Manual, Technical Report Y-87-1, U.S. Army Engineer Waterways Experiment Station, Vicksburg, Miss, 1987.
- [5] Office of Wetlands Protection, Wetland Identification and Delineation Manual (2 volumes), Environmental Protection Agency, Washington DC, 1988, pp. 1-63.
- [6] FICWD (Federal Interagency Committee for Wetlands delineation), Federal Manual for Identifying and Delineating Jurisdictional Wetlands, US Government Printing office, Washington DC, 1989, pp. 1-86.
- [7] P. Devillers, J. Devillers-Terschuren, P. Ledant, CORINE-Biotopes Manual, Habitats of the European Community, Data Specification Part 2, Commission of the European Communities, Luxemburg, 1991, pp. 96-135.
- [8] W.J. Mitsch, J.G. Gosselink, Wetlands, Van Nostrand Reinhold Company, New York, 1993, pp. 172-235.
- [9] M.-C. Kovacsazy, The wetlands, Report of the Evaluation Committee, Publisher La Documentation Française, Paris, 1994, pp. 85-140. (in French)
- [10] R.W. Tiner, Wetland Indicators: A Guide to Wetland Identification, Delineation, Classification, and Mapping, Lewis Publishers, Boca Raton, FL, 1999, pp. 17-43.
- [11] G. Barnaud, A. Dausse, Towards a standardisation of the identification, determination, delimitation methods for wetlands?, ZH, Infos 29 (2000) 7-9. (in French)
- [12] G. Romanescu, I. Minea, A. Ursu, M.C. Margarint, C. Stoleriu, Inventory and Typology of Wetlands from Moldavian Plateau, A Study for Iasi and Botosani Counties, Publisher Didactica si Pedagogica, Bucuresti, Romania, 2005, pp. 42-54. (in Romanian)
- [13] G. Kafle, J.B. Karki, Flora and Fauna of Ghodaghodi Lake Area (A Pocket Guide), Nepal, 2008, pp. 1-52.
- [14] G. Kafle, M. Cotton, J.R. Chaudhary, H. Pariyar, H. Adhikari, S.B. Bohora, et al., Status of and threats to waterbirds of rupa lake, Pokhara, Nepal, Journal of Wetlands Ecology 1 (1/2) (2008) 9-11.
- [15] G. Kafle, Review on research and conservation of otters in Nepal, IUCN/SCC Otter Specialist Group Bulletin 26 (1) (2009) 1-62.
- [16] M. Schram, D. Darabaneanu, A. Alexievici, Contributions to study the bottom sediments of lakes from Moldavian Plain, Romania, 1970, pp. 33-39. (in Romanian)
- [17] N. Florea, I. Munteanu, R. Mandru, Romanian Terrains Affected by Water Excess, Bucuresti, Romania, 1972, pp. 35-86. (in Romanian)
- [18] M.W. Lefor, W.C. Kennard, Inland wetland definition, Stors, Report 28, Institute of Resources, University of Connecticut, Conn., 1977, pp. 1-63.
- [19] M.M. Brinson, A hydrogeomorphic classification for wetlands, Technical Report WRP-DE-4, US Army Engineer Waterways Experiment Station, Vicksburg, MS, 1993, pp. 1-103, available online at: <http://www.wes.army.mil/el/wetlands/pdfs/wrpde4.pdf>.
- [20] P. Bernard, Wetlands, The wetlands, Les zones humides, Inter-Ministry Committee for the Evaluation of Public Policies, Evaluation Report, Publisher La Documentation Française, 1994, pp. 1-62. (in French)
- [21] E. Fustec, B. Frochot, Functions and values of wetlands, Applied Geology Lab of Paris VI and Ecology Lab of Dijon, Water Agency Seine-Normandie, 1996, pp. 1-134. (in French)
- [22] M.M. Brinson, R.D. Smith, D.F. Whigham, L.C. Lee, R.D. Rheinhardt, W.L. Nutter, Progress in development of the hydrogeomorphyc approach for assessing the functioning of wetlands, in: Proceedings of INTECOL International Wetland Conference, Perth, Australia, 1998, pp. 135-188.
- [23] R.D. Smith, Hydrogeomorphic Approach to Assessing Wetland Functions: Guidelines for Developing Regional Guidebooks, Chapter 3: Developing a reference wetland system, ERDC/EL TR-01-29, US Army Engineer Research and Development Center, Vicksburg, MS, 2001, pp. 1-18.
- [24] D.A. Goode, The significance of physical hydrology in the morphological classification of mires, in: Proceedings of the International Symposium, Glasgow, Helsinki, 1974, pp. 1-36.
- [25] V. Carter, Wetland hydrology, water quality, and associated functions, in: National Water Summary on Wetland Resources, United States Geological Survey, Water-Supply Paper 2425, Washington D.C., 1986, pp.

- 35-48.
- [26] W.E. Spencer, Physiological response to flooding for wetland indicator plants, Technical Note VN-DL-1.1., US Army Engineer Waterways Experiment Station, Vicksburg, MS, 1994, pp. 1-3.
- [27] H. Bendjoudi, E. Fustec, Wetlands and water regime in functions and values of wetlands, University Paris VI and Dijon, Water Agency Seine-Normandie, 1996, pp. 1-194. (in French)
- [28] S.W. Sprecher, A.G. Warne, Accessing and using meteorological data to evaluate wetland hydrology, Technical Report ERDC/EL TR-WRAP-00-01, US Army Engineer Research and Development Center, Vicksburg, MS, 2000, pp. 1-12, available online at: <http://www.wes.army.mil/el/wrap/pdf/wrap00-1/wrap00-1.pdf>.
- [29] G. Romanescu, Floods as Risk Factor, A Study for Siret's Floods from July 2005, Publisher Terra Nostra, Iasi, Romania, 2006, pp. 36-71. (in Romanian)
- [30] G. Romanescu, Siret river basin planning (Romania) and the role of wetlands in diminishing the floods, WIT Transaction on Ecology and the Environment 125 (2009) 439-453.
- [31] G. Romanescu, C. Dinu, A. Radu, L. Torok, Ecologic characterization of the fluvial limans in the south-west Dobroudja and their economic implications (Romania), Carpathian Journal of Earth and Environmental Sciences 5 (2010) 25-38.
- [32] J.S. Nogueira, L. Sanches, O.B. Pinto-Junior, E.D. Almeida, Seasonal patterns of nitrogen and phosphorous in the litter and soil surface of transitional Amazon Cerrado forest, Brazil, Journal of Environmental Science and Engineering 5 (2011) 5-14.
- [33] R. Barbault, Biodiversity, Publisher Hachette Supérieur, Paris, 1997, pp. 75-98. (in French)
- [34] R.E. Stewart, Wetlands as bird habitat, in: National Water Summary on Wetland Resources, United States Geological Survey, Water-Supply Paper 2425, Washington D.C., 1996, pp. 49-56.
- [35] T.R. Wentworth, G.P. Johnson, R.L. Kologiski, Designation of wetlands by weighted averages of vegetation data: A preliminary evaluation, Water Resources Bulletin 24 (1988) 389-396.
- [36] P.J. Mulholland, E.J. Kuenzler, Organic carbon export from upland and forested wetland watersheds, Limnology and Oceanography 24 (1979) 960-966.
- [37] G.W. Hurt, V.W. Carlisle, Delineating hydric soils, in: J.L. Richardson, M.J. Vepraskas, (Eds.), Wetland Soils: Genesis, Hydrology, Landscapes, and Classification, Lewis Publishers, Boca Raton, FL, 2001, pp. 183-206.
- [38] M.E. Kentula, Wetland restoration and creation, in: National Water Summary on Wetland Resources, United States Geological Survey, Water-Supply Paper 2425, Washington D.C., 1996, pp. 87-92.
- [39] Report EPA, Freshwater wetlands for wastewater management: Environmental statement, Report EPA 904/9-83-107, Region IV USEPA, Atlanta, GA, 1983, pp. 1-86.
- [40] G. Barnaud, Conservation of Wetlands, Concepts and Methods Applied to Their Assessment, MNHN, Paris, 1998, pp. 295-322. (in French)
- [41] B.O. Wilen, V. Carter, R.J. Jones, Wetland mapping and inventory, in: National Water Summary on Wetland Resources, United States Geological Survey, Water-Supply Paper 2425, Washington D.C., 1996, pp. 73-78.
- [42] E. Barbier, M. Acreman, D. Knowler, Economic valuation of wetlands, A guide for policy makers and planners, Ramsar Convention Bureau, University of York, IUCN, Draft 9/02/96, 1996, pp. 33-61.
- [43] G. Romanescu, Wetlands—between preservation and eradication, in: The Geographic Scientific Seminar “Dimitrie Cantemir”, Iasi, Romania, 2004, pp. 115-126. (in Romanian)
- [44] V. Bacauanu, N. Barbu, M. Pantazica, A. Ungureanu, D. Chiriac, Moldavian Plateau-Nature, Human, Economy, Publisher Stiintifica si Enciclopedica, Bucuresti, Romania, 1980, pp. 10-25. (in Romanian)
- [45] M. Branzila, Geology of South Moldavian Plain, Publisher Corson, Iasi, Romania, 1999, pp. 25-64. (in Romanian)
- [46] E. Erhan, Preliminary study regarding the climatic resources of Moldova, in: The Geographic Scientific Seminar “Dimitrie Cantemir”, Iasi, Romania, 2001, pp. 130-139. (in Romanian)
- [47] M. Pantazica, Hydrography of Moldavian Plain, Publisher Junimea, Iasi, Romania, 1974, pp. 15-74. (in Romanian)
- [48] I. Ujvari, The Water Geography of Romania, Publisher Stiintifica, Bucuresti, Romania, 1972, pp. 488-558. (in Romanian)
- [49] INCDD, Satellite Images for Iasi, Botosani, Vaslui, Galati, Suceava, Neamt, Bacau and Vrancea counties, INCDD, Tulcea, Romania, 2000.
- [50] IGFCOT, Topographic Maps, Publisher IGFCOT, Scara 1:50000, Bucuresti, Romania, 1978.
- [51] IGFCOT, Cadastral Maps, Publisher IGFCOT, Bucuresti, Romania, 1978.
- [52] V. Baican, The Geography of Moldova Reflected in Cartographic Maps from XVIII Century, Publisher Academia Romana, Bucuresti, Romania, 1996, pp. 13-24. (in Romanian)
- [53] M.A. Khan, Environmental contamination of hokersar wetland waters in Kashmir Himalayan valley, India, Journal of Environmental Science and Engineering 52 (2010) 157-162.

Test Bench for the Mechanical Distribution of Predators to Control Insect Pests

M. Khelifi, F. Paré and M. Aider

Department of Soil Science and Agri-Food Engineering, Université Laval, Quebec City G1V 0A6, Canada

Received: May 13, 2011 / Accepted: June 7, 2011 / Published: November 20, 2011.

Abstract: In agriculture, chemical insecticides are widely used to protect crops from insect pests. Over a period of years, some insects such as Colorado potato beetle (CPB) succeed in developing resistance to most of the registered chemical insecticides. Consequently, heavy applications of chemical insecticides to control this pest become ineffective on a long-term basis and can lead to serious health and environmental problems. The use of natural enemies to control CPB is an interesting alternative to chemical means. However, hand release of predators is not feasible on a large scale in the field. The main objective of this research study was to design and build a test bench to investigate the technical feasibility of mechanically releasing predators. The test bench consisted of a vertical chain conveyor mounted on two vertical shafts driven by an electric motor. Since the predators are small and fragile, they were placed in a specially designed container to preserve their physical integrity. Trials using this test bench showed that a carrier material was required, because most of the predators remained inside the container. The success of this mass predator release system will be highly valuable for the biological control of insect pests in many crops.

Key words: Insect pests, chemical insecticides, biological control, natural enemies, mass release, mechanical distributor.

1. Introduction and Literature Review

In agriculture, the most common way to protect crops against insect pests is regular applications of chemical insecticides. However, some insects such as Colorado potato beetle, *Leptinotarsa decemlineata* (Say), manage to develop resistance over time to most registered insecticides used for their control [1-3]. Currently, Colorado potato beetle is developing resistance to the imidacloprid-based insecticide Admire, an effective insecticide widely used since 1995 to control this insect pest [4-6]. As a result, massive applications of chemical insecticides to control such pests in potato crops become ineffective on a long-term basis [7] and may result in serious health and environmental problems. One of the most promising alternatives to the regular use of chemical insecticides is the use of natural predators to control

Colorado potato beetle populations. This biological and sustainable alternative strategy is the least developed in North America [8]. The effectiveness of the use of the predator stink bug *Perillus bioculatus*, which is indigenous to Quebec, as a natural predator to control Colorado potato beetle has been demonstrated on a small scale [9-12]. The effectiveness of *P. bioculatus* on a large scale has not been demonstrated, however, because hand release of this predator is not only time-consuming and labour-intensive but not even feasible.

The main challenge is therefore to identify the optimal method for mechanically releasing these small and fragile predators while preserving their physical integrity. The use of a mechanical release system must not inflict any damage on the predators, or else the viability of the control method would be compromised. For that reason, the release system has to be designed in a way that takes into account the physical characteristics of the predators (second-instar nymphs)

Corresponding author: M. Khelifi, associate professor, Ph.D., main research field: power and machinery. E-mail: mohamed.khelifi@fsaa.ulaval.ca.

and the distribution method. According to Ref. [13], the predators are capable of scattering after being released, as shown in Fig. 1, to look for food. It would be therefore more appropriate to opt for a source-point mass release rather than uniformly releasing the predators over the entire field.

Some attempts have been made to build mechanical release systems to control pest insects. Giles et al. [14] developed a mechanical system for the field distribution of predacious mites that was used to release commercial formulations of vermiculite carrier and *Phytoseiulus persimilis* in strawberry crops. Those authors found that the mechanical distributors permitted the uniform, accurate and controllable release of the mites. A similar design consisting of a rotary-disc fertilizer distributor was used by Grundy and Maelzer [15] to release the predator *Pristhesancus plagipennis* (Walker) (Hemiptera: Reduviidae). Nymphs of this predator were also mixed with vermiculite. That distribution method made it possible to establish and disperse nymphs in soybean, cotton and sunflower crops in a manner comparable to manual distribution.

Currently, the scientific and technical literature on the mechanical distribution of predators to control Colorado potato beetle is limited, and it also seems that no large-scale mechanical release systems for predators such as *P. bioculatus* are available on the market.

The main objective of this research study was to design and build a test bench to investigate the

technical feasibility of mechanically releasing large numbers of predators while preserving their physical integrity. If a mechanical system can safely release such predators, it will be possible to use this sustainable and environmental alternative on a large scale.

2. Design of the Test Bench

2.1 Design Criteria

The goal was to design a simple and efficient release system that could be mounted on a standard three-point tractor hitch and powered by the tractor's hydraulic or electrical system. Thus the release system would be compatible with any existing tractor equipped with a hydraulic or electrical system would be less expensive and would not require any specific operator training. The release system was intended for use with *P. bioculatus*, but the concept can be generalized for other predators to control insect pests in various crops. The system was designed to release large numbers of predators, at a rate of up to 75,000 second-instar nymphs per hectare. With such a release rate, adequate control of Colorado potato beetle in highly infested potato crops could be achieved. However, the number of predators that should be released in the field remains closely related to the population of Colorado potato beetles settled on potato plants.

Given that second-instar nymphs are known to be capable after release of dispersing in the field to

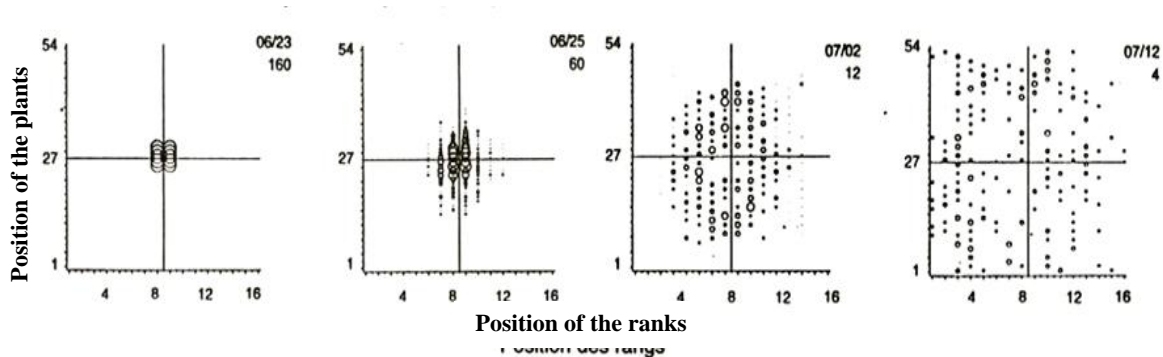


Fig. 1 Dispersion of second-instar *Perillus bioculatus* nymphs over time following a drop in the centre of a plot measuring 0.025 ha [13].

search for prey [16, 17], it was decided to opt for a source-point release approach. It was also decided to prevent any mechanical contact between the predators and moving parts in the release system, because the nymphs are small and fragile.

2.2 Laboratory Test Bench

Based on the source-point mass release approach, the concept of a conveyor of containers was selected. A vertical chain conveyor mounted on two vertical shafts driven by an electric motor (DC motor, model 0637, Emerson Electric Company, St. Louis, MO, USA) was therefore designed and built (Fig. 2). The release system carried a number of containers that could be opened to drop all the predator larvae at once when needed. The main idea behind using such containers was to eliminate any possible mechanical contact that could injure the predators. The number of predators per container would depend on the level of infestation and would need to be determined following field monitoring.

Each container was mounted on the chain using a sliding support (Fig. 3) to allow the container to be quickly and securely inserted and removed from the release system. The concept was simple enough to allow any producer to manually place the containers on the conveyor. At one end of the container, a trap held closed with a hinge spring was installed. When the container crossed a plastic rail (Fig. 4), the trap opened to allow the predators to drop to the ground. Fig. 4 also shows a container that is fully opened. The container was transparent to allow the behaviour of the predators to be viewed during the trials. The speed of the conveyor could be adjusted using a frequency modulator (Multi-drive, DC motor speed control, Penta KB Power No. 07114, Coral Springs, FL., USA).

3. Evaluation of the Test Bench

3.1 Preliminary Test

Preliminary tests were performed to evaluate the

test bench. Different conveyor speeds (2.5, 15 and 30 cm/s) were also tested. The most important observation resulting from these preliminary tests was that most of the larvae had the reflex to firmly cling to the inside walls of the containers, climb as far as they could to the top of the containers, and hence remain inside. To remedy this problem, a carrier material was required. Many carrier materials, namely peat, sawdust, cedar mulch, perlite, vermiculite, wood shavings, thin wood chips and charcoal, were then investigated (Fig. 5). For each test, 10 larvae mixed with 100 mL of a carrier material were used.

The results of the carrier material tests show that thin wood chips were the most appropriate carrier material. Thin wood chips are not compact or dusty, and they provide more space than the other materials to let the larvae move freely inside the containers. It was also concluded that it would be useful to remodel the container slightly and fill it completely with the carrier material to prevent the larvae from climbing to the top and clinging to the inside walls.

3.2 Main Tests

Based on the preliminary testing observations, some modifications were made to the container (Fig. 6) to prevent any possibility of the carrier material being retained inside the container.

Thin wood chips were used as the carrier material. It was also decided to test another carrier material, popcorn, which is also light, not compact and inexpensive. Popcorn seems to have the potential to protect predators and offer them great freedom of movement. The volume of the carrier material was set to 500 mL to completely fill each container during the experiments. The number of predator larvae in each container was increased in the same proportion, i.e. from 10 to 50 per container.

Under real field conditions, the release system would certainly be subject to strong vibrations. For this reason, only the highest speed, which generated the most vibrations, was used for the main tests (30

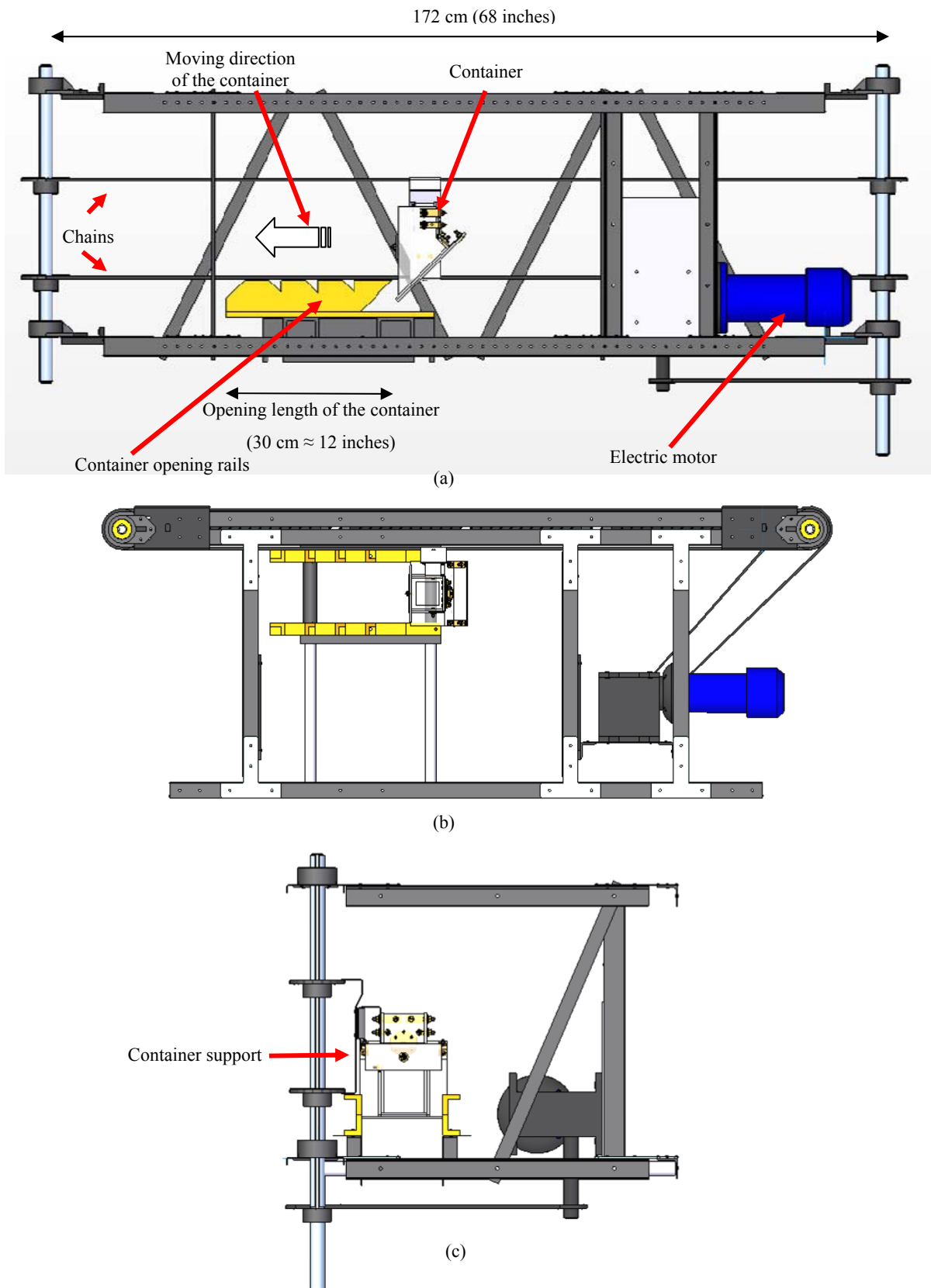


Fig. 2 Predator release system: (a) general view; (b) top view; and (c) side view.

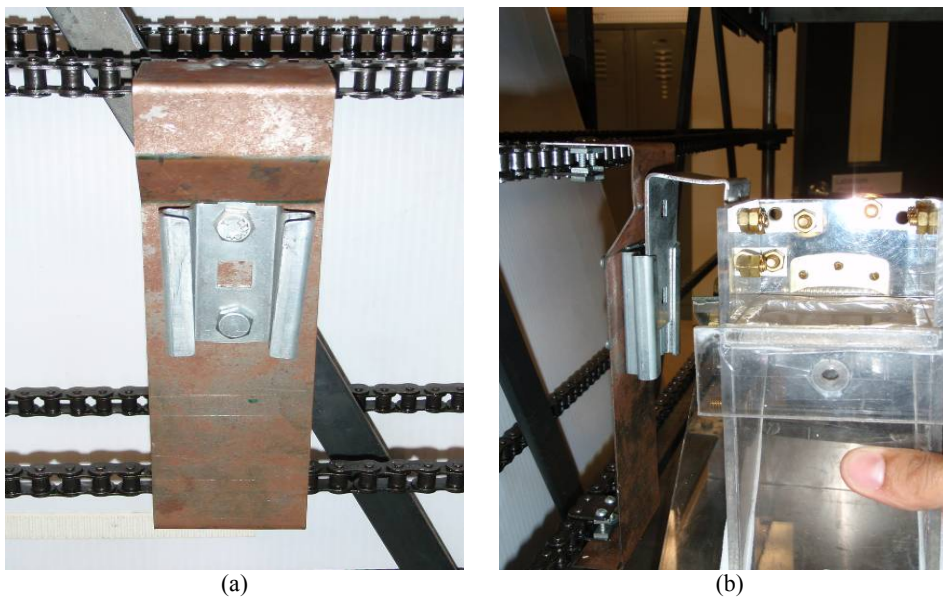


Fig. 3 Sliding support for the containers: (a) front view; and (b) side view.



Fig. 4 Plastic rail used to open the containers; the diagonal notches allowed the nymph predators remaining inside the container to be shaken out.

cm/s). This speed also allowed the containers to open quickly (in 1 s) to release their contents. The trials were carried out using two groups of larvae from two different generations, making it possible to check the effect of generation on the grasping ability of the larvae, which could represent a source of variation between predators. For each trial, 50 new larvae were used, and the mechanical system was activated for 15 min to subject the larvae to the same stress that they would likely experience during transportation and release in the field. The larvae were counted before and immediately after each release to determine the release rate. Each trial was replicated three times.

An analysis of variance (ANOVA) was performed

on the data using the GLM procedure of the SAS software program (SAS 2005) [18]. The measured variable was the release rate, and the independent variables were the generation of the predators (block) and the carrier material (thin wood chips and popcorn).

The ANOVA results presented in Table 1 reveal that there is no significant difference between the use of thin wood chips and the use of popcorn as the carrier material ($P = 0.6823$). Both carrier materials resulted in comparable release rates (Fig. 7). The rates are remarkable, because most of the predators successfully left the containers once they had been opened. This result clearly indicates that the



Fig. 5 Different carrier materials tested.

mechanical release system was appropriate for the mass release of young predators regardless of the carrier material.

The results also indicate no significant effect of generation on the release rates of predator larvae ($P = 0.0648$). It can therefore be presumed that the ability to cling to the inside of the containers was comparable for both generations of larvae.

The release of predator larvae using this mechanical system was successful, a result that indicates that this technique could be easily applied in potato fields to

control Colorado potato beetle. However, it would be appropriate to investigate the survival of young predators after mechanical release. Further testing is therefore required to check whether the mechanical release system preserves the physical integrity of the predator larvae. This testing could be achieved by observing the development of the larvae from the time of mechanical release until their passage to another growing stage.

The containers used in the experiments were intentionally oversized to provide a clear idea of the

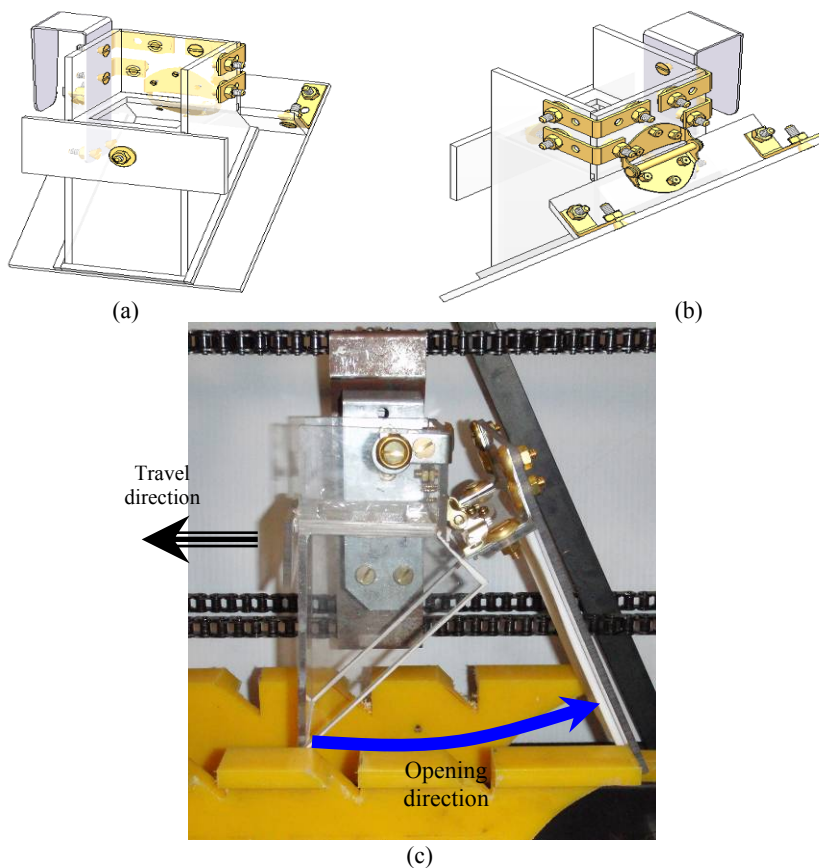


Fig. 6 Final design of the container: (a) front view; (b) top view; and (c) general view.

Table 1 ANOVA results for release rate efficiency.

Source of variation	DF	F-values	Pr > F
Block	1	4.42	0.0648 NS ^[a]
Carrier material	1	0.18	0.6823 NS
Error	9		

^[a] NS = not significant.

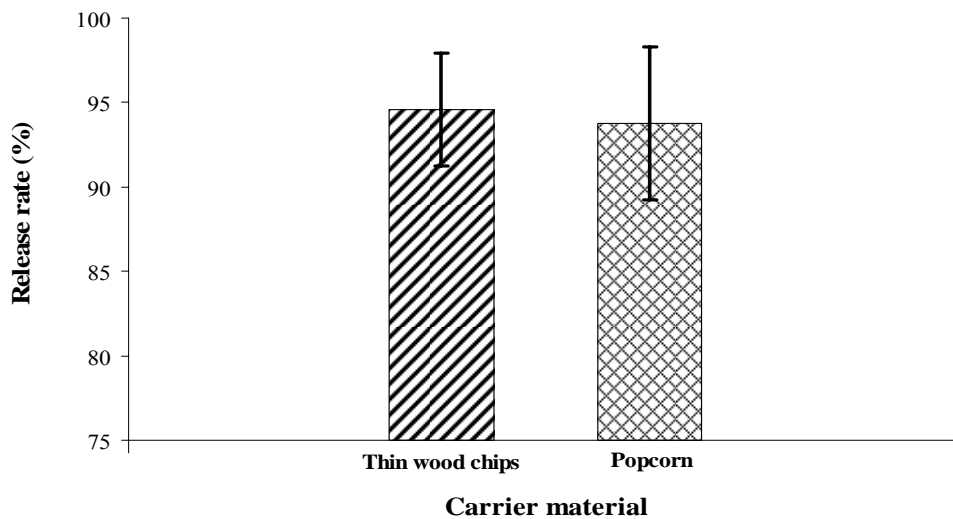


Fig. 7 Mean release rates for the predator larvae according to the carrier material.

behaviour of the predator larvae alone or when mixed with a carrier material. All the observations made throughout the experiments, in particular during the preliminary testing, were indeed highly valuable for refining the design of the release system and choosing the most appropriate carrier material. Based on the size of the predator larvae, the size of the containers could be further reduced.

4. Conclusions

- The results of the preliminary tests clearly show that it is necessary to use a carrier material to enhance the release of the predator larvae. The containers have to be completely filled with the carrier material to prevent the predator larvae from clinging to the inside walls of the containers.

- The preliminary tests also made it possible to establish the optimal characteristics for the most efficient carrier material: the material must be light and non-compact and must allow the predator larvae to move inside the container. The carrier material should also be easy to discharge from the container. The main tests proved that the mechanical release system is efficient in releasing masses of young predators. Indeed, most of the predators were successfully evacuated from the release containers.

- Thin wood chips and popcorn are the most appropriate carrier materials for enhancing the release of the predator larvae from the containers.

Acknowledgments

The authors gratefully acknowledge the financial support of the Natural Sciences and Engineering Research Council of Canada (NSERC).

References

- [1] A.J. Forgash, Insecticide resistance of the Colorado potato beetle, *Leptinotarsa decemlineata* (Say), in: J.H. Lashomb, R. Casagrande (Eds.), *Advances in Potato Pest Management*, Hutchinson Ross Publishing Co, Stoudsburg, 1981, pp. 34-46.
- [2] H. Parry, C.R. Harris, Insecticide resistance in New Brunswick populations of the Colorado potato beetle (Coleoptera: Chrysomelidae), *Canadian Entomologist* 119 (1987) 459-463.
- [3] M.E. Whalon, D.L. Miller, R.M. Hollingworth, E.J. Grafius, J.R. Miller, Selection of a Colorado potato beetle (Coleoptera: Chrysomelidae) strain resistant to *Bacillus thuringiensis*, *J. Economic Entomology* 86 (1993) 226-233.
- [4] A. Alyokhin, Colorado potato beetle management on potatoes: Current challenges and future prospects, in: P. Tennant, N. Benkeblia (Eds.), *Fruit, Vegetable and Cereal Science and Biotechnology, Special Issue 1*, Global Science Books, 2009, pp. 10-19.
- [5] A. Alyokhin, G. Dively, M. Patterson, C. Castaldo, D. Rogers, M. Mahoney, et al., Resistance and cross-resistance to imidacloprid and thiamethoxam in the Colorado potato beetle *Leptinotarsa decemlineata*, *Pest Mgmt. Sci.* 63 (2007) 32-41.
- [6] D. Mota-Sanchez, R.M. Hollingworth, E.J. Grafius, D.D. Moyer, Resistance and cross-resistance to neonicotinoid insecticides and spinosad in the Colorado potato beetle, *Leptinotarsa decemlineata* (Say) (Coleoptera: Chrysomelidae), *Pest Mgmt. Sci.* 62 (2006) 30-37.
- [7] D.N. Ferro, Biological control of the Colorado potato beetle, in: G.W. Zehnder, M.L. Powelson, R.K. Jansson, K.V. Raman (Eds.), *Advances in Potato Pest Biology and Management*, American Phytopathological Society Press, Minnesota, 1994, pp. 357-375.
- [8] M. Khelifi, C. Laguë, Y. de Ladurantaye, Physical control of Colorado potato beetle: A review, *Applied Engineering in Agriculture* 23 (2007) 557-569.
- [9] T. Jermy, The introduction of *Perillus bioculatus* into Europe to control the Colorado beetle, *European and Mediterranean Plant Protection Organization Bulletin* 10 (1980) 475-479.
- [10] J. Hough-Goldstein, J. Whalen, Inundative release of predatory stink bugs for control of Colorado potato beetle, *Biological Control* 3 (1993) 343-347.
- [11] J. Hough-Goldstein, J.A. Janis, C.D. Ellers, Release methods for *Perillus bioculatus* (F.), a predator of the Colorado potato beetle, *Biological Control* 6 (1996) 114-122.
- [12] C. Cloutier, G. Boiteau, M.S. Goettel, *Leptinotarsa decemlineata* (Say), Colorado potato beetle (Coleoptera: Chrysomelidae), in: P.G. Mason, J.T. Huber (Eds.), *Biological Control Programmes in Canada, 1981-2000*, CABI Publishing, Wallingford, U.K., 2002, pp. 145-152.
- [13] S. Lachance, Lutte biologique contre le doryphore de la pomme de terre par des lâchers inondatifs de la punaise *Perillus bioculatus*: Facteurs influençant la dispersion du prédateur (Biological control of the Colorado potato by inundative release of the stinkbug *Perillus bioculatus*:

- Factors affecting the dispersal of the predator), M.Sc. Thesis, Department of Biology, Université Laval, Quebec City, QC, Canada, 1996.
- [14] D.K. Giles, J. Gardner, H.E. Studer, Mechanical release of predacious mites for biological pest control in strawberries, *Transactions of the ASABE* 38 (1995) 1289-1296.
- [15] P.R. Grundy, D.A. Maelzer, Factors affecting the establishment and dispersal of nymphs of *Pristhesancus plagipennis* Walker (Hemiptera: Reduviidae) when released onto soybean, cotton and sunflower crops, *Australian Journal of Entomology* 41 (2002) 272-278.
- [16] S. Lachance, C. Cloutier, Factors affecting dispersal of *Perillus bioculatus* (Hemiptera: Pentatomidae), a predator of the Colorado potato beetle (Coleoptera: Chrysomelidae), *Environmental Entomology* 26 (1997) 946-954.
- [17] C. Cloutier, Facilitated predation through interactions between life stages in the stinkbug predator *Perillus bioculatus* (Hemiptera: Pentatomidae), *J. Insect Behavior* 10 (1997) 581-598.
- [18] SAS OnlineDoc, Ver. 9.1.3, available online at: <http://support.sas.com/documentation/onlinedoc/91pdf/index.html>.

Economic Analysis of CO₂ Emission Abatement Applying a Dynamic CGE Model with Endogenous Technological Change: Impacts of the Time Horizon

K. Matsumoto

School of Environmental Science, University of Shiga Prefecture, Hikone 5228533, Japan

Received: April 14, 2011 / Accepted: May 11, 2011 / Published: November 20, 2011.

Abstract: We evaluate economic and environmental impacts of climate change mitigation in a country scale considering various time horizons in the analysis applying a single-country dynamic computable general equilibrium model with endogenous technological change. Although there is a possibility that Gross Domestic Product (GDP) becomes larger for the abatement cases than the baseline case in the earlier years, it tends to be lower than that in the later years. The longer the time horizon and/or the more severe the abatement, the larger the negative impacts will be. When subsidizing R&D investment, increase in GDP compared to the baseline case is realized in the middle of the time horizon, and the larger increase tends to be observed for the longer-term cases. These results would be due to technological change induced by the subsidies and emission abatement. Environmental indicators are also improved. We showed that the results were influenced by the target time horizon when using an intertemporal dynamic model.

Key words: Endogenous technological change, intertemporal dynamic CGE, time horizon, economic impact, climate change policy.

1. Introduction

Climate change is one of the most significant environmental issues for the present society and policy discussions from mid- to long-term perspectives are continuing all over the world. Although the expected new protocol for the Post Kyoto Protocol was not established, the Copenhagen Accord was made at the fifteenth Conference of the Parties (COP) of the United Nations Framework Convention on Climate Change (UNFCCC) in 2009. Based on the accord, the Annex I countries of UNFCCC and some major non-Annex I countries such as China submitted their pledge on greenhouse gas (GHG) emission abatement [1]. As former Prime Minister of Japan, Yukio Hatoyama, stated at the United Nations Summit on Climate Change on September 22, 2009, the target Japanese government

submitted was a 25% abatement compared to the 1990 level. His cabinet had also submitted the Basic Act on Global Warming Countermeasures to the ordinary Diet session in 2010, which was later scrapped off. Promotion of innovative technological development has been one of the fundamental measures and policies in it. Furthermore, a target was set to raise the research and development (R&D) investment of the total private and governmental sectors to 4% of Gross Domestic Product (GDP) by 2020FY following the New Growth Strategy (Framework) determined at the extraordinary cabinet meeting on December 30, 2009. The Kan cabinet on June 18, 2010 then decided the New Growth Strategy. International actions considering the relationships between climate change measures, R&D investment, technological development, and economy preceded such movements [2, 3].

Corresponding author: K. Matsumoto, assistant professor, Ph.D., main research fields: environmental economics and policy. E-mail: matsumoto.k@ses.usp.ac.jp.

In order to address the additional costs and economic impacts that accompany the climate change

mitigation measures, importance of technological development and its diffusion is being particularly emphasized globally in the recent years. Technological change can be understood as an increase in outputs possible from a given level of inputs through the process of invention, innovation, and diffusion [4]. In other words, inputs such as natural resources necessary to produce a certain amount of outputs are reduced. Especially, a decline in fossil fuel requirement can be connected directly to mitigation in climate change. Thus, handling endogenous technological change (ETC) in the economic models would be of much significance for analyzing the relationships between climate change and its measures, technology, and economy as ETC implies incorporating a feedback mechanism by which policy can direct technological change towards carbon-saving technology [4]. However, computable general equilibrium (CGE) models that have been frequently used for economic analysis of climate change issues and its measures have considered the technological change as exogenous [4-7] and those with ETC are rare [4, 8-14]. In addition, several methods have been proposed for modeling ETC and no consolidation of the methods has been postulated [15]. When modeling ETC, mainly two methods have been suggested, the first being R&D investment and the second is technology learning. The latter is generally used in bottom-up models and the former is more appropriate for CGE models [14].

One of the most important studies of recent years on technological change and knowledge capital carried by Romer [16] examines the relationship between knowledge accumulation and technological change considering knowledge as one of input factors. This framework has also been applied to economic analysis in the environmental and energy fields that are closely related to climate change issues [8-14]. This is due to growing importance of climate change as one of the most significant social issues and the relevant policies are closely knitted to R&D

investment, resulting in technological changes.

In our previous study [17], a single-country dynamic CGE model with ETC targeting the Japanese economy had been developed. In the model, ETC is expressed as the accumulation of knowledge capital through R&D investment like the above studies. The study analyzes economic impacts of CO₂ emission abatement and subsidies on R&D investment, and finds that there is a possibility to have positive effects on economy when CO₂ emissions are abated. However, as it is assumed that the target period is between 2005 and 2020, such a short period would be insufficient for this kind of analysis, because climate change is a longer-term issue. Moreover, since the dynamic structure of the model is an intertemporal optimization type, the results can be affected by the time horizon. The purpose of this study is to analyze economic and environmental impacts of CO₂ emission abatement considering longer periods applying the abovementioned CGE model. We consider year 2020, 2030, 2050, and 2100, respectively, as the terminal points (i.e. planning periods).

2. Model

In order to analyze the economic impacts when CO₂ emissions are abated and technology is changed, a dynamic CGE model installing R&D investment and knowledge capital has been developed [17]. The model is a single-country (Japan) model and consists of 33 industrial sectors (Table 1). Knowledge capital appears in the production and dynamics. The summary of the model is described below (see Ref. [17] for the details).

2.1 General Structure and Data

In this study, the social accounting matrix (SAM) is developed based on the 2005 Input-Output Table for Japan. For households, government, and abroad, only one sector exists for each. The labor and capital tax data are from the System of National Accounts of Japan. The data on knowledge capital and R&D

Table 1 Classification of industrial sectors.

Code	Classification	Code	Classification
AGR	Agriculture, forestry, fisheries	ITQ	Information equipment
MIN	Mining	ECM	Electronic components
COA	Coal	TRQ	Transportation equipment
OIL	Crude oil	PRQ	Precision instruments
GAS	Natural gas	OMF	Other manufacturing
FOD	Foods	CNT	Construction
TEX	Textile	ELE	Electricity
PPP	Pulp, paper, wood	GSH	Gas & heat supply
CHE	Chemical	WTR	Water supply
PPR	Petroleum products	WST	Waste management
CPR	Coal products	COM	Commerce
CLY	Ceramic, stone, clay	FIN	Finance
STL	Ferrous metal	EST	Real estate
NFE	Non-ferrous metal	TRN	Transportation
MET	Metal products	ICT	Communication
MCH	General machinery	OSV	Other services
ELQ	Electric machinery		

investment are not represented in the Input-Output Table. The estimation method is described in section 2.4.

The data on CO₂ emissions are based on the Energy Balance Table for Japan 2005, in which emission data by energy and sector, including households, are shown. Direct CO₂ emissions are taken into account in the model.

2.2 Production Structure

Each industrial sector performs production activities using domestic and imported intermediate inputs and production factors owned by the household sector, and pays production tax to government. When energy goods are consumed, CO₂ emission permits corresponding to the amount of emissions from energy use are required. The model uses nested CES (constant elasticity of substitution) functions. The substitution relationship of knowledge capital is considered at the top level of the functions as in existing studies [8, 10, 12-14]. For the elasticity of substitution between knowledge capital and other inputs, several values are used in the literature. For example, Otto et al. [12], Sue Wing [13], and some

other studies use 1.0, Wang et al. [14] use 2.5, and Sue Wing [18] suggests 0.5-2.0. Thus, we use 1.5 for the value, being approximately the central value. According to our previous study [19], the difference of the substitution parameter does not largely affect the overall results and only affect the degrees of the changes. Thus, we do not conduct sensitivity analysis for the substitution parameter.

2.3 Household Consumption and Government Structure

The household sector determines its consumption and saving to maximize the present discounted value of the utility based on its consumption. It earns its income from labor and capital (physical and knowledge capital) supply, pays taxes imposed on its income, and consumes goods as Armington aggregations. It is also required to hold emission permits for energy use just as the industrial sectors are. The household utility function is a nested CES function. The intertemporal elasticity of substitution is 0.5 in the model.

Government determines its expenditure subject to its budget obtained from taxes (minus subsidies) and emission permit revenue. In this study, it is assumed that government allocates emission permits by auction when implementing CO₂ emission abatement measures. The government expenditure is also a nested CES function.

2.4 Endogenous Technological Change

Knowledge capital is used as a production factor and modeled to demonstrate the link between the knowledge accumulation and technological change based on the concept of endogenous growth theory [13, 20, 21]. It is accumulated due to R&D investment, the scale of which is determined endogenously in dynamic structure. This technological change affects economic growth, energy use, and CO₂ emissions. Knowledge capital is assumed to be distributed throughout the economy as well as physical capital.

Since both R&D investment and knowledge capital are not disaggregated in the Input-Output Table for Japan, they are estimated using the method of Terleckyj [22, 23]. First, the amount of R&D investment by sector is estimated based on the total expenditure on R&D of the Survey of Research and Development for Japan 2005. Knowledge factors are then separated from the intermediate input matrix of SAM using the data.

2.5 Dynamic Structure

Consideration of the temporal aspect is indispensable for analyzing the changes in environment and economy. Furthermore, the determination of the investment amount is a significant issue for this analysis. Thus, dynamic structure based on the Ramsey growth model, an intertemporal optimization, is applied in the model. In the Ramsey model, households maximize the present discounted value of the utility based on their consumption as shown in the Eqs. (1-5):

$$\max \sum_{t=0}^{\infty} \left(\frac{1}{1+\rho}\right)^t U(C_t) \quad (1)$$

$$\text{s.t. } Y_t = F(K_t, KNC_t, L_t) = C_t + I_t + RDI_t \quad (2)$$

$$K_{t+1} = (1-\delta)K_t + I_t \quad (3)$$

$$KNC_{t+1} = (1-\mu)KNC_t + RDI_t \quad (4)$$

$$L_{t+1} = (1+g)L_t \quad (5)$$

Where, $U(\cdot)$: utility function, $f(\cdot)$: production function, C_t : consumption, Y_t : income, K_t : physical capital, KNC_t : knowledge capital, L_t : labor, I_t : physical capital investment, RDI_t : R&D investment, ρ : discount rate, δ : depreciation rate of physical capital, μ : depreciation rate of knowledge capital, g : increase rate of labor, t : time.

To solve such dynamic models, it must be ensured that a dynamic stable equilibrium exists and the solution converges to the stable equilibrium from the initial state. However, it is not certain that the arbitrary initial state satisfies such conditions. Thus, it is often assumed that the initial state is also a stable equilibrium for analysis using this kind of dynamic

model [24-26]. The amount of investment is adjusted following these examples.

In this type of dynamic model, household sectors determine the optimum combination of their consumption and saving from the infinite horizon optimization problem. However, because it is not possible to consider infinite time in simulation analysis, a finite time is considered instead and the solution at the terminal point must be identical to that for infinite time. Thus, elaborating the condition under which rise in investment becomes equal to the economic growth rate at the terminal point is estimated [27]. In addition, the increase rates of labor in efficiency units, budget deficit, and current-account surplus are assumed to be equal to the growth rate (of the baseline case) to confirm the dynamic stable equilibrium condition from the initial to terminal points.

3. Baseline and Scenarios

3.1 Baseline Settings

Dynamic analysis is implemented from year 2005 (base year) to 2100 (interest rate: 5%/yr), because calculation until 2020, 2030, 2050, and 2100 brings identical results for the baseline case. Economic growth depends on labor (increase rate: 1%/yr) and capital accumulation. Physical capital and knowledge capital are accumulated through investment on each and assumed to be depreciated at 5% and 15% per annum, respectively. The range of the depreciation rate of knowledge capital is broad such as 9-15% [13] and 18-35% [12]. Thus, the above value, being approximately the central value, is adopted in this study. It has been proved that the difference of the depreciation rate does not largely affect the overall results according to our previous analysis [17], thus we do not conduct sensitivity analysis for the depreciation rate in this paper.

3.2 Scenario Cases

In this study, scenario cases in which emissions are

abated from 10% to 50% at the terminal points compared to the baseline case are analyzed to understand the economic impacts. In addition, larger abatement cases are calculated for the longest one. In each case, emission abatement starts in 2011 and is implemented at the same abatement rate every year between 2011 and each terminal point to achieve the abatement target.

When CO₂ emissions are abated, emission permit revenue is obtained. At first, the revenue is considered to be used for government expenditure (“no-subsidy cases”). In addition, it is also justifiable to utilize the revenue to further promote climate change efforts along with technological changes. Since technological change is expressed as the accumulation of knowledge through R&D investment in this study, we also analyze cases in which the revenue is used for subsidizing R&D investment (“subsidy cases”). The other assumptions are same as the no-subsidy cases.

4. Results and Discussions

4.1 No-Subsidy Cases

Observing the overall economic impacts, GDP increases compared to the baseline case for the 2020 cases (e.g. 3.5% in 2020 for 50% abatement) and larger abatement cases tend to bring higher GDP (Fig. 1). On the other hand, the other cases (i.e. 2030, 2050, and 2100 cases) tend to be different. In these cases, although GDP increases compared to the baseline case in earlier years, it decreases in later years. Depending on the abatement amount and terminal years, the turning points are around 2021-2035. The longer the time span, the smaller the increase in GDP and the larger the decrease in GDP will be. Moreover, the larger the abatement amount, the larger the decrease in GDP will be.

GDP consists of private (household) consumption, government expenditure, investment, and net exports. Examining these changes, household consumption and government expenditure show similar tendencies for all the cases (Fig. 2). Household consumption

decreases compared to the baseline case and the decrease is larger as the abatement amount is large. Government expenditure is opposite to it owing to the emission permit revenue.

On the other hand, investment changes differently depending on the cases. For the shortest cases, both physical capital investment and R&D investment are larger than the baseline case. However, both increase in earlier years, but decrease in later years for the longer cases (the turning points are around 2020-2030). From these results, it is found that change in investment is most influential to increase or decrease GDP. The model is an intertemporal optimization model, thus not only the present status but also the future status is considered for the decision-making. In the shorter term, increasing investment instead of household consumption would

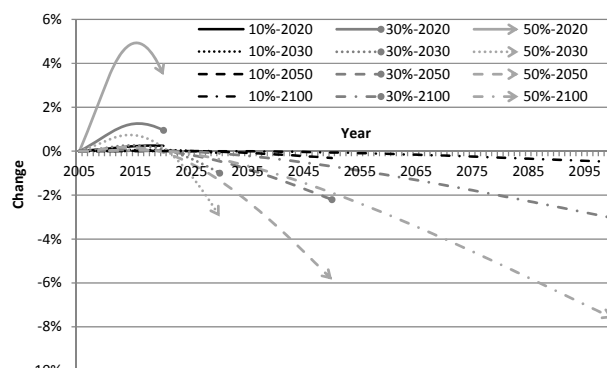


Fig. 1 Change in GDP for no-subsidy cases (e.g. 10%-2020: 10% abatement-2020 terminal point case).

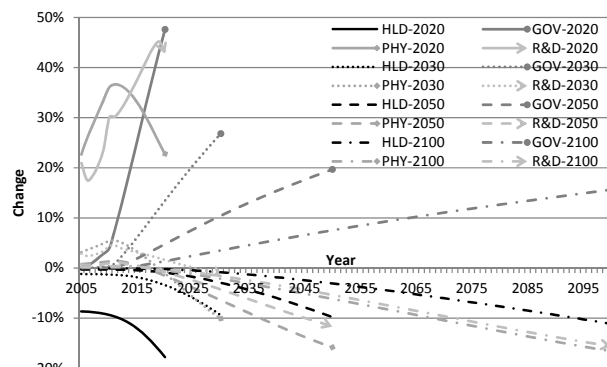


Fig. 2 Change in components of GDP for no-subsidy cases (50% abatement. HLD: household consumption; GOV: government expenditure; PHY: physical capital investment; R&D: R&D investment. e.g. HLD-2020: household consumption for the 2020 case).

be evaluated optimum in the model considering the present and future situations simultaneously. In addition, additional R&D investment indicates additional technological change, which accelerates economic growth. This effect is induced by CO₂ emission constraints. Considering the longer term, however, it is required to abate more CO₂ emissions because of continuous increase in the “amount” of CO₂ emissions in the baseline case. Consequently, both physical capital investment and R&D investment have to be reduced as well as household consumption. Since the model is an intertemporal optimization type, economic impacts appear before CO₂ emissions are actually abated.

Another important indicator to understand economic impacts of emission abatement is marginal abatement cost (MAC). MAC increases nonlinearly with increase in the abatement rate for the scenario cases (Fig. 3). Compared to the shorter cases, however, MAC does not increase exponentially over time for the longer cases and even decreases in later years for the longest cases because of the emission abatement pathways assumed in this study.

As for environmental aspects, emission intensity (CO₂ emissions/GDP) improves compared to the baseline case since decrease in CO₂ emissions is larger than that in GDP (Fig. 4). Decomposing it to carbon intensity (CO₂ emissions/energy use) and energy intensity (energy use/GDP), both of them improve. The former indicates a fuel switch to low-carbon energy and the latter indicates less energy use for economic growth. The larger the emission abatement rate, the lower these indicators will be.

In order to achieve such low carbon economy, industrial structure has changed. For example, the percentage of production from tertiary industry increases 2.7 percentage points and that from secondary industry decreases 2.8 percentage points in 2020 compared to the 2005 levels for the 2020 case (50% abatement). It is similar for the 2100 case, and the percentage of production from tertiary industry

increases 2.5 percentage points and that from secondary industry decreases 2.5 percentage points in 2100 (50% abatement). Especially, decreases in the percentages of production from energy intensive sectors such as steel industry are large.

4.2 Subsidy Cases

When subsidies on R&D investment are introduced, the results tend to be different from the no-subsidy cases. Observing the overall economic impacts, GDP decreases compared to the baseline case for the 2020 cases (e.g.-2.4% in 2020 for 50% abatement) and larger abatement cases tend to bring lower GDP (Fig. 5). On the other hand, the other cases tend to be different from them. In these cases, change in GDP can be positive or negative depending on the year, and the larger the abatement rate, the more greatly GDP

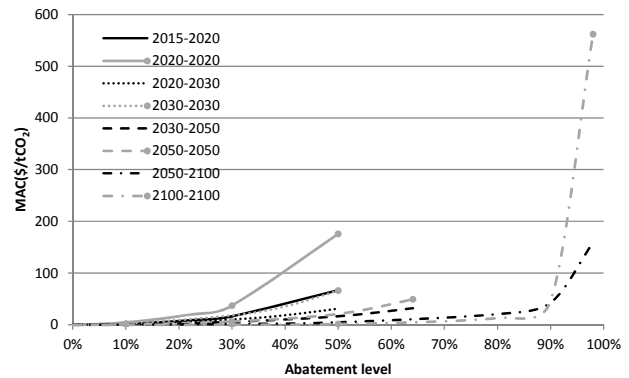


Fig. 3 MAC curves for no-subsidy cases (e.g. 2015-2020: MAC in 2015 for the 2020 cases).

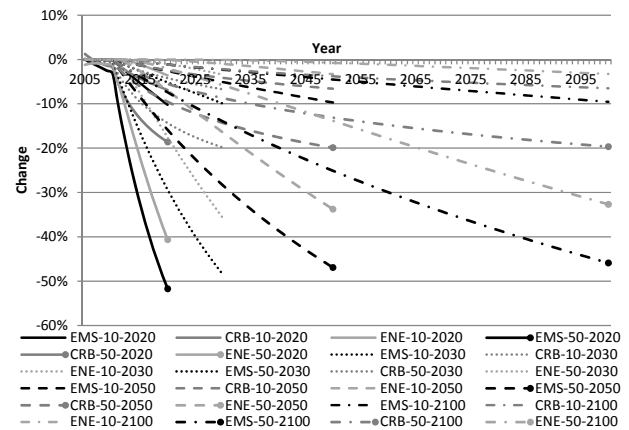


Fig. 4 Change in environmental indicators for no-subsidy cases (EMS: emission intensity; CRB: carbon intensity; ENE: energy intensity. e.g. EMS-10-2020: emission intensity for the 10% abatement-2020 terminal point case).

Economic Analysis of CO₂ Emission Abatement Applying a Dynamic CGE Model with Endogenous Technological Change: Impacts of the Time Horizon

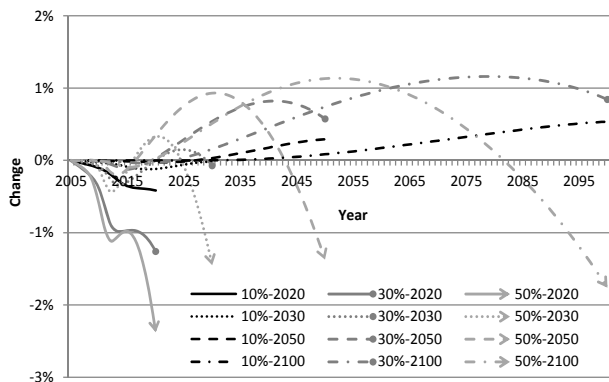


Fig. 5 Change in GDP for subsidy case.

changes.

In these cases, R&D investment plays an important role to raise GDP (Fig. 6). It is accelerated by CO₂ emission abatement and subsidies on it, especially the latter has the significant effect. This increase in R&D investment means technological improvement. The other components of GDP tend to decrease. Government expenditure decreases mainly because of subsidies on R&D investment. Decreases in consumption and physical capital investment are due to the substitution relationships. Increasing investment instead of household consumption would be evaluated optimum in the model. Furthermore, R&D investment is selected instead of physical capital investment, since the price of R&D investment becomes relatively cheaper by subsidizing R&D investment. Emission abatement constraints also contribute to these decreases.

The shapes of MAC for the subsidy cases are similar to those for the no-subsidy cases (Fig. 7). Comparing the two, there is a tendency that the larger the economy (GDP), the larger the MAC will be, and vice versa. This result can be interpreted that CO₂ emission abatement would be more economically difficult as the economy grows.

As for environmental aspects, all of the indicators improve as well as the no-subsidy cases (Fig. 8). Similar to the no-subsidy cases, industrial structure has changed to realize such the environmental improvement. For the 2020 case, the percentage of production from tertiary industry increases about 0.4

percentage points and that from secondary industry decreases about 0.5 percentage points in 2020 compared to the 2005 levels (50% abatement). As these changes are smaller than the no-subsidy cases, it would be due to the effects of technological change promoted by the subsidies. Because of the effects, secondary industry would be able to produce goods more energy-efficiently than the no-subsidy cases.

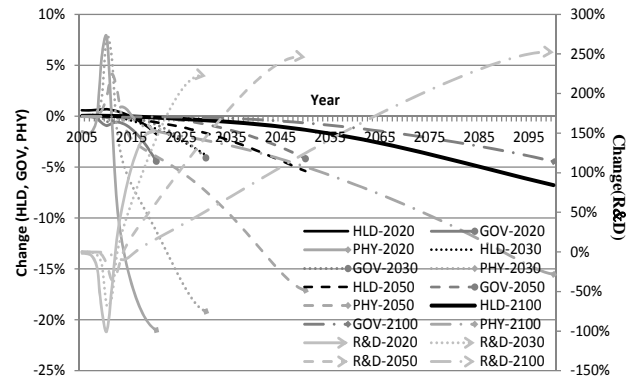


Fig. 6 Change in components of GDP for subsidy cases (50% abatement).

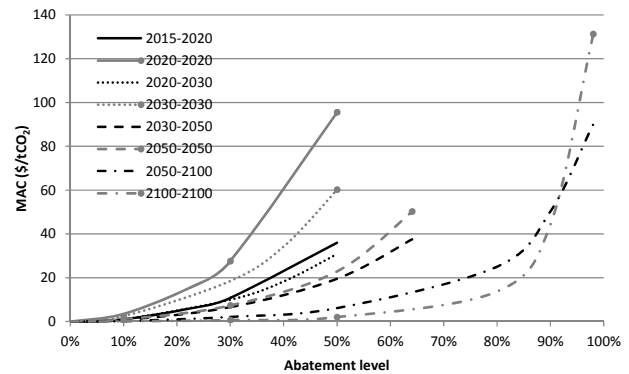


Fig. 7 MAC curves for subsidy cases.

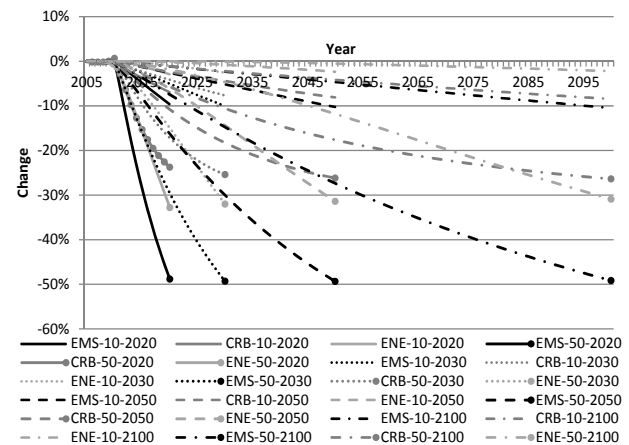


Fig. 8 Change in environmental indicators for subsidy cases.

Observing the 2100 case (50% abatement), to the contrary, the percentage of production from tertiary industry decreases 1.5 percentage points and that from secondary industry increases 1.6 percentage points in 2100. Since a possible trend toward service (or postindustrial) economy is not installed explicitly in the model, there is sufficient time for secondary industry to adapt to the emission abatement through technological change promoted by the subsidies.

4.3 Large Abatement Cases

In order to achieve low carbon economy, tremendous CO₂ emission abatement is required and understanding the economic consequences is important. Thus, we also analyze economic impacts of 90% emission abatement in 2100. The emission abatement pathway is determined as in the previous sections. In addition, we also analyze economic impacts considering the shorter terms using the same pathway to understand the impacts of the time horizon. The emission abatement rates compared to the baseline case are 22.6% in 2020, 40.1% in 2030, and 64.1% in 2050.

Overall, the relationships of changes in GDP between the cases are same with the previous comparisons (Fig. 9). For the no-subsidy cases, GDP increases compared to the baseline case in earlier years, but decreases in later years. In addition, the shorter-term cases show larger GDP if compared in the same year. For the subsidy cases, GDP decreases compared to the baseline case for the 2020 cases, but change in GDP can be positive or negative depending on the year in the other cases. Comparing these results with those for the lower abatement cases, the degrees of the changes are almost the same or slightly decline when increasing and expand when decreasing. The differences in the above results between the cases might be due to the way of handling the terminal condition. For the no-subsidy cases, since the amount of emission abatement is larger for the longer-term cases, the utility level is lowered more. Consequently,

investment is affected more severely and decrease in GDP becomes larger.

The components of GDP change as explained in the previous sections for all the cases (Fig. 10). In addition, MAC and the environmental indicators, too, change as in the previous sections (Figs. 3 and 7, and Fig. 11). In these cases, industrial structure also has

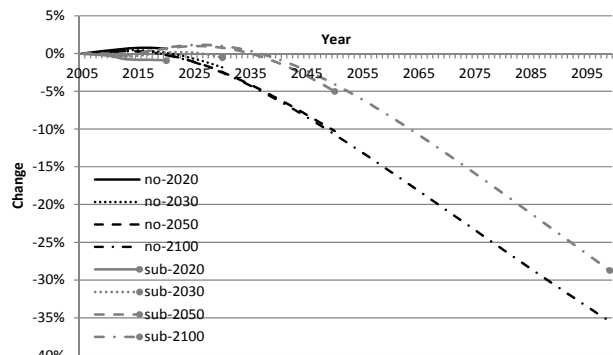


Fig. 9 Change in GDP for cases of 90% abatement in 2100 (no: no-subsidy case; sub: subsidy case. e.g. no-2020: no-subsidy-2020 terminal point case).

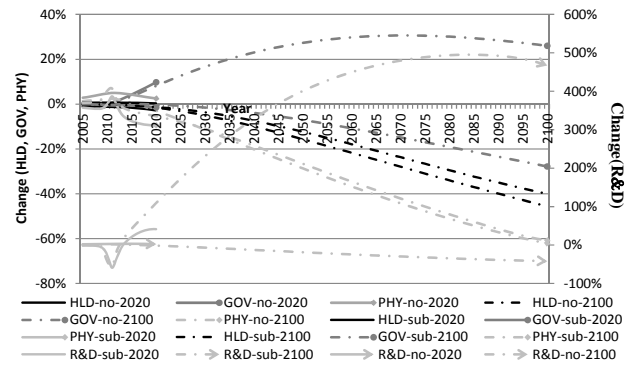


Fig. 10 Change in components of GDP for cases of 90% abatement in 2100 (e.g. HLD-no-2020: household consumption for the no-subsidy-2020 terminal point case).

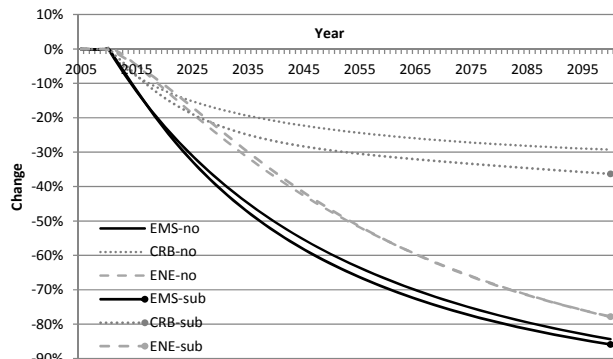


Fig. 11 Change in environmental indicators for cases of 90% abatement in 2100 (e.g. EMS-no: emission intensity for the no-subsidy case).

changed similar to the previous sections. For the 2100 without subsidies case, the percentage of production from tertiary industry increases 8.0 percentage points and that from secondary industry decreases 7.7 percentage points in 2100 compared to the 2005 levels, which are larger than the small abatement cases. For the 2100 with subsidies case, on the other hand, the percentage of production from tertiary industry decreases 4.0 percentage points and that from secondary industry increases 4.4 percentage points in 2100 because of the same reason mentioned in section 4.2.

5. Conclusions

In this paper, the authors have analyzed the impacts of CO₂ emission abatement as a climate change measure in Japan using a dynamic CGE model considering ETC developed by Matsumoto [17]. We compared the impacts by setting different terminal points in the model.

As a result, the authors found that the trends of GDP were different between the cases. For no-subsidy cases, while GDP increased compared to the baseline case when short periods were considered, it increased in earlier years and decreased in later years when longer periods were considered. The change in investment would determine increase or decrease in GDP in this analysis. For the subsidy cases, while GDP decreased compared to the baseline case for the 2020 cases, change in GDP could be positive or negative depending on the year for the other cases. In these cases, R&D investment or technological change, accelerated mainly by subsidies on R&D investment, played an important role to raise GDP. This effect was stronger in later years because of the larger subsidies.

In regard to the environmental aspects, emission intensity, carbon intensity, and energy intensity were improved for all the scenario cases, and the higher the abatement rate, the lower the intensities. Conversely, it suggests that improving these indicators simultaneously was indispensable to achieve CO₂

emission abatement targets.

To summarize, this study showed that although there was compatibility between economic growth and CO₂ emission abatement in the short term, the economic damage was observed in the long term. Because the amount of emission abatement becomes large in the far future, technological change and other factors could not cover the damage.

In this study, only one electricity sector (ELE) exists in the model. It means that although it is possible to consider the fossil fuel switches, it is not possible to consider the substitution effects between fossil fuels and renewables explicitly. However, such effects are significant to consider CO₂ emission abatement in the longer-term future. Thus, analysis taking account of multiple types of power generation would be a work for future. Furthermore, studies on modeling methodology of knowledge capital such as spillover effects of knowledge and sector-specific knowledge (technology) will be implemented.

References

- [1] UNFCCC, available online at: http://unfccc.int/files/press/news_room/press_releases_and_advisories/application/pdf/pr_accord_100201.pdf.
- [2] Green New Deal Group, A Green New Deal, New Economics Foundation, 2008.
- [3] UNEP, available online at: <http://www.unep.org/documents.multilingual/default.asp?documentid=548&articleid=5957&l=en>.
- [4] K.T. Gillingham, R. Newell, W.A. Pizer, Modeling endogenous technological change for climate policy analysis, *Energy Economics* 30 (2008) 2734-2753.
- [5] M.H. Babiker, J.M. Reilly, J. Mayer, R.S. Eckaus, I. Sue Wing, R.C. Hyman, The MIT emissions prediction and policy analysis (EPPA) model: Revisions, sensitivities, and comparisons of results, MIT JPSPGC Report 71, 2001.
- [6] K. Matsumoto, T. Masui, Economic implication of avoiding dangerous climate change: An analysis using the AIM/CGE[Global] model, *Journal of Environmental Science and Engineering* 7 (2010) 76-83.
- [7] P. Nijkamp, S. Wang, H. Kremers, Modeling the impacts of international climate change policies in a CGE context: The use of the GTAP-E model, *Economic Modelling* 22 (2005) 955-974.

- [8] L.H. Goulder, S.H. Schneider, Induced technological change and the attractiveness of CO₂ abatement policies, *Resource and Energy Economics* 21 (1999) 211-253.
- [9] C. Kemfert, Induced technological change in a multi-regional, multi-sectoral integrated assessment model (WIAGEM) impact assessment of climate policy strategies, *Ecological Economics* 54 (2005) 293-305.
- [10] A. Löschel, V.M. Otto, Technological uncertainty and cost effectiveness of CO₂ emissions reduction, *Energy Economics* 31 (2009) S4-S17.
- [11] V.M. Otto, A. Löschel, R. Dellink, Energy biased technical change: A CGE analysis, *Resource and Energy Economics* 29 (2007) 137-158.
- [12] V.M. Otto, A. Löschel, J. Reilly, Directed technical change and differentiation for climate change, *Energy Economics* 30 (2008) 2855-2878.
- [13] I. Sue Wing, Induced technical change in computable general equilibrium models for climate-change policy analysis, Ph.D. Thesis, Massachusetts Institute of Technology, Massachusetts, 2001.
- [14] K. Wang, C. Wang, J. Chen, Analysis of the economic impact of different Chinese climate policy options based on a CGE model incorporating endogenous technological change, *Energy Policy* 37 (2009) 2930-2940.
- [15] A. Löschel, Technological change in economic models of environmental policy: A survey, *Ecological Economics* 43 (2002) 105-125.
- [16] P.M. Romer, Endogenous technological change, *Journal of Political Economy* 98 (1990) S71-S102.
- [17] K. Matsumoto, Analyzing economic impacts of CO₂ abatement and R&D promotion in Japan applying a dynamic CGE model with endogenous technological change, *Journal of Global Environment Engineering* 16 (2011) 25-33.
- [18] I. Sue Wing, Induced technical change and the cost of climate policy, MIT JPSPGC Report 102, 2003.
- [19] K. Matsumoto, Economic implications of CO₂ emission abatement in Japan applying a dynamic CGE model with endogenous technological change: Considering use of emission permit revenue, *Environmental Economics and Policy Studies* submitted.
- [20] R.J. Barro, X. Sala-i-Martin, *Economic Growth*, 2nd ed., The MIT Press, Cumberland, 2003.
- [21] I. Sue Wing, Representing induced technological change in models for climate policy analysis, *Energy Economics* 28 (2006) 539-562.
- [22] N.E. Terleckyj, Effects of R&D on the productivity growth of industries: An exploratory study, National Planning Association Report 140, 1974.
- [23] N. Terleckyj, Direct and indirect effects of industrial research and development on the productivity growth of industries, in: J. Kendrick, B. Vaccara (Eds.), *New Development in Productivity Measurement*, University of Chicago Press, Chicago, 1980, pp. 359-386.
- [24] S. Paltsev, Moving from static to dynamic general equilibrium economic models, MIT JPSPGC Technical Note 4, 2004.
- [25] M. Babiker, A. Gurgel, S. Paltsev, J. Reilly, Forward-looking versus recursive-dynamic modeling in climate policy analysis: A comparison, *Economic Modeling* 26 (2009) 1341-1354.
- [26] K. Ban, Multi-regional dynamic computable general equilibrium model for the Japanese economy: Regional economic analysis based on the forward-looking view, RIETI Discussion Paper 07-J-043, 2007. (in Japanese)
- [27] M.L. Lau, A. Pahlke, T.F. Rutherford, Approximating infinite-horizon models in a complementarity format: A primer in dynamic general equilibrium analysis, *Journal of Economic Dynamics and Control* 26 (2002) 577-609.

Effect of Percolation Pattern on Yields and Accumulation of Copper and Cadmium in the Rice Plants with Soil Dressing Models

S.K. Paul¹, C. Sasaki², N. Matsuyama² and K. Kato²

1. The United Graduate School of Agricultural Sciences, Iwate University, Morioka 020-8550, Japan

2. Faculty of Agriculture and Life Science, Hirosaki University, Hirosaki-shi, Aomori 036-8561, Japan

Received: February 28, 2011 / Accepted: May 28, 2011 / Published: November 20, 2011.

Abstract: A greenhouse experiment was conducted using stratified paddy field models, which were prepared by polluted soil with 12.5 cm soil dressing. The paddy models were assembled with open and closed percolation system to focus the effect of percolation pattern on accumulation of copper (Cu) and cadmium (Cd) in rice plants in contaminated paddy field with soil dressing models. Percolation pattern has significant effect on soil environment, especially redox potential that may influence mobilization of Cd, Cu and other elements. In open system percolation models, the plowsole and subsoil were in oxidative condition (600 mV), whereas reduction condition (-200 mV) was measured in closed system percolation models. Accumulations of Cu and Cd in all parts of rice plants (roots, grains, stems and leaves) were found higher in an open system percolation with the paddy field model comparatively than in a closed system percolation. The soil redox (Eh) condition influenced by the percolation pattern might be one of the main factors for uptake and accumulation of Cu and Cd in rice plants. The plant height and stem number were found lower in open system percolation comparatively to closed system percolation. In the yields section, the average panicle length, number of panicle and rice grain/hill and weight of grain/hill were lower in open system percolation than the closed system percolation.

Key words: Rice plants, percolation system, soil dressing, cadmium and copper.

1. Introduction

In some regions of Japan, the paddy soils have been polluted with heavy metal especially cadmium (Cd), copper (Cu), lead (Pb) and zinc (Zn). Cadmium is a long-term problem as a toxic metal, which is contaminated in food chain from soil through plant to human beings, consequently causing health hazards. The increase of contaminants in agricultural farmland has a social issue due to production of safety food. Soil dressing with cheaper, effective and efficient technologies is the popular remediation method of heavy metal contaminated soils. Intake of high Cd content rice causes Itai-Itai disease which was first reported in Toyama-Prefecture, Japan [1]. For safety

of human beings, WHO-1992 set the cadmium level in rice grain 0.1 ppm but the Japan government set that value as 0.4 ppm. On the other hand, Cu is an essential micronutrient for plant. However, high concentration of Cu in soil causes Cu-toxicity in plant such as chlorosis and necrosis, stunting, leaf discoloration and inhibition of root growth [2]. Most of the roots growths in plow layer accumulation heavy metals by the root. So thickness of soil dressing is very effective to reducing uptake of heavy metals by rice plants. Favorable environment influence of Cu and Cd mobilization to the rhizosphere enhances uptake of such elements by the plant [3]. Soil air and microorganisms also regulate the growth of root and uptake of heavy metal by plants due to producing of soluble elements. Cd and Cu uptake by rice plants depends on a combination of soil and plants factors:

Corresponding author: S.K. Paul, Ph.D. student, research fields: agriculture and environmental engineering. E-mail: skumar paul79@yahoo.com.

concentration of Cd and Cu in soil, soil pH, redox condition and sorption capacity of soil [4]. The soil layer in saturated condition by water is an effective technology to minimize the uptake of heavy metal by plants because heavy metal is not dissolute. In the soil reduction condition, heavy metals are not dissolute so that principal was practiced with waterlogged soil environment in rice ecosystems by dissolution of Mn and Fe oxides [5] and less effective tiller, blacks of roots and rice yields decrease with Cu wastewater irrigated soil compared with non-wastewater irrigated soil [6]. Many methods have been developed to minimize the heavy metal pollution effect on plants. Soil dressing is the simple and widely used technique for heavily contaminated sites [7, 8]. And developed in-situ soil dressing system in applying removal of polluted soil replacing of unpolluted soil [9] has been practiced phytoremediation in different contaminated area [10, 11]. Many technologies have been developed and practiced for reduction of Cd and Cu by rice plants in agriculture sector such as Cd sorption by ferric oxide [12] and lime is a greatly effect in reducing Cd and Cu uptake in the Cd and Cu contaminated soil [13]. Cd complex decreases with carbonate and to remove hazardous metals from soil into aqueous solution with using extracting reagents [11]. Rice production and Cd and Cu accumulation depend on flood water three weeks before and after heading time of rice plants. Cd and Cu uptake by rice plants drastically decreased and showed effective growth and yields in applying continuously submerged paddy field after heading time [7]. Percolation pattern is one kind of hydraulic conductivities of the soil layers and can control the groundwater level [14], which may regulate soil redox potentials and influence to accumulation of Cd and Cu in rice plant. The rice plants roots grow up to plowsole and subsoil. Therefore, soil redox potential and air entry value of those soil layers are very important for uptake of Cd and Cu from polluted paddy fields. Many researchers conduct their research only in pot

device system which has not controlled the redox potential of plowsole and subsoil. Percolation pattern controls the redox potential of all soil layers which is actual to paddy field. So the aim of the study is to clarify the effect of percolation pattern on yields of rice plants and accumulation of Cd and Cu with soil dressing polluted paddy fields models.

2. Materials and Methods

2.1 Soil Properties

In this study, the used polluted soil (gray lowland soils) and andosol were collected from A-Prefecture (Japan) and chitose farm in Hirosaki which were loamy and silt clay loamy soil. The Physico-chemical properties of the soil were measured by the standard methods of soil chemical analysis [15]. In the polluted soil had 4.8% organic matter, MgO 496 mg/kg, Na₂O 114 mg/kg, CaO 2909 mg/kg, K₂O 311 mg/kg, Fe 2820 mg/kg, T-N 0.40%, T-P 0.15% and Cd 3.39 mg/kg respectively, in andosol, the value of MgO, Na₂O, CaO, K₂O, Fe and Cd were 918, 84, 1530, 159, 5683 and 0.19 mg/ kg and the T-N, T-P and OM were 0.44%, 0.60% and 6% respectively. In gravel, the value of MgO, Na₂O, CaO, K₂O, Fe and Cd were 147, 18, 539, 58, 600 and 0.13 mg/kg and the T-N, T-P and OM were 0.00%, 0.35% and 0.05% respectively.

2.2 Experimental Design

The experiments were conducted in green house and were made of open and closed system percolations of stratified paddy field models; each of stratified paddy fields model was imposed in three models. The open and closed system percolation models were M-1, M-2, M-3 and M-4, M-5, M-6 showed in Fig. 1. Each model has the dimension of 30 × 50 × 70 cm³, and it was practiced in iron box and constructed with three layers of soil material. Plow layer (I layer; 0-12.5 cm), plow sole (II layer; 12.5-22.5 cm), subsoil (III layer; 22.5-65 cm) were constructed with andosol (I layer), polluted soil (II layer) and gravel (III layer). Stratified paddy field

**Effect of Percolation Pattern on Yields and Accumulation of Copper and Cadmium
in the Rice Plants with Soil Dressing Models**

Soil layer	Stratified paddy field Model					
	Open system percolation			Closed system percolation		
	M-1	M-2	M-3	M-4	M-5	M-6
I	●	●	●	●	●	●
Plow layer (12.5 cm)	Andosol	Andosol	Andosol	Andosol	Andosol	Andosol
II	○	○	○	●	●	●
Plowsole (10 cm)	Polluted soil	Polluted soil	Polluted soil	Polluted soil	Polluted soil	Polluted soil
III	○	○	○	●	●	●
Subsoil (42.5 cm)	Gravel	Gravel	Gravel	Gravel	Gravel	Gravel
	●	●	●	●	●	●

Fig. 1 Overview of the experimental design (○: open system percolation; ●: closed system percolation; Andosol soil: Chitose farm is part of Hirosaki University, Japan; Polluted soil: Cd soil was collected from A-Prefecture, Japan; Gravel: gravel from Iwaki mountain).

models were the controlling ground water level at 57.5 cm and 12.5 cm in open and closed system percolation with using a subsurface drainage pipe.

There were 15 rice plants (*Oryza Sativa*, Cultivar: Tsugaru-Roman), and they were transplanted in each paddy field model with 10 cm planting distance, which has the length range between 19.0-22.0 cm. Fertilizers were applied as recommended rate for Tsugaru-Roman cultivar.

2.3 Measurement and Analysis of Rice Plants

Oxidation-reduction potential (ORP) of each soil layer was measured by electrometrically using ORP meter (Central Science Co., Ltd., model UC-203) from planting to harvesting period. The height, number of stem and Soil Plant Analyzer Development (SPAD-502) of rice plants were observed continuously from transplanting to harvest and the yields survey was measured by number of panicle, rice grain and weight of grains. Moreover, determined the cadmium and copper contains in rice grain, roots, stem and leaf which were extracted by nitric acid and sulfuric acid and then analyzed by Atomic Absorption Spectrophotometer (Model Z-2000, Hitachi Corporation) as described by The Ministry of

Agriculture, Forestry and Fisheries of Japan [16].

3. Results and Discussion

3.1 Redox Potential of Soil Layers (Eh)

Oxidation-reduction potential (ORP) condition is known as a redox potential (Eh). The oxidation-reduction value in soil more than 300 mV is an indicator of oxidation condition and lower than 300 mV indicates reduction condition [17]. Oxidation and reduction potential in different soil layer varied with different percolation pattern. In both percolation systems, the Eh value in plow layer was about -200 mV as shown in Figs. 2 and 3 due to saturated condition of soil layer. In open system percolation, the Eh values in plowsole and subsoil layer were above 600 mV in Fig. 2 and those layers became oxidized in unsaturated condition, as a result, Eh value was greater than 300 mV. The Eh value of gravel layer was decreased slowly due to less growth of microorganisms in the gravel layer presenting low amount of organic matters [18].

In closed system percolation, the average Eh value of all soil layers was about -200 mV during June to September, 2009 as showed in Fig. 3. In principle, soil

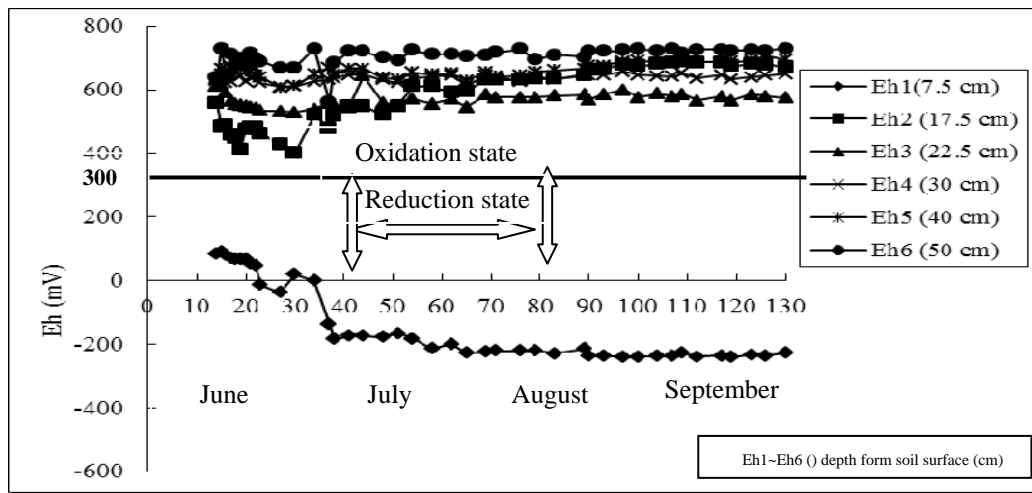


Fig. 2 Oxidation-reduction condition of soil layer in open system percolation model.

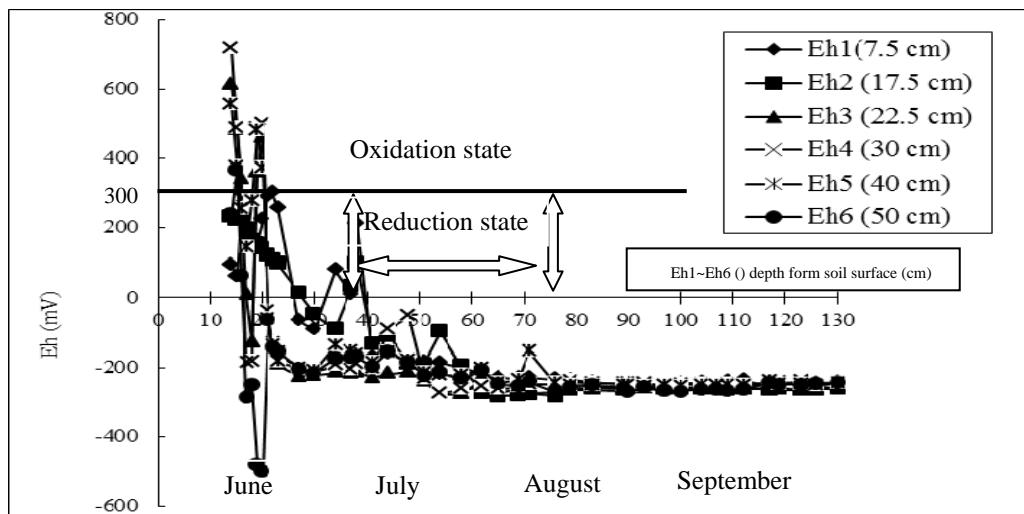


Fig. 3 Oxidation-reduction condition of soil layer in closed system percolation model.

layer with oxidation condition promotes the accumulation of cadmium and copper for plant. Many scientists have reported that most of the metals are uptaken by rice plants during the blooming period. And in the present study, the time of soil condition status was marked in Figs. 2 and 3. Absorption and accumulation of Cd and Cu are significantly reduced with diminishing Eh in reductive conditions formed by flooding rice fields [19]. The proportion of soluble cadmium decreases abruptly with the decrease of soil redox potential [17]. So in closed system percolation models, the Cd and Cu dissolve decreased comparatively to the open system percolation models.

3.2 Plant Length

The average plants length in open system percolation (105.9 cm) was smaller and significantly different to compared with the closed system percolation (111.7 cm) shown in Fig. 4. This result might be occurred due to the effect of groundwater level and soluble metal availability in the soil layer. As a result, in open system percolation stunted the plant length. Cd and Cu are toxic elements for plant growth, so availability of soluble Cd in soil decreases the rice plants length [20] which is supported to the present study.

Effect of Percolation Pattern on Yields and Accumulation of Copper and Cadmium in the Rice Plants with Soil Dressing Models

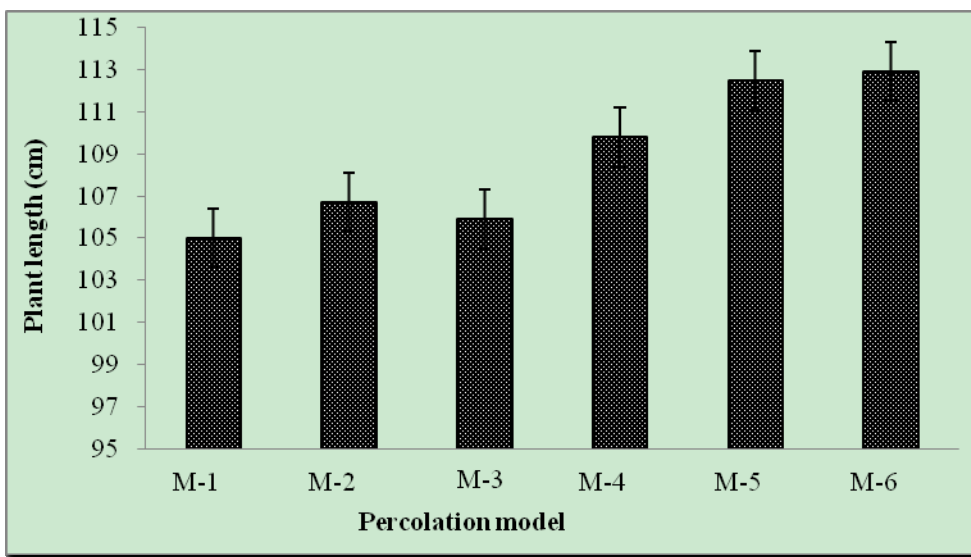


Fig. 4 The rice plants length in different percolation systems.

3.3 Stem Number

Average stem number of rice plants in open system percolation was significantly affected by percolation pattern. In closed and open system percolation, the average numbers of stem of rice plants were found 14.4 and 12.4 respectively shown in Fig. 5. The lowest average stem number was found 12.0 in M-1 open system percolation and the highest number was found 14.6 in closed system percolation (M-5 and M-6) model which might be due to the effect of different percolation patterns using polluted soil.

3.4 SPAD (Soil Plant Analyzer Development)

The chlorophyll meter provides a simple, quick, portable, and non-destructive method for estimating leaf chlorophyll content. The decrease of chlorophyll amount in rice blade was measured using soil and plant analyzer development (Type of No. SPAD-502) during plant growth stage to harvesting period. The highest SPAD value was measured from planting to early blooming stage in both percolations. The average SPAD value was about 43 in early blooming stage of open and closed system percolation models

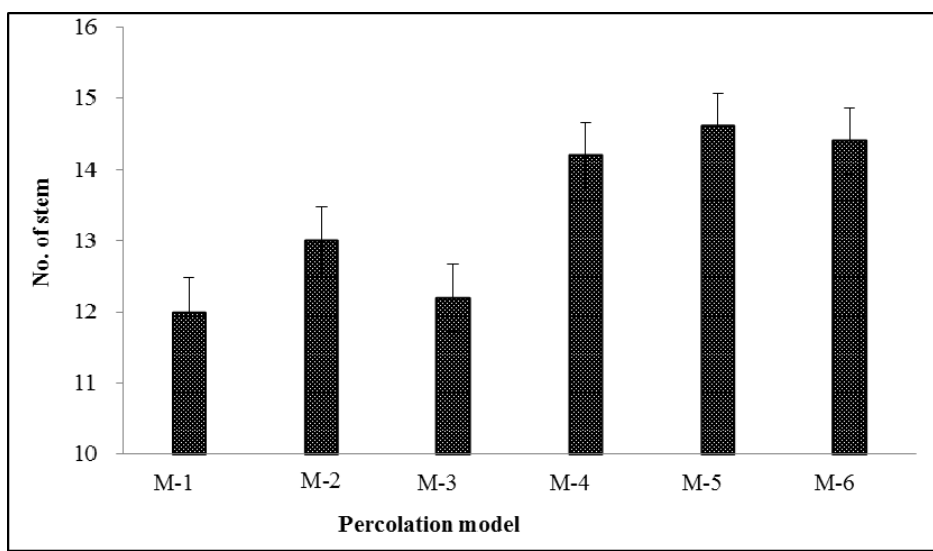


Fig. 5 The stem number of rice plants in different percolation system.

but that value gradually decreased with the increasing cultivation period. The average SPAD value in M-1, M-2, M-3, M-4, M-5 and M-6 were 26.2, 25.8, 26.5, 28.2, 28.4, 29.0. Finally, in open system percolation, the average amount of chlorophyll decreased faster than that in closed system percolation as shown in Fig. 6. The photosynthesis of leaf has been affected by cadmium [21] and the SPAD value increased with the increase of N levels, and decreased with the increase of Cd contents in solution [22]. In the present study, the SPAD value of rice plants in open system percolation model were affected due to availability of soluble Cd and Cu ions in the soil layer.

3.5 Root Weight

The vegetative root growths of each soil layer were weighted in closed and open system percolation models. Rhizosphere is an important environmental interface connecting plant roots and soil. Roots excrete some organic substances to rhizosphere during the growth and rhizosphere controls the entrance of nutrients, water and other chemicals, beneficial or harmful to plants. The vegetative roots growths were observed of plowlayer, plowsole and subsoil of open system percolation models. There were about 78% root's growth in plow layer of both percolation

models. For both closed and open system percolation, the dried weights of roots in plow layer were comparatively higher than other soil layers. However, in plowsole layer, the dried root weight in open system percolation was higher than closed system percolation due to the oxidizing condition of soil layer as shown in Fig. 7. In sterile and non-sterile hydroponic conditions, roots growth stressed with the presence of Pb and Cd availability in soil [23].

3.6 Yield of Rice Plants

The average length, number and weight of panicle per hill were 16.5 cm, 6.9 and 14.7 gm in open system percolation, which were lower than 18.2 cm, 8.9 and 20.4 gm in the closed system percolation as shown in Table 1. The average number of rice grain and weight of rice grain were measured by meant of polished of rice. In the yields section, the mean of the total weight of perfect rice grain per hill and number of perfect rice grain per hill were 12.0 g and 562 in open system percolation, which were comparatively lower than 15.3 g and 713 in closed system percolation as shown in Table 1.

The above results might be occurred explained by availability of soluble Cd and Cu in soil due to

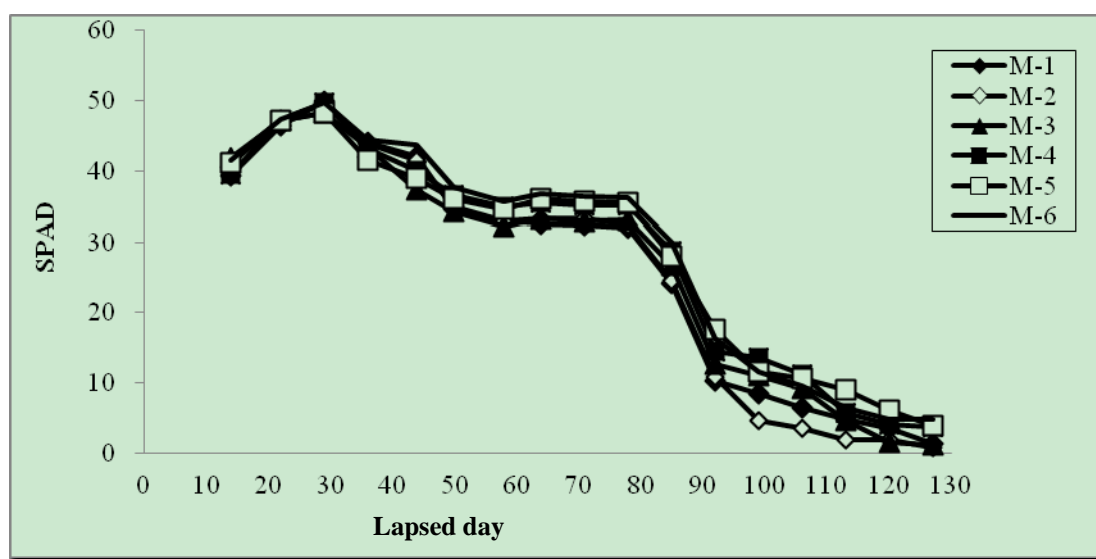


Fig. 6 SPAD values of rice plants in open and closed system percolation.

**Effect of Percolation Pattern on Yields and Accumulation of Copper and Cadmium
in the Rice Plants with Soil Dressing Models**

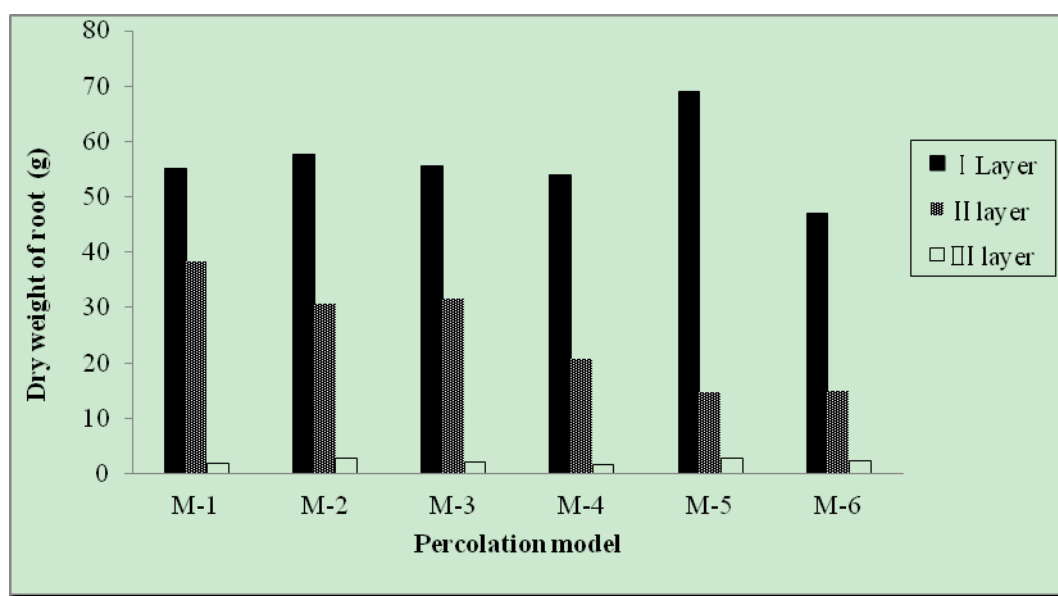


Fig. 7 Dry weight of roots in each soil layer of open and closed system percolation.

Table 1 Panicle length and number, weight of panicles and rice grains in experimental models.

Model	Length (cm)*	No. of panicles/hill (Pieces)*	Weight of panicles/hill (gm)*	No. of rice grains/hill (Pieces)*	weight of grains/hill (gm)*
M-1	16.9 ^b ± 0.9	6.8 ^b ± 1.3	15.1 ^b ± 1.1	530 ^b ± 26	11.9 ^b ± 1.4
M-2	15.9 ^b ± 0.5	7.4 ^{ab} ± 1.1	15.9 ^b ± 1.1	579 ^{ab} ± 51	13.2 ^{ab} ± 1.0
M-3	16.9 ^b ± 0.7	6.6 ^b ± 1.1	13.3 ^b ± 1.6	520 ^b ± 24	11.3 ^b ± 1.3
M-4	18.1 ^a ± 1.2	8.3 ^{ab} ± 1.1	19.6 ^{ab} ± 1.9	665 ^{ab} ± 68	14.3 ^a ± 0.4
M-5	19.4 ^a ± 1.0	9.2 ^a ± 1.3	20.7 ^a ± 1.5	717 ^a ± 71	14.4 ^a ± 1.7
M-6	18.1 ^{ab} ± 0.8	9.2 ^a ± 0.8	20.6 ^a ± 2.2	731 ^a ± 57	14.7 ^a ± 2.0

Means within the same row followed by the * letter are not significantly different to each other at $p > 0.01$ by DMRT.

oxidation of soil which easily affected the rice plants yields in open system percolation. Many scientists have reported that the heavy metal affects on rice plants growth and yields, such as Cd contamination in soil at concentrations ranging from 20 to 40 mg/kg caused severe damage to rice plants and plant height was reduced by 64.7% and the number of tillers and the rice yield declined by 80%, compared to the control [24]. The root and straw dry weight and grain yields decreased quickly with the increase of soil Cu levels [25]. And Cd content in rice grain was negatively correlated with the weight of grains [26]. In a concluded ward from above the study, rice yields and growth declined if the excess amount of Cd and Cu presence in soil and easily soluble and accumulation of rice plants. In the present study

plowsole and subsoil were exposed and oxidized in open system percolation and thus produced soluble Cd and Cu which affected on the yield of rice plants.

3.7 Cadmium and Copper Concentration in Stem and Leaf of Rice Plants

Accumulation of average Cd and Cu in stem and leaf by rice plants in open system percolation was higher (0.9 and 1.7 mg/kg), compared to the closed system percolation (0.5 and 1.2 mg/kg) that is not statistically significantly different at $p > 0.01$ respectively, as shown in Fig. 8. In soil reduction condition, the presence of sulfate ion can be converted to sulfide ion which reacts with Cd and Cu and produces relatively insoluble cadmium and copper-sulfide [27], that mechanisms supported to the

closed system percolation and that is why low uptake of Cd and Cu by rice plants. In open system percolation, the Cd and Cu accumulation by rice plants was much due to soil oxidation status.

3.8 Cadmium and Copper Concentration in Brown Rice

Results on Cd and Cu concentration in brown rice revealed that percolation system influences the uptake of Cd and Cu and mobilization in rice plants. This mobilization depends upon the soil oxidation-reduction condition. The average amounts of Cd and Cu content in brown rice were higher in open system (0.2 and 4 mg/kg) than in closed system percolation (0.1 and 2.5 mg/kg), due to the oxidation in submerging paddy field as shown in Figs. 9 and 10. Cu concentrations in rice paddy vary due to application of trace elements contents soil and contaminated water [28]. Many scientists have reported that accumulation of Cd, Cu and other heavy metals by rice plants is decreased in submerging conditions of the soil layer. Closed system percolation models are related to submerging condition of soil layer with 12.5 cm groundwater level.

3.9 Cadmium and Copper Concentration in Roots of Rice Plants

Accumulation of Cd and Cu in roots of all soil layers in closed system percolation has no significant difference ($p > 0.01$) with the open system percolation. In open and closed system percolation, accumulation of Cd in the I, II and III soil layer's root were 7.5, 33, 5.4 mg/kg and 4.3, 18, 3.2 mg/kg but in case of Cu accumulation by roots were 62.7, 150 and 207 mg/kg and 42.8, 110 and 120 mg/kg, respectively, as shown in Figs. 11 and 12. The above results showed that the more of the Cu and Cd amassed in the II layer's roots and the higher uptake in open system percolation compared to closed system percolation. Concentrations of Cd and Cu in roots were higher than the stem and leaf and rice grain due to directly diminish within the soil. Accumulation of Cd in roots

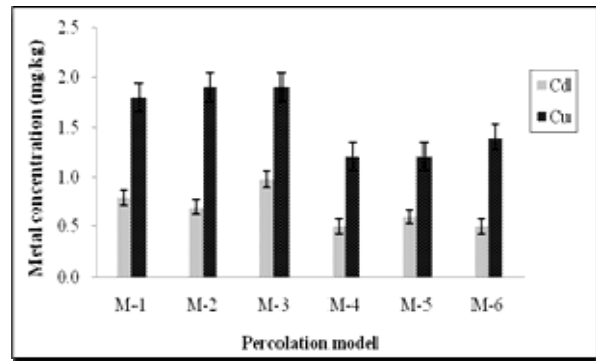


Fig. 8 Cd and Cu concentration in stem and leaf of rice plants.

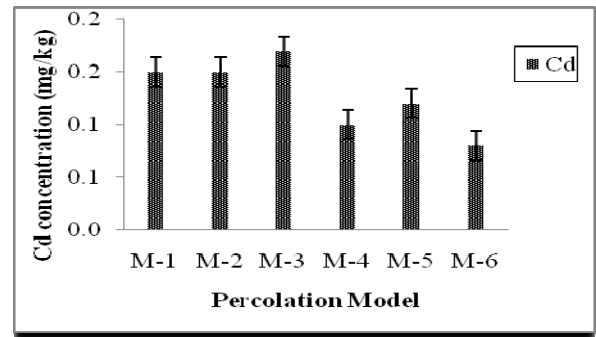


Fig. 9 Cd concentration in rice grain.

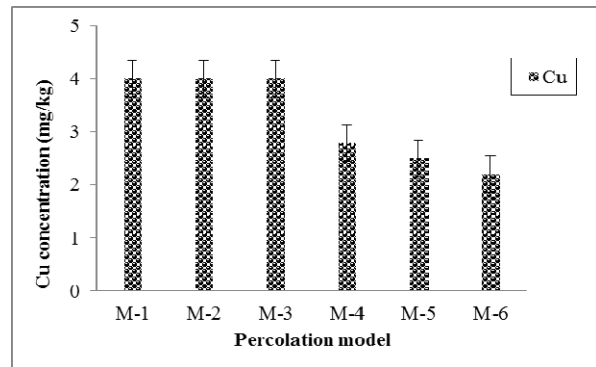


Fig. 10 Cu concentration in rice grain.

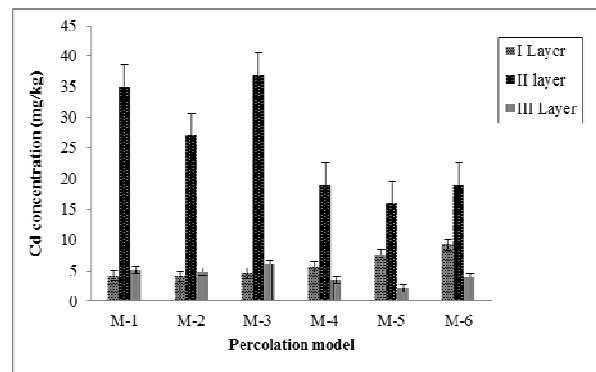


Fig. 11 Cd concentration in different soil layer's roots of rice plants.

Effect of Percolation Pattern on Yields and Accumulation of Copper and Cadmium in the Rice Plants with Soil Dressing Models

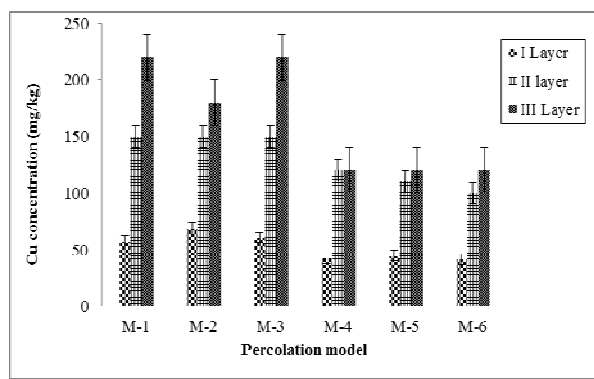


Fig. 12 Cu concentration in different soil layer's roots of rice plants.

was the highest of the total Cd in plant [29, 30] which is sustenance to the present study.

4. Conclusion

The difference of percolation system affected not only rice growth and yields but also accumulation of Cd and Cu by rice plants. Percolation pattern controls the oxidation–reduction status of soil, consequently uptake of heavy metal by rice plants. In oxidation condition of soil, plants more uptakes of Cd and Cu due to mobilize of soluble of heavy metals. Cd and Cu concentration in brown rice was higher in open system percolation than the closed system percolation; this result suggested that open system percolation promotes Cd and Cu uptakes in rice plants due to oxidizing condition of soil layers. So a closed system percolation will be an effective tool to reduce uptake of Cd and Cu with soil dressing in a polluted paddy field.

References

- [1] J. Kobayashi, Pollution by cadmium and the itai-itai disease in Japan, in: F.W. Oehme (Ed.), Toxicity of Heavy Metals in the Environment, part 1, Marcel Dekker, New York, 1978, pp. 47-158.
- [2] F. Van Assche, H. Clijsters, Effects of metals on enzyme activity in plants, *Plant Cell Environment* 13 (1990) 195-206.
- [3] O. Onyatta, P.M. Huang, Phosphate-cadmium release from soils, in: Proc. of 17th WCSS, Vol. 79, 2002, pp. 1-7.
- [4] B.J. Alloway, Heavy Metals in Soils, John Wiley and Sons, New York, 1990, pp. 29-39.
- [5] F.N. Ponnampuruma, The chemistry of submerged soils, *Adv. Agron.* 24 (1972) 26-92.
- [6] Z.H. Cao, Z.Y. Hu, Copper contamination in paddy soils irrigated with wastewater, *Chemosphere* 41 (2000) 3-6.
- [7] K. Sakurai, P.M. Huang, Influence of potassium chloride on desorption of cadmium sorbed on hydroxyaluminosilicate-montmorillonite complex, *Soil Science and Plant Nutrition* 42 (1996) 475-481.
- [8] J. Vangronsveld, S.D. Cunningham, Introduction to the concepts, in: J. Vangronsveld, S.D. Cunningham (Eds.), *Metal-Contaminated Soils*, Springer, Berlin, 1998, pp. 1-15.
- [9] N. Yamada, Remediation of heavy metal contaminated soils by soil dressing and sustainability of the remediation effects, *J. Soil Sci. Plant Nutr.* 78 (2007) 411-416.
- [10] S.S. Suthersan, Phytoremediation, in: *Natural and Enhanced Remediation System*, CRC Press Inc., Florida, 2002, pp. 239-267.
- [11] H.A. Elliot, L.M. Herzig, Oxalate extraction of Pb and Zn from polluted soils: Solubility limitations, *Journals of Soil Contamination* 8 (1999) 105-116.
- [12] S. Kuo, B.L. McNeal, Effects of pH and phosphate on cadmium sorption by hydrous ferric oxide, *Soil Sci. Soc. Ame. J.* 48 (1984) 1040-1044.
- [13] X. Xian, Effect of chemical form of cadmium, zinc and lead in polluted soil on their uptake by cabbage plants, *Plant Soil* 113 (1989) 257-264.
- [14] K. Adachi, C. Sasaki, Percolation and seepage, in: M. Mizutani, S. Hasegawa, K. Koga, A. Goto, V.V.N. Murty (Eds.), *Advanced Paddy Field Engineering*, Shinzan-sha Sci. & Tech, Tokyo, 1992, pp. 71-88.
- [15] National Institute of Agricultural Science and Technology, Methods of soil chemical analysis, 1988, available online at: <http://www.icar.org.in/files/ICAR-ITP/iiss.pdf>.
- [16] MAFF (The Ministry of Agriculture, Forestry and Fisheries of Japan), The foundation of environmental paddy field and investigation of paddy field, water quality and crop analysis method, in: *National Conference of Paddy Field Preservation*, Tokyo, 1979, pp. 113-115.
- [17] K. Iimura, Metal Stress in Rice Plants, Japan Scientific Societies Press, Tokyo, 1981, p. 19.
- [18] C. Sasaki, M. Inagaki, K. Enari, K. Koseki, Influence of percolation pattern on the removal of soluble ions in stratified paddy field with rice and gravel under the plowsole, *REE* 41 (2001) 78-89.
- [19] R.K. Lu, L.M. Xiong, Z.Y. Shi, A review about studies on cadmium in soil-crop ecosystem, *Soils* 24 (1992) 129-132, 137-141.
- [20] N.Q. Nguyen, H.B. Le, Heavy metal pollution in paddy soils near Ho Chi Minh city caused by waste water discharge and

the influence of cadmium on rice, 2005, available online at:
<http://academic.research.microsoft.com/Paper/6478307.aspx>.

- [21] L. Sanitá di Toppi, R. Gabbrielli, Response to cadmium in higher plants, *Environ. Exp. Bot.* 41 (1999) 105-130.
- [22] Q. Du, M.X. Chen, R. Zhou, Z.Y. Cao, Z.W. Zhu, G.S. Shao, et al., Cd toxicity and accumulation in rice plants vary with soil nitrogen status and their genotypic difference can be partly attributed to nitrogen uptake capacity, *Rice Science* 16 (2009) 283-291.
- [23] Q. Lin, Y.X. Chen, H.M. Chen, C.M. Zheng, Study on chemical behavior of root exudates with heavy metals, *Plant Nutr. Fertil. Sci.* 9 (2003) 425-431.
- [24] N.N. Quynh, V.D. Khanh, N.H. Viet, Effects of Cadmium pollution in soil and in irrigation water on growth and development of rice plant, Department of Agriculture and Forestry Extension, Ministry of Agriculture and Rural Development-MARDI, *Science & Technology Journal of Agriculture and Rural Development* 3 (2002) 227-230.
- [25] J. Xu, L. Yang, Z. Wang, G. Dong, J. Huang, Y. Wang, Toxicity of copper on rice growth and accumulation of copper in rice grain in copper contaminated soil, *Chemosphere* 62 (2006) 602-607.
- [26] T. Ishikuro, N. Yamada, Difference in cadmium accumulation in hulled grains of paddy rice among position in the ear, *Soil Sci. Plant Nutr.* 68 (1997) 629-633.
- [27] K. Ono, M. Gamo, J. Nakanishi, Factors affecting cadmium concentration in rice in Japanese paddy fields, in: *Proc. of 24th Annual Meeting: North America, The Society of Environmental Toxicology and Chemistry (SETAC)*, 2003, p. 71.
- [28] S.T. Abbas, M. Sarfraz, S.M. Mehdi, G. Hassan, O.U. Rehman, Trace elements accumulation in soil and rice plants irrigated with the contaminated water, *Soil & Tillage Research* 94 (2007) 503-509.
- [29] S.C. Jarvis, L.H.P. Jones, M.J. Hopper, Cadmium uptake from solutions by plants and its transport from roots to shoots, *Plant and Soil* 44 (1976) 179-191.
- [30] Y. Cui, X. Zhang, Y. Zhu, Does copper reduce cadmium uptake by different rice genotypes?, *Journal of Environmental Sciences* 20 (2008) 332-338.

Comparative Study of the Impact of Climate Variability on Prevalence of Urinary Schistosomiasis: Cases at Sunyani Regional Hospital and among School Children in Atronie, Sunyani

S.C.K. Tay¹, L.K. Amekudzi² and G. Tagoe³

1. School of Medical Sciences, Kwame Nkrumah University of Science and Technology (KNUST), Kumasi 1908, Ghana

2. Meteorology and Climate Science Unit, Department of Physics, Kwame Nkrumah University of Science and Technology (KNUST), Kumasi 1908, Ghana

3. Laboratory Department, Kumasi South Hospital, Kumasi 1908, Ghana

Received: March 11, 2011 / Accepted: May 12, 2011 / Published: November 20, 2011.

Abstract: A study has been conducted to determine the impact of climate variability on *Schistosoma haematobium* infection among patients and school children in Sunyani between 2006 and 2009. Urine samples from the subjects were collected and examined in the laboratory using the Filtration technique for the detection and quantification of *Schistosoma haematobium* eggs. The prevalence rate of urinary schistosomiasis at the Sunyani Regional Hospital for 2006, 2007, 2008 and 2009 were found to be 0.24%, 0.55%, 0.55% and 0.75% respectively while that for Methodist Junior High School in 2008 and 2009 were 60.1% and 60.3% respectively. A decrease in the relative humidity and average annual rainfall were identified as factors contributory to the increase in urinary schistosomiasis prevalence rate. The temperature values obtained throughout the study period did not have any significant effect on the prevalence rate. The temperature values, however, were those that enhanced cercarial incubation (15-35 °C) with a resultant increase in shedding of cercariae leading to more infections among water contacts. The infection rate due to the stream Amama was 20.1%, while that due to river Tano was 36.6%. The highest risk group was children aged 15-19 years. Praziquantel was administered to treat the infection, producing a cure rate of 93%. Recognition of urinary schistosomiasis as a public health problem in Ghana is the main challenge to prevention and control of the disease.

Key words: Tropical disease, *Schistosomiasis haematobium*, praziquantel, climate variability.

1. Introduction

Schistosomiasis is the second most prevalent tropical parasitic disease after malaria, affecting about 200-300 millions people world-wide [1]. Five to six million people are at risk and this has mainly been associated with river basin projects [2].

Schistosomes are platyhelminthes and members of the digenetic blood trematodes commonly called blood flukes, in the genus *Schistosoma* [3]. The three main

species of this genus affecting humans are *Schistosoma haematobium*, *Schistosoma japonicum* and *Schistosoma mansoni*. Two other species more localized geographically are *Schistosoma mekongi* and *Schistosoma intercalatum* [4]. *Schistosoma mekongi* is found in Southeast Asia while *Schistosoma intercalatum* is found in central West Africa. In addition, other species which parasitize birds and mammals can cause cercarial dermatitis in humans [5]. *Schistosoma haematobium* causes urinary schistosomiasis and the species contain several strains. It is mainly endemic in Africa and the eastern

Corresponding author: L.K. Amekudzi, Ph.D., main research field: effect of climate on humans and biogeochemical cycle. E-mail: lkamekudzi.sci@knust.edu.gh.

Mediterranean [6].

Schistosomiasis is mostly common in areas where the water is contaminated with freshwater snails, which serve as intermediate host [4]. The disease affects many people, particularly children who may acquire the disease by swimming or playing in contaminated fresh water [7]. Snails of the *Bulinus* genus are the natural intermediate reservoir hosts of the parasite [8]. A major factor associated with the intensification of schistosomiasis infection in sub-Saharan Africa is water development projects, particularly man-made lakes, dams for hydroelectric power and irrigation schemes, which can lead to shifts in snail vector populations [9].

Climate change affects the spread of certain diseases. These are diseases transmitted by arthropods and other diseases transmitted from animals to people, which are called zoonoses [10]. According to Ref. [11] and references therein, more than 150,000 deaths and a burden of 5.5 million disability-adjusted life years (DALYs) can be attributed to climate change and climate variability each year.

Perturbations in key climate variables affect the global hydrologic cycle, precipitation, and pronounced changes in water availability [10]. Changes in water availability will affect diseases spread by snails, such as schistosomiasis, because changes in rainfall will have an impact on flow of rivers and levels of lakes [10].

Infections that will spread with climate change have some commonalities. They are focal, and their distribution is limited by the ecology of their reservoir. They usually have a two- or three-host life cycle, thus in addition to infecting people, they infect a vector and sometimes a wild vertebrate animal host [12]. The range of the reservoir is delineated by temperature and sometimes water. In order to survive global climate change the infectious agent will need to have reservoirs that will survive; they will probably survive by moving in a polar direction, north in the Northern Hemisphere, in order to find a temperature range that is ecologically

permissive [10]. According to Ref. [13], if the infectious agent and reservoir are successful in the newly warmer climate, the infectious agent can be expected to multiply more rapidly, and if the reservoir is an arthropod or snail, it will develop more rapidly (it may also have a shorter life).

Sunyani which is the capital of Brong-Ahafo Region is in the forest zone of Ghana (see Fig. 1) and has several inland water bodies. Several farmers depend on these water bodies for irrigation. Children living along these water bodies swim in them. Two distinct seasons are experienced in this climate zone. These are the Harmattan or dry season (from November to February) and the wet or rainy season from April to early November. The rainfall pattern in Sunyani is shown in Fig. 2, in general, high variability in the rainfall between 1976 and 2009 is observed. Two distinct rainy seasons (see Fig. 3(a)), called the major and minor seasons, are seen. The rainy seasons which span from March to June is the major season and the minor season is the rainy season from September to early November [14].

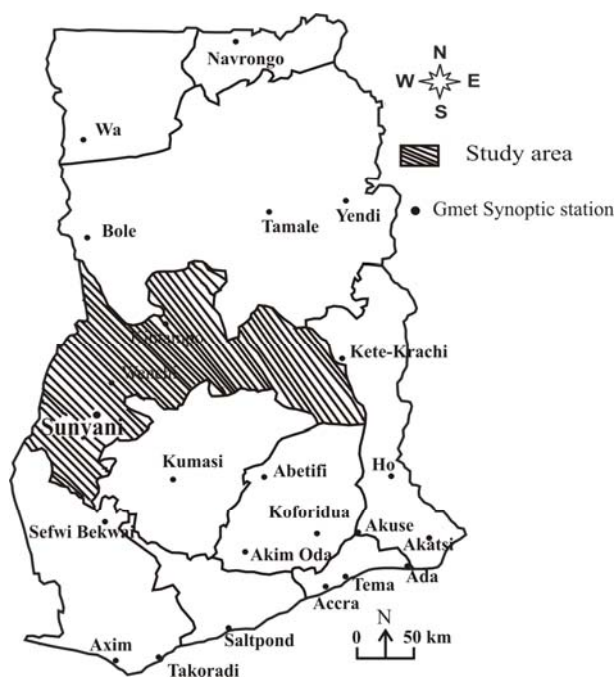


Fig. 1 Map of Ghana showing all synoptic stations of Ghana Meteorological Agency. The shaded region is the study area.

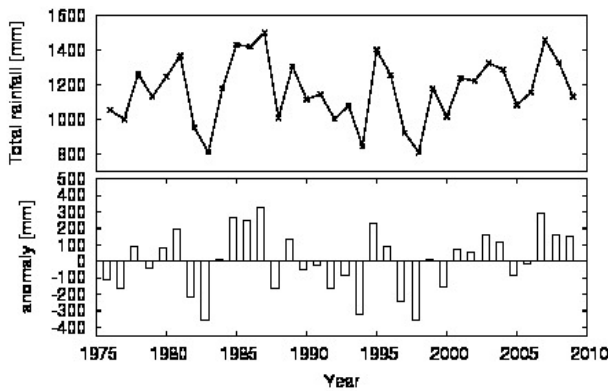


Fig. 2 Annual rainfall pattern for Sunyani municipality from 1976 to 2009.

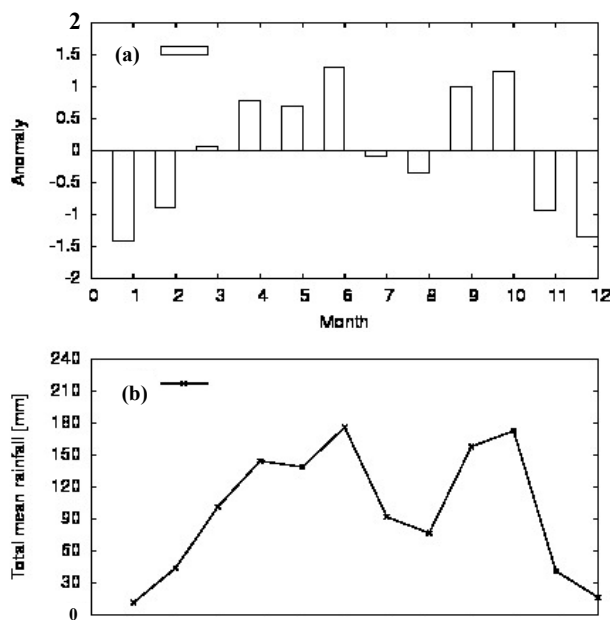


Fig. 3 (a) Monthly mean total rainfall averaged for all the data set for the period 1976-2009, showing clearly the two rainy season; (b) the monthly rainfall standardized anomaly index for the same period.

Urinary schistosomiasis usually responds well to drug therapy. Two drugs which have been extensively used in the treatment of schistosomiasis are Metrifonate and Praziquantel [15, 16]. Schistosomiasis is readily treated using a single oral dose of the drug Praziquantel [17], which is the drug of choice for the treatment of any of the human schistosome species. This drug can be prescribed to persons of all ages at a dose of 40 mg/kg body weight [18]. Metrifonate is given orally in a dosage of 7.5 mg/kg body weight every other week in three doses [7]. While drug

treatment is effective for eliminating parasites already in the body, it does not prevent new infections [19]. There is however an ongoing and extensive research into developing a schistosomiasis vaccine that will prevent the parasite from completing its life cycle in humans [20].

Control programs based on oral drug delivery have been developed and partially implemented as a means to control morbidity in endemic areas [18]. Water sanitation, mass chemotherapy and health education to highlight the disease are some preventive measures available to control *Schistosoma haematobium* infection [20].

The goal of this paper is to present a comparative study of the impact of climate variability on prevalences of urinary schistosomiasis cases at Sunyani regional hospital and Atronie community in Sunyani. The paper is structured as follows: in section 2 laboratory investigations and data analysis methods are described. This is followed by discussion of results in section 3 and finally the conclusions are given in section 4.

2. Methods and Data

The study was carried out at the Sunyani Regional Hospital, Parasitology Laboratory and the Methodist Junior High School at Atronie, Sunyani. Ethical clearance was obtained from Komfo Anokye Teaching Hospital and the School of Medical Sciences, KNUST Ethics and Research Committee before the sampling began. The excretion of *Schistosoma haematobium* eggs in urine was highest between 10.00 am and 14.00 pm, with a peak around midday [4] for which reason the urine sample was collected between 12:00 noon and 14:00 local time [7]. Patients were given a clean, dry, leak proof universal container to void their own urine usually between the hours of 8:00 and 12:00 noon. Patients were advised to exercise vigorously prior to voiding the urine. The terminal urine was however preferred. The volume of urine required was about 10 mL. Questionnaire was designed and used as the data

collection tool. It covered some behavioural activities in water bodies. Also, data on rainfall, temperature and relative humidity spanning the period 1976 to 2009 were collected from the Ghana Meteorological Agency office in Sunyani. The rainfall trends and season were determined over the Sunyani Municipality (see Fig. 3). Urine was examined using the filtration technique for detecting and quantifying *Schistosoma haematobium* eggs in urine.

Data was doubly-entered using GraphPad Prism (version 5.2), cross checked and subsequently analysed with GraphPad Prism (version 5.2) and Excel.

3. Results and Discussion

In all, 46 (0.44%) out of 10534 patients were found to have urinary schistosomiasis in the hospital while 963 (60.2%) out of 1600 pupils were found to have urinary schistosomiasis in the school. Prevalence of urinary schistosomiasis in the Sunyani Regional Hospital was very low (0.44%) with some months registering prevalence of 0.0%. The vast difference in prevalence rate can be attributed to the fact that majority of the people who access health care at the Sunyani Regional Hospital, live in Sunyani where out of a population of about 80,245, 5488 individuals have access to pipe-borne water in addition to about 162 community standpipes [21] compared to Atronie which is in the outskirts of Sunyani, with only a few boreholes available compelling majority of people in Atronie to rely on the stream, Amama for drinking and other domestic activities. Also, the children in Atronie lack playing and sporting facilities compelling most of them to take to swimming as a form of recreation. This is consistent with the findings of Mafiana et al. [21] who showed that increase in socio-economic activities and improved water supply reduced the propensity of people especially children to swim in the rivers and therefore reduce the prevalence of *Schistosoma haematobium* infection.

Prevalence of *Schistosoma haematobium* infection decreases as relative humidity increases in both study

sites (see Fig. 4). This is because increase in relative humidity will lead to more evaporation and hence enhanced convective activity such as, clouds formation and eventually rainfall. Higher relative humidity values lead to increases in rainfall which will result in decreasing prevalence as shown in Fig. 5.

There was a variability in the total average annual rainfall from year to year (see Fig. 2). As a result there was less water available for irrigation and other activities in some years, resulting in more water contacts among persons living in Atronie. Etim et al. [22] reported that the snail vector populations fluctuate strongly, decreasing at the peak of the rainy season.

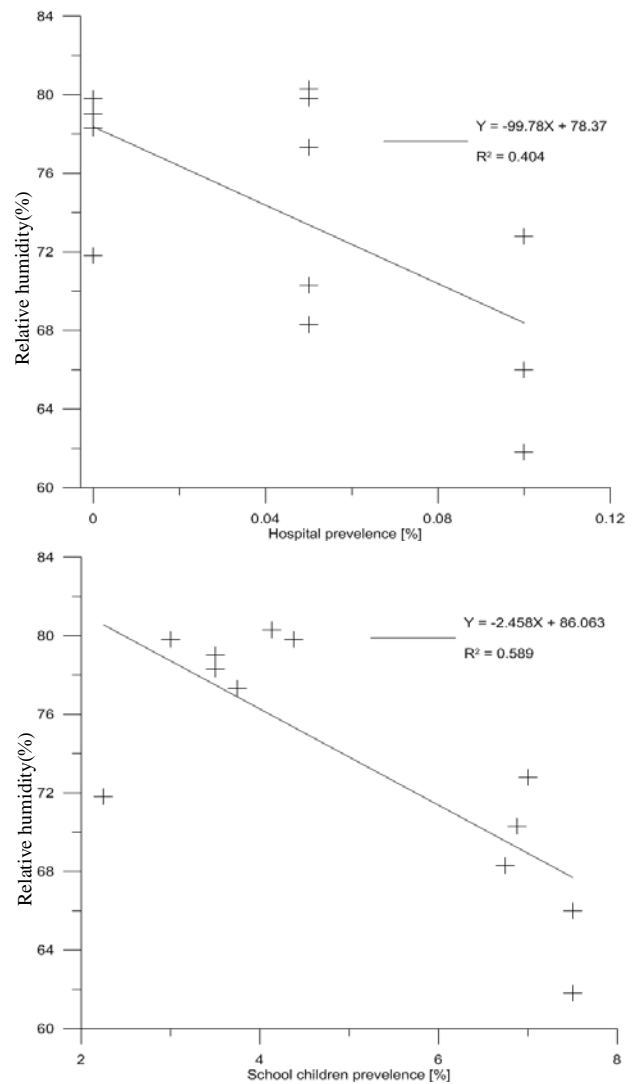


Fig. 4 Regression analysis of relative humidity as a function of prevalence rate (top in Hospital, down among school children).

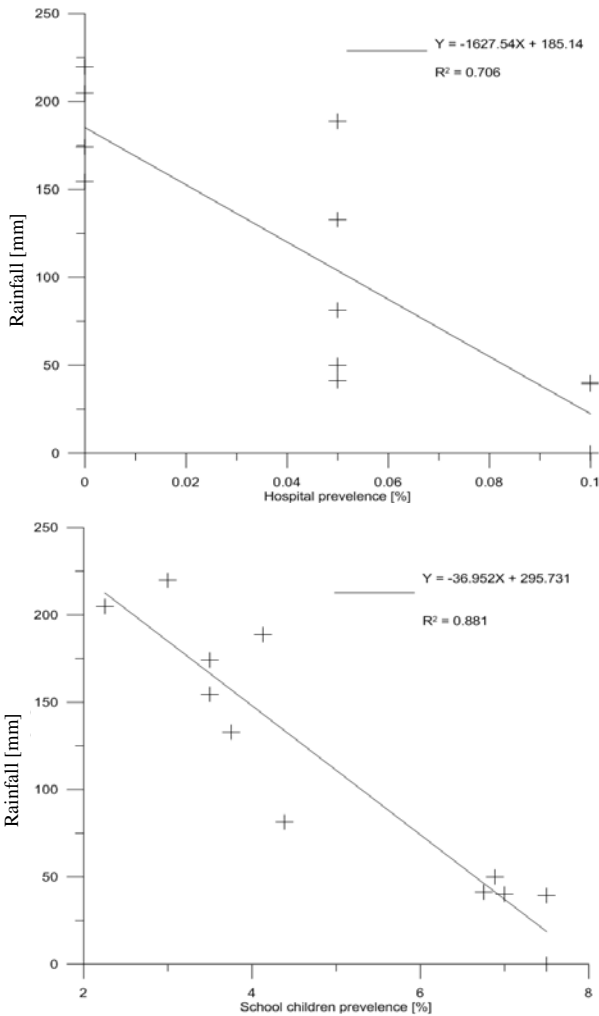


Fig. 5 Regression analysis of rainfall (mm) as a function of prevalence rate (%) (top in Hospital, down among school children).

This implies that decrease in rainfall will lead to an increase in the snail vector population and hence a spread in *Schistosoma haematobium* infection. During the dry season, more people go swimming in order to cool off, which means longer and more frequent water contact with a resultant increase in infection rate [23].

From the study, the overall prevalence of *Schistosoma haematobium* infection in the dry season was 5.0% while that in the rainy season was 2.8%. This shows that *Schistosoma haematobium* infection rate is higher in the dry season than in the rainy season. This can be attributed to the fact that more snails are found in water bodies with low-flow velocities [24] during the dry season. In the dry season, the rains are less

hence the water bodies contain less water with a resultant reduction in the flow velocities. Availability of more snails during the dry season will mean more vectors to aid in the propagation of the infection hence the higher prevalence rate in the dry season than in the rainy season.

An experiment conducted by Anderson et al. [25] showed that the suitable temperature range for larval development in the laboratory was between 15 °C to 35 °C, with an optimum temperature for intramolluscan development of 25 °C. Although the temperature figures (Figs. 6 and 7) obtained throughout

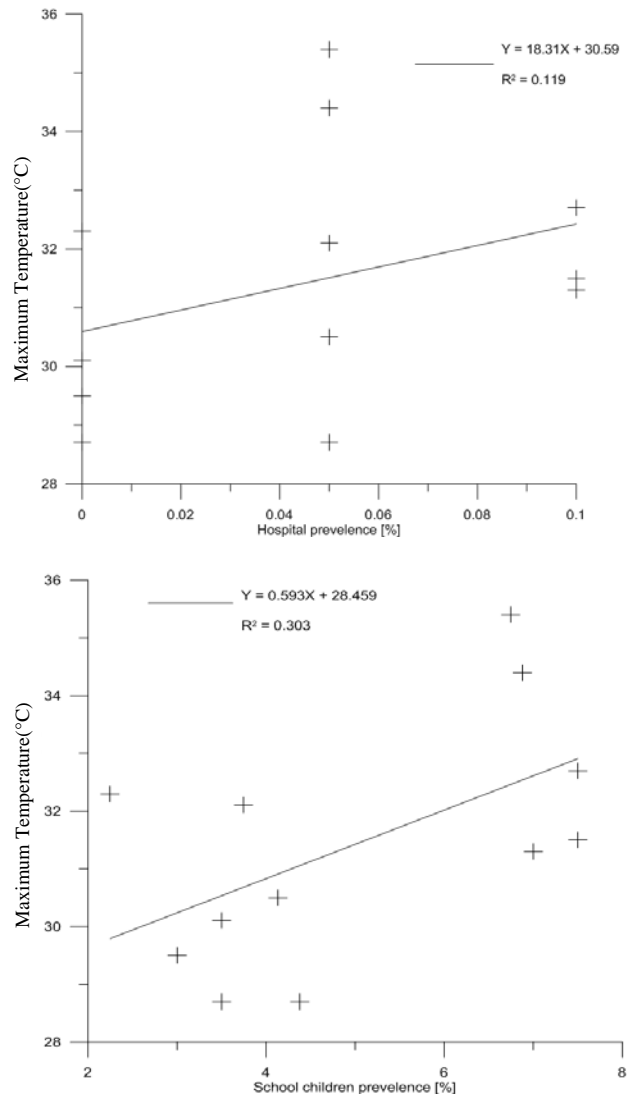


Fig. 6 Regression analysis of maximum temperature as a function of prevalence rate (top in Hospital, down among school children).

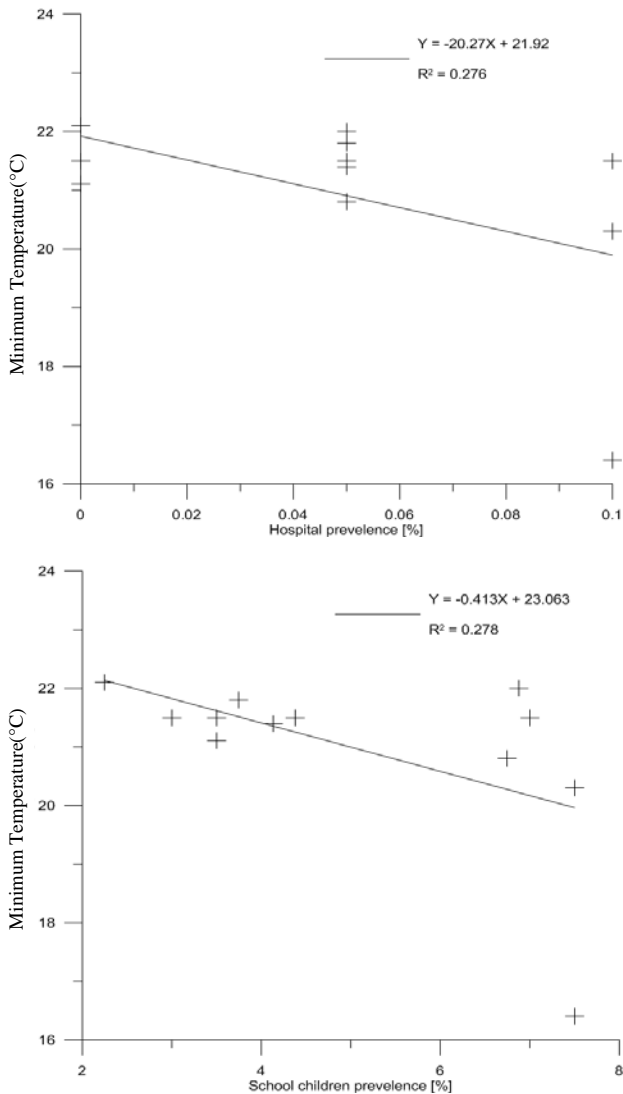


Fig. 7 Regression analysis of minimum temperature as a function of prevalence rate (top in Hospital, down among school children).

the study period did not have any significant effect on prevalence rate, the figures recorded were those that enhanced cercarial incubation with a resultant increase in shedding of cercariae leading to more infections among water contacts [26].

Prevalence of infection rose from 0.73% among children aged 5 years to a peak of 5% among persons in the 15-19 years group as shown in Fig. 8. The prevalence of infection began to drop from age 20 years with prevalence rate of 0% being detected among persons from 40 years and above. The young (below 26 years) appear to be at increased risk of infection

probably because fetching of water, bathing/swimming in water bodies, among others, which have been identified to be risk factors by some earlier studies [27-30], are frequently carried out by them. The downward trend of prevalence rate of infection with advancing age after the peak age is attained may also be explained on the basis of a host reaction arising from humoral response to infection with a possible immunity mechanism coming into play [31].

Behavioral and occupational factors that exposed people to *Schistosoma haematobium* infection (Fig. 9) were swimming (71.4%), household chores (40.6%), irrigation (54.9%), fishing (60.6%) and drinking (32.1%). According to Ref. [32], univariate statistics

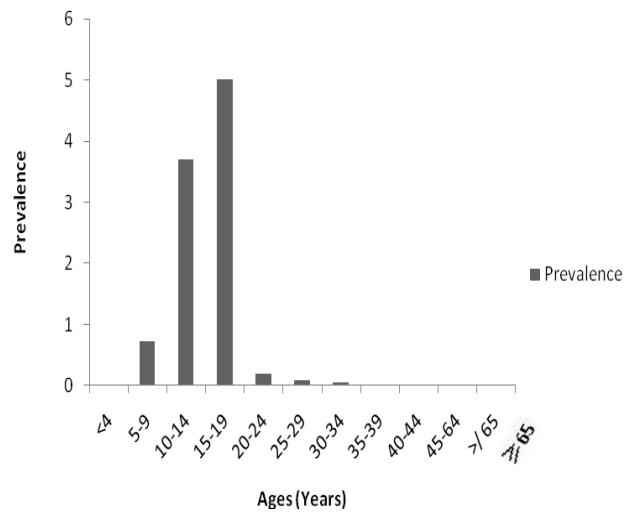


Fig. 8 Prevalence of *schistosoma haematobium* infection among various age groups.

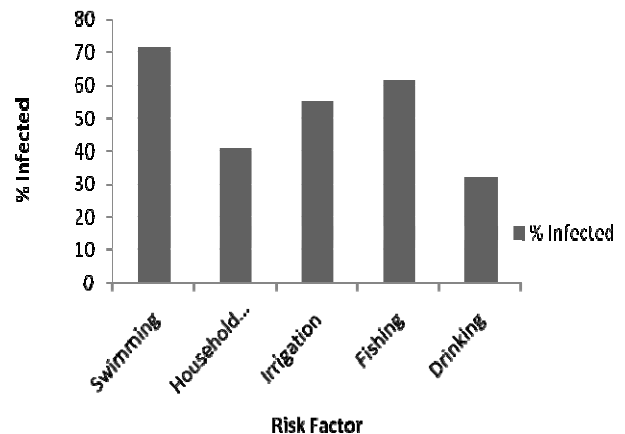


Fig. 9 Prevalence of *schistosoma haematobium* infection among various risk groups.

Table 1 Water body contacted by infected persons.

Water body	No. of contacts	No. of positive contacts	Prevalence (%)
Amama stream (Atronie)	609	501	20.1
River Tano	1351	911	36.6
Others	532	231	9.3
Total	2492	1643	65.9

revealed significant associations between infection and specific water-contact activities, including washing/bathing and playing in streams/ponds.

Amama stream and River Tano were the major sources of infection among school children in Atronie and in the Sunyani Regional Hospital with prevalence rates of 20.1% and 36.6% respectively. Other smaller water bodies within Sunyani, some water bodies outside Sunyani, for example Akosombo Dam in the Eastern Region of Ghana and some water bodies within West Africa, for example Mali and Niger accounted for 9.3% (see Table 1). In a multivariate analysis by Ref. [32], the strongest predictor of infection was proximity of the child's home to a site harbouring *S. haematobium*-infected *Bulinus* species, suggesting that geography was a better proxy for exposure.

About 300 of the 963 school children who were infected with *Schistosoma haematobium* infection were treated with single-day oral treatment with praziquantel (20 mg/kg bid). 279 of the 300 pupils had urine negative for *Schistosoma haematobium* when urine quantitation for *Schistosoma haematobium* eggs was conducted five months after treatment, this gives a cure rate of 93.1% after treatment, which is consistent with the findings of Ref. [33]. Satayathum et al. [33] treated 113 infected pupils with praziquantel (40 mg/kg body weight) and subsequently re-screened 5 months after the administration of the chemotherapy. Results showed that a single dose of praziquantel conferred a 94.44% cure rate.

4. Conclusions

The impact of climate variability on prevalences of urinary schistosomiasis has been studied. We observed that the prevalence of *Schistosoma haematobium*

infection at the study sites is influenced by climate variables such as rainfall and relative humidity. The infection rates at the Sunyani Regional Hospital though low occurred during the dry season (November-April; July-August) compared to high rates at Atronie which also occurred in the dry season. High rainfall and high relative humidity lead to low *Schistosoma haematobium* infection in both Sunyani Regional Hospital and Atronie.

The prevalence rate of urinary schistosomiasis at the Sunyani Regional Hospital for 2006, 2007, 2008 and 2009 were found to 0.24%, 0.55%, 0.55% and 0.75% respectively while that for 2008 and 2009 from the Methodist Junior High School were 60.1% and 60.3% respectively. A reduction in the average annual rainfall was identified as a contributory factor to the increase in prevalence. It was observed that the enhanced cercarial incubation temperature were in the range of 15-35 °C with a resultant increase in shedding of cercariae leading to more infections among water contacts. The stream Amama was identified as the source of infection in Atronie with infection rate of 20.1% while river Tano was seen as the main source of infection at the Sunyani Regional Hospital with infection rate of 36.6%. The dry season was found to have the highest infection rate (5.0%). Behavioral and occupational factors such as irrigation, swimming, fishing and drinking were identified as risk factors to contracting the infection. In addition, it was found that infection in children was more than in adults with the peak level of infection being found in persons in the 15-19 year group (5%). Praziquantel was found to have a cure rate of 93%.

No snail (concentration) population data was collected at the study sites. Analysis was based on the biology of the aquatic snail intermediate host of *Schistosoma haematobium*. Due to lack of funds, only 300 of the school children in Atronie received treatment even though according to the World Health Organization (WHO) standard guidelines, a prevalence exceeding 50% warranted mass treatment. With the National Health Insurance Scheme in place, funding

should be sourced to treat all infected children in future studies.

The main challenge to urinary schistosomiasis prevention and control in Ghana is the lack of recognition of the disease as a public health problem. Control strategies including case-detection (laboratory diagnosis in health facilities, mass screening), malacological surveillance (snail monitoring, mollusciciding), chemotherapy (individual and mass treatment) and health education must be vigorously undertaken on the effect of climate change on the spread of *Schistosoma haematobium* infection in Ghana. A general rise in living standards in the country, together with improved sanitation and water supplies, construction of wells in rural areas, and a significant improvement in medical care is also needed as it can help in the elimination of the disease in endemic areas.

Praziquantel treatment for long-term control of schistosomiasis may not be possible because of variable efficacy of the drug, high rates of post-treatment reinfection, and the possible development of drug resistance [33]. Vaccine research and development needs to be considered in Ghana. Since there is no immunization against *Schistosoma haematobium* in Ghana, the result of this study should be used to provide prophylactic treatment for all children from the ages of 5-19 years during the dry season to control the morbidity associated with the infection.

Future studies to identify species of aquatic snails at the study sites and also to isolate cercariae from aquatic snail collected at the study sites in the laboratory using Polymerase chain reaction (PCR) is ongoing. The studies of the potential impact of regional climate change on the transmission of schistosomiasis at the present study sites with respect to the demographic, ecological and economic changes will be considered in future studies.

Acknowledgments

The authors are grateful to the following institutions

and persons: The management and staff of Sunyani Regional Hospital, Ghana Meteorological Agency (GMET), Sunyani, the Headmaster, staff and pupils of Methodist Junior High School, Atronie, Sunyani.

References

- [1] C. Lengeler, J. Utzinger, M. Tanner, Questionnaires for rapid screening of schistosomiasis in sub-Saharan Africa, *Bull World Health Organ* 80 (2002) 235-242.
- [2] D.W.T. Crompton, P. Peters, Working to overcome the global impact of neglected tropical diseases, WHO Tropical Diseases Report, 2010.
- [3] G. Oliveira, N.M. Rodrigues, A.J. Romanha, D. Bahia, Genome and genomics of schistosomes, *Canadian Journal of Zoology* 82 (2004) 375-390.
- [4] M. Cheesebrough, *District Laboratory Practice in Tropical Countries*, 2nd ed., Cambridge University Press, New York, 2005, pp. 236-239.
- [5] E. Chidozie, S. Daniyan, Urinary schistosomiasis epidemiological survey of children in selected schools: A preliminary study in Minna, Nigeria, *African Journal of Biotechnology* 7 (2008) 2273-2776.
- [6] N.R. Bergquist, Schistosomiasis: From risk assessment to control, *Trends in Parasitology* 18 (2002) 309-314.
- [7] S. Parija, *Medical Parasitology (Protozoology & Helminthology)*, 2nd ed., All India Publishers, India, 2000.
- [8] L. Roberts, J. Janovy, *Foundations of Parasitology*, 5th ed., Wm. C. Brown Publishers, Dubuque, Iowa, 1996.
- [9] J.A. Patz, T.K. Graczyk, N. Geller, A.Y. Vittor, Effects of environmental change on emerging parasitic diseases, *Int. J. Parasitol* 30 (2000) 1395-1405.
- [10] R.E. Shope, Impacts of global climate change on human health: Spread of infectious disease, in: S.K. Majumdar, L.S. Kalkstein, B. Yarnal, E.W. Miller, L.M. Rosenfeld, (Eds.), *Global Climate Change: Implications, Challenges and Mitigation Measures*, 1992, pp. 63-70.
- [11] X.N. Zhou, G.J. Yang, K. Yang, X.H. Wang, Q.B. Hong, L.P. Sun, et al., Potential impact of climate change on schistosomiasis transmission in China, *Am. J. Trop. Med. Hyg.* 278 (2008) 188-194.
- [12] G.T. Strickland, B.L. Ramirez, *Hunter's Tropical Medicine and Emerging Infectious Disease*, 8th ed., W.B. Saunders Company, Philadelphia, 2000, pp. 804-832.
- [13] V.R. Southgate, D. Rollinson, L.A. Tchuem-Tchuente, P. Hagan, Towards control of schistosomiasis in sub-Saharan Africa, *Journal of Helminthology* 79 (2005) 181-185.
- [14] K. Oduro-Afriyie, D.C. Adukpo, Spectral characteristics of annual mean rainfall series in Ghana, *West Africa Journal of Applied Ecology* 9 (2006) 118-126.
- [15] A. Danso-Appiah, J. Utzinger, J. Liu, P. Olliaro, Drugs for

1482 **Comparative Study of the Impact of Climate Variability on Prevalence of Urinary Schistosomiasis: Cases at Sunyani Regional Hospital and among School Children in Atronie, Sunyani**

- treating urinary schistosomiasis, *Cochrane Database of Systematic* 3 (2008) 53-57.
- [16] S. Toure, Y. Zhang, E.K.C. Bosque-Oliva, A. Ouedraogo, A. Koukounari, A.F. Gabrielli, et al., Two-year impact of single praziquantel treatment on infection in the national control programme on schistosomiasis in Burkina Faso, *Bull World Health Organ* 86 (2008) 780-787.
- [17] WHO, Prevention and control of schistosomiasis and soil-transmitted helminthiasis, Report of a WHO Committee, 2002, pp. 1-57.
- [18] A. Capron, M. Capron, D. Dombrowicz, G. Riveau, Vaccine strategies against schistosomiasis: from concepts to clinical trials, *Int. Arch Allergy Immunol.* 124 (2001) 9-15.
- [19] A. Elderderly, M. Eltoun, A. Babiker, B. Hani, Schistosomiasis in Sudan and beyond, *Urological Cancer* 3 (2008) 18-19.
- [20] O.F. Ati, E.O. Iguisi, Recent trends in the duration of the rainy season in some stations north of latitude 9° N of Nigeria, *Journal of Applied Sciences Research* 3 (2007) 1737-1745.
- [21] C.F. Mafiana, Y.O. Beyioku, *Schistosoma haematobium* infection in Abeokuta, *African Journal of Medicine and Medical Sciences* 27 (1998) 5-7.
- [22] S.E. Etim, The epidemiology of urinary schistosomiasis in Biase area, Cross River State and its implications for control, *The Nig. J. Parasitol* 19 (1998) 77-83.
- [23] K.Y. Chu, I.K. Dawood, Cercarial transmission season of *Schistosoma mansoni* in the Nile Delta Area, *Bull Wld. Hlth. Org.* 42 (1970) 575-580.
- [24] E. Boelee, H. Laamrani, K. Khallaayoune, H. Madsen, Malacological length profile of irrigation canals in Morocco, emphasizing *Bulinus truncatus*, intermediate host of urinary schistosomiasis, in: *Proceedings of the 18th Symposium of the Scandinavian Society for Parasitology*, 1997, pp. 22-24.
- [25] R. Anderson, R. May, Prevalence of schistosome infections within molluscan populations: Observed patterns and theoretical predictions, *Parasitology* 79 (1979) 63-94.
- [26] O.F. Ati, C.J. Stigter, E.O. Oladipo, A comparison of methods to determine the onset of the growing season in northern Nigeria, *International Journal of Climatology* 22 (2002) 731-742.
- [27] Y. Wagatsuma, M.E. Aryeetey, F.K. Nkrumah, D.A. Sack, S. Kojima, Highly symptom-aware children were heavily infected with urinary schistosomiasis in southern Ghana, *Cen. Afr. J. Med.* 49 (2003) 16-19.
- [28] M.F. Useh, G.C. Ejezie, Modification of behaviour and attitude in the control of schistosomiasis, observations on water-contact patterns and perception of infection, *Ann. Trop. Med. Parasit.* 93 (1999) 711-720.
- [29] M.J. Enk, A. Amorim, V.T. Schall, Acute schistosomiasis outbreak in the metropolitan area of Belo Horizonte, Minas Gerais: Alert about the risk of unnoticed transmission increased by growing rural tourism, *Mem. Inst. Oswaldo Cruz.* 98 (2003) 740-750.
- [30] A.K. Jeans, M.P. Schweltnus, The risk of schistosomiasis in Zimbabwean triathletes, *S. Afr. Med. J.* 84 (1994) 756-758.
- [31] B.L. Blas, V.F. Prella, A.B. Ofelia, E.S. Edgardo, B.C. Jose, B.S. Edgardo, Epidemiology and control of schistosomiasis in the MR-9 Philipines: Progress report as of 1987, *Mem. Inst. Oswaldo Cruz Rio de Janeiro Supp. I* 84 (1989) 105.
- [32] J.W. Rudge, J.R. Stothard, M.G. Basanez, A.F. Mgeni, A.N. Khamis, D. Rollinson, Micro-epidemiology and pattern of *S. haematobium* infection among school children in Zanzibar, *Acta. Trop.* 105 (2008) 45-54.
- [33] S.A. Satayathum, Factors affecting infection or reinfection with *Schistosoma haematobium* in coastal Kenya: Survival analysis during a nine-year, school-based treatment program, *American Journal of Tropical Medicine and Hygiene* 75 (2006) 83-92.

Effect of Soil and Water Conservation Measures on Selected Soil Physical and Chemical Properties and Barley (*Hordeum spp.*) Yield

Tadele Amdemariam¹, Yihnew G. Selassie², Mitiku Haile³ and C. Yamoh³

1. Department of Natural Resources Management, College of Agriculture and Natural Resources, Debremarkos University, Debremarkos, Ethiopia

2. Department of Natural Resources Management, College of Agriculture and Environmental Sciences, Bahir Dar University, Bahir Dar, Ethiopia

3. Department of Land Resource Management and Environmental Protection, College of Dry Land Agriculture and Natural Resources, Mekele University, Mekele, Ethiopia

Received: March 4, 2011 / Accepted: April 19, 2011 / Published: November 20, 2011.

Abstract: A study was conducted in 2007/2008 at Absela locality, Banja Shikudad District of the Amhara National Regional State, Ethiopia to evaluate the effects of soil bunds stabilized with vetiver grass (*V. zizanioides*) and tree lucerne (*C. palmensis*) on soil physical and chemical properties, bund height, inter-terrace slope and barley (*Hordeum vulgare* L.) yield. Data were analyzed using one-way analysis of variance (ANOVA) and mean values for the treatments were separated using Duncan's Multiple Range Test. Results indicated that the non-conserved fields had significantly ($p \leq 0.05$) lower organic carbon and was found to contain 66% less OM from the average of the conserved treatment. 9-year old sole soil bund, the 9-year old soil bund stabilized with tree lucerne, the 9-year old soil bund stabilized with vetiver, and the 6-year old soil bund stabilized with tree lucerne had 71.20, 68.56, 52.30, and 36.12%, respectively higher percent OM than the control treatment. The trend was similar for total nitrogen. The non-conserved treatment had a higher bulk density when compared to the conserved fields. Fields with soil bunds stabilized with vetiver grass had the highest bund height and the lowest inter-terrace slope than fields treated with the rest of remaining conservation measures. Barley grain yields were significantly ($P < 0.05$) greater in both the soil accumulation and loss zones of the conserved fields than the non-conserved (control) treatment. Practicing soil conservation measures and curtailing causes of land degradation could improve the soil physical and chemical properties thereby increase land productivity of the conserved land.

Key words: Organic carbon, soil bund, total N, tree lucerne, vetiver.

1. Introduction

Soil degradation can be described as a reduction of resource potential by combination of processes acting on the land, such as soil erosion by water and wind, bringing about deterioration of the physical, chemical and biological properties of soil [1]. The principal environmental problem in Ethiopia is land degradation

and it is manifested mainly in the form of soil erosion, gully formation, soil fertility loss, and crop yield reduction. The excessive dependence of the Ethiopian rural population on natural resources, particularly land, as a means of livelihood is an underlying cause for land and other natural resources degradation [2].

Some forms of land degradation are the result of normal natural processes of physical shaping of the landscape and high intensity of rainfall. The scale of the problem, however, dramatically increased due to the increase in deforestation, overgrazing,

Corresponding author: Yihnew G. Selassie, associate professor, Ph.D., main research fields: soil chemistry, land management, environmental science. E-mail: yihnewgs@yahoo.com; yihnewgs@gmail.com.

over-cultivation, inappropriate farming practices, and increasing human population. Removing vegetative cover on steep slopes for agricultural expansion, firewood and other wood requirements as well as for grazing space has paved the way to massive soil erosion. Forest cover in the Ethiopian highlands as a whole decreased from 46% to 2.7% of the land area between the 1950s and the late 1980s [3].

It is estimated that over 1.9 billion tons of soils are lost from high lands of Ethiopia annually [4]. The Ethiopian highlands, which are the center of major agricultural and economic activities, have been the victim of soil erosion for many years. It is concluded that about half of the highland's land area (about 27 million hectares) is significantly eroded and over one-fourth (14 million hectares) are seriously eroded. Moreover, 2 million ha of land is permanently degraded that the land is no longer able to support cultivation [4].

In the Amhara region, the soil loss due to water erosion is estimated to be 58% of the total soil loss in the country [5]. This has already resulted in a reduction in agricultural productivity of 2 to 3% per year, taking a considerable area of arable land out of production. The situation is becoming catastrophic because increasingly marginal lands are being cultivated, even on very steep slopes [5].

Mechanical conservation structures are designed to control runoff and soil erosion in fields where biological control practices alone are insufficient to reduce soil erosion to permissible level and to support agronomic measures and soil management [6, 7]. The structures are designed to intercept and reduce runoff velocity, pond and store runoff water, convey runoff at non-erosive velocities, trap sediment and nutrients, promote formation of natural terraces over time, protect the land from erosion, improve water quality, enhance biodiversity of downstream water, prevent flooding of neighboring lands, reduce sedimentation of waterways, streams and rivers, improve land productivity and provide diverse ecosystem

services [6].

To mitigate land degradation problems in Ethiopia, the government has taken different soil and water conservation measures. Nevertheless, the rate of adoption of the interventions is considerably low. Space occupied by soil and water conservation (SWC) structures, impediment to traditional farming activity, water logging problems, weed and rodent problems and huge maintenance requirement are some of the reasons that cause farmers refrain from SWC works. In addition, top down approach in the extension activity, focusing mainly on structural soil and water conservation technologies, and land security issues contribute much to the failure of SWC works [8]. The present study was conducted by superimposing the treatments on one of the few successful SWC structures stabilized with biological measures to investigate the effects of integrating physical and biological conservation measures on some soil physical and chemical properties and subsequently on yield of crops and it is hypothesized that soil bunds stabilized with vetiver grass and tree lucerne will help to control erosion and improve soil physical and chemical properties and yield of crops when compared to non-conserved land.

2. Materials and Methods

2.1 Description of the Study Area

The study area was located in Absela Kebele, Banja Shikudad District, Amhara National Regional State (ANRS), Ethiopia between 10°45'-10°48' N latitude and 37°03'-37°04' E longitude. The mean annual rainfall of the study area ranges from 170 cm to 256 cm, with mean monthly minimum and maximum temperature ranging from 7 °C to 12 °C, and 18 °C to 25 °C, respectively (Fig. 1). The area has wet-cold locally known as *wet dega* agro-climatic zone [9]. The study area has an altitude that ranges between 2220 and 2600 meters above sea level with undulating topography. Its slope ranges from 15-25%. The dominant soil type of the research area is Nitosols with

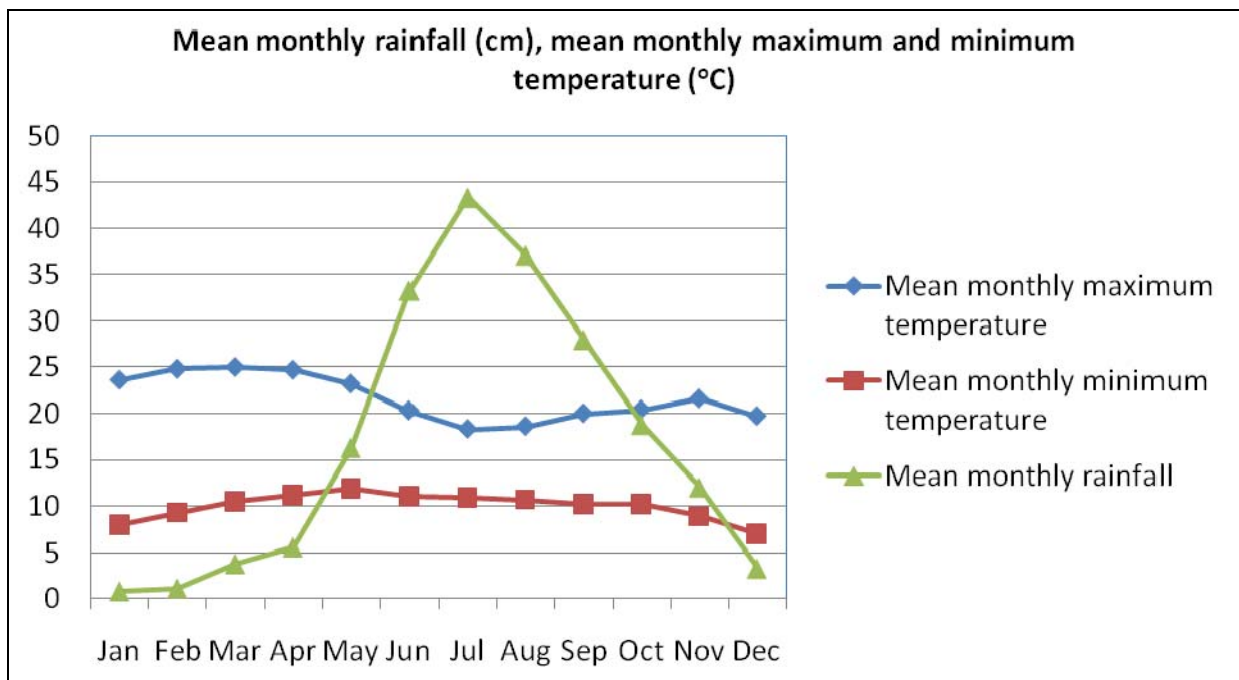


Fig. 1 Mean monthly rainfall, maximum and minimum temperature of the study area.

catchment that was treated with different type of soil and water conservation measures was about 126 ha. The length of growing period of the study area ranges between 240 and 270 days [10]. The farming system of the area is mixed farming, which includes crop such as barley, wheat, teff, pulse crops, and livestock (mainly sheep and cattle).

2.2 Characterization of the SWC Structures Considered in the Study

All soil and water conservation measures in the catchment area were installed for the purpose of demonstration; to diffuse extension service related to natural resource conservation to the farming community by the district and zonal agricultural bodies. The catchment area was delineated and different soil and water conservation activities were practiced since 1998. Various ages of soil bund stabilized with biological measure such as vetiver grass (*V. zizanioides*), tree lucerne (*C. palmensis*), sesbania (*Sesbania sesban*) and phalaris grass (*Phalaris spp.*) are found in the catchment.

The specific experimental field had original slope of

21% (slope percent prior to the construction of the structures) and 2 m vertical interval was used for the spacing of bunds. All the soil bunds were constructed in such a way that a trench was excavated to a depth of 60 cm and 50 cm wide along a contour at 1% gradient towards the waterway and the soil was thrown down hill, with which an embankment of soil having bottom width of 75 cm and top width 50 cm were established.

Where the bunds were stabilized with vetiver, tillers of the same were planted at the upper position of the soil bund with a spacing of 30 cm in a single row and where it was stabilized with tree lucerne, the seedlings were planted at the top of the soil embankment with 50 cm spacing in a single row. Planting of vetiver tiller and tree lucerne seedlings were done in the same year after installing the structures but in summer (Ethiopian rain season). The trees used to stabilize the bund were pruned each year before the onset of the main rainy seasons to avoid the shading effect after once they got matured. The pruned materials were largely used as source for fuel wood consumption, fodder material for cattle and sometimes as a fencing material. The pruned materials had never been incorporated to the soil as part

of a management practice to serve as source for organic matter except that some few fallen plant parts were added to the soil occasionally and insignificantly. There were also bunds left unplanted and area of lands not terraced where the later was used as control to the experiment.

2.3 Experimental Design and Layout

The experiment had five treatments, replicated 4 times which included:

- (1) Control (non-conserved plots);
- (2) 6 years soil bund + tree Lucerne;
- (3) 9 years soil bund + tree Lucerne;
- (4) 9 years soil bund + vetiver;
- (5) 9 years soil bund.

The pictures taken on the experimental fields are indicated in Figs. 2-4.

2.4 Sampling Technique

For soil analysis, composite soil samples representing the treatments were collected from each replication situated at soil deposition zone from within 30 cm soil depth using simple random sampling

technique. The size of the plots from which the composite soil samples were taken was 3 m × 10 m, the longest side along the contour.

In order to relate changes in the soil physical and chemical properties brought by the different treatments in the experiment with yield performance, a trial was conducted using test crop barley, which were planted both at the deposition (accumulation zone) and soil loss zone (erosion zone) with a seeding rate of 200 kg·ha⁻¹. The plots to which the crop planted had a size of 6 m × 3 m with the longest side parallel to the bunds. Wheat was the precursor crop for all treatment used in the research. Land preparation, method of planting and management practices for treatments were similar and followed the conventional procedure adopted by the farmers. Agronomic yield and yield component data were collected. These included plant height, number of plants m⁻², number of spike m⁻², number of spiklets/spike, and grain yield. Numbers of spiklets/spike were counted at field while the crop was standing just before harvesting through simple random sampling technique (100 samples of spikes per plot were considered).

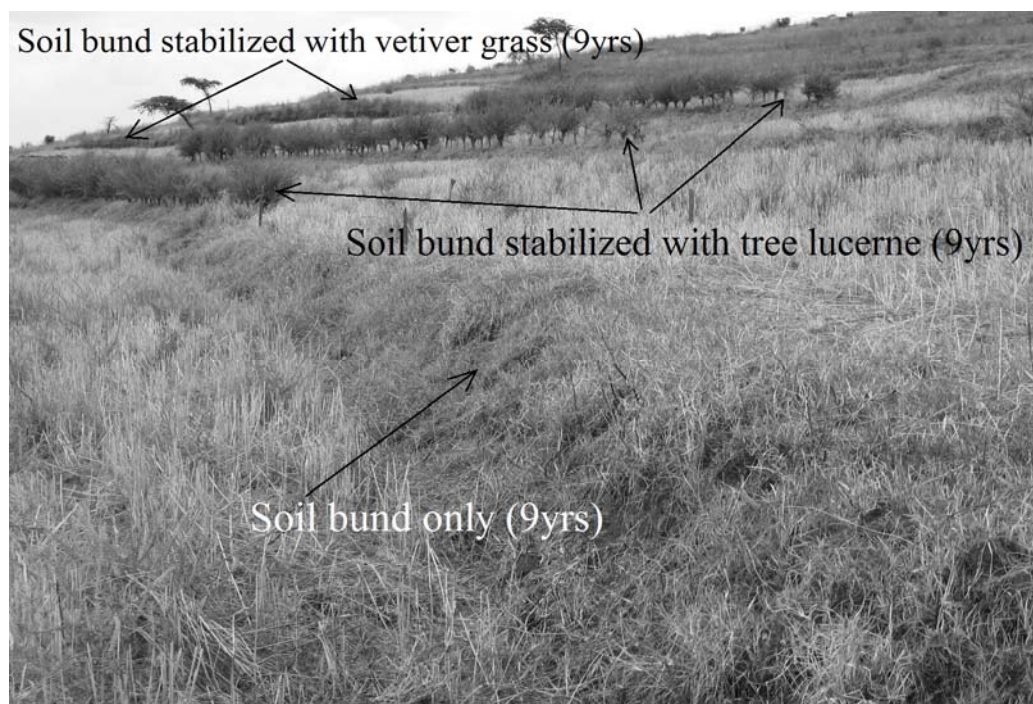


Fig. 2 Partial view of the experimental plots showing three treatments along with their replication (9-year soil bund stabilized with vetiver, 9-year soil bund stabilized with tree lucerne, and sole 9-year soil bund).

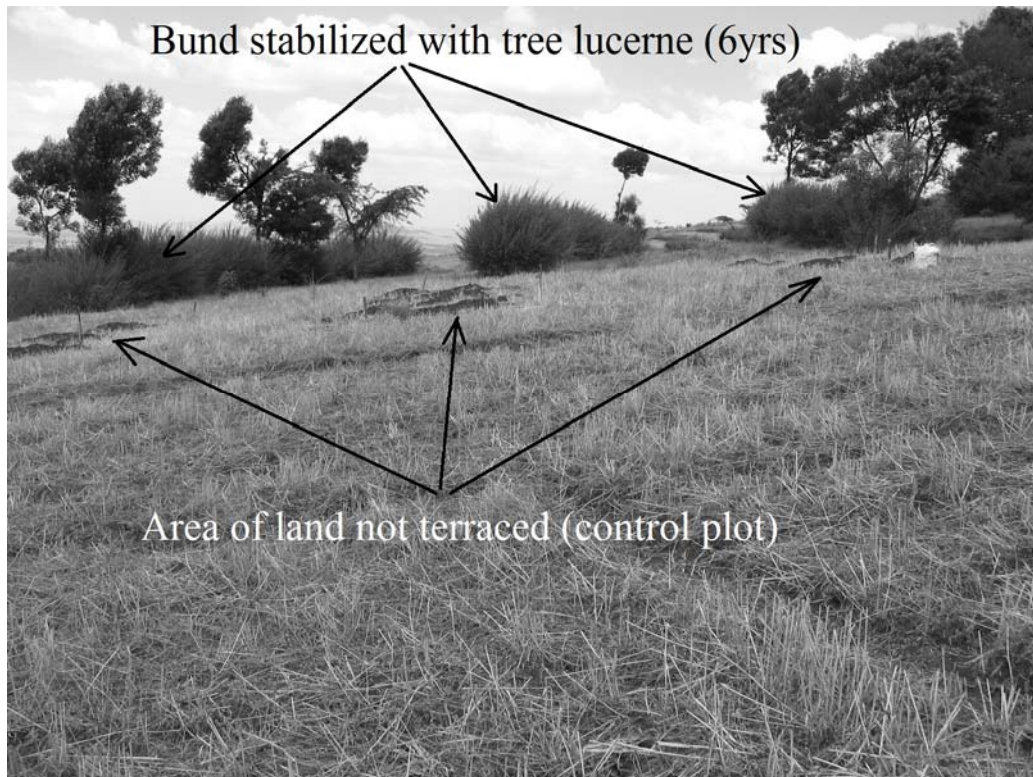


Fig. 3 Partial view of experimental plots showing the remaining two treatments (6-year soil bund stabilized with tree lucerne and the control plot).



Fig. 4 9-year soil bund stabilized with vetiver grass.

2.5 Data Analysis

The data obtained from laboratory and field measurements were analyzed statistically with JMP-5 using one-way analysis of variance (ANOVA) at $p \leq 0.05$ level of significance [11].

Soil textures were analyzed using hydrometer method [12]. Infiltration rate was measured using double ring infiltrometer and the soil bulk densities were determined from the oven dry (at 110 °C for 24 hrs) mass of soil in the core sampler and volume of the undisturbed soil cores using core sample method [12] and the relationship:

Bulk density ($\text{g}\cdot\text{cm}^{-3}$) = Oven dry soil mass (g)/Core volume (cm^3)

Soil organic carbon (OC) was determined following the wet digestion method [12]. Organic matter (OM) content was computed from organic carbon by multiplying each value of SOC by 1.724. Total Nitrogen (TN) was determined by the Kjeldahl method [12].

3. Results and Discussion

3.1 Effect of Soil Conservation Measures on Soil Chemical and Physical Properties

3.1.1 Organic Matter and Total Nitrogen

Results of the experiment indicated that there was a highly significant ($p \leq 0.05$) difference in OM content among the treatments. The 9-year old soil bund stabilized with tree lucerne and the 9-year old sole soil bund have significantly higher OM content than that of the 9-year old soil bund stabilized with vetiver, the 6-year old soil bund stabilized with tree lucerne, and the non-conserved treatments. The 9-year old soil bund stabilized with vetiver had statistically lower percent OM than the 9-year old sole soil bund treatments and the 9-year soil bund stabilized with tree lucerne, but it had significantly ($p \leq 0.05$) highest percentage of OM than the 6-year old soil bund stabilized with tree lucerne, and the non-conserved treatment (Table 1).

The non-conserved plots had significantly lowest

mean value of OM than all other treatments considered in the study. On relative basis, the 9-year old sole soil bund, the 9-year old soil bund stabilized with tree lucerne, the 9-year old soil bund stabilized with vetiver, and the 6-year old soil bund stabilized with tree lucerne had 71.20, 68.56, 52.30, and 36.12%, respectively higher percent OM than the control treatment. The result agrees with the finding by Million [13] who found that organic matter content of three terraced sites with original slopes of 15, 25, and 35% were higher than the corresponding non-terraced sites of similar slope. A study conducted by Kinati [14] in Enebsie Sar Mider district, Amhara region also showed that the organic matter content of non-conserved land for a slope range between 10 and 15% were lower (mean = 1.12%) than the terraced land of corresponding slope class (mean = 2.33%).

According to Bot and Benites [15], organic matter accumulation is often favored at the bottom of hills for two reasons: One is they are wetter than at mid- or upper slope positions, and the other is organic matter would be transported to the lowest point in the landscape through run off and erosion. The same holds true for terraced land where soils are actively eroded from the soil loss zone and deposited to the soil accumulation zone, creating spatial variability in terms of moisture and nutrient availability within the inter-terrace space.

The result for total nitrogen appeared to follow

Table 1 Effect of SWC measures on organic matter and total nitrogen contents of the soil.

Treatments	Organic matter (%) [*]	Total nitrogen (%) [*]
Control (non-conserved land)	1.577 ^d	0.125 ^c
6-yrs old soil bund + tree lucerne	2.470 ^c	0.173 ^{bc}
9-yrs old soil bund + tree lucerne	5.017 ^a	0.277 ^a
9-yrs old soil bund + vetiver	3.306 ^b	0.215 ^b
9-yrs old soil bund	5.478 ^a	0.284 ^a
CV (%)	14.00	17.48
SE \bar{x}	0.249	0.0187

^{*}Means in a column followed by the same letter are not statistically different at $p \leq 0.05$.

similar trend as that of organic matter (Table 1). Million [13] also found that the mean total nitrogen contents of the terraced site with the original slope of 15, 25, and 35% were higher by 26, 34, and 14%, respectively compared to the average total nitrogen contents of their corresponding non-terraced slope.

Although the 9-year soil bunds stabilized with tree lucerne were significantly higher in its organic matter content and total nitrogen, it was not significantly higher from that of sole 9-year soil bund. These could largely attribute to the way how the pruned tree lucerne materials were used by the landholders. In the study, area, the pruned materials were largely used as a source of fodder, firewood and fencing. It was neither used as mulch nor incorporated to the crop land to increase the fertility condition of the soil. Agroforestry practices such as alley-cropping systems modify the availability of soil nutrients in various ways. Generally, the inclusion of woody species on farmlands improves soil fertility by improving the organic content of soil through the addition of leaf litter and other parts from trees. Several studies, however, revealed that the nutrient from the hedgerows of alley cropping would be less if there is an off-take of pruning from the plots for various purposes [16].

3.1.2 Soil Texture

The analysis of variance computed for the different treatments with respect to the soil separates showed that sand, silt and clay content among the treatments were found significantly ($p \leq 0.05$) different with R^2 of 0.86, 0.83 and 0.90, respectively. Among the treatments, the non-conserved land had the highest mean value of percent clay and the lowest percent sand, which were significantly different, from those other treatments that are managed through different SWC measures.

In a study conducted by Million [13], to investigate the role of indigenous bund on soil productivity, he found high clay content at the upper slope position of the inter-terrace area, where sever erosion were expected to occur, regardless of the original ground slope and width of treatments considered in the study.

Considering bunds of similar age, the 9-year soil bund stabilized with vetiver grass had significantly highest proportion of clay soil separates than the 9-year soil bund stabilized with tree lucerne and the 9-year soil bund treatment (Fig. 5). The presence of highest clay percent in 9-year soil bund stabilized with vetiver treatment when compared to the other conservation measures could be related to the significant increase of

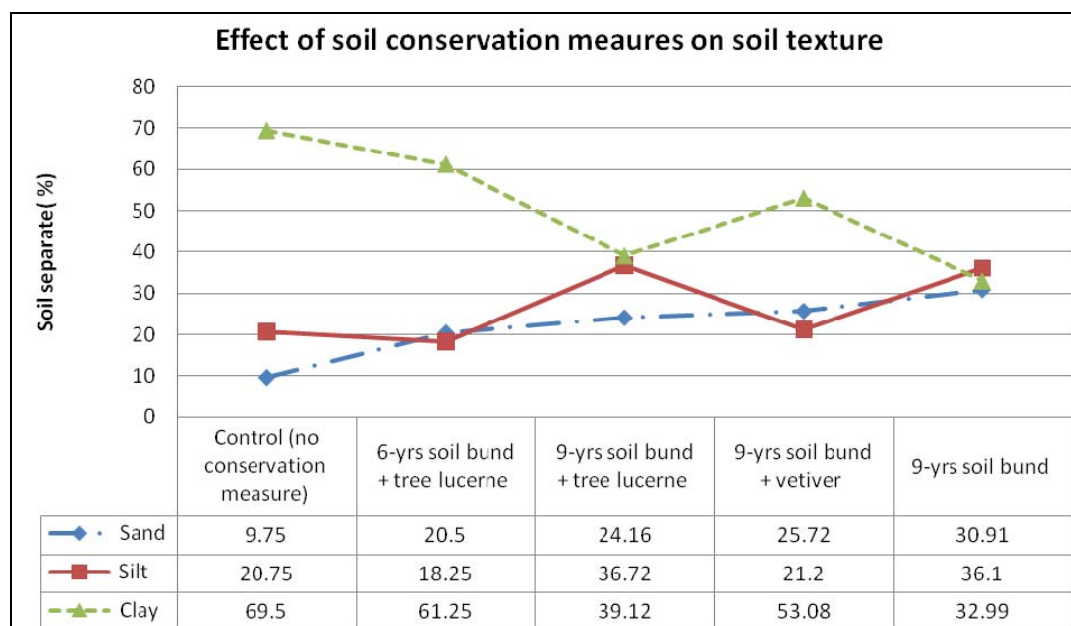


Fig. 5 Effect of soil and water conservation measures on soil texture.

bund height for the same that encouraged the deposition of sub soil materials eroded from the loss zone. Herweg and Ludi [17] pointed out that the complete removal of topsoil at the loss zone causes the subsoil (dominated by clay material) to move down slope and deposited on the top of the fertile accumulation. Herweg and Ludi [17] also discussed that tillage and water erosion causes colluviums to be deposited in the lower part of fields while soil profiles are truncated in the upper part. A study conducted by Desta et al. [18] revealed that the annual mass of soil displaced down slope from the truncation area by tillage erosion for 202 study plots was $39 (\pm 23) \text{ kg}\cdot\text{yr}^{-1}$, the maximum and the minimum values of unit soil loss rate being 7.5 and 122 $\text{kg}\cdot\text{yr}^{-1}$.

When bunds of different age were considered, the 9-year soil bund treatment had significantly lower percent of clay fraction than the 6-years soil bund that was stabilized with tree lucerne. Treatment that were stabilized with similar vegetation measure but had different age also had significantly different amount of clay soil separates in their sample. Therefore, the 6-years soil bund stabilized with tree lucerne had higher clay percent than the 9-year soil bund stabilized alike. Relative to the non-conserved treatment, the 6-years soil bund stabilized with tree lucerne, the 9-year soil bund stabilized with veriver, the 9-year soil bund stabilize with tree lucerne, and the 9-year soil bund treatment had 11.9, 23.6, 43.7, and 52.5%, respectively lower clay percent.

Delayed exposure of sub-soil in the depositional

zone of the terraced area particularly the 9-year soil bund stabilized with tree lucerne and the 9-year soil bund could cause less proportion of clay particles. Highest clay content in the control treatment was due to the exposure of the sub soil to serious level of erosion, which is naturally high in clay content. The 9-years soil bund stabilized with vetiver was dominated by clay and this could be the result of sub soil accumulation in the deposition zone because of soil erosion.

3.1.3 Bulk Density and Infiltration Rate

The one-way analysis of variance revealed the presence of significant difference ($p \leq 0.05$) in mean value of bulk density among the treatments. The non-conserved treatment was found to exhibit significantly higher mean bulk density than the remaining treatments. There was no, however, significant difference in mean bulk density among the rest of the treatments, which were managed through a range of conservation measures irrespective of the establishment year. The relatively lower bulk density associated with treatments conserved with various measures (Table 2) could be attributed to the presence of significantly ($p \leq 0.05$) higher organic matter content in those treatments.

The one-way analysis of variance also indicated the presence of statistically significant difference ($p \leq 0.05$) in mean infiltration rate among the treatments. The 9-year old soil bund and 9-year old soil bund stabilized with tree lucerne had the highest mean infiltration rate than the other treatments. The non-conserved treatment had the lowest mean infiltration rate (Table 2).

Table 2 Effect of SWC measures on soil bulk density and infiltration rate.

Treatments	Soil bulk density ($\text{g}\cdot\text{cm}^{-3}$)*	Infiltration rate ($\text{cm}\cdot\text{hr}^{-1}$)*
Control (non-conserved land)	1.38 ^a	0.24 ^b
6-yrs old soil bund + tree lucerne	1.26 ^b	0.28 ^b
9-yrs old soil bund + tree lucerne	1.29 ^b	0.73 ^a
9-yrs old soil bund + vetiver	1.25 ^b	0.82 ^a
9-yrs old soil bund	1.27 ^b	0.88 ^a
CV (%)	2.43	4.48
$SE_{\bar{x}}$	0.015	0.109

*Means in a column followed by the same letter are not statistically different at $p \leq 0.05$ and $p \leq 0.01$ for bulk density and infiltration rate, respectively.

The organic matter and percentage of clay soil separates in the treatments seemed to play crucial role for the variation in infiltration rates. Organic carbon content positively correlated ($p \leq 0.01$; $R^2 = 0.54$) with the infiltration rate (Fig. 6); while clay percentage negatively correlated ($p \leq 0.01$; $R^2 = 0.52$) with the same (Fig. 7). Moreover, infiltration rate was negatively correlated with bulk density of the soil. According to the rating of Landon [19] the non-conserved, the 6-year old soil bund stabilized with tree lucerne had slow infiltration rate while the 9-year old sole soil bund treatment, the 9-year old soil bund stabilized with tree lucerne and the 9-year old soil bund stabilized with vetiver treatments had moderately faster infiltration rate.

3.1.4 Slope Transformation

Results of the experiment indicated that the mean values of inter-terrace slope for the treatments are significantly different ($p \leq 0.05$ and $R^2 = 0.98$). The 9-year old soil bund stabilized with vetiver had significantly the lowest inter-terrace slope than all other treatments considered in the study signifying the effectiveness of vetiver grass in bund stabilization and slope transformation ability when compared to the

other bund stabilization techniques.

Differences in year of bund installation also brought a variation in inter-terrace slope, which was realized by having a lower inter-terrace slope for the aged bund than the younger one. Therefore, all 9-year old soil bund treatments (irrespective of bund stabilization technique) had the lowest mean value of inter-terrace slope percent than the 6-year old soil bund stabilized with tree lucerne. Considering age of bunds and the type of material used to stabilize them, the 9-year old soil bund stabilized with tree lucerne had significantly lower inter-terrace slope than the 6-year old soil bund stabilized with similar plant species (Fig. 8).

The deposition of soil materials and debris on the upper position of soil bund (usually called accumulation zone) causes the height of the bunds to rise year after year, thereby reducing the inter-terrace slope between two successive structures.

Similar to inter-terrace slope, the mean value of bund height was affected by age of the bunds. The older the bund, the higher was its bund height. Thus, the 9-year old soil bund treatments had higher mean bund height than the 6-year old soil bund (Fig. 9). Herweg and Ludi [17] pointed out that in the course of

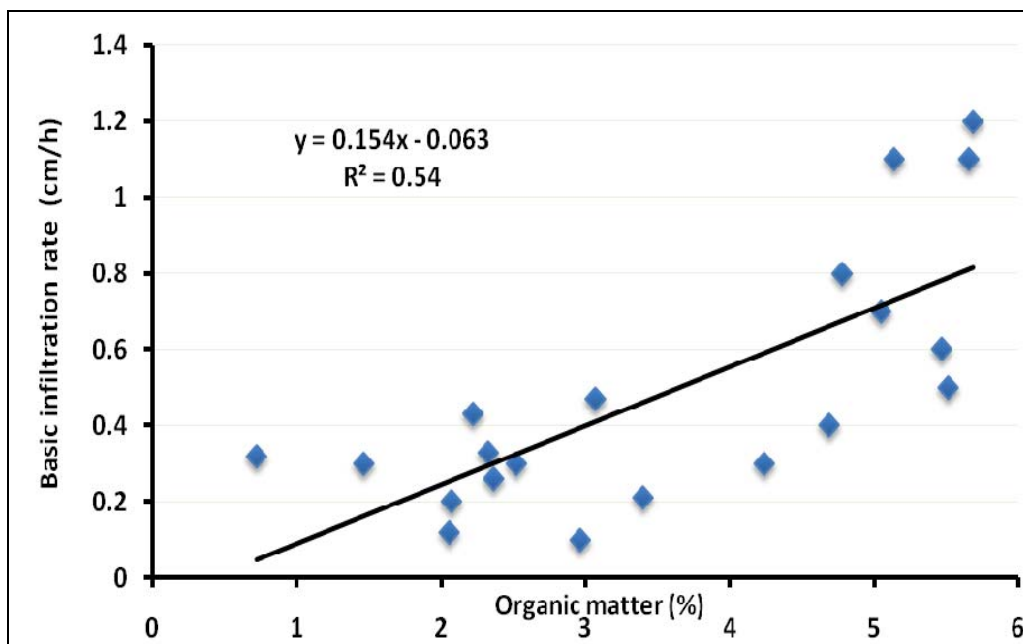


Fig. 6 Regression plot for basic infiltration rate vs. organic matter.

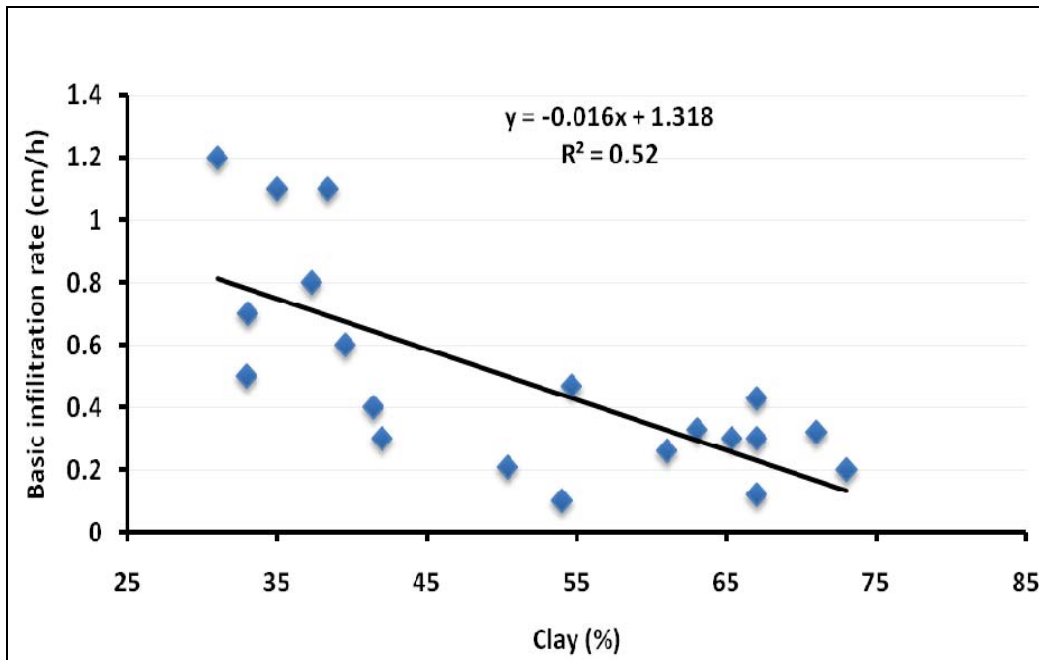


Fig. 7 Regression plot for basic infiltration rate vs. clay percentage.

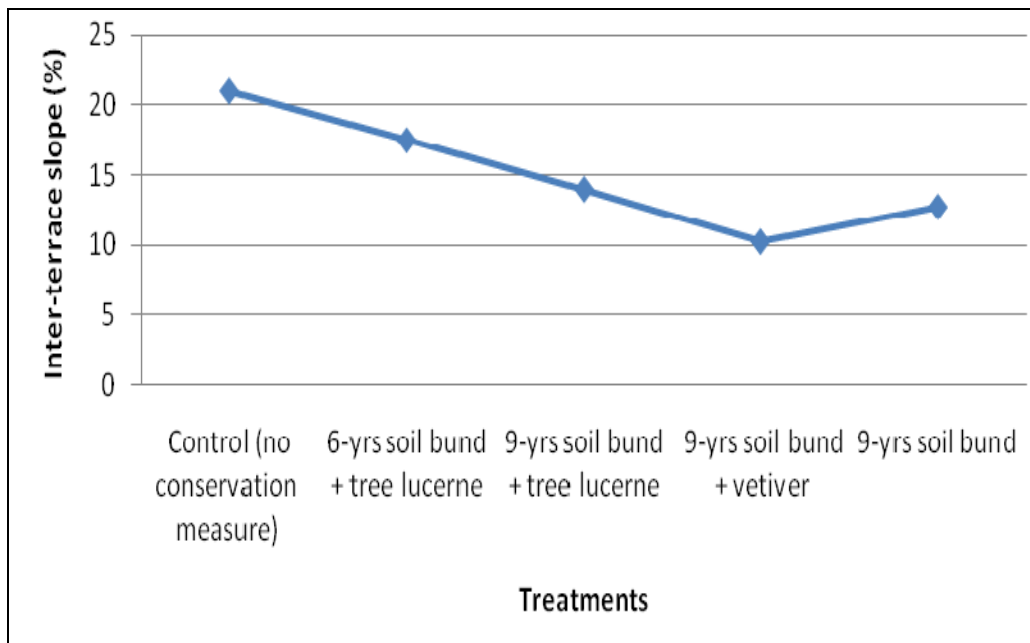


Fig. 8 Effect of SWC measures on inter-terrace slope.

erosion process that forms the terrace, the topsoil below the structure would gradually move down a slope and accumulate above the next SWC structure. This would eventually increase the bund height in gradual processes. According to Desta et al. [18], the rate of sediment accumulation by bunds is correlated with the soil loss by tillage because all the soils

displaced by tillage remains in the accumulation zone.

3.2 Effect of the Conservation Measures on Barley Yield

The one-way analysis of variance computed for the various treatments showed that grain yield varied significantly ($p \leq 0.05$). The 9-year old soil bund

stabilized with tree lucerne was found to give significantly ($p \leq 0.05$) higher mean value of grain yield than the 9-year old soil bund, 9-year old soil bund stabilized with vetiver, 6-year old soil bund stabilized with tree lucerne and the non-conserved treatment (Table 3). The 9-year old soil bund stabilized with tree lucerne had significantly higher grain yield than the 9-year old soil bund treatment. The non-conserved treatment had significantly lower mean grain yield compared to all other treatments. The yield components also showed similar trend in performance as that of the grain yield at the deposition zone.

Higher yield associated with the conservation measures could be attributed to the presence of high level of organic matter and total nitrogen in these treatments. A regression analysis computed for the grain yield performance with organic matter and nitrogen had confirmed this fact. Organic carbon and total nitrogen were directly related ($R^2 = 0.74$ and 0.71 , respectively at $p \leq 0.01$) to the grain yield of barley.

When yield in the accumulation and the loss zones are compared, the average grain yield obtained from the accumulation zones (averaged over all the treatments) was 29.8% higher than the average grain

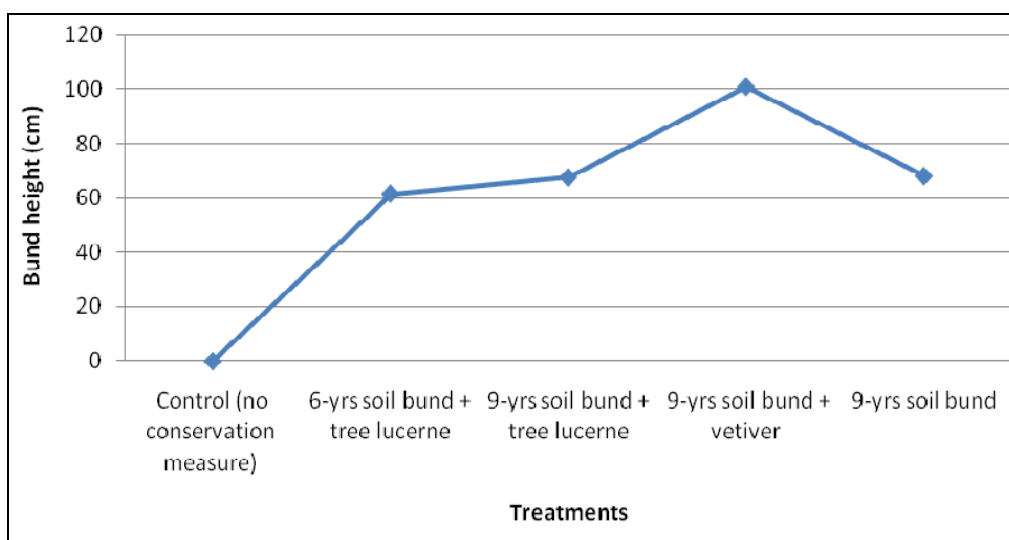


Fig. 9 Effect of SWC measures on bund height.

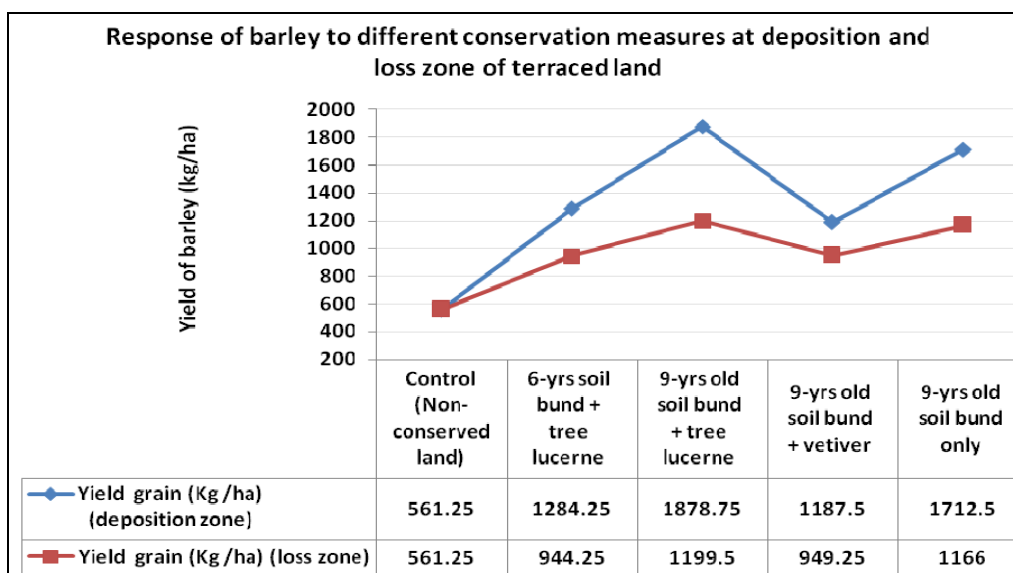


Fig. 10 Response of barley to different conservation measures at soil deposition and soil loss zone of terraced land.

Table 3 Effect of conservation measures on grain yield and yield components at the soil deposition zone.

Treatments	Grain yield (kg·ha ⁻¹) (a)	No. of plants m ⁻² (ab)	No. of spikes m ⁻² (a)	No. of spikelets/spike (a)	Plant height (cm) (a)
Control (non-conserved land)	561.25 ^d	404 ^b	350 ^c	7.0 ^c	44.50 ^c
6-yrs old soil bund + tree lucerne	1284.25 ^c	431 ^b	397 ^{ab}	15.75 ^b	57.75 ^b
9-yrs old soil bund + tree lucerne	1878.75 ^a	478 ^a	426 ^a	18.25 ^a	75.75 ^a
9-yrs old soil bund + vetiver	1187.50 ^c	417 ^b	396 ^{ab}	16.00 ^b	69.00 ^{ab}
9-yrs old soil bund	1712.50 ^b	435 ^b	375 ^{bc}	17.25 ^{ab}	77.75 ^a
CV (%)	7.82	5.79	6.55	7.01	11.5
SE \bar{x}	51.80	12.52	12.73	0.52	3.74

^aMeans in a column followed by the same letter are not statistically different at $p \leq 0.05$.

^bNo. of plants include all mother plants and tillers found in each plot.

yield obtained from the loss zones. This signifies the presence of fertility gradient within the inter-terrace space and highest yield in the deposition zone of the conserved treatments seemed to associate with the level of OM and total nitrogen contained in the same, coupled with other desirable changes in soil physical and chemical property brought by the implemented conservation measures (Fig. 10).

4. Conclusions and Recommendations

The experiment confirmed that compared to non-conserved plots, soil and water conservation measures can better control soil erosion problem in steep slope lands and yields some desirable effect on some physical and chemical properties of the soil which in turn improves the productive capacity of the land. Bund installation improved soil organic matter, total nitrogen, infiltration rate, soil bulk density, inter-terrace slope and bund height. Some soil properties were also found to vary significantly in response to bund age.

Organic matter and total nitrogen were significantly higher in all plots treated with different types of soil and water conservation measures irrespective of the age and type of plant used to stabilize the bunds than that of non-treated plots. When soil bunds of different age compared, older bunds produced significantly higher soil organic matter and total nitrogen. The research proved that mere stabilization of bunds with different type of plants did not result superior benefit and less improvement were observed in terms of soil

properties such as total nitrogen and organic matter contents when compared to soil conservation structures of similar age unless the pruned plant material are returned to the soil in the form of mulch or are used as green manure and incorporated to the soil for its improvement.

The research also discloses that inter terrace slope could be improved with the making of physical structures but that does not necessarily insure the improvement of land productivity in the entire area unless some agronomic and vegetative soil management practices are employed in between bunds.

The highest yields obtained in the accumulation zone of the conserved land signify the presence of fertility gradient within the inter-terrace space. Highest yield in the deposition zone of the conserved treatments seemed to associate with the level of organic matter and total nitrogen contained in the same.

As recommendation it is necessary to rehabilitate degraded agricultural lands through the implementation of integrated soil and water conservation measures (physical and biological measures) in order to increase their productivity to a significant level. Stabilization of bunds with tree species should be accompanied with the addition of the pruned to the soil for better effect.

Acknowledgments

This paper is partially based on work conducted within the framework of the Swiss National Centre of Competence in Research (NCCR) North-South:

Research Partnerships for Mitigating Syndromes of Global Change. Ministry of Agriculture, Ethiopia; Mekelle University, Ethiopia; and Center for Development and Environment, Bern University, Switzerland are also acknowledged for financially supporting the research.

References

- [1] J.M. Maitima, J.M. Olson, Guide to field methods for comparative site analysis for the land use change, impacts and dynamics (LUCID), Project Working Paper Series Number 15, International Livestock Research Institute, Nairobi, Kenya, 2001.
- [2] EPA (Environmental Protection Agency), National Action Programme to Combat Desertification, Federal Democratic Republic of Ethiopia Environmental Protection Authority, Addis Ababa, 1998, p. 30.
- [3] United States Agency for International Development (USAID), Ethiopia land policy and administration assessment, Final Report with Appendices, USAID Contract No. LAG-00-98-00031-00, Task Order No. 4, 2004, p. 110.
- [4] EHRS (Ethiopian Highland Reclamation Study), Final Report, Vol. I, FAO, Rome, 1986.
- [5] F. Tesfahun, A. Osman, Challenge and prospects of food security in Ethiopia, in: Proceeding of the Food Security Conference, UNNCC, Aug. 13-15, Addis Ababa, Ethiopia, 2003, p. 223.
- [6] R. Blanco, R. Lal, Principles of Soil Conservation and Management, Springer, New York, 2008, p. 285.
- [7] R.P.C. Morgan, Soil Erosion and Conservation, Blackwell Publishing, 3rd ed., USA, 2005, p. 303.
- [8] H. Mitiku, K. Herweg, B. Stillhardt, Sustainable Land Management-A New Approach to Soil and Water Conservation in Ethiopia, Land Resources Management and Environmental Protection Department, Mekelle University, Ethiopia, and Swiss Centre for Development and Environment, National Centre of Competence in Research (NCCR) North-South University of Bern, Switzerland, 2006, p. 269.
- [9] A practical guide for development agent in Ethiopia, Ethiopia, European Development Fund (EDF) Project No. 6.ACP.ET. 026, International Agricultural Training Programme, 2005, p. 35.
- [10] EMA, The Length of the Growing Period in Ethiopia, PMGSA-MoA-Land Use Planning and Regulatory, Department/UNDP-FAO Assistance to Land Use Planning Project-ETH/78/003, Addis Ababa, Ethiopia, 1982.
- [11] SAS (Statistical Analysis System) Institute Inc., Statistical Analysis System, Cary, NC, USA, 2003.
- [12] S. Sahelemedhin, B. Taye, Procedures for soil and plant analysis, Technical Paper No. 74, National Soil Research Center, Ethiopia Agricultural Research Organization, Addis Ababa, Ethiopia, 2000, p. 110.
- [13] A. Million, Characterization of indigenous stone bunding (Kab) and its effect on crop yield and soil productivity at Mesobit-Gedba, North showa zone of Amhara region, M.Sc. Thesis, Alemaya University, Alemaya, Ethiopia, 2003.
- [14] C. Kinati, The effect of integrated soil and water conservation measures on soil physical and chemical properties, a case for Enebsie Sar Midir Wereda, Ethiopia, M.Sc. Thesis, Mekelle University, Mekelle, Ethiopia, 2006.
- [15] A. Bot, J. Benits, The Importance of Soil Organic Matter—Key to Drought Resistant Soil and Sustained Food and Production, FAO, Rome, 2005, p. 78.
- [16] J. Shibu, C.A. Samuel, P.K. Ramachandran, Tree-crop interactions: Lessons from temperate alley cropping systems ecological basis of agroforestry, in: J. Shibu, C.A. Samuel, P.K. Ramachandran (Eds.), CRS Press, London, 2008, pp. 15-36.
- [17] K. Herweg, E. Ludi, The performance of selected soil and water conservation measures-case studies from Ethiopia and Eritrea, *Catena* 36 (1999) 99-114.
- [18] G. Desta, J. Poesen, J. Decker, H. Mitiku, G. Govers, J. Moeyerdons, Effectiveness of stone bunds in controlling soil erosion on cropland in the Tigray Highlands, northern Ethiopia, *Soil Use and Management* 21 (2005) 287-297.
- [19] J.R. Landon, Booker Tropical Soil Manual, A Handbook for Soil Survey and Agricultural Land Evaluation in Tropics and Sub Tropics, Longman Scientific and Technical Publishers, New York, 1991, p. 474.

Beta Diversity of Mbuna in Lake Malawi

L.G. Kanyumba¹, W.J. Changadeya¹, A.J.D. Ambali², L.A. Kamwanja³ and E.K.W. Kaunda⁴

1. Department of Biology, University of Malawi, Zomba, Malawi

2. NEPAD Planning and Coordinating Agency, Pretoria, South Africa

3. University of Malawi, Zomba 278, Malawi

4. Department of Aquaculture and Fisheries Science, University of Malawi, Lilongwe, Malawi

Received: April 19, 2011 / Accepted: June 9, 2011 / Published: November 20, 2011.

Abstract: Molecular and field studies suggest that Mbuna have limited migration range and are restricted by habitat discontinuities especially in areas where rocky habitats are separated by stretches of sand. This study estimated regional diversity of Mbuna in Lake Malawi. The estimated β -diversity for all sites was 114.5 Mbuna suggesting that there was high level of allopatrism for the species complex. Sympatric index was low in the two regions of southern and northern lake and the observed high-end richness strongly correlated with minimum species richness. The sympatric index for the whole lake was 0.8, with non-monotypic species complexes showing declining values of sympatric index and the decline was dependent on the geographical scale of the area covered. The northern region sites had mean habitat ranking of 84.5% while the southern sites had habitat ranking of 56.7% supporting the observation that there are more rocky habitats in the northern part of the lake than in the southern. Implications of habitat ranking are discussed in terms of species abundance and richness.

Key words: Mbuna, beta diversity, species richness, species abundance.

1. Introduction

Diversity is recognised at three levels, α , β and γ , where α -diversity measures the diversity within a particular area or ecosystem and is usually expressed by the number of species (i.e. species richness). β -diversity estimates the total number of species that are unique to each of the ecosystems being compared by determining the amount of species change between ecosystems [1]. γ -diversity is a measure of the overall diversity for the different ecosystems within a region. It is also referred to as “geographical-scale species diversity” [2]. β -diversity explains spatial variability in assemblage structure and is one of the fundamental themes of contemporary community ecology [3, 4]. It provides an explanation of the ecological interactions of populations with their environment, random events that influence population abundance within a habitat

and rates of species dispersal between habitat patches [5]. It is based on the observation that an assemblage with high functional overlap among species is less diverse than an assemblage in which species are less functionally similar [6]. Although estimation of β -diversity is important for formulation of species preservation procedures, limited studies have analysed β -diversity of Lake Malawi cichlids [7, 8].

The species distribution and abundance of Mbuna have been linked to three processes: limited dispersal ability, environmental determinism and stochastic events. Mbuna are known to have limited horizontal and vertical dispersal thus they have strong habitat fidelity within stretches of continuous habitat [9, 10]. Molecular studies by Ref. [11] suggested that limited migration of Mbuna is due to restriction imposed by habitat discontinuity where by stretches of sandy bottom or deep waters even impose barrier to gene flow. The low dispersal has, therefore, led to allopatric populations which have been linked to the evolution

Corresponding author: W.J. Changadeya, senior lecturer, Ph.D., main research fields: fish population genetics, plant population genetics, biodiversity conservation. E-mail: wchanga@chanco.unima.mw, wisdomchangadeya@gmail.com.

of differing breeding colouration. The environmental determinism is brought about by sympatric species that appear anatomically indistinguishable but are different in their ecological characters. Hence spatial differences in abundance are due to availability of resources upon which they depend and rates of predation and parasitism. The two most important environmental factors are substrate composition and habitat depth. Stochastic events are those that subject the populations to such events like predation which in return have an effect on population abundance.

The species richness of Mbuna depends on phenotypic variables like breeding colours and trophic morphology which play a major role. It has been observed that the co-occurring taxa with different breeding colours are reproductively isolated, although they may share several other morphological traits. It can therefore be ascertained that anatomically similar sympatric populations with contrasting breeding colours are true species. It has also been shown that anatomically similar populations occupying adjacent habitats that share breeding colours are on average genetically more closely related than similar sympatric populations with different breeding colours [12]. It is, therefore, reasonable to assume that adjacent allopatric populations sharing the same colour traits and anatomical characters are representatives of the same species. It is estimated that Mbuna “species” present in Lake Malawi have total allopatric distributions of about 70%, the assignment of such allopatric populations to species should severely affect measures of beta diversity because the phenotypic traits being employed are unreliable indicators of biological species. Morphological characters alone can not reliably take into consideration phenotypic differences along geographical clines [13]. Therefore, use of morphologically defined species can provide inaccurate assessments of regional species richness [14].

There are limited rules that govern the types and degrees of differences in phenotypic or genotypic

traits that are used to distinguish species in such species assemblages. This has led to systematicists using phenotypic trait information with differing degree of importance as a result there is inconsistency in the assignment of populations to categories such as species, subspecies, megaspecies or allospecies. There is, therefore, need for a quantitative procedure that enables estimates to be standardized for comparative work. A procedure that generates a measure of minimum regional species richness, as a standardized alternative without necessarily replacing the observed “high-end” measures has been suggested by Ref. [8]. The information uses the species absence-presence data of identified taxa and disregards information associated with colour or any other phenotypic differentiation, with the assumption that currently recognised taxa within defined genera and subgenera, also called “complexes”, are allopatric populations of the same species, unless they co-occur at least at one location. There is no empirical evidence yet as to whether breeding colours would result in prezygotic isolation in the case of allopatric populations being united hence the hypothesis of conspecific status of allopatric taxa can not be rejected [4].

Lake Malawi offers great opportunity for testing the conspecific status of allopatric taxa because it inhabits several rock-dwelling cichlids which have been identified into several species and there are several others that have not yet been fully identified. In this paper, the suggested approach has been applied to biogeographical data collected during this survey to determine minimum species richness estimates in order to compare it with high-end measures.

2. Materials and Data

2.1 Sampling Sites

Underwater observations with the aid of Scuba diving were employed in studying Mbuna in Lake Malawi during the period August 2004-October 2005. SCUBA surveys were undertaken in the following areas: Chinyamwezi rock, Chinyankhwazi rock,

Thumbi West Island (11 sites), Nkhudzi Spit, Kanchedza Island, Crocodile Rocks, Nkopola, and Boadzulu Island (4 sites) in the southern part of the lake, Mbenji Island (4 sites) in the central part of the lake, Kande (2 sites), Nkhata-Bay (2 sites), Chilumba (2 sites), Likoma Island (6 sites) and

Chizumulu Island (3 sites) in the northern region of the lake (Fig. 1; Table 1). Same sites surveyed by Ref. [15] were studied, except in Chilumba where a new site was added (Table 1).

Sites in southern and central Malawi were sampled during the period August-November 2004 while sites

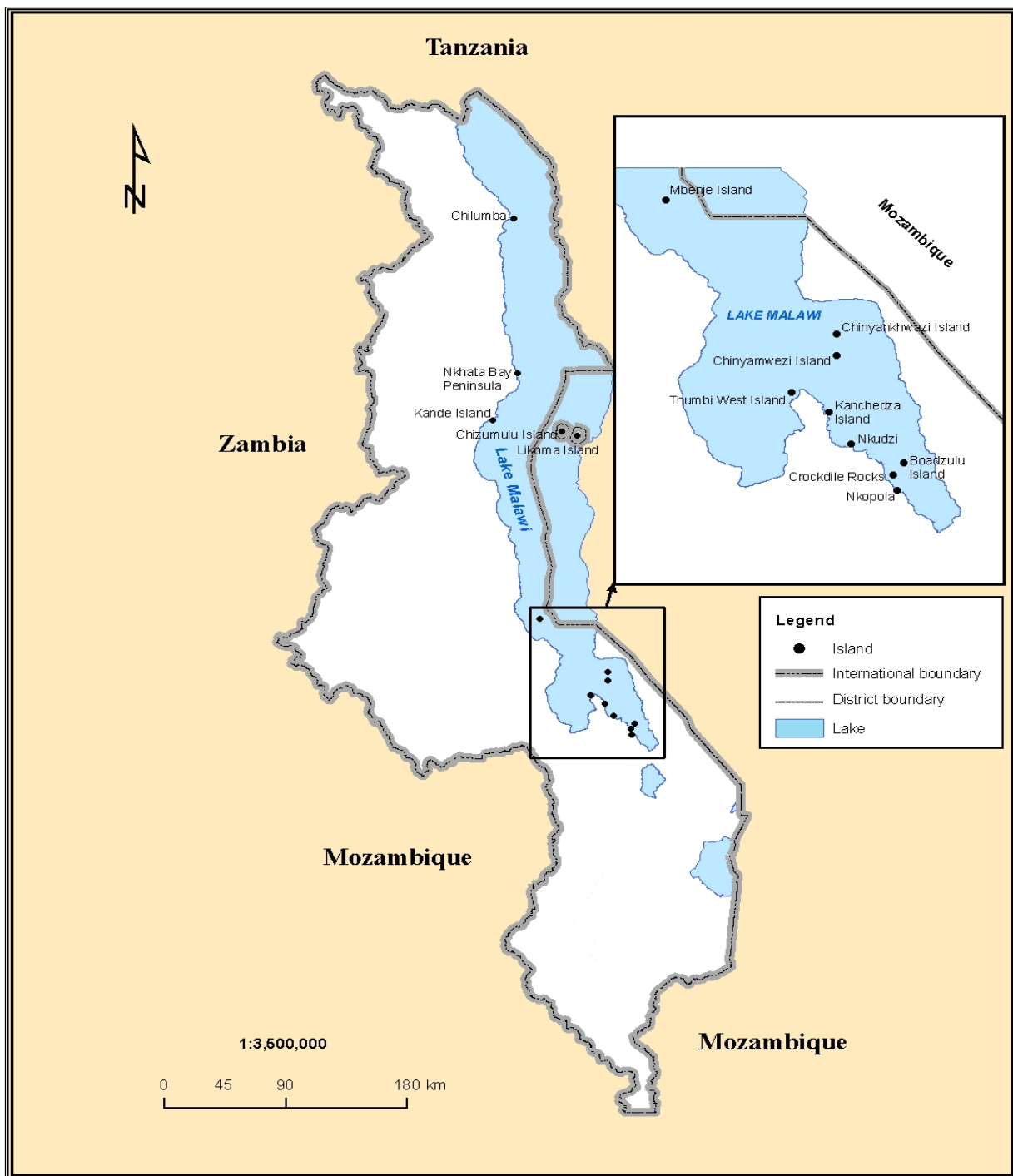


Fig. 1 Map of Malawi showing major sampling sites.

Table 1 Sampling sites and their locations.

Locations	Sampling sites	District	Region
Thumbi West Island	A	Mangochi	South
	B		
	B+1		
	C		
	C+2		
	D		
	E		
	E+3		
	E+4		
	E+5		
	F		
South East Arm	Kancedza	Mangochi	South
	Nkudzi		
	Crocodile rocks		
	Nkopola		
	Boadzulu–A		
	Boadzulu–B		
	Boadzulu–C		
	Boadzulu–D		
Chinyamwezi	One site	Mangochi	South
Chinyankhwazi	One site		
Mbenji Island	A	Salima	Centre
	B		
	C		
	D		
Nkhata Bay	A	Nkhata Bay	North
	B		
Kande	A	Nkhata Bay	North
	B		
Chilumba	Mpanga rocks	Nkhata Bay	North
	Chitande		
Likoma	Membe	Likoma	North
	Maingano		
	Mbako point		
	Ndumbi rocks		
	Makulawe point		
	Masimbwe		
Chizumulu	A-Mkanila Bay	Likoma	North
	B-Machili Islet		
	C-Membe Islet		

in northern region were surveyed during the period July-October 2005. No sampling was done during the

rainy season due to turbidity which is high in the inshore waters.

2.2 Fish Identification/Taxonomy

Prior to the underwater observation, a list of expected fish taxa at each site was compiled based on Ref. [15]. All special documented features of specific fish taxa such as body colour, size and shape, habitat type and depth preferred were compiled in advance to assist with identification during SCUBA diving, following Ref. [15, 16]. Although some of the species have subsequently been described, names used by Ref. [15] were used in order to facilitate comparison of species presence, abundance and richness between this study and Ref. [15].

2.3 Fish Census Methods

Line transects were used to record fish species and their abundance. A transect comprised of two poles with 2 holes drilled two meters apart connected with two ropes of 25 m length tied through the two holes. Each line transect covered an area of 2 m × 25 m (50 m²). It was used in more or less uniform size bottom substratum offering a regular terrain where a uniform depth contour could be followed. Fish taxa and their abundance in transect were recorded by two divers. Only areas sampled by Ref. [15] using line transects were sampled hence sites which required point transects were not covered during this survey so that data could be subjected to robust comparative statistical analyses.

In almost all the sites, except Kande and Crocodile rocks, transects were laid at six depths, namely 1 m, 3 m, 5 m, 10 m, 15 m, and 20 m. Sampling beyond 20 m depth was not done for the safety of divers. Most Mbuna species are likely to have been encountered as they are restricted to the waters of 20-meter depth [15]. Sampling was done during the daytime and all sites were visited once. After setting transect lines, the fish were allowed to recover from the effect of diver disturbance and then counting was done. Data collected included name of species observed and number of individuals for each species.

2.4 Data Analysis

In the following analyses, sites surveyed were grouped into two namely: (1) southern sites which included Lake Malawi South East Arm sites, Chinyankhwazi, Chinyamwezi, Thumbi West Island and Mbenji Island; and (2) northern sites which included Kande, Nkhata-Bay, Chilumba, Likoma Island and Chizumulu Island. A third cluster identified as “all sites” included all the 40 sites together.

2.4.1 Estimating β -Diversity of Mbuna in the Surveyed Regions

β -diversity as a measure of increases in species diversity along transects was computed using the SDR-IV programme [17]. The measure determined the number of distinct habitats within a region and the replacement of species by another between disjoint parts of the same habitat. In this study, this turnover of species was measured using presence/absence data and by calculating Cody's β -diversity index [17, 18]. Cody's β -diversity uses Eq. (1) [17]:

$$\beta_c = [g(H) + l(H)] / 2 \quad (1)$$

where, $g(H)$ is the number of species gained and $l(H)$ is the number lost moving along the transect and β_c is the Cody's β -diversity.

The Index is one of the eight recommended by Ref. [19] because it has capacity to focus on compositional differences rather than on species richness and it also gives higher scores where the proportion of shared species is low and the percentages of species gained and lost are similar [20].

2.4.2 Estimating Minimum Species Richness

The procedure outlined in Ref. [7] was used to estimate minimum species richness. It is based on the null hypothesis that conspecific status of two currently identified taxa within recognized complexes can only be rejected if they occur in sympatry. In this case, if taxa within a complex have allopatric distributions totally, they are treated as geographically disjunct forms of the same species. The approach has the potential of reducing regional and beta diversity, yet maintains alpha species richness.

The species presence-absence matrices were generated based on classifications of Ref. [15] and minimum regional species richness was calculated from these data using an iterative procedure. Within each species assemblage (i.e. lake), complexes were identified on the basis of the best available taxonomic information, and within each, putative species were sorted in descending order by the number of sites in which they occurred. The species present at the largest number of sites (A) was selected and if the next most frequently occurring taxon (B) was sympatric with A, then it was considered to be a distinct species. Otherwise it was considered to be an allopatric population of A, and the distribution of B was added to that of A. Next species were resorted in descending order by the number of sites on which they were present and the iterative process continued with the next taxon, if present. The process was continued until it had been applied to all taxa within the evolutionary lineage, so no two taxa could have totally allopatric distributions. In a case where two taxa were present at the same number of sites, then the procedure was applied to taxa in alphabetical order [4, 8].

2.4.3 Estimating Sympatric Index

A Sympatric Index was then derived by dividing the minimum species richness of each complex by its “observed species richness” based on present species classifications. The sympatric index values ranged between 0 and 1; lower values of the Sympatric Index indicated that proportionally more species within the complex did not co-occur in the region. Further analysis also involved determining whether monotypic complexes had more observed species than other complexes and to what extent did the variation in the bottom substrate relate with Sympatric Index.

2.4.4 Habitat Analysis

The description of the bottom habitats where sampling was carried out is provided in Table 2. Considering the volume of the data generated, a 11 point ranking of the habitats was developed based on the composition of rocks and sand in each of the

quadrats. The ranking was developed based on the hypothesis that rocky habitats have high Mbuna abundance and species richness. The habitat which had its bottom comprised of rocks only was given higher ranking than one composed of sand or silt and weeds. The 11 point ranking developed by this study is provided in Table 2.

3. Results

3.1 β -Diversity

Cody's β -diversity estimates are provided in Table 3. Among the islands, the lowest β -diversity was observed at Boadzulu Island and in their increasing order followed by Chinyamwezi and Chinyankwazi, Chizumulu Island, Mbenji, Thumbi and Likoma

Table 2 Classification of bottom habitats of the various sites surveyed.

	Habitat description	Rating
1	Mud and weeds	0
2	Sand and snail shells with isolated weeds	1
3	Sand throughout or rocks completely covered with mud	2
4	More than 50% sand and isolated small rocks	3
5	More than 50% sand and isolated big rocks	4
6	50% small rocks and 50% sand	5
7	50% big rocks and 50% sand	6
8	Medium/small rocks throughout	7
9	More than 50% medium/small rocks mixed with big rocks	8
10	More than 50% big rocks mixed with small rocks	9
11	Open rock spread throughout in the depth of more than 10 m	10

Table 3 Cody's β -diversity values for various islands and regions on Lake Malawi.

Site	α -diversity	Cody's β -diversity
Thumbi Island	40	13
Boadzulu Island	15	1
Chinyamwezi & Chinyankwazi	14	4.5
Mbenji	25	5.5
Likoma Island	35	14
Chizumulu Island	27	4.5
Southern	75	53.5
Northern	78	56
All sites	136	114.5

Island. The southern sites had lower β -diversity than northern sites and all the sites combined had a total regional diversity of 114.5. The difference between α -diversity and β -diversity within the Islands suggests that most of them share a large proportion of species among their localities with Boadzulu Island showing a much higher degree of uniformity among sites in terms of species composition.

3.2 Minimum and Maximum Regional Species Richness

The difference between maximum regional species

richness and minimum species richness is higher in the northern sites (45) than the southern sites (32) (Tables 4 and 5). The Sympatric Index is higher in the southern sites than in the northern, with a range of 0.3 -1.0 in the southern and 0.2-1.0 in the northern. The *Cyanotilapia* genus is more allopatric in the southern than in the northern sites whereas *Labichromis* shows the opposite trend. *Pseudotropheus* species complex has lower Sympatric Index in northern sites than in the southern sites. Overall there was strong positive correlation between observed high-end species richness and minimum species richness (southern: (1)

Table 4 Maximum regional species richness and minimum regional species richness for southern sites (Thumbi West Island, Southeast Arm, Chinyankhwazi and Chinyamwezi).

Taxa	Maximum regional species	Minimum regional species	Sympatric index
<i>Cyathochromis</i>	1	1	1.0
<i>Cynotilapia</i>	4	1	0.3
<i>Genyochromis</i>	1	1	1.0
<i>Gephyrochromis</i>	1	1	1.0
<i>Iodotropheus</i>	1	1	1.0
<i>Labeotropheus</i>	3	3	1.0
<i>Labidochromis</i>	8	5	0.6
<i>Melanochromis</i>	12	8	0.7
<i>Petrotilapia</i>	7	4	0.6
<i>Pseudotropheus aggressive</i>	5	5	1.0
<i>Pseudotropheus elongatus</i>	13	5	0.4
<i>Pseudotropheus tropheops</i>	1	1	1.0
<i>Pseudotropheus</i>	18	7	0.4
	Total = 75	Total = 43	Mean = 0.8

Table 5 Maximum regional species richness and minimum regional species richness for northern sites (Kande, Nkhata Bay, Chizumulu, Likoma and Chilumba).

Taxa	Maximum regional species	Minimum regional species	Sympatric index
<i>Cyathochromis</i>	1	1	1.0
<i>Cynotilapia</i>	4	3	0.8
<i>Genyochromis</i>	1	1	1.0
<i>Gephyrochromis</i>	1	1	1.0
<i>Iodotropheus</i>	1	1	1.0
<i>Labeotropheus</i>	1	1	1.0
<i>Labidochromis</i>	10	3	0.3
<i>Melanochromis</i>	9	3	0.3
<i>Petrotilapia</i>	7	2	0.3
<i>Pseudotropheus aggressive</i>	4	3	0.8
<i>Pseudotropheus elongatus</i>	4	2	0.5
<i>Pseudotropheus tropheops</i>	11	5	0.5
<i>Pseudotropheus williamsi</i>	2	1	0.5
<i>Pseudotropheus zebra</i>	6	3	0.5
<i>Pseudotropheus</i>	16	3	0.2
	Total = 78	Total = 33	Mean = 0.6

all species combined, $n = 13$, $r^2 = 0.8$; (2) each complex with > 1 species represented a single independent data point, $n = 8$, $r^2 = 0.6$) and (northern: (1) all species combined, $n = 15$, $r^2 = 0.6$; (2) each complex with > 1 species represented a single independent data point, $n = 10$, $r^2 = 0.3$).

3.3 Sympatric Index of Monotypic and Non-mono-typic Complexes

With sites combined, the sympatric index of the non-monotypic complexes showed overall decline compared to regional sites. This suggests that non-monotypic complexes are dependent on the geographical scale of the area covered, thus with increase in the number of sites, more species tend to have totally allopatric distribution (Table 6). This is also demonstrated by the mean sympatric index for all sites which is lower than the two regional sites.

3.4 Abundance and Habitat Ranking

There were more Mbuna per site in the southern

sites than in the northern sites (Table 7) and the difference was significant ($p < 0.05$), however, the species richness per site was not significantly different between the two site clusters. Most of the sites in the southern region had bottoms comprised of a mixture of sand and rocks (mean 56.7% habitat ranking) while the sites in the northern region were mostly rocky bottoms (mean 84.5% habitat ranking).

4. Discussion

This study supported the fact that the level of endemism of Mbuna in Lake Malawi is high with β -diversities of about 72%, 71% and 84% in southern, northern and all sites, respectively. The southern most site surveyed showed that although there are high number of species at Boadzulu Island, the species may be well distributed in all the sampling sites hence low β -diversity value. The Island has habitat ranking of 42 suggesting that bottom substrate is predominantly rocky hence the Mbuna could move a greater distance than a comparable area with breaks of sandy and

Table 6 Number of sites species were present, the maximum regional species richness and minimum regional species richness for all sites sampled on Lake Malawi.

Taxa	Maximum regional species	Minimum regional species	Sympatric index
<i>Cyathochromis</i>	1	1	1.0
<i>Cynotilapia</i>	7	3	0.4
<i>Genyochromis</i>	1	1	1.0
<i>Gephyrochromis</i>	1	1	1.0
<i>Iodotropheus</i>	1	1	1.0
<i>Labeotropheus</i>	3	3	1.0
<i>Labidochromis</i>	15	5	0.3
<i>Melanochromis</i>	17	7	0.4
<i>Petrotilapia</i> 'chitande'	12	4	0.3
<i>Pseudotropheus aggressive</i>	5	1	0.2
<i>Pseudotropheus elongatus</i>	13	3	0.3
<i>Pseudotropheus tropheops</i>	20	5	0.3
<i>Pseudotropheus williamsi</i>	3	1	0.3
<i>Pseudotropheus zebra</i>	10	2	0.2
<i>Pseudotropheus</i>	26	5	0.2
	Total = 135	Total = 43	Mean = 0.5

Table 7 Mean \pm SE abundance, species richness and habitat ranking.

Region	Number of sites	Abundance	Richness	Habitat ranking (%)
Southern	25	821 \pm 79.4	19.3 \pm 1.4	56.7 \pm 4.3
Northern	15	467 \pm 48.6	18.3 \pm 0.9	84.5 \pm 2.3
All sites	40	688 \pm 59.1	18.9 \pm 0.9	67.5 \pm 3.5

0.2-1.0 with mean of 0.6 in the northern sites. This suggests that most of taxa in the lake occur in isolation but may not be necessarily true species. Allopatrism is higher among the northern region habitats than in the southern region. The difference between the two arbitrary clustered regional groups may not be conclusive at this stage given that the number of sampling sites covered are less than the number required (35 sites) to reach asymptote.

The fact that the non-monotypic complexes tended to have their sympatric index decline with increase in the number of sites supports the doubt about whether or not all these allopatric species in the lake have valid species status and that probably more rigorous approach of designating species status needs to be adopted which should be complemented with phylogenetic evidence. A study by Ref. [8] has shown that the scale of species differences among complexes has never been quantified hence it is not known as to whether some complexes possess more genuine morphological differentiation among allopatric populations or not.

There were more Mbuna in the southern sites than in the northern sites probably due to the fact that a large proportion of sampling in the south covered protected areas of Thumbi West Island where the populations are conserved. Mbuna are mostly distributed in the rocky areas and a trend that emerged from habitat ranking was that there were more Mbuna with high habitat ranking than those that have low ranks at similar depth. In addition to the nature of the bottom substrate, other factors that contribute to species abundance and richness include turbidity, nutrient content of the bottom substrate, water depth, etc.. It was outside the scope of the present study to investigate each of these environmental variables. However, Hanssens et al. [26] have reported correlation between depth and abundance of Mbuna being more pronounced in rocky habitats than in the sandy and soft bottom.

5. Conclusions

This paper provides more insights into the diversity of Mbuna in Lake Malawi. The α -diversity is generally high on the Islands like Thumbi West Island, Likoma Island and Mbenji Island but their β -diversity decreases to varying degree due to the fact that spatial variability is higher on some islands than others. For instance there are more unique species on Likoma Island than on Thumbi Island.

The species designation of the Mbuna of Lake Malawi which is predominantly based on morphological and behavioural characters requires more in depth studies in order to revise some of the names. Most of the species occur in allopatry to the extent that estimation of minimum species richness casts further doubt in the species status of some of the taxa. At least 42% of the species occur in allopatry hence their species status could not be ascertained using the method applied in this study. The difference between maximum regional species and minimum regional species was more pronounced in the non-monotypic species complexes than in the monotypic complexes especially as the number of sites increased.

The bottom of the sampling sites in the northern region were more rocky than those in the southern region, although there were more Mbuna in the southern than in the northern sites which was mainly due to sampling error as the number of sites were less than the number required (35 sites) to reach asymptote. There were fewer sites covered in the northern region than in the southern region.

References

- [1] I. Harrison, M. Leverty, E. Sterling, Alpha, beta and gamma diversity, 2004, available online at: <http://cnx.org/content/m12147/1.2/>.
- [2] D. Pameroy, A. Lewis, Bird species richness in tropical Africa: Some comparisons, *Biological Conservation* 40 (1987) 11-28.
- [3] H. Tumiosto, K. Ruokolainen, M. Yli-Halla, Dispersal,

- environment and floristic variation of western Amazonian forests, *Science* 299 (2003) 241-244.
- [4] M.J. Genner, O. Seehausen, D.F.R. Cleary, M. Knight, El. Michel, G.F. Turner, How does the taxonomic status of allopatric populations influence species richness within African cichlid fish assemblages?, *Journal of Biogeography* 31 (2004) 93-102.
- [5] D. Borcard, P. Legendre, P. Drapeau, Partialing out the spatial component of ecological variation, *Ecology* 73 (1992) 1045-1055.
- [6] C. Ricotta, S. Burrascano, Beta diversity for functional ecology, *Preslia* 80 (2008) 61-71.
- [7] G.F. Turner, O. Seehausen, M.E. Knight, C.J. Allender, R.L. Robinson, How many species of cichlid fishes are there in African lakes?, *Molecular Ecology* 10 (2001) 793-806.
- [8] M.J. Genner, O. Seehausen, D.F.R. Cleary, M. Knight, El. Michel, G.F. Turner, Beta diversity of rock-restricted cichlid fishes in Lake Malawi: Importance of environmental and spatial factors, *Ecography* 27 (2004) 601-610.
- [9] E. Hert, Homing and home-site fidelity in rock-dwelling cichlids (Pisces: Teleostei) of Lake Malawi, Africa, *Africa Environmental Biology of Fishes* 33 (1992) 229-237.
- [10] M.J. Genner, G.F. Turner, S.J. Hawkins, Resource control by territorial male cichlid fish in Lake Malawi, *Journal of Animal Ecology* 68 (1999) 522-529.
- [11] M.E. Arnegard, J.A. Markert, P.D. Danley, J.R. Stauffer, A. Ambali, T.D. Kocher, Population structure and colour variation in the lithophilous cichlid *Labeotropheus feullebornii* Ahl along a recently formed archipelago of rocky habitat patches in southern Lake Malawi, *Proceedings of the Royal Society of London Series B* (266) (1999) 119-130.
- [12] C. Rico, P. Bouiteillon, M.J.H. Van Oppen, M.E. Knight, G.M. Hewitt, G.F. Turner, Extreme microallopatric divergence in a cichlid species from Lake Malawi, *Molecular Ecology* 11 (2003) 37-46.
- [13] E. Mayr, J. Diamond, *The Birds of Northern Malenesia: Species, Ecology, and Biogeography*, Oxford University Press, New York, 2001.
- [14] D. Kassam, S. Seki, B. Rusuwa, A.J.D. Ambali, K. Yamaoka, Genetic diversity within the genus *Cynotilapia* and its phylogenetic position among Lake Malawi's Mbuna cichlids, *African Journal of Biotechnology* 4 (2005) 1195-1202.
- [15] A.J. Ribbink, B.A. Marsh, A.C. Ribbink, B.J. Sharp, A preliminary survey of the cichlid fishes of the rocky habitats of Lake Malawi, *South African Journal of Zoology* 18 (1983) 155-309.
- [16] A. Konings, *Konings Book of Cichlids and All Other Fishes of Lake Malawi*, T.F.H. Publications, 1990, p. 495.
- [17] R.M. Seaby, P.A. Henderson, *Species Diversity and Richness, Version 4*, Pisces Conservation Ltd., Lymington, England, 2006.
- [18] M.L. Cody, Bird diversity components within and between habitats in Australia, in: R.E. Ricklefs, D. Schuler (Eds.), *Species Diversity in Ecological Communities*, Chicago Press, 1993, pp. 147-158.
- [19] P. Koleff, K. Gaston, J.J. Lennon, Measuring beta diversity for presence-absence data, *Journal of Animal Ecology* 72 (2003) 367-382.
- [20] F. Escobar, J.M. Lobo, G. Halffter, Assessing the origin of neotropical mountain dung beetle assemblages (Scarabaeidae: Scarabaeidae): The comparative influence of vertical and horizontal colonization, Unpublished Paper, Open-University of Pretoria, 2007.
- [21] A.J.D. Ambali, L.B. Malekano, B.J. Mkoiko, G.P. Mwale, W. Changadeya, Assessment of impacts and potential mitigative interventions of fishing and other anthropogenic activities on the 100-metre aquatic zone of Lake Malawi, Report submitted to the Department of National Parks and Wildlife, Lilongwe, Malawi, 2002.
- [22] G.F. Turner, Lake Malawi benthic haplochromine cichlids, 2004, available online at: http://www.hull.ac.uk/cichlids/benthic_cichlids.htm.
- [23] M.J.H. Van Oppen, C. Rico, J.C. Deutsch, G.F. Turner, G.M. Hewitt, Isolation and characterization of microsatellite loci in the cichlid fish *Pseudotropheus zebra*, *Molecular Ecology* 6 (1997) 387-388.
- [24] I. Kornfield, P.F. Smith, African cichlid fishes: Model systems for evolutionary biology, *Annual Reviews in Ecology and Systematics* 31 (2000) 163-196.
- [25] M.E. Knight, G.F. Turner, Reproductive isolation among closely related Lake Malawi cichlids: Can males recognize conspecific females by visual cues?, *Animal Behaviour* 58 (1999) 761-768.
- [26] M. Hanssens, J. Snoeks, Mbuna distribution and species richness, in: J. Snoeks (Ed.), *The Cichlid Diversity of Lake Malawi/Nyasa/Niassa: Identification, Distribution and Taxonomy*, Cichlid Press, El Paso, USA, 2000, p. 360.

Counteracting the Effects of Sea Level Rise in Southeast Florida

F. Bloetscher¹, B.N. Heimlich² and T. Romah¹

1. Department of Civil, Environmental and Geomatics Engineering, Florida Atlantic University, Boca Raton, FL 33431, USA

2. Center for Environmental Studies, Florida Atlantic University, Boca Raton, FL 33431, USA

Received: April 8, 2011 / Accepted: June 22, 2011 / Published: November 20, 2011.

Abstract: Over the past 100 years, worldwide surface temperatures have increased at an unprecedented rate, contributing to warming of the oceans, melting ice fields and glaciers, and other adverse climatic effects. Southeast Florida's vulnerability derives from its geographic location, low elevation, porous geology, unusual ground and surface water hydrology, subtropical weather patterns, and proximity to the Atlantic Ocean. The region is especially susceptible to sea level rise. After several millennia of stable sea levels prior to the 20th century, sea levels have been rising at accelerating rates due to thermal expansion of the oceans and from land-based ice melt. The Everglades ecosystem and the water supplies for southeast Florida are particularly vulnerable as neither can be protected without significant expenditures of public dollars, and even these efforts may not prove to be successful. New approaches may be required to improve the resilience and prolong the sustainability of the region's water resources and ecosystem. The efforts to adapt to sea level changes in both the urban area and ecosystem as outlined herein are date and incident based-climate changes may occur earlier or later so instead of spending limited public dollars early, expenditures can be adjusted given future information.

Key words: Sea level rise, water supply, Everglades.

1. Introduction

The 2007 IPCC report on global scientific consensus regarding climate change stated that the "warming of the climate system is unequivocal, as is now evident from observations of increases in global average air and ocean temperatures, widespread melting of snow and ice, and rising global average sea level" [1]. Recent reports [2, 3] indicate that global average sea level may rise by 2 to 4 feet or more by 2100. There are a number of possible causes that may contribute to changes in the world-wide climate, including greenhouse gases [1], solar activity [4], land use changes [5] and even a coming change in the pole location [6]. The only sure thing is that the climate will change in the future. Southeast Florida, with a population of 5.5 million [7], is among the ten coastal metropolitan areas in the world most vulnerable to climate change [8]. Rapidly

growing interest in this subject can be found in Florida [9], California [10], King County, Washington [11], and New York City [12], some of those areas most vulnerable infrastructure to sea level rise and other impacts of climate change, especially in low coastal regions like south Florida, are water, wastewater and stormwater utilities.

1.1 Climate Change in Florida

If global temperatures rise, it is reasonable to expect that Florida's existing climate zones will move northward and the zones of more tropical climate will enlarge, however, this has not been the case to date because Marshall et al. [5] pointed out that while temperatures have increased, there have been greater variation-colder winters and warmer summers. Mulkey [13] noted that the direction and magnitude of precipitation changes for the Florida peninsula are more uncertain than other sections of the continent of North America due to limitations in existing global

Corresponding author: B.N. Heimlich, fellow, main research field: climate change. E-mail: barryces@bellsouth.net.

climate models. There may be “slightly increased runoff in the southeast (United States)”, but it is unclear if such a trend would apply to the Florida peninsula (U. S. Climate Change Science Program). Freas et al. [14] suggest there is a potential for lower overall annual average precipitation in subtropical areas similar to peninsular Florida. More extreme seasonal variations in precipitation patterns will pose challenges for South Florida since topography limits storage of excess precipitation for use during the anticipated extreme dry periods. Extremes in weather phenomena are not new to Florida, where hurricane occurrence cycles have occurred about every 20 years and periodic droughts are noted to occur in roughly seven year cycles. The concern is that these extremes may worsen as a result of climate change.

Marshall et al. [5] found a long-term increasing trend in temperatures, higher highs and lower low temperatures and a decrease of 12 percent in convective (summer) rain. The effects of climate change may already be influencing weather in southeast Florida. Rainfall has decreased over the past 30 years, and the daily summer pattern of convective storm activity appears to be the most affected [5]. Marshall et al. [5] state that “because sea breezes are driven primarily by contrasting thermal properties between the land and adjacent ocean, it is possible that alterations in the nature of land cover of the peninsula have had impacts on the physical characteristics of these circulations”. This mechanism accounts for the primary wet season precipitation contributing over 70 percent of the annual rainfall. Their modeling suggests that land use changes have reduced total rainfall by 12 percent since 1900, especially in the summer, probably as a result of land use changes that have resulted in the loss of wetlands. Future changes in climate will likely worsen these effects. Additional research and high resolution climate modeling for the Florida peninsula is needed before definitive conclusions can be drawn.

For Florida, changes in precipitation and rising sea level may pose the most significant problem faced by

the region, which will require water users to expand planning and monitoring, and construct protective measures in the coming years. Coastal areas will see migration of seawater into previously fresh aquifers. More rain should increase the potential for percolation, but excessive rain will tend to runoff reducing recharge, which is of particular interest in a state where 93 percent of water use comes from groundwater [15].

1.2 Sea Level Rise

There is clear scientific evidence that sea level has steadily risen over the past 100 years and is accelerating. Sea level rise, not changes in precipitation patterns, may pose a greater challenge for southeast Florida. Measurements in Florida [16] show an average rate of sea level rise of 2.27 ± 0.04 mm per year from 1915 to 2005 based upon tide gauge readings in Key West, which are the Western Hemisphere’s longest sea level record. From 1913-1999 sea level in Miami has risen 2.39 ± 0.22 mm/yr [17]. Barrier islands in the Tampa Bay (2.3 mm/yr) region are experiencing significant beach erosion due to sea level rise, compounded by high storm surge. Numerous researchers are modeling sea level rise projections, but it appears that sea level rise is increasing (see Fig. 1).

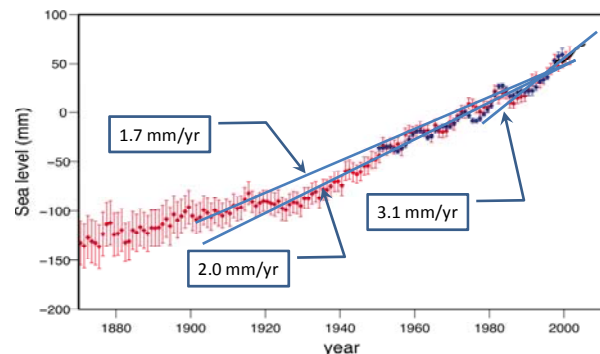


Fig. 1 The present rate of both global and local sea level rise is approximately 12 inches per century. This chart reflects the rise of sea levels since the nineteenth century and the accelerated pace over the last few decades. The trend line shows reconstructed data since 1870, with darker points showing coastal tide gauge measurements since 1950. The solid lines show the changes in trend that has occurred, increasing from 1.7 to 2.0 to 3.1 mm/yr (from Intergovernmental Panel on Climate Change [1]).

The authors reviewed data for all sea level monitoring stations in Florida. Of interest was whether the IPCC trend is different than that of Florida. Figs. 2-4 show the changes in sea level at the stations on the Atlantic Ocean, Gulf of Mexico and the Panhandle. In all cases, the stations show an increase in the level of the sea.

Combining these together, Fig. 5 shows that:

- (1) Relative 95% Conf Limits vary inversely with Time Span;
- (2) Florida avg. sea level rise is 2.10 ± 0.49 mm/yr for all 14 Florida locations;
- (3) All but one location is within the 95% Conf

Limits range;

- (4) Exception is Panama City which has a very short time span;
- (5) Therefore, none of SLR rates differ statistically;
- (6) Average global SLR for 1920-2000 was 2.0 mm/yr-within 95% Conf Limits for Florida locations.

The conclusion is that the global projections of SLR are in line with the results seen as the Florida stations excepting Panama City, Florida.

Table 1 outlines a few of these sea level rise models. Many of the models focused on in this report stem from

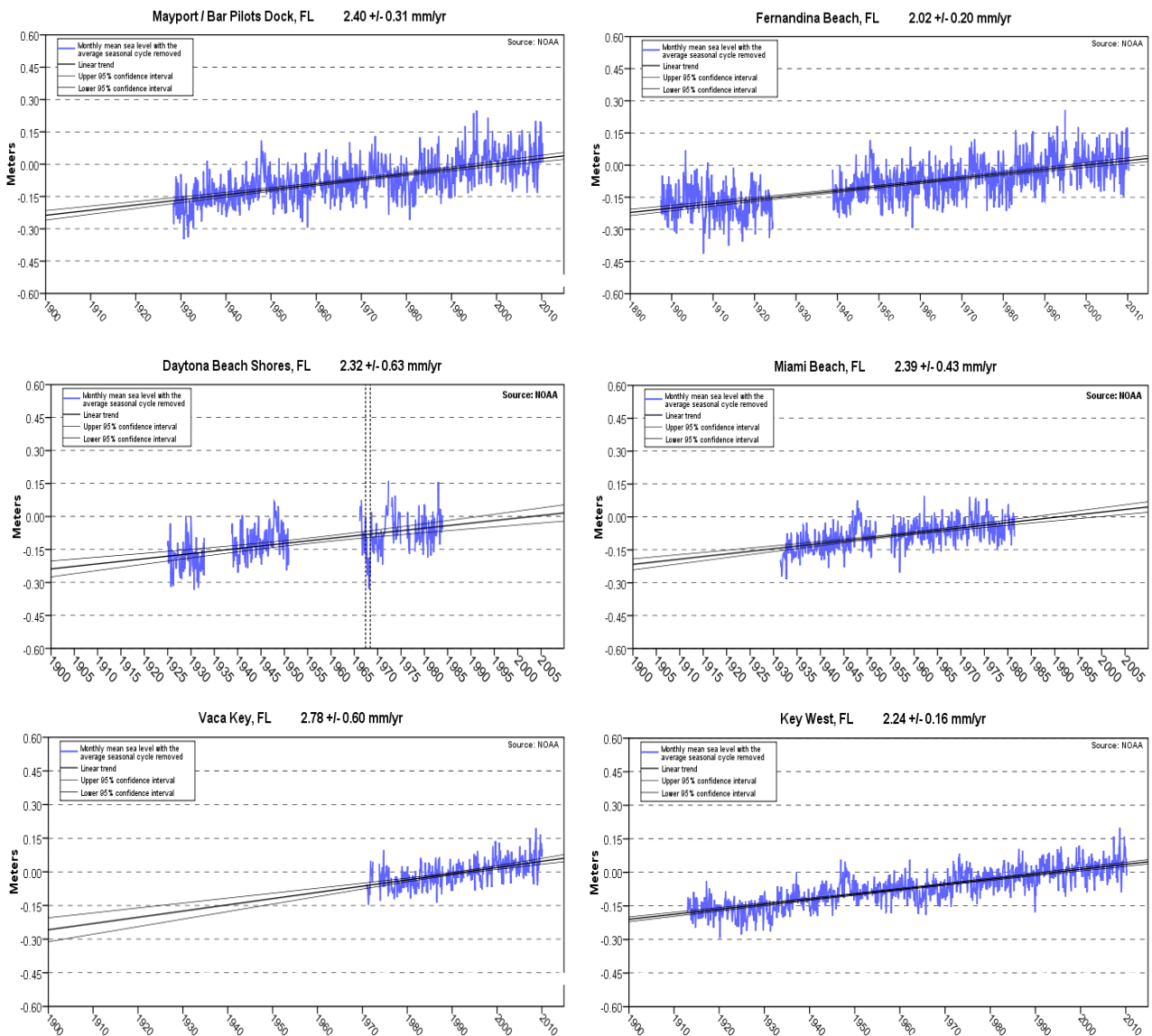


Fig. 2 Results of stations and sea level rise on the Atlantic Ocean (horizontal axis is years).

Counteracting the Effects of Sea Level Rise in Southeast Florida

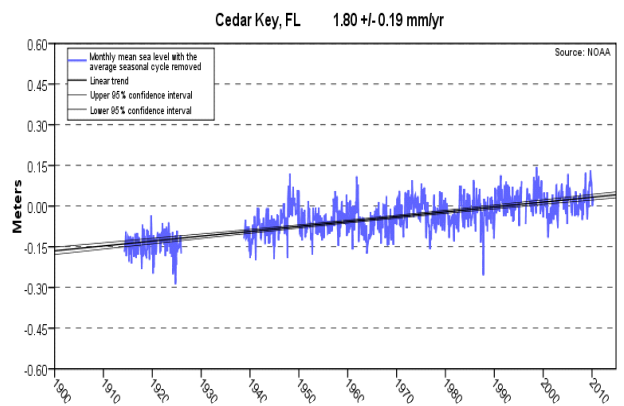
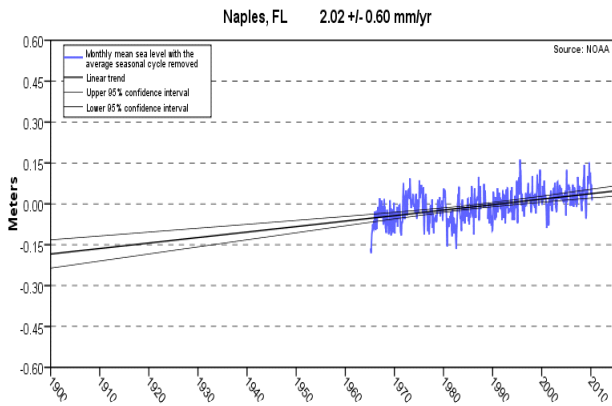


Fig. 3 Results of stations and sea level rise on the Gulf of Mexico. (horizontal axis is years).

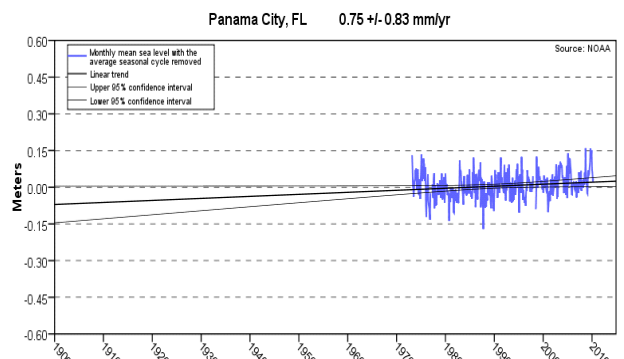
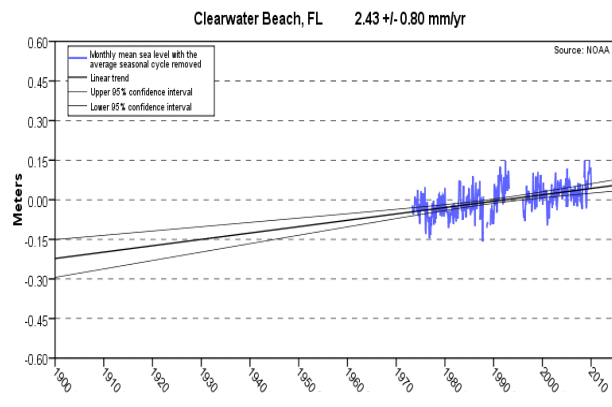
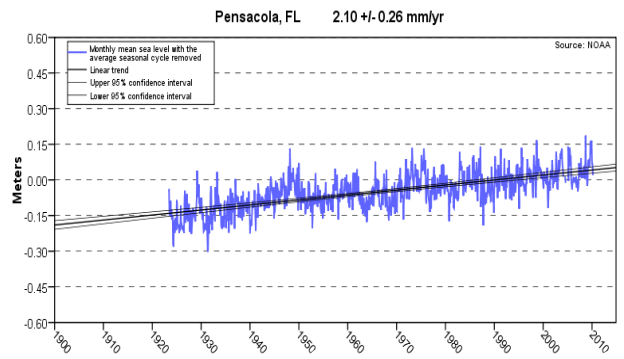
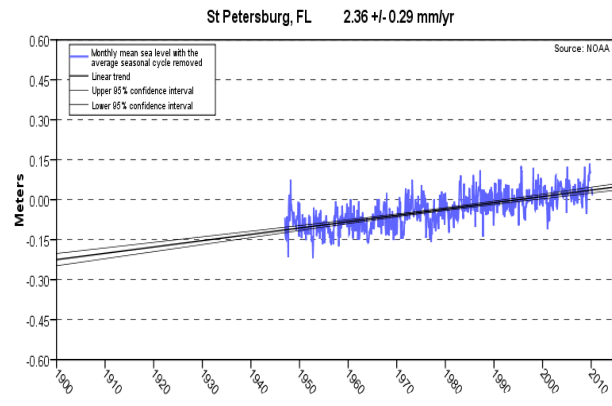
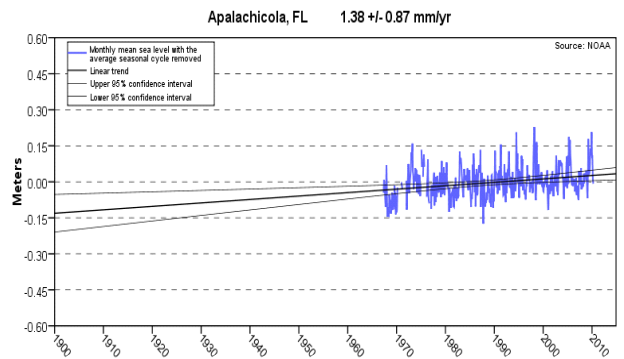
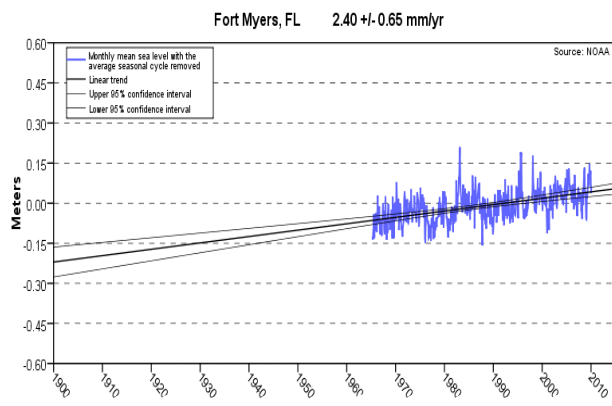


Fig. 4 Results of stations and sea level rise on the Gulf of Mexico in the Panhandle (horizontal axis is years).

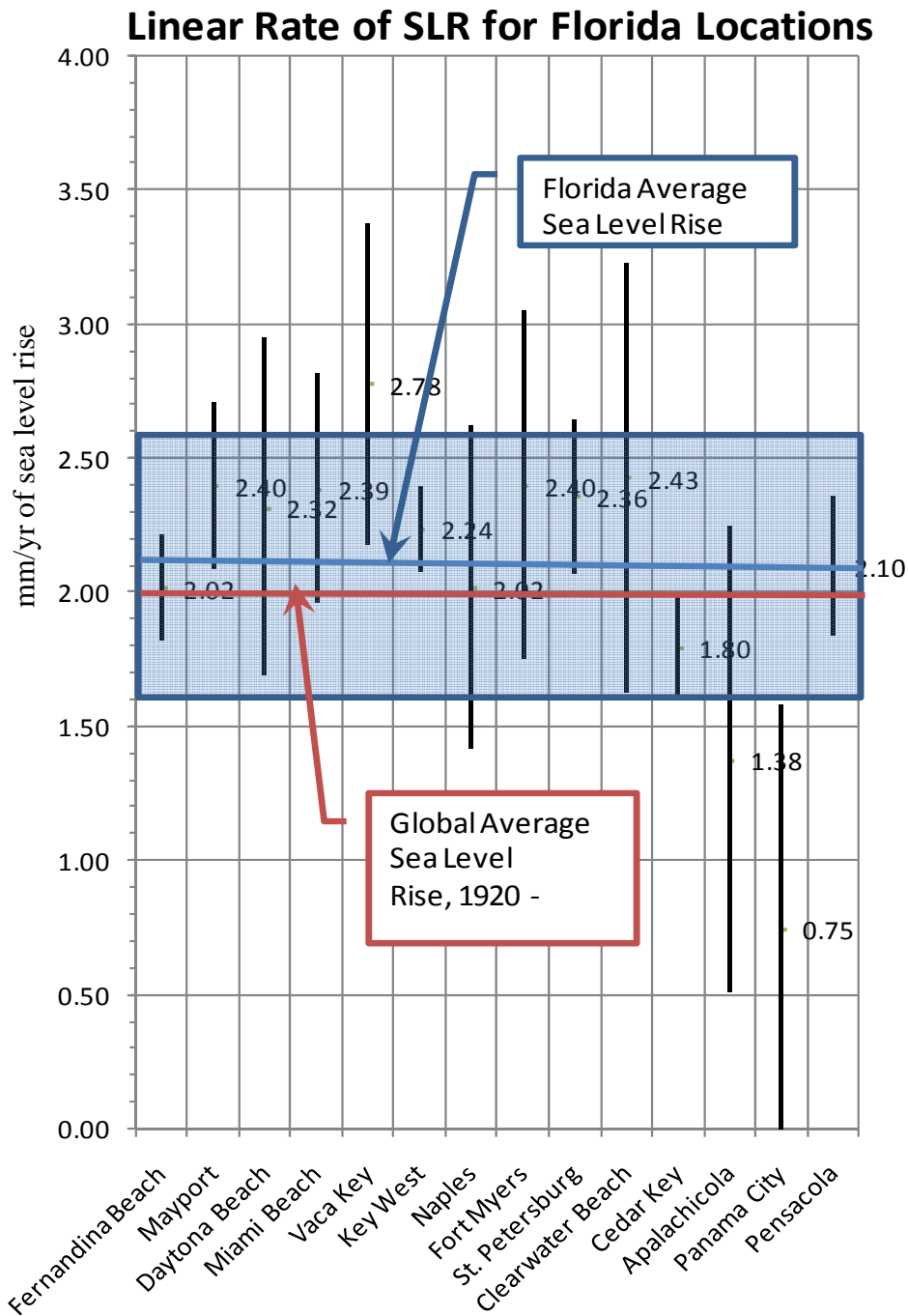


Fig. 5 The results of analysis of the 14 stations in Florida. The Florida average sea level rise is 2.10 ± 0.92 mm/yr.

sea level rise research based in Florida. Most of the sea level rise predictions are expecting an increase between 2.5 to 5 feet by 2100 (see Fig. 6). A 3 ft sea level rise appears to be an appropriate value for planning purposes.

FAU’s recent publication related to climate change, entitled Southeast Florida’s Resilient Water Resources:

Adaptation to Sea Level Rise and Other Impacts of Climate Change [18], outlines the knowledge of the climate change issues as they relate to water, wastewater and stormwater utility operations [12]. The study is a follow-up to Murley et al. [9] which proposed a state policy framework for adaptation to climate change for coastal Florida. These studies outline why

Table 1 Model result of projected sea level rise.

Sea level rise projections/predictions chart					
Region	Sea level rise projections/predictions in feet	Range/time frame	Data source	Date published	Model(s)/method used
Global	0.26-2 ft	2100	IPCC	2007	Hierarchy of several models
Global	1.9-5.25 ft, with confidence limits of 1.93 and 5.9 ft	2100	Jeverjeva, Moore and Grinstead	2010	Inverse statistical model
Global	1.6, 3.2, and 4.9 ft	2100	USACE	2009	Modified NRC curves with modified equations and IPCC projections
Global	4.27-20.67	Not given	Mitrovica	2008	Modified calculations and models (Fingerprinting, IPCC)
Global	2.5-6.2 ft	2100	Vermeer and Rahmstrof	2010	Semi-empirical dual model
Global	2.6-6.5 ft	2100	Pfeffer et al.	2008	Calculation of ice sheet dynamics
Global	1 ft	2100	Church and White	2006	Statistical analysis of historic sea level data/trends
Global	3.12-3.94 ft	2250	MIT-IGSM	2009	Integrated global systems model
Florida	In-progress	In-progress	Gulf Coast Alliance	2014	
Florida	3-5 ft	2100	Heimlich et al.		Quadratic equation
Florida	3-5 ft	2100	Miami-Dade Climate Change Advisory Task Force	2008	Modified IPCC
Florida	0.59-4.4 ft	2100	SWFRPC	2010	Modified EPA and Stanton and Ackerman

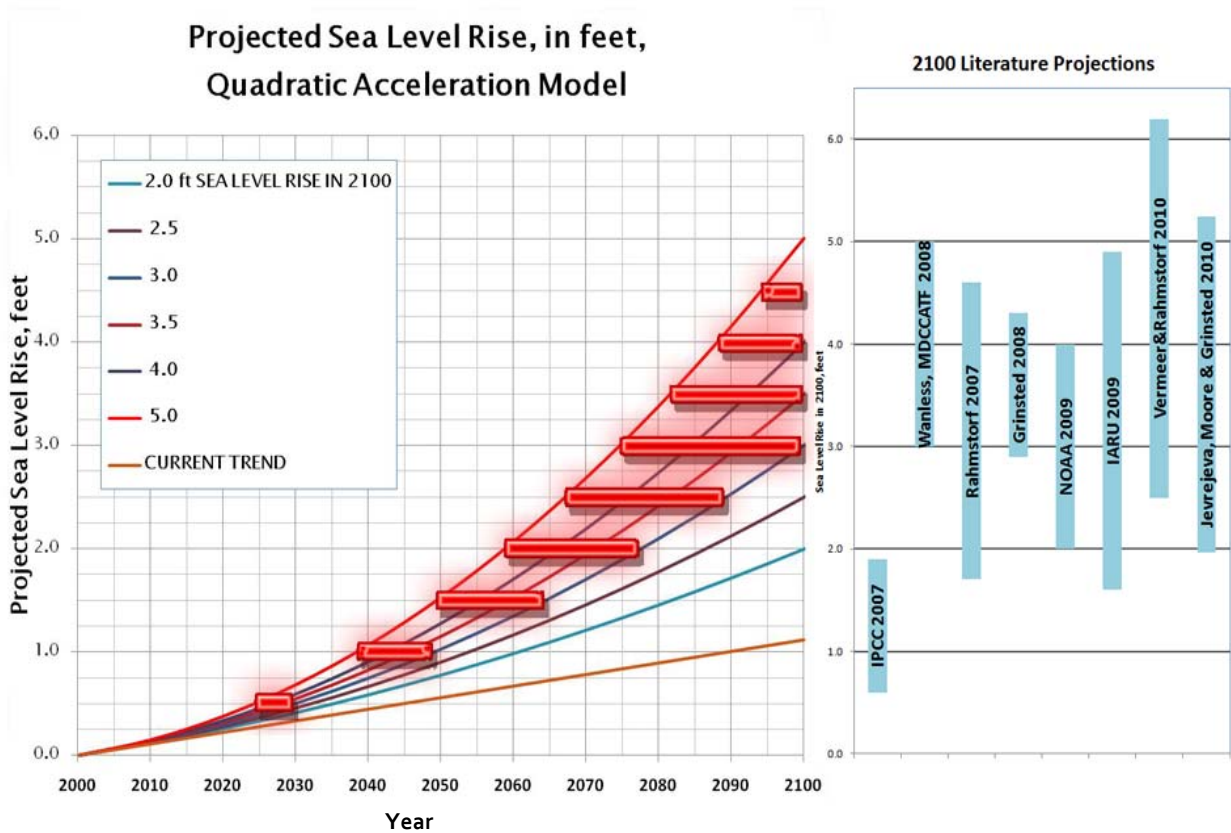


Fig. 6 Prediction of sea level rise using a Quadratic Acceleration Equation [18, 19]; The graph outlines the average, and 1 and 2 standard deviations form the average of the current models (Table 1); The horizontal bars outline the ranges when the sea level rise could occur.

more frequent and damaging floods are likely to become an ever-increasing problem as sea level continues to rise. Murley et al. [9] identified: (1) inundation of barrier islands and coastal property; (2) beach erosion; (3) encroachment of coastal wetlands including the southern Everglades with significant modification of wetland habitat as the water becomes more saline; and (4) impacts on the region’s water resources, namely the water supply and groundwater and surface water hydrology through: (a) increasing levels of interior ground and surface waters; (b) reduced groundwater flow through the aquifer; and (c) increasingly compromised stormwater drainage systems, as the major issue that will impact southeast Florida [19].

1.3 Saltwater Intrusion in the Southern Everglades

Water supply, water quality and Everglades’s ecosystem health are intrinsically linked in south Florida. When attempting to evaluate the ecological

health of southeast Florida, one must look at the entire southern portion of the peninsula of Florida. Historically there were no barriers or canals to direct or control the path of water (see Fig. 7). The canal system permanently reduced groundwater levels along the coast (which enabled the development that exists today see Fig. 8). As a result of reduced groundwater levels, combined with lessened historical flows to the Everglades and less water standing in the Everglades during the summer months, the Biscayne Aquifer does not recharge as it once did [19].

As sea level rises, the saltwater intrusion zone in the southern Everglades (see Fig. 9) will move northward. Saline water would inundate the surface waters of the southern Everglades watershed. As salinity levels in the ground and surface waters in the southern Everglades migrate northward, it would eventually threaten the wellfields in southwest Miami-Dade County by contaminating the southern Biscayne Aquifer at its head waters in the Everglades.

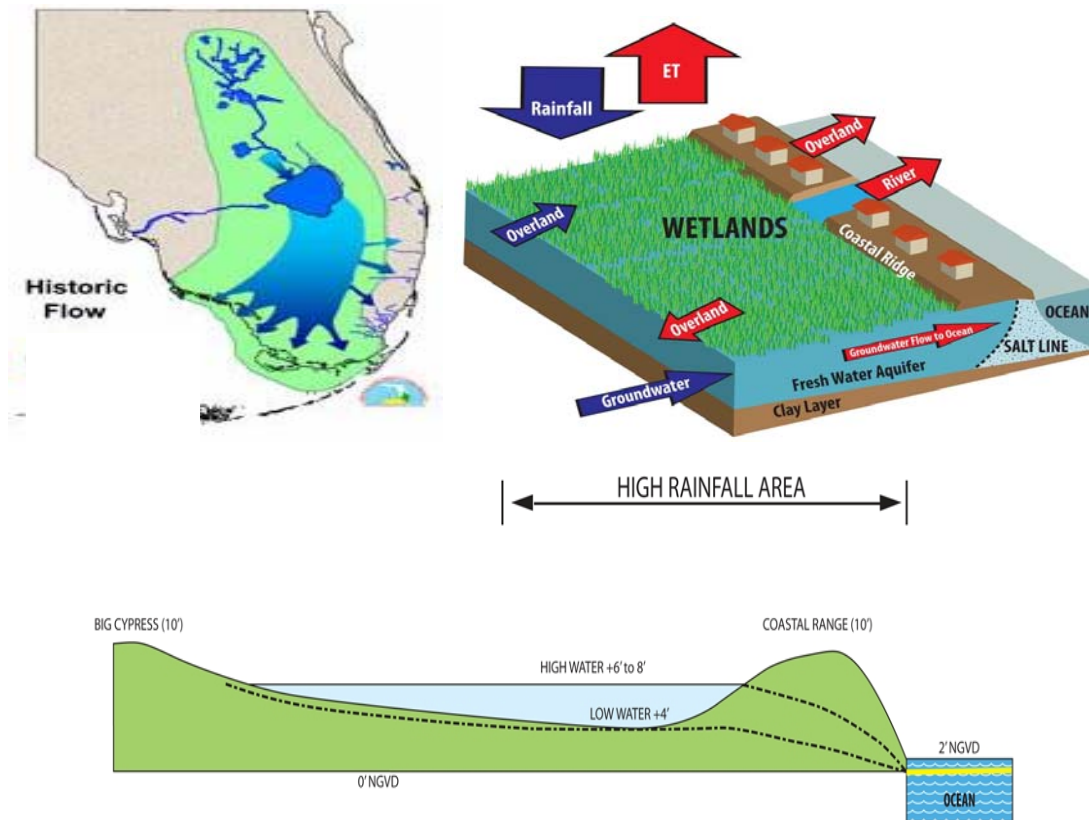


Fig. 7 Historical Everglades flow pattern and cross-section [18].

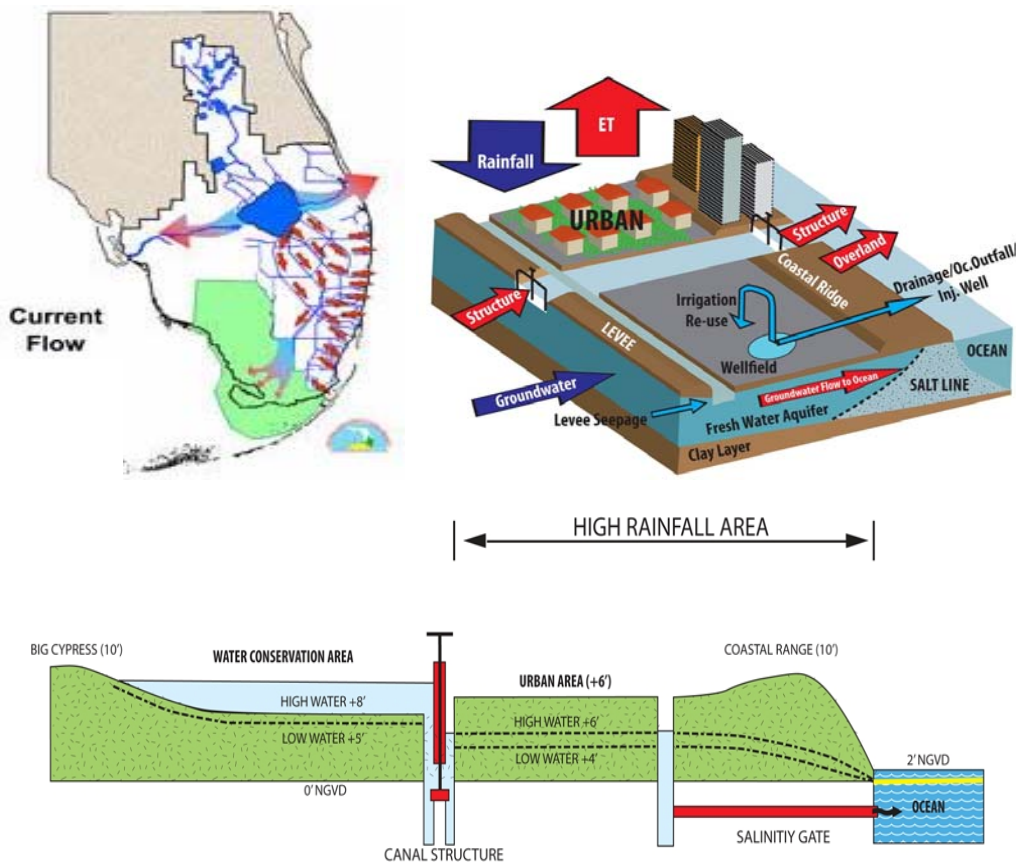


Fig. 8 Current Everglades flow pattern and cross-section [18].

The Everglades is a shallow, wide, slow moving river, although during the dry winter and spring season there is little flow. There are wet and dry cycles in the Everglades. The fauna and flora are adapted to this wet/dry variation. However, the ecosystem is dependent on this region having fresh water. The groundwater table is just below the surface. The deepest part of the Everglades is Shark Valley, which has an elevation of 4 ft based on the 1929 national geodetic vertical datum (ngvd) at the Tamiami Trail and increases approximately 0.1 ft/mile. In 100 miles from south to north, the elevation of the Everglades rises about 10 ft. As a result, as sea level rises, there are few obstacles to the progression of saltwater up Shark Valley. With the increase in sea level, the wet/dry cycles will be compromised, and ecological changes will result. Sawgrass prairies, pinelands, hardwood hammocks, and cypress swamps will not tolerate saltwater. The Everglades has the potential to become

one of the world’s largest saltwater marshes unless steps to address the saltwater advance are taken.

Groundwater is also susceptible. As shown in Fig. 10, the Biscayne aquifer is wedge-shaped its bottom surface slopes downward from the Everglades toward Biscayne Bay and the Atlantic Ocean. Surface water percolates into the aquifer and then eastward towards the ocean. As a result, inundation of the Everglades would potentially contaminate the aquifer system. Furthering the concern is that change in the land use along the coast has resulted in water falling on impervious surfaces where development has taken place causing water to collect in pools or run off rapidly, further reducing the potential for recharge.

Ponding in impervious regions often results in large-scale flooding because high rates of rainfall during intense storms can overwhelm drainage systems. Drainage canals are used to discharge this excess runoff to the ocean to minimized flooding. The net

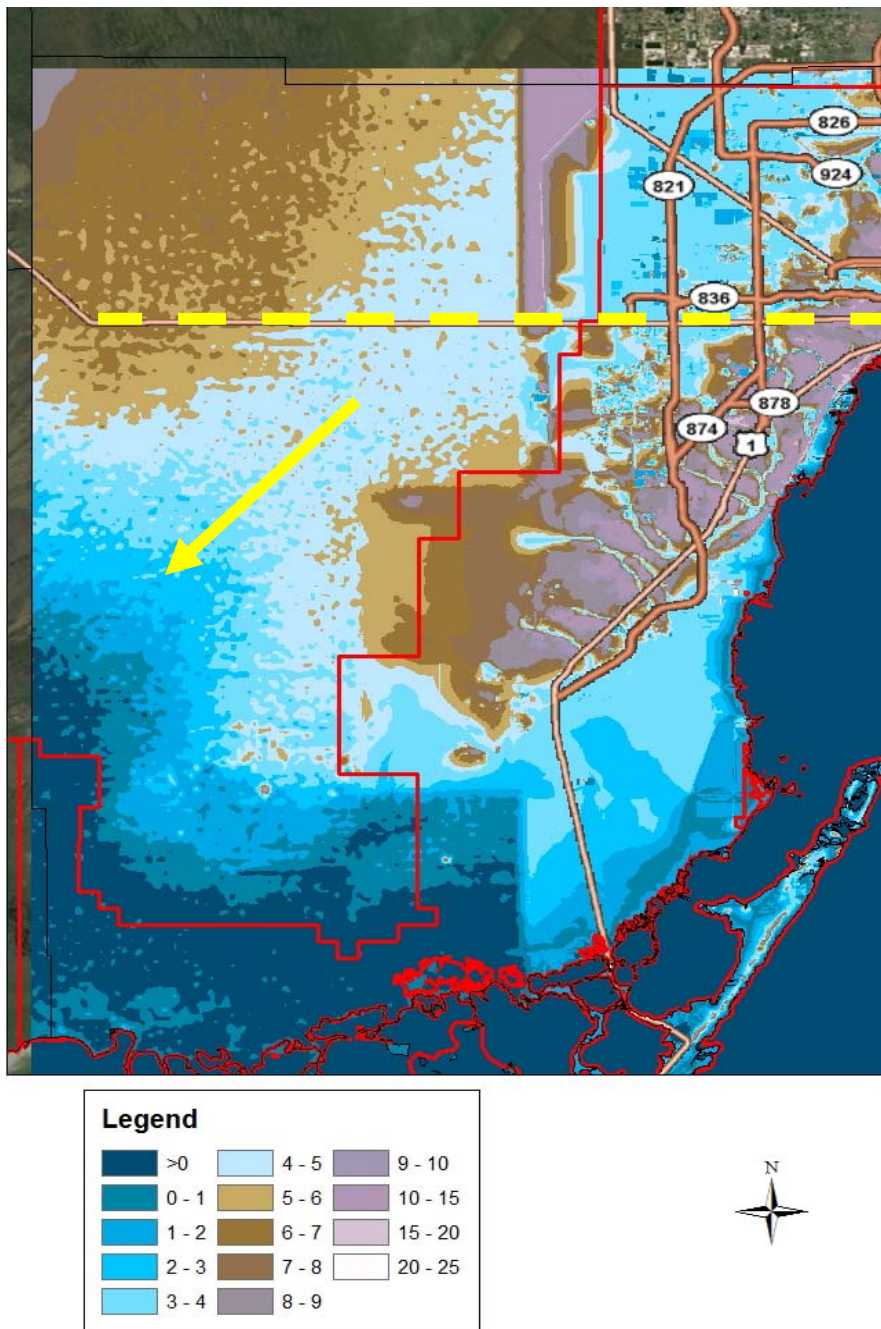


Fig. 9 Location of Tamiami Trail (yellow dashed line) showing areas with elevation of 5 ft ngvd and less in red, and a topographic depiction of the Everglades (yellow arrow showing the direction of surficial water flow); What this shows is that much of the lower Everglades would be inundated with saltwater; Note does not account for tidal action or surface or groundwater hydrology.

result is that historical groundwater storage is reduced, causing a reduction in available fresh water supplies during the dry season. This coincides with increased resident population and peak irrigation season for lawns and agriculture in winter. These improvements

may not provide adequate protection to south Florida from recurrent “droughts” during the drier months of winter and spring when crops fail and the potential for saltwater intrusion in coastal wellfields is highest.

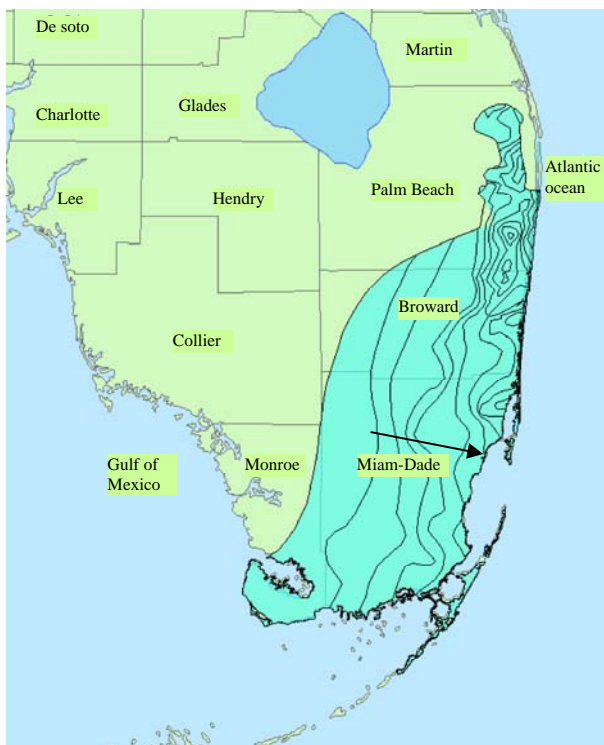


Fig. 10 Natural water movement of the Biscayne aquifer (black arrow shows direction of groundwater movement [20]).

2. Planning for Change

The literature on climate change focuses on two plausible strategic responses: “mitigation of climate change” which relies primarily on policies to reduce greenhouse gas (GHG) emissions, and “adaptation to climate change” consisting of actions to offset the vulnerability to climate change impacts [1, 20]. To reduce the impact of sea-level rise on coastal communities, three types of adaptive responses can be undertaken: planned retreat (zoning to discourage development in coastal zones), accommodation (retrofitting buildings), or protection (levees and seawalls) [21-23].

2.1 Reducing Risk vs. Creating Resiliency

While uncertainties in the scale, timing and location of climate change impacts can make decision-making difficult, response strategies can be effective if planning is initiated early. Because vulnerability can never be estimated with 100% accuracy, the

conventional anticipation approach should be replaced or supplemented with one that recognizes the importance of building resiliency. The resilience approach focuses on adaptive capacity, which can be seen as the innate ability of a natural or social system to cope with extreme events, respond, learn from mistakes, and recover (hopefully even stronger). This is what adaptation is all about, and policies that aim to strengthen adaptive capacity/resiliency not only avoid potential impacts, but create benefits, regardless of the actual occurrence of any or all events.

2.2 The Cost of a Coastline in Crisis

According to the Florida Department of Environmental Protection (DEP) almost 400 miles or nearly 50 percent of Florida’s 825 miles of beaches are currently “critically eroded” [24]. For every foot in sea-level rise, Florida’s beaches have receded anywhere from 100 to 2,000 feet [21]. Seawalls and beach re-nourishment projects are expensive and have adverse ecological consequences. According to the U.S. EPA, the cost of replenishing Florida’s beaches under a 1/2 meter rise in sea-level would be \$1.7 billion, and upwards of \$11.8 billion with a 2 meter rise [24]. Additionally, a Tufts University study finds that economic losses due to climate change, such as decreases in tourism revenue, hurricane damage, and potential loss of real estate could cost Florida \$327 billion by 2100 [24].

2.3 Reducing Property Vulnerability

Florida’s economic vitality is also at risk. The Federal Emergency Management Agency’s (FEMA) National Flood Insurance Program (NFIP) ranked Florida third in the nation for repetitive-loss properties (which have two or more flood insurance claims within a 10 year period) [24]. To reduce the costs associated with maintaining, insuring, and rebuilding flood prone properties, a number of strategies can be employed, such as: rolling easements, targeted coastal land acquisition, tax incentives for landward relocation,

stricter setbacks, reclassifying hazard zones, conservation easements, restrictions on rebuilding after storm destruction, and improved comprehensive planning [21, 24, 25].

2.4 Coastal Ecosystem Management

The relationship between natural systems and the ability to protect and adapt to anticipated impacts of climate change are also important to recognize. Coastal wetlands provide habitat for wildlife, including nurseries for fish and rookeries for birds, and critical functions for humans, such as the natural cleaning of ground and surface water, as well as flood and storm protection [26, 27]. Wetlands are under enormous pressure already, largely due to human density, infrastructure and water management practices. Taking these into consideration, as much as 70% of the world's wetlands might be lost by the year 2080 [23].

Protecting coastal, freshwater wetlands is a complex matter. Climate change adaptation strategies like flood protection can reduce the ability of freshwater wetlands to migrate inland ahead of saltwater marshes. Wetland changes will be manifested in a variety of ways. First, developers will note the inland migration of mangroves. Wading birds will likely migrate to more favorable areas, but higher water levels may complicate the survival of suitable wetlands. Peat collapse, coastal erosion and sediment changes will also be factors along the coast. The loss of marine nurseries and coastal habitat are potential results.

Thus, as sea-level rises, all the elements in a coastal wetland (salt marshes, mangrove forests, cypress swamps, etc.) can be caught between development and a revised coastline and, effectively, become "squeezed" out [20, 26, 27]. Wetlands are a critical part of an area's natural infrastructure and water supply recharge. As a result, this resource should be protected through good coastal management and careful infrastructure and land use planning.

Likewise, beaches are extremely vulnerable to erosion due to sea level rise in combination with coastal storms. Beaches are a critical element of

Southeast Florida's tourist economy and the way of life sought by a large number of its residents. Environmentally, beaches represent important and sometimes essential habitat for birds, fish, and sea turtles. South Florida's beaches support a large and critical venue for sea turtle nesting. They also absorb wave movement and retard wave migration.

3. Potential Solutions

As much as 1 to 2 feet or more of sea level rise by the mid- to late-21st century will present southeast Florida with some unprecedented challenges. Much of these will be manifested through its water resources. Water management plans until recently have only begun to consider the potential impacts of sea level rise. For the most part, planning until now has assumed "stationarity", i.e. the assumption that the status quo and historical norms will remain intact. However, in the face of climate change induced sea level rise and changes in temperature and precipitation patterns, this assumption is no longer valid. There has yet to be any substantial rethinking of long range goals and plans that takes the impacts of climate change into account. As noted, climate change could affect the feasibility of a number of alternative water supply, wastewater reuse, and stormwater programs. Furthermore, plans for Everglades restoration should be thoroughly reviewed through the lens of climate change. For these reasons and in order to stimulate discussion and debate of these matters, some new ideas for consideration are presented, some of which may have been regarded as unthinkable until now.

3.1 Re-engineering Canal Systems, Control Structures, and Pumping

Sea level rise will inundate coastal property. Since most of southeast Florida's stormwater drainage depends on gravity flow, drainage capacity will suffer as sea level rises reducing the head differential between interior surface waters and tide. Saltwater intrusion will be exacerbated. Furthermore, reduced soil storage capacity, groundwater flow and stormwater drainage

capacity will contribute to increased flooding during heavy rain events in low-lying areas below 5 ft elevation (over half of Broward and Miami-Dade Counties).

Water managers in southeast Florida use the drainage canal network to control water table levels and prevent flooding by discharging stormwater to tide in coastal areas. The current placement and design of coastal control structures did not anticipate sea level rise and changes in precipitation patterns. Repositioning of coastal control structures might prevent or substantially reduce the inland migration of seawater in canals and the saltwater intrusion front (see Fig. 11). By maintaining high water levels in the canals, the aquifer retains water that would otherwise be lost to tide, while protecting against saltwater intrusion.

The South Florida Water Management District maintains and operates the primary canal system. According to their estimates, approximately 13% of the control structures (see Fig. 12) would lose 100% of their capacity with sea level rise above 4 inches, about 67% with an 8 inch sea level rise, and over 80% of the structures with a 1.5 foot rise in sea level [29]. Capacity of the system is reduced even further [18], since control structures would lose capacity as sea level rises. Consequently, estimated total system capacity loss is estimated to be about 30% with sea level rise of 4 inches and 70% with an 8 inch sea level rise. These estimates do not take into account the additional runoff rates that will result as groundwater levels rise along with sea level. The dilemma is that as control structures lose capacity due to decreased head differential, stormwater runoff rates will increase substantially resulting in increased surface water ponding. As a result, stormwater management during the rainy season and major rainfall events, especially tropical storms and hurricanes, will become increasingly difficult as sea level continues to rise to levels approaching and exceeding current groundwater elevations.

There are currently only three coastal pumping stations in Southeast Florida, the S-13 on the C-11

canal in Broward County and the S-25 and S-26 on the Miami River and one of its tributaries in Miami-Dade County. The S-13 is designed to assist stormwater drainage as needed from the C-11 canal which is barely above current mean tide and is often below high tide. The S-13 has a rated capacity of 540 cubic feet per second against a static head of 4 feet (cfs). The cost was nearly \$100 million. The SFWMD is evaluating solutions such as additional pumping stations on the most vulnerable control structures, but pumping comes with major capital investment, operating costs, and increased energy consumption. Public interests, with interests in open ocean access, private property rights, inverse condemnation, etc., will resist construction of salinity structures closer to the ocean, and such installations may exacerbate inundation and flooding of low lying coastal areas. Furthermore, not only is low-lying property near the coast at risk, so are low-lying communities much farther inland in flood plains that were previously part of the Everglades.

Stormwater management regionally and in local communities during the wet season and major rainfall events will become increasingly difficult as sea level rises. Groundwater levels are tied to sea levels in coastal regions, so south Florida should expect sea level rise to cause corresponding increases in groundwater levels unless actions are taken to reduce groundwater levels in low lying areas through increased pumping. Currently groundwater levels are controlled by the SFWMD and local drainage districts using gates and pumps. As sea level rises to about 1-2 feet pumping to control groundwater levels will increase the risk of saltwater intrusion. As sea level rises by 2-3 feet or more, it will be increasingly difficult to control groundwater levels during intense rain storms as the drainage system becomes more compromised. Increased groundwater levels diminish soil storage capacity (i.e., the amount of rainfall that can percolate into the soil) and compromise the flow capacity of storm drainage systems and coastal structures. Modest increases in sea level could lead to

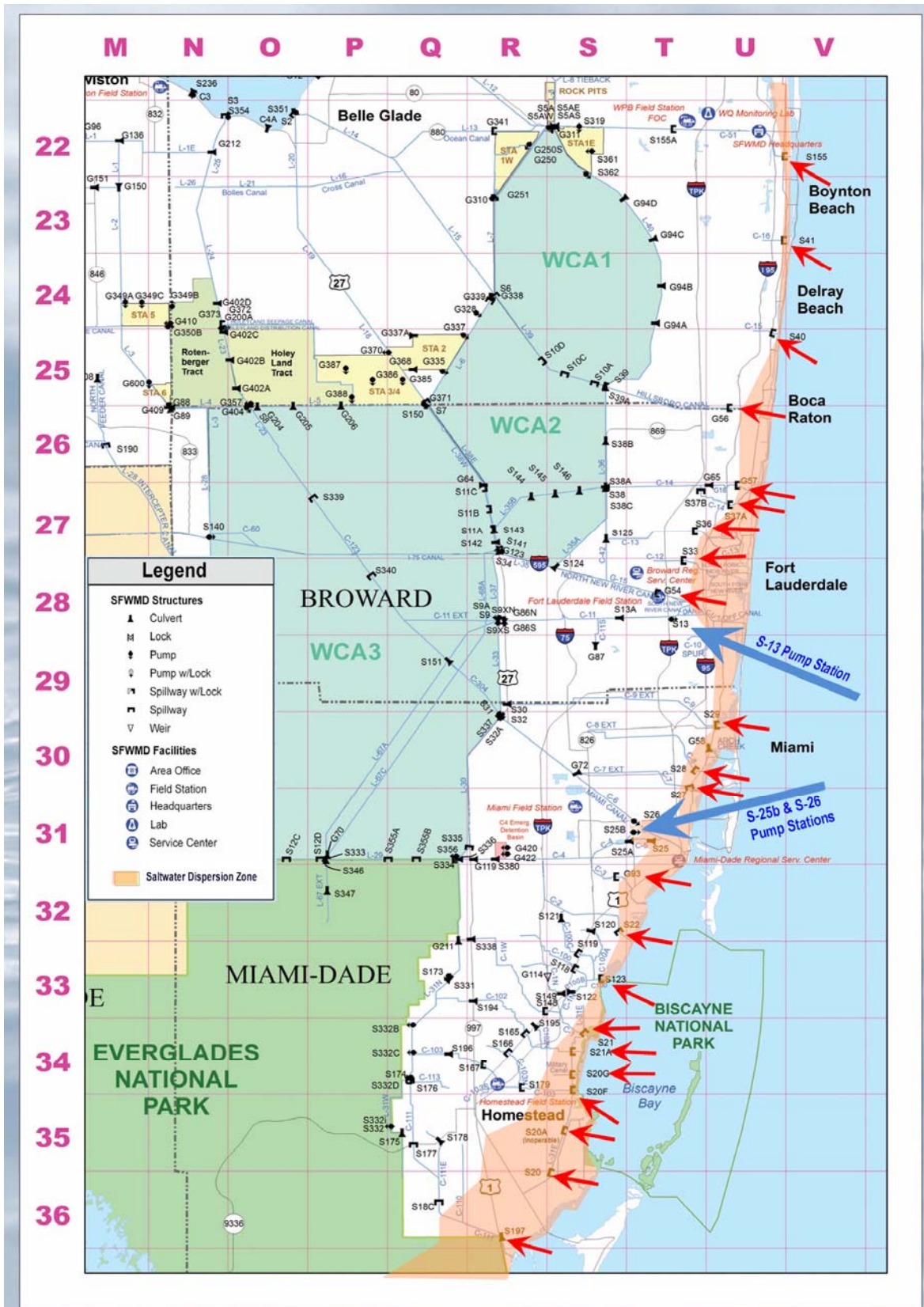


Fig. 11 Location of salinity structures in southeast Florida. The migration of saltwater intrusion matches the salinity structures, which matches the location of the salinity structures [28].

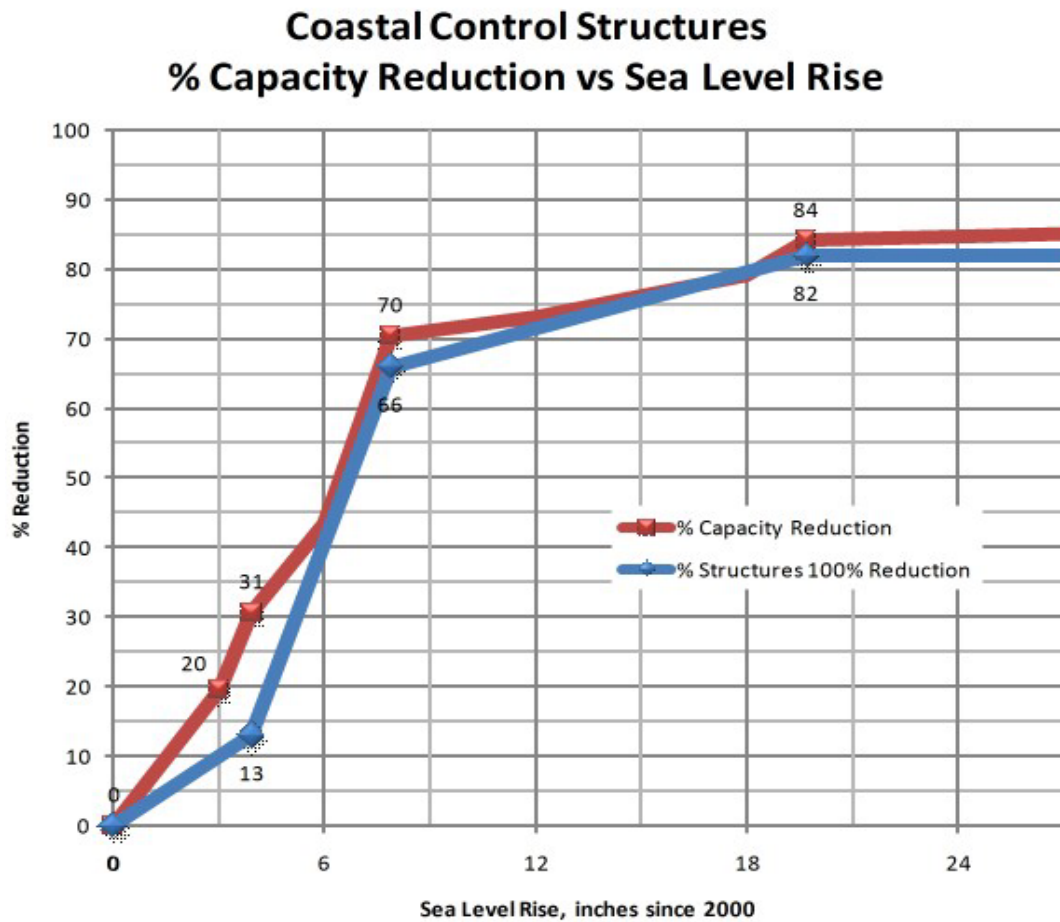


Fig. 12 Effect of sea level rise on capacity of coastal flood control (salinity) structures in Southeast Florida; The blue curve is data from Ref. [28] showing the percent structures losing 100% of their capacity versus sea level rise; The red curve shows estimated total system capacity loss as a function of sea level rise [18].

the potential for severe flooding of large areas after typical rainstorm events. Some communities in southeast Florida have areas that already flood regularly. The problems will worsen with time as more areas begin to lose soil storage capacity.

In low lying areas, exfiltration trenches will become impractical due to increased ponding as water tables rise with sea level, and dry retention will become wet retention. Additional local pumping stations on secondary canals will be needed to supplant the storm drainage system in order to prevent unacceptable ponding. Design capacities of these stations will depend on local rain patterns, drainage basin size and secondary canal system design, but could range from \$1.5 million for small local stations to over \$50 million for larger, regional stations. And many will operate

continuously, which means ongoing operations will increase substantially. Hundreds of pumping stations may be needed in larger southeast Florida communities. Permits will be a major challenge due to contaminants in the runoff as regulated by MS 4 Stormwater permits, and the inability to treat this water under the current structure. The cost and energy required for stormwater treatment would be a major concern going forward. Communities will have to obtain up-to-date LIDAR topography and ground truthing and perform additional stormwater modeling to prioritize areas that will need drainage and pumping improvements. Stormwater utilities will be faced with dramatic, currently unanticipated increases in capital expenditures and operating costs, and time will be needed for planning, design, securing permits and compliance.

3.2 Increasing Flows to the Everglades

A 3 foot sea level rise will create significant adverse impacts on the lower Everglades. Major changes will result as fresh water ecologies convert to one of the world's largest saltwater marshes unless steps are taken to address the advance of saltwater (see Fig. 13 and previously in Fig. 9). However, an alternative water supply solution worth considering would be to redirect treated urban stormwater runoff and wastewater effluent.

Presently, most of the treated wastewater generated in the US is discharged to surface waters. In California, Texas, Arizona and Nevada significant amounts of wastewater are reclaimed, and Florida is among the leaders in reclaimed water use in the United States with some 400 facilities using reclaimed water for a variety of purposes. Public access reuse systems, where accessible, can provide irrigation for residential lawns, golf courses, cemeteries, parks, landscaped areas, and highway medians. For these purposes, reclaimed water must be filtered to less than 5.0 mg/L of suspended solids before application of disinfectant to assure deactivation of viruses and other pathogens. Filtration also removes protozoan pathogens (*Cryptosporidium* and *Giardia*).

With sea level rise, irrigation in low lying areas would be less beneficial because of the aforementioned

potential of ponding and stormwater flooding. However, a potential beneficial use of treated wastewater and stormwater runoff could be to offset saline water invasion in the lower Everglades while creating a natural barrier to the migration of salt water northward. A comprehensive solution previously suggested by Ref. [31] may be to augment the Everglades restoration plan by providing regional advanced treatment facilities that raise wastewater quality to the level required for direct aquifer recharge (reverse osmosis, ultraviolet disinfection and oxidation). This water could then be discharged to the Everglades Water Conservation Areas (WCAs) and/or regional recharge areas, as needed.

Everglades recharge with treated wastewater would follow the 40 year precedent in Orange County, California for aquifer recharge. Regionalization of state-of-the-art facilities would provide economies-of-scale to lower costs of operation and investment in capital equipment. In addition, the amount of secondary treated wastewater disposed to deep injection wells and ocean outfalls without beneficial use would be substantially reduced. The concept could make a major contribution to ecosystem restoration by providing fresh water (over 500 MGD is available) needed to counteract the northward migration of saltwater in the southern Everglades caused by sea level rise.

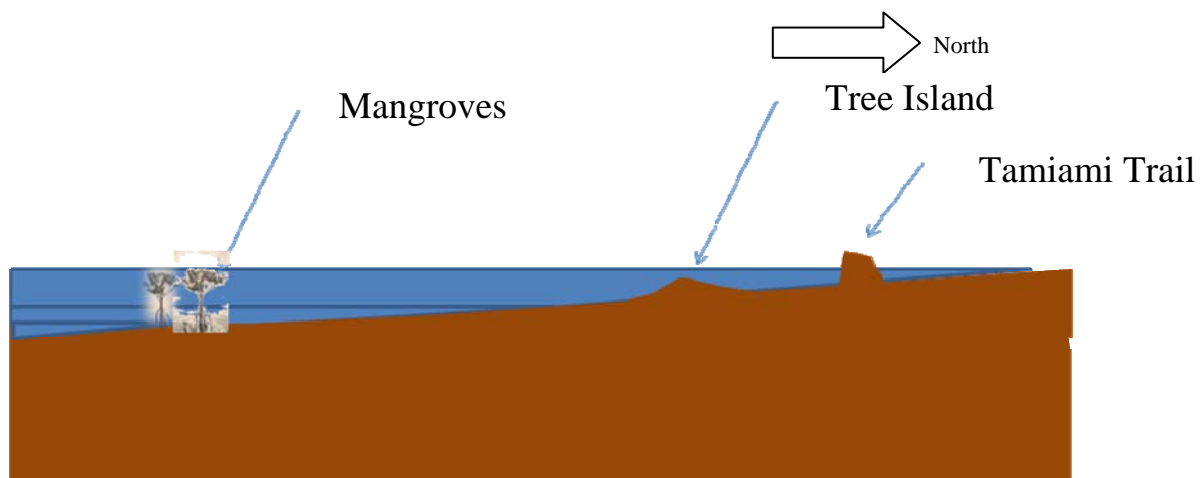


Fig. 13 Progression of inundation into the Everglades. As sea level rises, the level of water will migrate further north; At 3 ft rise, high tide will be at current 5 ft NGVD, which will mean the saltwater has the potential to extend north of the Tamiami Trail [30].

A regionalization plan would consist of the following components: a piping network to deliver secondary treated wastewater to the requisite number of regional advanced treatment facilities and a network of 50-100 MGD advanced treatment facilities using media filtration, cartridge filtration, ultraviolet disinfection, reverse osmosis, advanced oxidation, and other advanced treatment technologies deemed appropriate. The high quality treated wastewater produced in this option could then be discharged directly to the WCAs providing more consistent hydration year-round for ecosystem restoration. This would also recharge the Biscayne aquifer at its headwaters and increase the available water supplies for the region. Release to the urban canal systems could also augment aquifer recharge during periods of extended drought. Under this scenario, current wells and treatment facilities would continue to operate as designed, maximizing utilization of local infrastructure. It may also be possible to delay development of other water supply alternatives. Currently Miami-Dade County, Plantation, Sunrise, Davie and Pembroke Pines have or are currently testing the process, and results of these tests will be forthcoming.

In addition, to facilitate flood control in the increasingly vulnerable low-lying flood plains west of the coastal ridge, the same concept could be applied to

treating and delivering stormwater during the rainy season to the Everglades Water Conservation Areas (WCAs) and additional Stormwater Treatment Areas (STAs), where it could be stored and delivered as necessary to the urban areas and the southern Everglades. This would require reengineering the stormwater drainage system in order to collect and convey stormwater to treatment facilities before pumping to the WCAs. The proposed concept envisions a partnership between utilities and regulators to address technical, economic, environmental and regulatory issues to meet the growing demands of the region. It is possible that existing canals could be modified to transfer stormwater to treatment facilities located close to the edge of the WCAs. Feeder canals would then be used to recharge the surficial aquifer locally as deemed appropriate. Fig. 14 shows the concept.

3.3 Barriers to Flow Migration

Unlike the urban area, there are limited structures in the lower Everglades. There are a levee and control structures along the Tamiami Trail, an east-west highway traversing the Everglades that connects Miami with Naples, Florida, that was constructed nearly 90 years ago. A canal parallels the north upstream side of the Trail. A limited number of gated

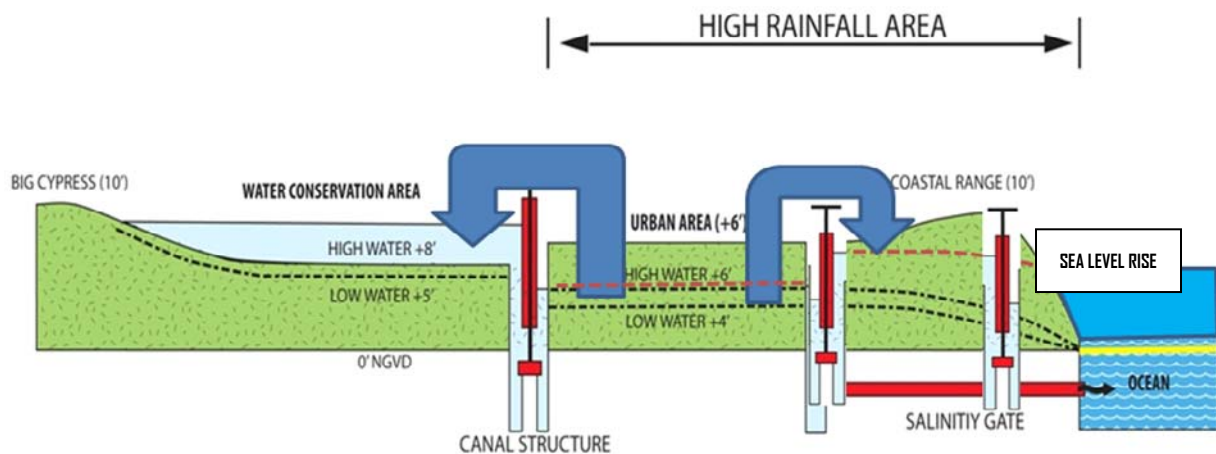


Fig. 14 Suggested drainage system reengineering concept; Treated stormwater west of the coastal ridge and treated wastewater using advanced techniques to remove nutrients and contaminants could be pumped westward to add freshwater to the Everglades; Additional gates would create locks that could elevate water tables in the coastal ridge to provide salinity barriers to the east while controlling flooding in developed areas west of the ridge [30].

conduits pass under the Trail. The Tamiami Trail has been a point of contention for many years between environmentalists and water supply managers.

In its current configuration, the Trail prevents adequate fresh water from flowing southward into Everglades National Park depriving the park of a major portion of its historical hydration. A primary goal of the Comprehensive Everglades Restoration Plan is to restore sheet flow to Everglades National Park by eliminating the blockage caused by the Trail. Ground was broken recently for the first 1 mile elevated section of the Tamiami Trail to eliminate the impediment to sheet flow.

An alternative plan to restore sheet flow proposed by the Miccosukee Tribe is to excavate a new spreader canal on the south side of the Trail connected to the north side canal by numerous gated conduits. This could maximize use of current infrastructure at significantly less cost than the elevated highway. Another consideration is that this approach would retain the levee that might be useful in the future as a means of controlling migration of saltwater northward as sea level rise progresses to 3 feet or more. Miami-Dade County has a major water wellfield a short distance north of the Trail that supplies fresh water to most of the southern portion of the County. Migration of brackish waters north of the Trail would contaminate this wellfield and subsequently the Everglades Conservation Areas that are the headwaters of southeast Florida's water supply. The Tamiami Trail and levee might, with suitable upgrading, be thought of as "a line in the sand" to protect southeast Florida's water supply from sea level rise. The decision to elevate a large section of the Tamiami Trail should be revisited in consideration of the possibility that sea level rise could exceed 3 feet by the end of the 21st century.

4. Conclusions and Recommendations

Southeast Florida is one of the most vulnerable areas in the world to sea level rise resulting from climatic

changes. Recent reports have focused on the urban issue, but the ecosystem impacts may be even more significant. South Florida is home to the Everglades, the only environment of its kind in the world. It is home to numerous endangered species and a unique ecosystem that supports the mid-Atlantic marine food chain and fisheries. It is also the headwaters for the water supplies of the region. As a result, ecosystem impacts would have significant impacts on the urban environment as well.

To protect the Everglades and water supplies in south Miami-Dade County, it is critical to slow the northward migration of saltwater in the southern Everglades. This is best accomplished by increasing fresh water flow to the southern Everglades, which is the primary goal of the Comprehensive Everglades Restoration Program (CERP). Sea level rise makes the case for CERP even more compelling. Quantitative predictions of these concepts using hydrological models are needed.

There are several issues that can be pursued to protect southeast Florida's ecosystem and its water supplies. Among the issues are:

- Evaluation of the redirection of wastewater treatment to permit recharge to the Everglades Water Conservation Areas to increase southward water flows. This option offers advantages that are far-reaching despite the potential costs. The concept would provide a major contribution to ecosystem restoration by providing the water needed to counteract the northward migration of saltwater in the southern Everglades caused by sea level rise;
- Major replumbing of the current drainage systems that exhibit decreased performance as sea level rises, necessitating major investments in regional and local stormwater infrastructure;
- In light of sea level rise, review of the decision to elevate the Tamiami Trail, which would remove a potential barrier to northward migration.

These strategies should be pursued in a more fully developed framework of research, collaboration, and

policy formulation. Planning for climate change will take creative ideas, significant effort and commitment. The authors hope that this paper will stimulate further consideration of the daunting challenges facing Southeast Florida and result in new solutions.

References

- [1] Intergovernmental Panel on Climate Change 2007: The Physical Science Basis, available online at: http://ethree.com/downloads/Climate%20Change%20Readings/Climate%20Science/IPCC%20Reports/AR4WG1_FrontMatter-v2.pdf (accessed 10/1/2010).
- [2] Climate change: Global risks, challenges & decisions, Synthesis Report, International Alliance of Research Universities, Copenhagen, 2009.
- [3] T.R. Karl, R. Thomas, J.M. Melillo, T.C. Peterson (Eds.), Global Climate Change Impacts in the United States, U.S. Global Change Research Program, Cambridge University Press, 2009, available online at: <http://www.globalchange.gov/publications/reports/scientific-assessments/us-impacts/full-report>.
- [4] F.E. Singer, Nature, not human activity, rules climate change, summary for policy makers, The Nongovernmental International Panel on Climate Changes, The Heartland Institute, Chicago, IL, 2008.
- [5] C.H. Marshall, H. Curtis, R.A. Pielke, Sr., L.T. Steyaert, D.A. Willard, The impact of anthropogenic land-cover change on the Florida peninsula sea breezes and warm season sensible weather, Monthly Weather Review 132 (2003) 28-52.
- [6] C.H. Hapgood, Path of the Pole, 2nd ed., Adventures Unlimited Press, Kempton, IL, 1999.
- [7] US Census, Latest estimate for Miami-Dade, Broward, Palm Beach and Monroe Counties, 2008, available online at: http://factfinder.census.gov/servlet/ADPTable?_bm=y&-qr_name=ACS_2008_1YR_G00_DP2&-geo_id=05000US12011&-ds_name=ACS_2008_1YR_G00_-&-lang=en.
- [8] R.J. Nicholls, OECD, Ranking Port Cities with High Exposure and Vulnerability to Climate Extremes: Exposure Estimates, Organization for Economic Co-Operation and Development, OECD Publishing, 2008.
- [9] J. Murley, Charting the Course, Where Is South Florida Heading, Florida Atlantic University, Boca Raton, FL, 2006.
- [10] California Natural Resources Agency, California Climate Adaptation Strategy: A Report to the Governor of the State of California in Response to Executive Order S-13-2008, 2009, available online at: <http://www.climatechange.ca.gov/adaptation/>.
- [11] J.S. Littell, M. McGuire, L.C. Elsner, W. Binder, A.K. Snover (Eds.), The Washington Climate Change Impacts Assessment: Evaluating Washington's Future in a Changing Climate, Climate Impacts Group, University of Washington, Seattle, Washington, 2009, available online at: www.cses.washington.edu/db/pdf/wacciaexecsummary638.pdf.
- [12] New York City Department of Environmental Protection, Report 1: Assessment and Action Plan-A Report Based on the Ongoing Work of the DEP Climate Change Task Force, New York, USA, (2008. May).
- [13] M. Stephen, Climate change and land use in Florida: Interdependencies and opportunities, A Report prepared for the Century Commission for a Sustainable Florida, Sept. 30, 2007.
- [14] K. Freas, R. Bailey, A. Muneavar, S. Butler, Incorporating climate change in water planning, JAWWA 100 (2008) 93-99.
- [15] F. Bloetscher, The potential impact of climate change on groundwater recharge, available online at: <http://www.gwpc.org/meetings/forum/2008/proceedings/Opening%20Session/BloetscherOpening.pdf>.
- [16] G.A. Maul, Florida's changing sea level, shoreline: Florida shore and beach preservation association, May, 2008, 3 p. available online at: <http://www.fsbpa.com/publications.html>.
- [17] USEPA, Synthesis and Assessment Product 4.1, Coastal Sensitivity to Sea Level Rise: A Focus on the Mid-Atlantic Region, U.S. Climate Change Science Program, Washington DC, 2009.
- [18] B.N. Heimlich, F. Bloetscher, D.E. Meeroff, J. Murley, Southeast Florida's resilient water resources: Adaptation to sea level rise and other climate change impacts, Florida Atlantic University, 2009, available online at: http://www.ces.fau.edu/files/projects/climate_change/SE_Florida_Resilient_Water_Resources.pdf.
- [19] F. Bloetscher, D.M. Meeroff, B.N. Heimlich, A.R. Brown, D. Bayler, M. Loucraft, Improving the resilience of a municipal water utility against the likely impacts of climate change: A case study: City of Pompano beach, Florida water utility: City of Pompano beach, FL, JAWWA 102 (2010) 36-46.
- [20] H.M. Füssel, R.J.T. Klein, Climate change vulnerability assessments: An evolution of conceptual thinking, Climatic Change 75 (2006) 301-329.
- [21] R.E. Deyle, K.C. Bailey, A. Matheny, Adaptive response planning to sea level rise in Florida and implications for comprehensive and public-facilities planning, Florida Planning and Development Lab, Department of Urban and Regional Planning, FSU, 2007.

- [22] R.J.T. Klien, R.J. Nicholls, S. Ragoonaden, M. Capabianco, J. Aston, E.N. Buckley, Technological options for adaptation to climate change in coastal zones, *Journal of Coastal Research* 17 (2001) 531-543.
- [23] R.J. Nicholls, F.M.J. Hoozemans, M. Marchand, Increasing flood risk and wetland loss due to global sea-level rise: Regional and global analyses, *Global Environmental Change* 9 (1999) S69-S87.
- [24] Florida Coastal and Ocean Coalition (FCOC), Preparing for a sea change in Florida: A strategy to cope with the impacts of global warming on the state's coastal and marine systems, available online at: <http://www.flocoastalandocean.org/> (accessed on Dec. 15, 2008).
- [25] R.P. Stumpf, J.W. Haines, Variations in tidal level in the gulf of Mexico and implications for tidal wetlands, estuarine, *Coastal and Shelf Science* 46 (1998) 165-173.
- [26] J.G. Titus, Greenhouse effect and coastal wetland policy: How Americans could abandon an area the size of Massachusetts at minimum cost, *Environmental Management* 15 (1) (1991) 39-58.
- [27] B. Poulter, R.L. Feldman, M.M. Brinson, B.P. Horton, M.K. Orbach, S.H. Pearsall, et al., Sea level rise research and dialogue in north Carolina: Creating windows for policy change, *Ocean and Coastal Management* 52 (2009) 147-153.
- [28] SFWMD, Facilities and Infrastructure Location Index Map, 2005, available online at: http://www.sfwmd.gov/portal/page/portal/xrepository/sfwmd_repository_pdf/facility_map_overview.pdf
- [29] J.S. Obeysekera, Climate Change & Water Management: Planning for Sea Level Rise, Broward Climate Change Task Force, Science & Technology Subcommittee, Fort Lauderdale, 2009.
- [30] F. Bloetscher, B.N. Heimlich, Counteracting the effects of sea level rise on southeast Florida's water resources, in: Greater Everglades Ecosystem Restoration (GEER) Conference, Naples, FL, July, 2010, available online at: <http://conference.ifas.ufl.edu/GEER2010/Presentations/Thursday/Royal%20Palm%201-2/pm/0420%20B%20Heimlich.pdf>.
- [31] F. Bloetscher, A. Muniz, Water supply in South Florida-The new limitations, in: Sustainable Water Sources (Reno) Conference Proceedings, Denver, CO: AWWA, 2008.

A “Trojan” in Climatic Change: The Urban Effect

J. Quereda Sala, E. Montón Chiva and J. Escrig Barberá

Climate Laboratory, Faculty of Agriculture, University Jaume I, Castellón 12006, Spain

Received: March 24, 2011 / Accepted: April 20, 2011 / Published: November 20, 2011.

Abstract: This paper sets out the preliminary results of an experimental research plan aimed at analysing the thermal processes inherent to the urbanisation effect. Although this effect is undeniable, the extent of its impact is a matter of controversy. The results obtained in this study show both the nature of the phenomenon and its considerable magnitude. Failure to take this process into account might seriously bias any analysis of thermal evolution, the cornerstone of the climate change hypothesis.

Key words: Temperatures, urban heat island effect (UHI), homogeneity, climatic change.

1. Introduction

Much research has been devoted in the past three decades to climate change and mankind's influence on the climate. This intense research activity is justified by the current hypotheses regarding the future of the climate. However, despite the great striving to control data quality, many uncertainties still persist in this domain, in which middle-degree, or perhaps larger, oscillations should be examined with circumspection, since they could be caused by a simple change of shelter or relocation of the observatories.

Thus, the evolution of temperature through the historical series available at the world's main laboratories cannot be readily analysed, because certain non-climatic processes need to be taken into account. Of these processes, the subtlest and most important is undoubtedly the urban thermal effect. Though this effect is undeniable, its importance is a matter of controversy. Cities have become cells or bubbles with very different climate conditions from those of the surrounding atmospheric or rural environment. This process is known as the urban heat island effect (UHI).

The existence of the UHI effect is undeniable. The more buildings, pavement, inhabitants and activities accumulated in an area, the stronger the changes observed in the temperature trends, and even in the precipitation records. Cities have become nuclei or bubbles with specific climate conditions, quite different from the atmospheric rural environments that surround them. Therefore, during the day the urban temperature records are only a little higher than the rural ones, as much in summer as in winter. But during the nighttime urban temperatures are warmer than those on the outskirts, with differences in readings that can exceed 5 or 6 °C.

Some of the energetic processes that lead to the generation of UHI are: the heat capacity and conductivity of building and paving materials, increased absorption of short-wave radiation due to canyon geometry, increased long-wave radiation loss because of the reduction of the sky view factor, anthropogenic heat sources, increased sensible heat storage and decreased evapotranspiration due to construction materials, decreased total turbulent heat transport due to wind reduction caused by canyon geometry, and lastly, the atmospheric pollution of the air covering the cities, which is capable of containing long-wave radiation, thereby increasing the latent heat. That effect may be a true Achilles heel when it comes

Corresponding author: J. Quereda Sala, professor, Ph.D., main research fields: climatology, climatic change, hydric resources, remote sensing, dendroclimatology and dendrochronology. E-mail: quereda@his.uji.es.

to analysing temperature evolution.

The phenomenon was first investigated and described by Luke Howard in the 1810s [1]. The urban heat island (UHI) is a metropolitan area which is significantly warmer than its surrounding rural areas. The question being asked is, have urban areas contributed to the observed trend of warming temperature and influenced our knowledge of global warming? A view often held by sceptics of global warming is that much of the temperature increase seen in land based thermometers could be due to an increase in urbanization and the siting of measurement stations in urban areas. In such a way it can be concluded that about half of the observed warming trend could be accounted for by the residual UHI effects in the corrected temperature data set they studied [2], so the rapid warming measured over the last century could be just a record of the urbanisation [3]. Consequently, researchers must remove heat island effects from temperature records to accurately estimate climate change.

Thus, whilst some climatologists now think that the warming in the temperature record from some small urban area is partly the result of UHI, other prominent scientific and the IPCC have concluded that the impact of the urban heat island on the temperature records is real but local and has only a negligible effect on regional or global trends. However while the “heat island” warming is an important local effect, there is no evidence that biases trends in historical temperature record [4, 5]. Studies that have looked at hemispheric and global scales conclude that any urban-related trend is an order of magnitude smaller than decadal and longer time-scale trends evident in the series [6, 7]. Parker [8] noted that warming trends in night minimum temperatures over the period 1950 to 2000 were not enhanced on calm nights, which would be the time most likely to be affected by urban warming. The infrared AVHRR imagery shows the relevance of that phenomenon. This effect is visible in all the seasons during the night but it differs during the day in the

maximum temperature records [3]. Thus, the global land warming trend discussed is very unlikely to be influenced significantly by increasing urbanisation [8, 9].

This all requires awareness of the enormous difficulties involved in verifying the climate warming hypothesis, because of the great heterogeneity in temporal thermal series. Indeed, despite rigorous use of the most sophisticated statistical analytical techniques, this uncertainty in detecting significant trends remains present in all conclusions concerning the magnitude of the observed warming [10-15]. A major process in this uncertainty is the urbanisation effect [16-19].

2. Experiment

The temperature evolution in the Spanish Mediterranean region displays a significant climate warming trend. The value of this trend for the century would be appreciable, 1.6 °C, equivalent to 1 °C for the period 1950-2010. However, this value becomes even more striking if one considers that it only began to be detected after 1980, following a relatively cool decade (Fig. 1).

However, both the sharp post-1980 increase and the different magnitude of the warming recorded between these observatories, which lie quite close to each other, namely + 0.03 °C/year in Castellón, + 0.02 °C/year in Valencia, + 0.016 °C/year in Alicante and a mere 0.014 °C/year in Murcia, together with the varying behaviour of the maximum and minimum temperatures, have cast doubts on the anthropogenic or natural nature of the change, as well as on its actual existence [20] (Fig. 2).

Data used in the analysis belong to the network of meteorological stations for the Murcia Region and the Province of Alicante (Spain). That zone has an extensive weather station network with long-term series of more than 50 years. This network consists of four first order stations and thirty second order stations (Fig. 3). The analysis was done over the monthly mean minimum and maximum temperatures from the Instituto Nacional de Meteorología (INM).

Given that the validity of all conclusions on the evolution of the climate depend on the quality of the data, all the temperature series have undergone a rigorous process of quality control consisting of three steps. In the first step, a continuity and spatial coherence test has been applied to the data. If the data

were loss or missing, they were reformed. Within this step, the records that have not reached a confidence level of 99% were rejected. The second step was the application of the homogeneity test. Firstly, an internal homogeneity test (sequence and Helmert methods) was applied and afterwards a relative homogeneity test.

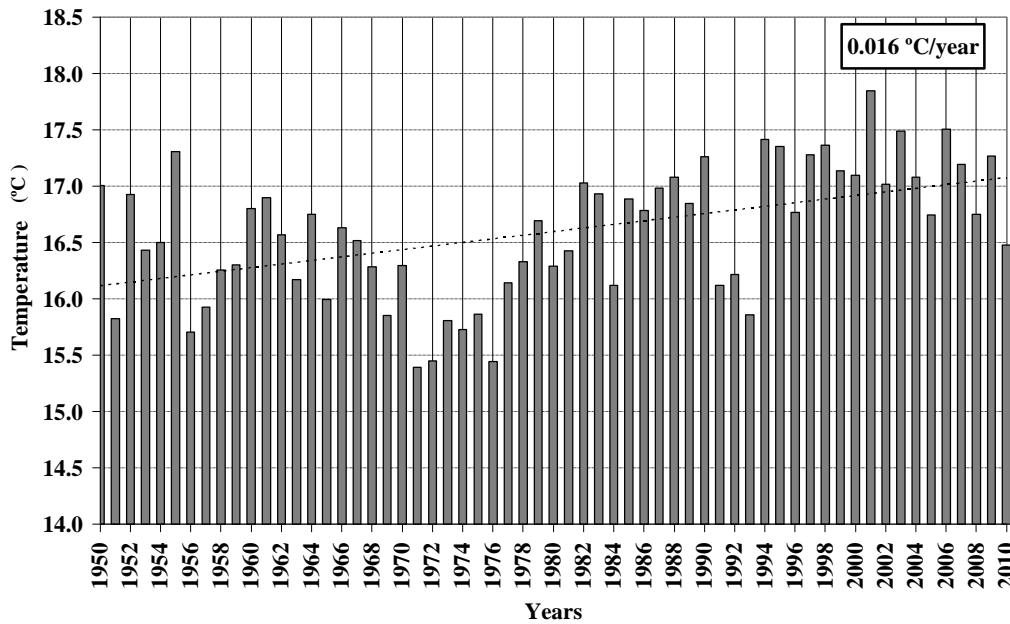


Fig. 1 Evolution of the homogenised mean annual temperatures in the Murcia and Valencia Region, INM [21].

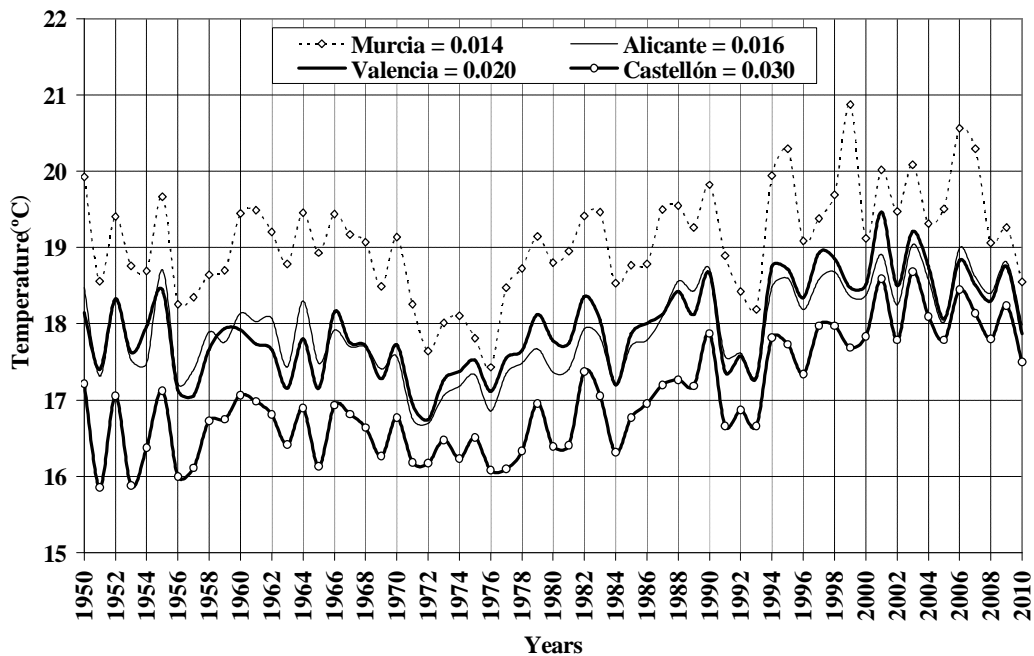


Fig. 2 Evolution of mean annual temperatures at the Murcia, Alicante, Valencia, and Castellón observatories.

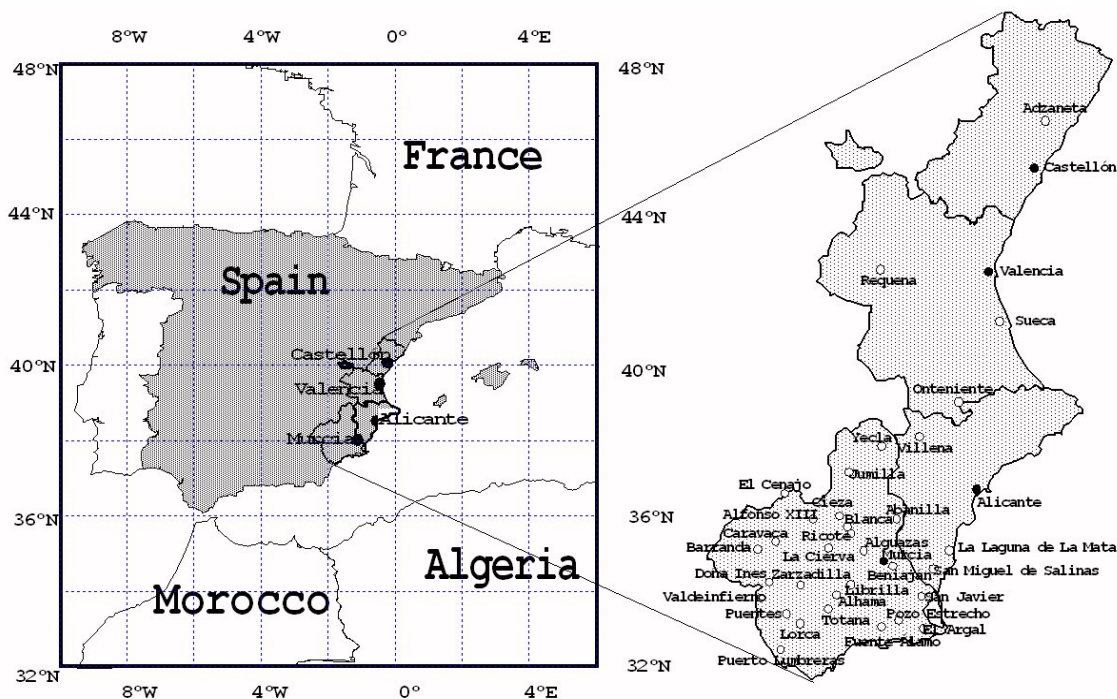


Fig. 3 Map of the major Spanish Mediterranean observatories used in this study (1950-2010).

That second step was used to ensure that most of the long-term series were not contingent. Consequently, a certain number of homogeneity tests and heterogeneity correction were applied to all the used records. The techniques used have been described exhaustively [22]. The third and last step consisted of a heterogeneity correction, which established the difference between the mean of the period of the series to be corrected and the mean of the period of the homogeneous series. That difference has been added to the difference of the values of the series to be corrected. Correlation coefficients between both series must be higher than 0.7 to be considered.

In this respect, after performance of the complex and laborious homogenisation process to correct the heterogeneities [13, 20, 22, 23], the assumption may be made that part of this temperature increase, 1 °C in the period 1950-2010, is due to the urbanisation effect. An effect that has materialised progressively and cumulatively as the observatories has been gradually engulfed by city growth.

The result of this process may be reflected in the fact

that most of the thermal increase has occurred in the minimum temperatures, with a value of 1.4 °C in the period 1950-2010. The evolution of the maximum temperatures, with an increase of 0.4 °C in the same period, would have been responsible for barely a third of this rise in temperature (Fig. 4).

As a result, the urban heat generation process continues to be one of the major uncertainties in the climate change hypothesis. And with good reason, since this scientific hypothesis is based on the records of historical observatories which, in the case of the Mediterranean observatories, were established at the end of the 19th century on town outskirts, and which have been progressively swallowed up by urban growth, with effects that need to be determined because they could be disguising real climate trends. Failure to take these effects into account might seriously bias the results and lead to errors in verifying the magnitude and nature of climate warming. This is evinced by the great difference in the trend value between the observatories located in large cities and those in smaller towns (Fig. 5).

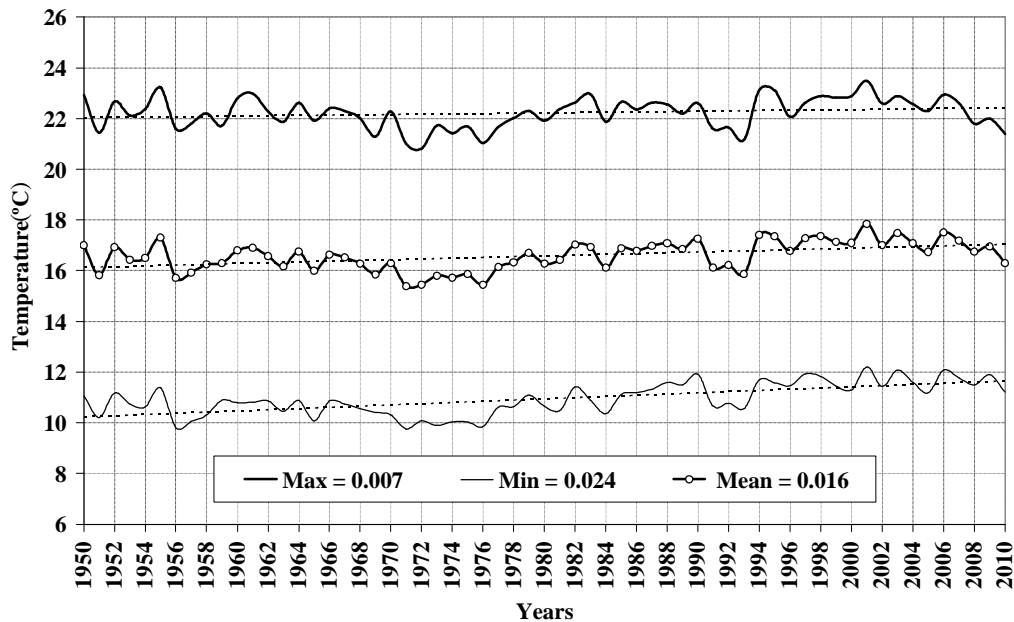


Fig. 4 Evolution and trend of the mean annual, maximum, and minimum temperatures at 34 major observatories in the Murcia and Valencia Region, INM [21].

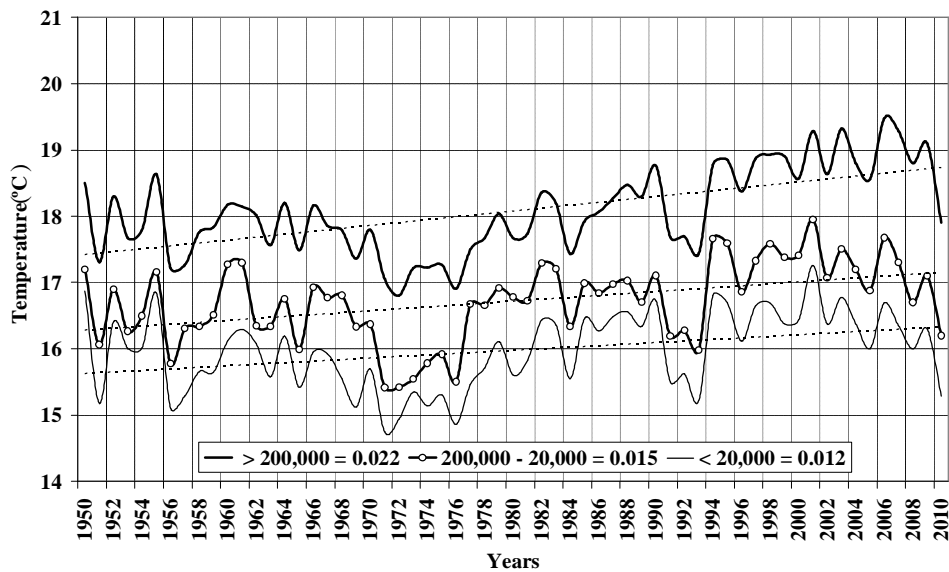


Fig. 5 Evolution and trend of the mean annual temperatures at the observatories in the cities of Murcia, Elche, Alicante, Valencia and Castellón and at the more rural observatories (towns with more than 200,000 inhabitants, and with fewer than 200,000 inhabitants and with fewer than 20,000 inhabitants), INM [21] and self generated.

3. Results and Discussion

The foregoing analyses suggest that the true “natural increase” in temperature, corrected for the urbanisation effect, could be much smaller than that posited by

current studies and models, or possibly non-significant. In addition, the analyses justify further research into a process that could be seriously biasing the study of thermal evolution, the cornerstone of the climate change hypothesis [8, 17, 20].

3.1 The Observational Arrangement

In the present study, the urban thermal effect has been examined by installing three duly calibrated, automatic meteorological stations (Davis-Casella). These three stations have been located in the Castellón city area, a city that has undergone marked demographic growth in recent years (from 53,000 inhabitants in 1950 to 190,000 inhabitants in 2010) (Figs. 6 and 7).

The locations, shown in Fig. 8, were chosen to record the temperature at the city centre (Casino Antiguo station, 51 m), at the Mediterranean Sea surface (marine station on the BP Oil Platform, 12 m), on the western outskirts of the city (Universitat Jaume I, UJI station, 79 m), and at the INM observatory, (Instituto Nacional de Meteorología, 42 m) which is located on the southwestern outskirts of the city, around 4 Km of the Casino Antiguo station. The four stations are located on an E-W diagonal of just 10 km on the coastal plain. The marine station records two temperatures: air and the sea surface temperature (Fig. 9).

3.2 Results of the Analysis

The meteorological records analysed here cover the

first ten years of the 21th century, from 2001 to 2010. During this period the three automatic meteorological stations (Casino Antiguo, UJI and marine station) have been constantly controlled and have functioned perfectly. Thus, though the observational period has been short, data recording and processing have been rigorous, making this a valuable experiment in regard to the process being studied.

3.2.1 Mean Annual Temperature

The mean annual temperature (Fig. 10) shows the great difference between the values of the meteorological station installed on the terrace of the Casino Antiguo in the centre of Castellón and the values at the marine station (BP Oil Platform), the university station (UJI) and the INM observatory located outside the built-up area. The mean annual temperature for the (2001-2010) period was 20.1 °C in the city centre, while it was only 17.8 °C at the sea surface air (18.9 °C, SST) and 18.1/18.2 °C on the outskirts of town (UJI and INM respectively). These values suggest that the mean temperature at the Casino station exhibits the considerable magnitude of the urbanisation effect.

3.2.2 Maximum and Minimum Temperatures

The difference between the mean annual maximum

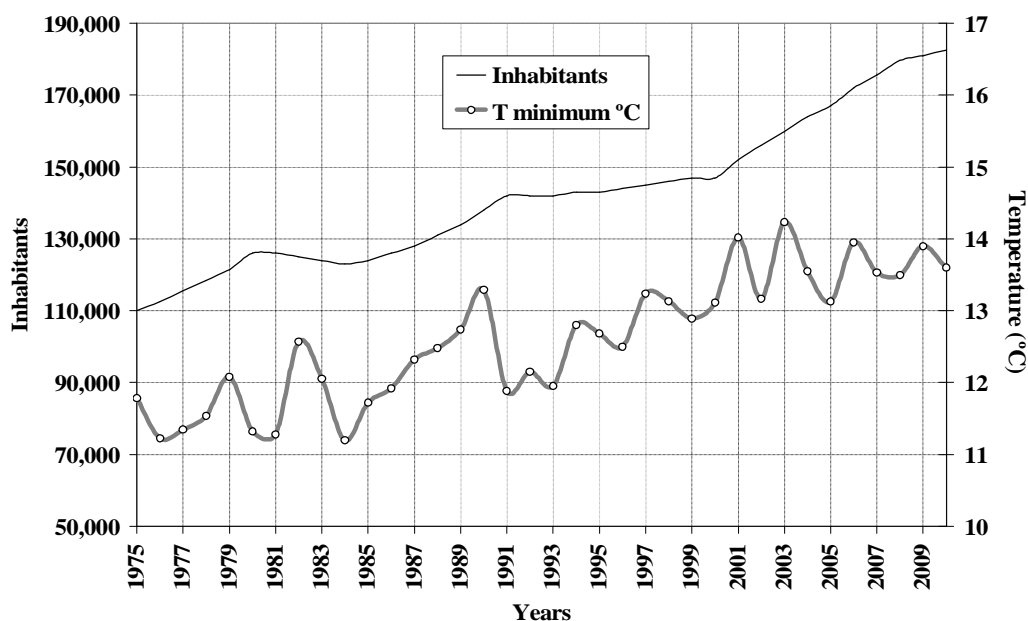


Fig. 6 Evolution of the inhabitants and the minimum temperature in the Castellón city area (1975-2010).



Fig. 7 Castellón city centre in 1950 and in 2010, with the Casino Antiguo building on the left.

temperatures is significant. Thus, a mean maximum value of 24.3 °C was recorded at the city centre, while this was 22.4 °C at the UJI station and 22.8 °C at the INM observatory. The sea temperatures presented a value of 20.8 °C, reflecting the thermal air regime in the surface waters of the sea (Fig. 11).

The behaviour of the minimum temperatures is even more significant. The annual minimum temperature

regime exhibits an even greater difference between the urban values (16.5 °C) and those recorded to the west of the city, on the university campus (13.7 °C) and 13.6 °C at the INM observatory (Fig. 12). The marine temperature (air) presented a value of 14.8 °C.

4. Conclusions

Though the records obtained in the experimental



Fig. 8 Network of stations used in this study: Casino Antiguo, marine station on the BP Oil Platform (Islet), University Jaume I station (UJI) and at the INM observatory on the western outskirts of the city.



Fig. 9 Marine station on the BP Oil Platform (Islet) in the left side of the photograph. The geographic co-ordinates are: 39°56'42''N and 00°01'36''E.

meteorological network only cover the first ten years of the 21th century, from 2001 to 2010, they allow some very interesting conclusions to be drawn regarding the effect of urban growth on temperature. The analysis performed has allowed assessment of the magnitude of this heat effect in Castellón, a city of 190,000

inhabitants. Urban heat generation has been shown in both the maximum and minimum temperatures. However, the minimum temperatures have exhibited the greatest effect. Thus, the differences between the city centre temperatures (Casino Antiguo) and those at the periphery (university campus) are quite high: 2 °C

in the maximum temperatures, and 3 °C in the minimum temperatures. Such differences entail a strong bias in the determination of the mean temperatures.

These results pose an important question. What would be the real current temperature obtained in the historical data if the urban effect was eliminated? This paper highlights the nature and significance of this

process in the Spanish Mediterranean region. The heat island effect is undeniable and of great magnitude. The notable differences in temperature between the city centre and the outskirts demonstrate the need for further analysis of the process. This should commence with a careful examination of the thermal evolution recorded at observatories far from human activity, as set out in the current regulations on atmospheric

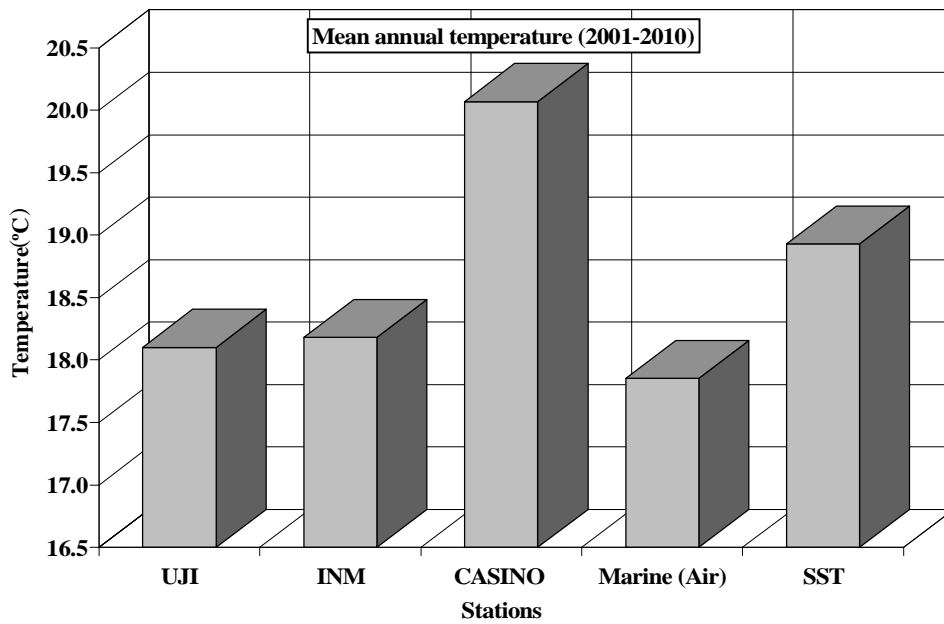


Fig. 10 Mean annual temperatures at the city centre and peripheral stations (2001-2010).

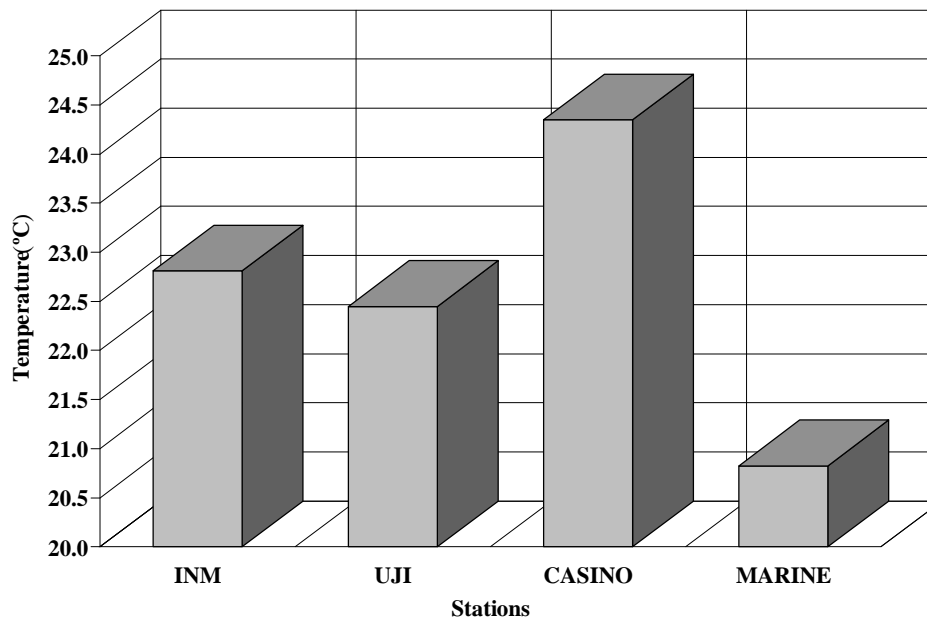


Fig. 11 Differences in the mean annual maximum temperatures between the city centre and peripheral stations.

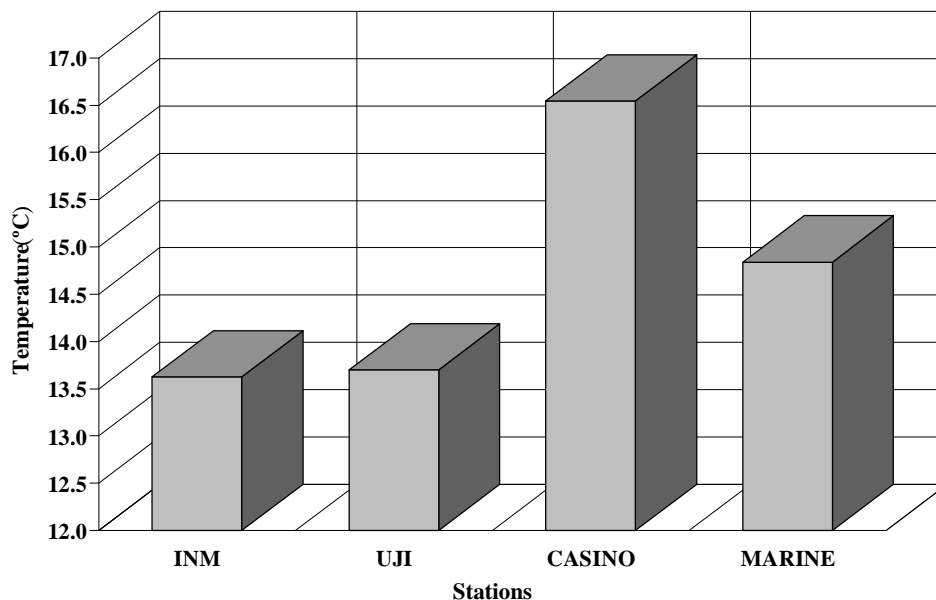


Fig. 12 Thermal differences in the minimum temperatures between the city centre and the peripheral stations.

pollution in special ecosystems.

Acknowledgments

This research was funded by BANCAJA with the research project 08I421.01.1 “Verification of the magnitude of climate change in the Mediterranean region”.

References

- [1] L. Howard, The climate of London, deduced from meteorological observations, made at different places in the neighbourhood of the metropolis, London, W. Phillips, 2 vols. 1818, p. 183. Rev.ed. 1833, Harvery and Darton, London.
- [2] R.R. McKittrick, P.J. Michaels, Quantifying the influence of anthropogenic surface processes and inhomogeneities on gridded global climate data, *J. Geophys. Res.* 112 (2007) 1-14.
- [3] J. Quereda, A. Ruescas, E. Monton, J. Escrig, B. Mollá, Detection of the urban effect over temperature trend by means of NOAA-AVHRR imagery, MeCeo, in: First Mediterranean Conference on Earth Observation, Belgrade, 2004, pp. 32-39.
- [4] IPCC Working Group I Third Assessment Report, Climate Change 2001: The Scientific Basis, available online at: <http://www.gcric.org/online.html>.
- [5] K.E. Trenberth, P.D. Jones, P. Ambenje, R. Bojariu, D. Easterling, A.K. Tank, et al., IPCC Fourth Assessment Report-Chapter 3-Observations: Surface and Atmospheric Climate Change, Intergovernmental Panel on Climate Change, 2007, available online at: <http://www.ipcc.ch/pdf/assessment-report/ar4/wg1/ar4-wg1-chapter3.pdf>.
- [6] P.D. Jones, P.Y. Groisman, M. Coughlan, N. Plummer, C. Wang, T.R. Karl, Assessment of urbanization effects in time series of surface air temperature over land, *Nature* 347 (1990) 169-172.
- [7] T.C. Peterson, Assessment of urban versus rural in situ surface temperatures in the contiguous United States: No difference found, *Journal of Climate* 16 (2003) 2941-2959.
- [8] D.E. Parker, Climate: Large-scale warming is not urban, *Nature* 432 (2004) 290.
- [9] D.E. Parker, A demonstration that large-scale warming is not urban, *Journal of Climate* 19 (2006) 2882-2891.
- [10] J.R. Mitchell, J.M. Dzerdzevskii, H. Flohn, W.L. Hoymeyr, H.H. Lamb, K.N. Rao, et al., *Climatic Change*, T. Note No.79 WMO, Ginebra, 1966, p. 78.
- [11] R. Sneyers, On the statistical analysis of the series of observations, Technical Note No. 143, World Meteorological Organization, Geneva, 1975, p. 192.
- [12] D.R. Easterling, T.C. Peterson, Techniques for detecting and adjusting for artificial discontinuities in climatological time series: A review, in: 5th International Meeting on Statistical Climatology, Toronto, June 22-26, 1992, pp. J28-J32.
- [13] Ph. Lamarque, S. Jourdain, Production of long and homogeneous climatological series for the study of the climatic evolution, *The Meteorology* 8th Series 7 (1994) 61-69.

- [14] D.R. Easterling, B. Horton, P.D. Jones, T.C. Peterson, T.C. Karl, D.E. Parker, et al., Maximum and minimum temperatures trends for the globe, *Science* 277 (1997) 364-367.
- [15] A. Moberg, H. Alexandersson, Homogenization of Swedish temperature data, Part II: Homogenized gridded air temperature compared with a subset of global gridded air temperature since 1861, *International Journal of Climatology* 17 (1997) 35-54.
- [16] G. Kukla, J. Gavin, T.R. Karl, Impact of urban heating on recent temperature trends in eastern and central North America, in: *Third Conference on Climatic Variations and Symposium on Contemporary Climate 1850-2100*, American Meteorological Society, Los Angeles, California, 1985, pp. 23-24.
- [17] D.O. Lee, Urban warming? An analysis of recent trends in London's heat island, *Weather* 47 (1992) 50-56.
- [18] J.G. Lockwood, Future trends in daytime and night-time temperatures, *Weather* 53 (1998) 72-78.
- [19] J. Quereda, E. Monton, J. Escrig, Evaluation of the climate change and of his impact on the water resources in the basin of the Júcar, Valencian Autonomous Government, 2009, p. 165.
- [20] J. Quereda Sala, A. Gil Olcina, J. Olcina Cantos, A. Rico Amorós, E. Montón Chiva, J. Escrig Barberá, Climatic warming in the Spanish Mediterranean, natural trend or urban effect, *Climatic Change* 46 (2000) 473-483.
- [21] INM (National Institute of Meteorology), *Iberian Climate Atlas (1950-2010)*, AEMET, State Agency of Meteorology, 2011.
- [22] H. Alexandersson, A. Moberg, Homogenization of Swedish temperature data, part i: Homogeneity test for linear trends, *International Journal of Climatology* 17 (1997) 25-34.
- [23] H. Alexandersson, A homogeneity test applied to precipitation data, *International Journal of Climatology* 6 (1986) 661-675.

Seasonal Effect on Atmospheric Refractivity in Diverse Terrains

Y.O. Olasoji and M.O. Kolawole

Department of Electrical & Electronics Engineering, Federal University of Technology, Akure, Nigeria

Received: November 15, 2010 / Accepted: March 7, 2011 / Published: November 20, 2011.

Abstract: Air masses in the atmosphere have contrasting temperature, humidity and moisture, which influence radio signals traversing the atmosphere. The influence of the atmosphere on refractivity is strongly determined by its temporal and spatial variability. This paper uses meteorological measurements to investigate the impact of meteorological structures on diverse environments evident in Nigeria. The study hypothesises that refractivity measures could serve as indicators of diurnal radio wave degradation traversing the atmosphere.

Key words: Radiosonde, refractivity, radio signal, hydrostatic component, Longley-Rice model.

1. Introduction

The current cost of performing radiosonde measurements limits the optimum spacing of the operational radiosonde network to 250 km in the horizontal direction [1]. From the radiosonde measurements, the air refractive index can be estimated. The changes in the refractive index of air in the troposphere determine the nature of the radio-wave propagation. Multipath effects arise due to large-scale variations in atmospheric radio refractive index, such as horizontal layers with very different refractivity [2]. This effect becomes noticeable, when the same signal takes different paths to its target and the rays arriving at different times thereby interfering with each other during propagation through the troposphere. The consequence of this large-scale variation in the atmospheric refractive index is that radiowave propagating through the atmosphere becomes progressively curved towards the earth. Thus, the range of the radiowaves is determined by the height dependence of the refractivity. Therefore, the

refractivity of the atmosphere will not only affect the curvature of the ray path but will also provide some insight into the fading of radio waves through the troposphere [3]. In the planning and design of microwave communication links, the structure of the radio refractive index in the lower part of the atmospheric boundary layer is very important.

The refractive property of the neutral atmosphere is related to pressure, temperature and water vapour partial pressure. Troposphere—the lowest part of the atmosphere that extends from the earth surface up to about 10 km—is a non-dispersive medium and its refraction effect estimation is possible only by modelling the tropospheric medium. The atmospheric parameters like pressure, temperature and water vapour undergo variations based on the geographical locations and seasons. The first step is to estimate the refractivity of the atmosphere. The refractive index of the neutral atmosphere is related to atmospheric parameters as [4, 5]:

$$N = k_1 \frac{P}{T} + k_2 \frac{e}{T} + k_3 \frac{e}{T^2} \quad (1)$$

where N is termed as refractivity, T is temperature (K), e is the water vapour (hPa) and P is the hydrostatic atmospheric pressure (in hPa). The constants k_1 , k_2

Corresponding author: Y.O. Olasoji, Ph.D., research fields: atmospheric science, telecommunication engineering. E-mail: yoolasoji@yahoo.com or yoolasoji@futa.edu.ng.

and k_3 have values 77.6848, 71.2952 and 375463 respectively [6]. These are found to be valid for the estimation of N for frequency up to 30 GHz and for normally encountered ranges of pressure, temperature and humidity. The tropospheric refractivity given by Eq. (1) consists of two parts [7]: the hydrostatic component or dry component (N_D)—represented by $\left\{N_D = k_1 \frac{P}{T}\right\}$, and the other non-hydrostatic component or wet component (N_w)—represented by $\left(N_w = k_2 \frac{e}{T} + k_3 \frac{e}{T^2}\right)$.

The dry gases in the troposphere like N_2 , O_2 , etc., contribute for hydrostatic component while water vapour causes primarily the wet component [8]. The water vapour is mostly confined to lower part of troposphere and shows significant temporal and spatial variability, while the variability of P and T is well defined. For the latitude of Nigeria, the water vapour pressure e is derived from the relative humidity H [%] using the expression [9]

$$e = 0.061121H \exp\left\{\frac{17.502t}{t + 240.97}\right\} \quad (2)$$

where, t corresponds to temperature in degree Celsius ($^{\circ}\text{C}$). A look at related expression that considers use of the dew point temperature, T_d ($^{\circ}\text{C}$) expressed by [10]

$$e = 6.1078 \times 10^{\frac{7.5T_d}{237.3+T_d}} \quad (3)$$

excludes the relative humidity. Dew point and relative humidity are related. Eqs. (2) and (3) have application in different climatic conditions: Eq. (2) in the humid tropics, while Eq. (3) in temperate region. The difference between the two expressions is small: mean of 0.072 and standard deviation of 0.136 for 99.93% humidity for a measureable temperature of up to 60°C .

These tropospheric factors—such as variations of radio refractive index and its “normal” change with height—enable radiowave propagation over a greater than line-of-sight range. This effect was taken into approximate account by assuming an increased radius for the Earth, e.g. by a factor of $4/3$ as in

Longley-Rice model [11]. The Longley-Rice model is simple calculation, which uses the horizontal difference, but neglects the vertical section information, therefore may not be accurate [12]. A modified refractivity M that accounts for the curvature of the earth is thus defined as

$$M = N + \frac{z}{r_g} \quad (4)$$

therefore improving the Longley-Rice model; where z is altitude (km) and r_g is the geometric radius due to the elliptical nature of the Earth’s orbit (in km). The geometric radius r_g depends on the latitude/longitude of the region under consideration, specifically at any particular longitude, as [13]

$$r_g \approx r_e \left(0.99832 + 0.001684 \cos 2\theta_{lat} - 0.000004 \cos 4\theta_{lat} \dots\right) \quad (5)$$

Where, r_e is the radius of the earth at the equator (in km) and θ_{Lat} is the location latitude in degree.

In view of Eq. (5) in Eq. (4), the effect of modified refractivity M characterizes propagation conditions factoring the curvature of the ray path along the Earth’s surface.

When characterizing the radio propagation environment, it is natural to consider the refractivity gradient of the atmosphere [14]. The dependence of refractivity on the physical structure of the atmosphere implies that changing meteorological conditions can lead to changes in radio wave propagation [15]. This paper uses meteorological measurements to investigate the variability of these meteorological structures on different terrain, from which radio-wave propagation loss profile may be inferred.

2. Methods

There is a wide range of variations in the climate of Nigeria—a country between Longitude 3.80°E , Latitude 03.94°N and Longitude 13.80°E , Latitude 13.94°N . The climate ranges from the typical thick evergreen rain forest to Sahel savannah type peculiar to the tropics. Hence the modeling of selected cities cut across those range within the tropic. In order to model, the meteorological data for different locations

were collected over a period of six years. The selected locations are Abuja (07.00°E, 09.25°N), Jos (08.85°E, 9.63°N) and Maiduguri (13.08°E, 11.85°N). Radiosonde data were collected, and obtained between years 2000 and 2005 from the Nigerian Meteorological Organisation for a given location and time, which were used to determine the corresponding refractivity profile for these cities. The study areas are within the 250 km-axis recommended by WMO-ITU (2009) for operational radiosonde network for successful extrapolation and interpretation for radio communication operations. The radiosonde data were analysed for these towns to observe the seasonal effects on atmospheric refractivity. There are three primary seasons in Nigeria namely: harmattan season, dry season and raining or wet season, whose peaks approximate to month of December, March and August respectively. The seasons could strictly speaking be classified as dry and raining given that the harmattan season can be refreshingly cold in the early part of the morning but hot during the day, blowing dusty dry wind south from Sahara and picking up fine dust particles, nominally between 0.5 and 10 μm . The effect of the fine dust particles on the radio waves can be telling, hence the inclusion of the harmattan season in the study.

3. Results and Discussion

Daily representative graphs of the three major seasons in Nigeria are shown in Figs. 1-3. The close study of all the Figs. 1-3 obtained from the calculated modified refractivity M values showed that within the period of 12:00 and 16:00 hours, there is depression in the responses, an indication of the effect of temperature showing that a considerable amount of hydrostatic particulates suspended in the atmosphere. This demonstrates that any changes in meteorological conditions—substantiated with expressions in Eq. (4)—can lead to changes in radio wave propagation.

In Fig. 1, the evergreen terrain, refractivity decreases as temperature picks up with most depression occurring at peak temperature parts of the day and increases as the temperature cools down. The refractivity values remain relatively constant during the dry and harmattan seasons within the range, i.e., as in Table 1, 327.7 and 333.63 and standard deviation of 8.0 and 9.0.

In Fig. 2, the semi-temperate terrain of Jos appears to have crossover refractivity as the day breaks. The dry period appears to still have suspended water particles that affect refractivity. Jos environ is relatively cooler region with occasional flaky ice at

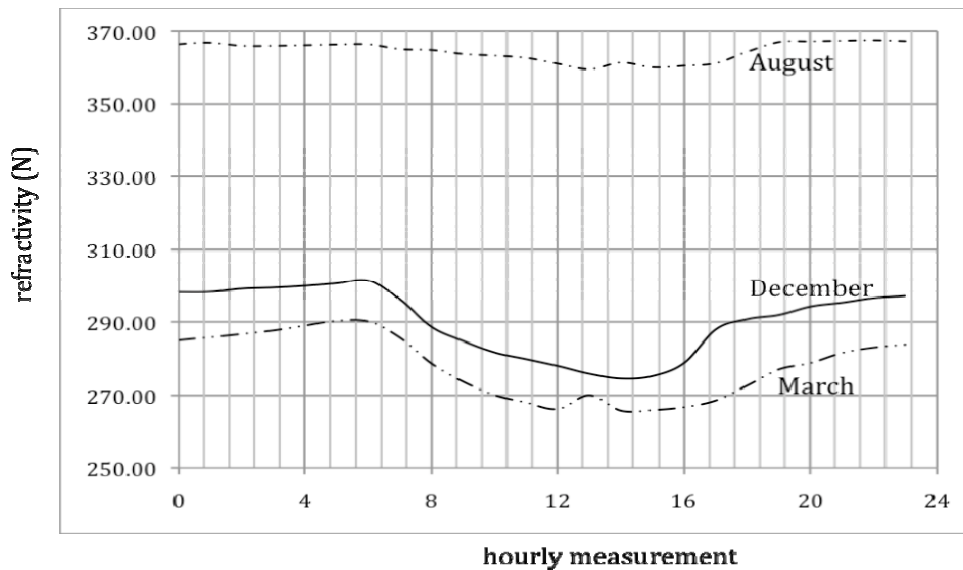


Fig. 1 Representative seasonal-hourly refractivity for Abuja, Nigeria.

Seasonal Effect on Atmospheric Refractivity in Diverse Terrains

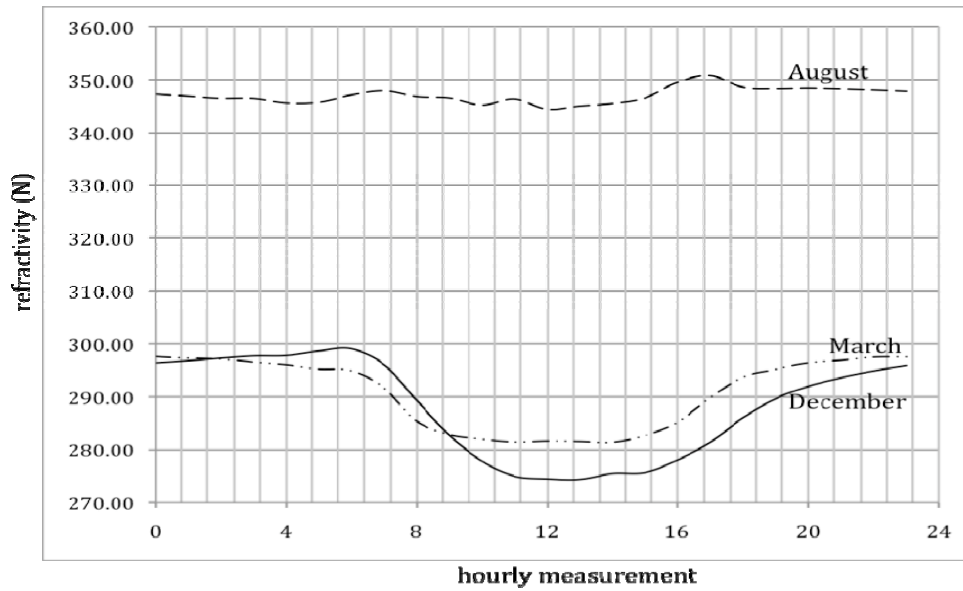


Fig. 2 Representative seasonal-hourly refractivity for Jos, Nigeria.

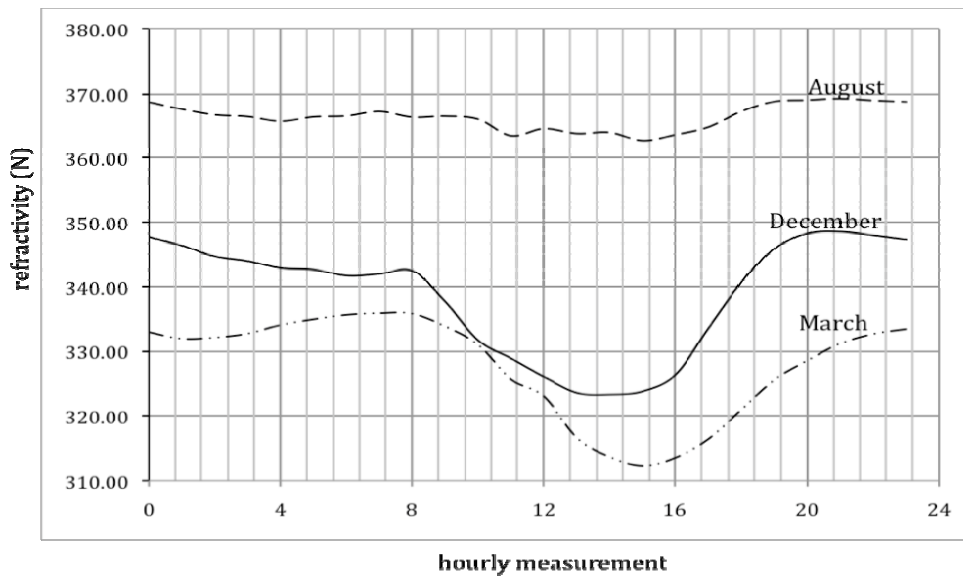


Fig. 3 Representative seasonal-hourly refractivity for Maiduguri, Nigeria.

night. The refractivity values remain relatively constant during the dry and harmattan seasons within the narrow range, i.e., as in Table 1, 288.08 and 290.62 and standard deviation of 8.0 and 9.34.

In Fig. 3, the Sahel terrain, and close to desert environment, instead of the refractivity increases as in Abuja and Jos environs, the refractivity increases during harmattan period. This is attributed to the encroachment of the desert sands, which tend to maintain relatively high temperature except during the raining period. The fluctuation in refractivity profiles

of the evergreen and Sahel environments is similar, about 11.93 ± 1.0 and 12.2 ± 0.53 respectively.

Table 1 Statistical variations of mean seasonal modified refractivity, <M>, and standard deviation, σ , for Nigerian terrain.

Seasons	Parameters	Evergreen	Semi-temperate	Sahel
Harmattan	<M>	333.63	290.62	290.12
	σ	9.00	6.68	9.26
Dry	<M>	327.7	288.08	277.92
	σ	8.00	9.34	8.73
Raining	<M>	368.8	347.07	364.51
	σ	1.94	1.51	2.54

Regardless of the seasons and terrain considered, the refractivity is at the highest in the raining period, averaging between 347.07 and 368.8 and standard deviation of 1.51 and 2.54. The high values of refractivity can be attributed to dampened particulates. Consequently, more radio signals penetrate the atmosphere with lesser attenuation than the dry seasons when the atmosphere is precipitated with dry hydrostatic particulates. This study thus suggests that refractivity values could be used as a measure of diurnal radio wave degradation traversing the atmosphere. This inference is the subject of another paper that is being empirically analyzed.

4. Conclusions

The influence of the atmosphere on refractivity is strongly determined by its temporal and spatial variability. This implies that changing atmospheric conditions can lead to changes in radio wave propagation. The study suggests that similar trends as refractivity could serve as expected fluctuation in propagation signal losses traversing the atmosphere. We are currently pursuing this objective with signal strength measurements and the results will be reported in the next paper.

References

- [1] World Meteorological Organisation-International Telecommunication Union, Use of Radio Spectrum for Meteorology: Weather, Water and Climate Monitoring and Prediction, Radiocommunication Bureau, Geneva, 2009.
- [2] M. Grabner, V. Kvicera, Clear-air propagation modelling using parabolic equation method, *Radio Engineering* 12 (2003) 50-54.
- [3] T.O. Adediji, M.O. Ajewole, Vertical profile of radio refractivity gradient in Akure south-west Nigeria, *Progress in Electromagnetics Research C* 4 (2008) 157-168.
- [4] G.D. Thayer, An improved equation for the radio refractive index of air, *Radio Science* 9 (1974) 803-807.
- [5] H.J. Liebe, G.G. Gimmestad, J.D. Hopponen, Atmospheric oxygen microwave spectrum-experiment versus theory, *IEEE Transactions on Antennas and Propagation* 25 (1977) 327-335.
- [6] J.M. Rüeiger, Refractive index formulae for electronic distance measurement with radio and millimetre waves, Unisurv Report S-68, School of Surveying and Spatial Information Systems, University of New South Wales, Sydney, Australia, 2002, pp. 1-52.
- [7] J. Saastamoinen, Atmospheric correction for the troposphere and stratosphere in radio ranging of satellites, in: *The Use of Artificial Satellites for Geodesy*, American Geophysical Union, 1972, pp. 247-251.
- [8] J.L. Davis, T.A. Herring, I.I. Sharipo, A.E.E. Rogers, G. Elgered, Geodesy by radio interferometry: Effects of atmospheric modelling errors on estimates of baseline length, *Radio Science* 20 (1985) 1593-1607.
- [9] T.O. Adediji, M.O. Ajewole, S.E. Falodun, O.R. Oladosu, Radio refractivity measurement of 150 m altitude on TV tower in Akure, south-west Nigeria, *Journal of Engineering and Applied Sciences* 2 (2007) 1308-1313.
- [10] J.A. Hermann, A.S. Kulesa, C. Lucas, R.A. Vincent, J.M. Hacker, C.M. Ewenz, Impact of elevated atmospheric structures upon radio-refractivity and propagation, in: *Proceedings of the Workshop on the Applications of Radio Science*, 2002, pp. 20-22.
- [11] A.G. Longley, P.L. Rice, Prediction of tropospheric radio transmission loss over irregular terrain: A computer method, U.S. Government Printing Office, Washington, DC, July, 1968.
- [12] W. Zullang, Z. Mao, W. Juan, Z. Linhua, Improved algorithm of atmospheric refraction error in Longley-Rice channel model, *Journal of Systems Engineering and Electronics* 19 (2008) 683-687.
- [13] M.O. Kolawole, *Remote Sensing for Spatial Scientists and Practitioners*, Springer-Verlag, Berlin, 2011, p. 27.
- [14] J. Bech, B. Codina, J. Lorente, D. Bebbington, The sensitivity of single polarization weather radar beam blockage correction to variability in the vertical refractivity gradient, *Journal of Atmospheric and Oceanic Technology* 20 (2003) 845-855.
- [15] Y.O. Olasoji, Propagation loss model of UHF radio signal in multilayer and anisotropic environment, Ph.D. Thesis, University of Technology Akure Nigeria, 2011.

Review Article of Landscape Metrics Based on Remote Sensing Data

A.F. Petrosyan and V. Karathanassi

Laboratory of Remote Sensing, School of Rural and Surveying Engineering, National Technical University of Athens, Athens 15780, Greece

Received: February 19, 2011 / Accepted: May 19, 2011 / Published: November 20, 2011

Abstract: This article describes metrics in order to quantify landscape structure. Landscape metrics are offered and designed to be as versatile as possible using several programs. In this paper it is attempted to (a) collect all the metrics found in the literature, (b) classify them, and (c) evaluate them through their use. An extensive investigation of the literature has been performed. Small discussion of each metric is provided to its concept, definition, use, way of calculation and in some cases contribution to the sustainable development. The frequency of used papers per each index has been taken into account. The most used to the least used six metrics have the following order: Area/Density/Edge; Isolation Proximity; Diversity; Contagion Interspersion; Shape; Connectivity. Moreover, the frequency of used papers is divided into five groups, i.e. group A till group E. Concluding, it has been provided an explanation of the results regarding to the four indices of group A and two indices from the group B.

Key words: Landscape, ecology, structure, metrics, class, indices.

1. Introduction

Indicators are investigative and interpretive tools of ecological dynamics [1]. In this sense, landscape ecology is very useful to define indicators even though it is not the only scientific field where they can be used successfully. Landscape ecology often uses not only “structural” indicators [2-8] which are connected with the various components of the areas being studied and with how they have become organized (e.g. the size of the patches, which reveals a series of features linked to it), but also “functional” [9-11] indicators.

Identifying ecological indicators is an important element in illustrating an ecological system, instituting latent metrics of change, and constructing an effective environmental monitoring system [12]. The suite of indicators signify the range of ecological conditions in

the ecological system, serve as signals of environmental change, and is simple enough to permit cost-effective monitoring and modelling [13-17]. Landscape pattern, environmental change, and fragmentation are central points of landscape ecology as they have an important role in driving ecological processes [18-20].

Landscape metrics that comprise quantifiable measures of landscape indicators have been expanded to detain important aspects of landscape pattern in a few numbers [21-23]. These numbers can often be correlated with land-use change and ecological processes. By using such metrics to observe and measure landscape patterns through time, researchers may determine the long-term impacts of previous land use [24-25]. Landscape metrics can capture changes in pattern, be executed along a variety of spatial scales, and be useful indicators of land-cover changes due to prior land use and management. Remote sensing data significantly contributed to the estimation of the landscape metrics.

Corresponding author: A.F. Petrosyan, Ph.D. student at NTUA, main research fields: landscape ecology, evaluation of biodiversity, environmental economics, sustainable development, remote sensing and GIS. E-mail: mariamarita2002@yahoo.com.

In the literature, a large number of landscape metrics have been used to monitor environmental quality at regional scales [26]; to measure and monitor landscape change [27]; to examine habitat fragmentation [28, 29]; to quantify ecological processes [30-33]; to study the effects of society on landscape [34, 35] and to aid in landscape design [36]. Moreover, recent studies have demonstrated that land use and landscape changes have significantly affected biodiversity [37, 38].

2. Methods

In this paper, an extensive investigation of the literature has been performed in order to (a) collect all the landscape metrics based on remote sensing data, that are found in the literature, (b) classify them, and (c) evaluate them through their use. Their classification resulted in six main groups:

- Area/Density/Edge, which is classified into 10 subcategories and uses 22 papers;
- Shape, which is classified into 13 subcategories and uses 17 papers;
- Isolation Proximity, which is classified into 2 subcategories and uses 15 papers;
- Connectivity, which is classified into 2 subcategories and uses 5 papers;
- Contagion Interspersion, which is classified into 8 subcategories and uses 12 papers;
- Diversity, which is classified into 9 subcategories and uses 20 papers.

In section 3, each group is further classified to subcategories with a brief description, some definition and/or some metrics' relations to sustainable development. Each subcategory represents an index of Class or/and Landscape Metrics. A table with chosen authors, correspondingly utilized remote sensing data and programs is given to each index. Generally, 32 papers were used to be referenced for each index during constructions of tables. In addition, all types of remote sensing data, i.e., very high, high, medium resolution, aero-photographs and even simulated data, are considered accordingly per author's work.

Categorization of metrics and indices was initially established by the Fragstat program and then adopted by other remote sensing programs.

3. Landscape Metrics

3.1 Area/Density/Edge

3.1.1 Class Area (CA)–Class Metrics; Total Area–Landscape Metrics

Class area (CA) is a measure of landscape composition; specially, how much of the landscape is comprised of a particular patch type. Class area is a sum of areas of all patches belonging to a given class, in map units [39]. Total landscape area (TA) often does not have a great deal of interpretive value for evaluating landscape structure, but it is important because it defines the extent of the landscape [40].

Papers	Data	Program
[39]	IKONOS images	ArcGIS 9.0; Fragstat
[41]	Landsat 7 ETM + and 5 TM; VHR RS images; HRSC; soil map; IKONOS	Tool extension (V-LATE) calculated within ArcGIS 8.x [42]
[43]	Aerial photographs	ArcViewTM (ESRI)
[44]	Simulated data	3Q programme
[45]	Topographic maps; Aerial photographs	GIS
[46]	Landsat TM; AVHRR; MODIS; TIGER DLG	GIS
[47]	Aerial photographs	GIS; Fragstat
[48]	Landsat TM	ArcView 3.2; Fragstat [40]

3.1.2 Percentage of Land (CPLAND)-Class Metrics

Percentage of land is a measure that computes the percentage of landscape (%LAND) occupied by each patch type [40]. Percentage of land is the proportion of each land use in the study area, which represents the landscape composition [49]. Percentage of land is the percentage of area occupied by certain land cover class [50]. Percentage of landscape quantifies the proportional abundance of each patch type in the

landscape [51]. If one class dominates completely the landscape then it will provide little support for multi-habitat species [52]. At its lowest limit, there is only one land-use type and landscape lacks diversity. The arrangement of coarse/fine-grained areas within the landscape is doubtless key factor to achieve a sustainable environment [19].

Papers	Data	Program
[39]	IKONOS images	ArcGIS 9.0; Fragstat
[46]	Landsat TM; AVHRR; MODIS; TIGER DLG	GIS
[49]	Aerial photographs	GIS; Fragstat version 3.1
[50]	IKONOS	Fragstat version 3.3.
[51]	Data are derived from land-use map sheets	ArcGIS; Fragstat version 3.3 [53]
[54]	Aerial photography	Fragstat version 3.2
[55]	CORINE, Landsat MSS & TM, IRS-IC data, aerial photo; land & soil maps	ERDAS Imagine; Fragstat

3.1.3 Number of Patches (NP)—Class Metrics, Landscape Metrics

Number of patches (NP) of a particular habitat type may affect a variety of ecological processes, depending on the landscape context; for example, the number of patches may determine the number of subpopulations in a spatially dispersed population, or metapopulation, for species exclusively associated with that habitat type. The number of subpopulations could influence the dynamics and persistence of the metapopulation [56]. Number of patches equals the number of patches of the corresponding patch type [51]. If mean patch size is small and number of patches is high it can indicate a fragmented landscape [52].

Papers	Data	Program
[1]	Regional technical map	GIS
[39]	IKONOS images	ArcGIS 9.0; Fragstat
[41]	Landsat 7 ETM+ and 5 TM; VHR RS images; HRSC; soil map; IKONOS	Tool extension (V-LATE) calculated within ArcGIS 8.x

Papers	Data	Program
[43]	Aerial photographs	ArcViewTM (ESRI)
[44]	Simulated data	3Q programme
[45]	Topographic maps; Aerial photographs	GIS
[51]	Data are derived from land-use map	ArcGIS; Fragstat version 3.3
[57]	Landsat TM and ETM	MiraMon Software; Fragstat
[12]	Landsat ETM and MSS images	Imagine; ArcView; Fragstat; ATtILA [58]
[59]	Raster data layers	ARCGIS; Fragstat
[60]	Landsat MSS; TM and ETM+	ERDAS Imagine 8.7; ARCGIS 9.0 (ESRI); Fragstat

3.1.4 Patch Density (PD)—Class Metrics, Landscape Metrics

Patch density is the number of patches per 100 ha [49]. Patch density is the number of patches per unit area [61]. Patch density equals the number of patches of the corresponding patch type divided by total [51]. Patch density is the number of patches per area [50].

Papers	Data	Program
[1]	Regional technical map	GIS
[18]	Digitized from true color orthophoto	ArcGIS 8.1 (ESRI); Fragstat
[39]	IKONOS images	ArcGIS 9.0; Fragstat
[47]	Aerial photographs	GIS; Fragstat
[48]	Landsat TM	ArcView 3.2; Fragstat
[49]	Aerial photographs	GIS; Fragstat version 3.1
[50]	IKONOS	Fragstat version 3.3.
[51]	Data are derived from land-use map	ArcGIS; Fragstat version 3.3
[54]	Aerial photography	Fragstat version 3.2
[55]	CORINE, Landsat MSS & TM, IRS-IC data, aerial photo; land & soil maps	ERDAS Imagine; Fragstat

Papers	Data	Program
[57]	Landsat TM and ETM	MiraMon Software; Fragstat
[61]	Land use data is derived from Map	Idrisi Kilimanjaro; Fragstat
[62]	Soil data is derived from the Estonian Soil Map (1: 10,000)	Idrisi Kilimanjaro [63]; Fragstat version 3.3

3.1.5 Largest Patch Index (LPI)–Class Metrics, Landscape Metrics

A largest patch index (LPI) is computed at the class and landscape levels that quantifies the percentage of total landscape area comprised by the largest patch [40]. Indicators for change in landscape structure caused by urbanization provided information about specific aspects of landscape structure and thus were helpful to “guide” process of urbanization towards sustainability [64, 65]. Largest patch index is the percentage of total area occupied by the largest patch [50].

Papers	Data	Program
[12]	Landsat ETM and MSS images	Imagine TM; ArcView TM; Fragstat; ATtILA
[18]	Digitised from true color orthophoto	ArcGIS 8.1 (ESRI); Fragstat
[39]	IKONOS images	ArcGIS 9.0; Fragstat
[47]	Aerial photographs	GIS; Fragstat
[50]	IKONOS	Fragstat version 3.3.
[51]	Data are derived from land-use map	ArcGIS; Fragstat version 3.3
[54]	Aerial photography	Fragstat version 3.2
[57]	Landsat TM and ETM	MiraMon Software; Fragstat
[60]	Landsat MSS; TM and ETM+	ERDAS; ARCGIS; Fragstat

3.1.6 Landscape Shape Index (LSI) and Normalized Landscape Index (NLSI)–Class Metrics, Landscape Metrics

Landscape shape index measures the perimeter-to-area ratio for the landscape as a whole. This index is identical to the habitat diversity index

proposed by [66]. Landscape shape index is ratio of the total edge to the minimum total edge. Normalized landscape shape index is ratio of the total edge to the minimum total edge per class, rescaled according the proportion of the classes [50].

Papers	Data	Program
[18]	Digitized from true color orthophoto	ArcGIS 8.1 (ESRI); Fragstat
[48]	Landsat TM	ArcView 3.2; Fragstat
[50]	IKONOS	Fragstat version 3.3
[54]	Aerial photography	Fragstat version 3.2
[67]	Cartographic data; Landsat 5 TM & 7 ETM; Digital vegetation photographs	GIS; Fragstat version 3.3

3.1.7 Total Edge (TE)–Class Metrics, Landscape Metrics

Total edge (TE) is an absolute measure of total edge length of a particular patch type (class level) or of all patch types (landscape level). In applications involving comparisons of landscapes of different sizes, this index may not be useful [40].

Papers	Data	Program
[12]	Landsat ETM and MSS images	Imagine TM; ArcView TM; Fragstat; ATtILA
[57]	Landsat TM and ETM	MiraMon Software; Fragstat
[59]	Raster data layers	ARCGIS; Fragstat

3.1.8 Edge Density (ED)–Class Metrics, Landscape Metrics

Edge density is the total length of patch edge per ha [49]. Edge density is total length of edge per unit area [50]. Edge density is the total length of all edge segments per ha for the landscape of consideration [61].

Papers	Data	Program
[1]	Regional technical map	GIS
[18]	Digitized from true color orthophoto	ArcGIS 8.1 (ESRI); Fragstat

Papers	Data	Program
[48]	Landsat TM	ArcView 3.2; Fragstat
[49]	Aerial photographs	GIS; Fragstat version 3.1
[50]	IKONOS	Fragstat version 3.3
[54]	Aerial photography	Fragstat version 3.2
[57]	Landsat TM and ETM	MiraMon Software; Fragstat
[61]	Land use data is derived from Map	Idrisi Kilimanjaro; Fragstat
[62]	Soil data is derived from Soil Map	Idrisi Kilimanjaro; Fragstat

3.1.9 Patch Area Distribution (AREA_X)–Class Metrics, Landscape Metrics

Mean (AREA_MN): Patch area is the area of a patch [49]. Patch area is size of the patches [50]. Patch area mean equals to the sum, across all patches of the corresponding patch type, of the corresponding patch metric values, divided by the number of patches of the same type [40].

Weighted Mean (AREA_AM)–Class Metrics; Landscape Metrics: Patch area-weighted mean equals the sum, across all patches of the corresponding patch type, of the corresponding patch metric value multiplied by the proportional abundance of the patch [40].

Coefficient of Variation (AREA_CV)–Class Metrics, Landscape Metrics: Patch area coefficient of variation equals the standard deviation divided by the mean, multiplied by 100 to convert to a percentage, for the corresponding patch metric [40].

Papers	Data	Program
[12]	Landsat ETM and MSS images	Imagine TM; ArcView TM; Fragstat; ATtILA
[18]	Digitized from true color orthophoto	ArcGIS 8.1 (ESRI); Fragstat
[49]	Aerial photographs	GIS; Fragstat version 3.1

Papers	Data	Program
[50]	IKONOS	Fragstat version 3.3.
[54]	Aerial photography	Fragstat version 3.2
[59]	Raster data layers	ARCGIS; Fragstat
[62]	Soil data is derived from Soil Map	Idrisi Kilimanjaro; Fragstat

3.1.10 Radius of Gyration (GYRATE_X)–Class Metrics, Landscape Metrics

Mean (GYRATE_MN); Weighted Mean (GYRATE_AM); Coefficient of Variation (GYRATE_CV): GYRATE equals the mean distance (m) between each cell in the patch and the patch centroid [50]. Radius of gyration is a measure of patch extent; thus it is affected by both patch size and patch compaction [40].

Papers	Data	Program
[18]	Digitized from true color orthophoto	ArcGIS 8.1 (ESRI); Fragstat
[50]	IKONOS	Fragstat version 3.3
[54]	Aerial photography	Fragstat version 3.2

3.2 Shape

3.2.1 Perimeter Area Fractal Dimension (PARFAC)–Class Metrics, Landscape Metrics

Perimeter area fractal dimension patch is shape complexity measure, which approaches 1 for shapes with simple perimeters and 2 for complex shapes.

Papers	Data	Program
[50]	IKONOS	Fragstat version 3.3

3.2.2 Perimeter Area Ratio Distribution (PARA_X)–Class Metrics, Landscape Metrics

Mean (PARA_MN); Weighted Mean (PARA_AM); Coefficient of Variation (PARA_CV): Perimeter area ratio is patch shape complexity measure that measures perimeter per area [50]. “Heterogeneity per se appears useful to planning a sustainable environment, but more important is the actual arrangement of patches and corridors”. “Geometry patterns are indicators of human disturbance (roads, urban areas)” [19].

Papers	Data	Program
[12]	Landsat ETM and MSS images	Imagine TM; ArcView TM; Fragstat; ATtILA
[18]	Digitized from true color orthophoto	ArcGIS 8.1 (ESRI); Fragstat
[50]	IKONOS	Fragstat version 3.3
[51]	Data are derived from land-use map	ArcGIS; Fragstat version 3.3
[54]	Aerial photography	Fragstat version 3.2

3.2.3 Shape Index Distribution (SHAPE_X)–Class Metrics, Landscape Metrics

Shape index equals 1 when all patches are circular; increases with complexity of patch shapes; independent of patch size [50]. Shape index is the patch complexity of the focal class, where shape is defined by perimeter–area relationships [54]. SI_i is the patch shape index for patch i , P_i the perimeter of the patch, a_i the area of the patch i . It assumes that the patch shape index = 1 when the patch is circular, and increases without limit as patch shape becomes more irregular [45].

Mean (SHAPE_MN): Mean patch shape complexity equals 1 when all patches are square and increases without limit as patch shape becomes more irregular. It is the simplest and most straightforward measure of overall shape [49].

A patch-level shape index (1) averaged over all patches in landscape:

$$SHAPE_MN = \frac{\sum_{i=1}^m \sum_{j=1}^n \left(\frac{P_{ij}}{\sqrt{\pi a_{ij}}} \right)}{N} \quad (1)$$

where P_{ij} is the perimeter and a_{ij} is the area of patch ij , and N is the total number of patches in the landscape (unitless) [61].

Weighted Mean (SHAPE_AM);

Coefficient of Variation (SHAPE_CV)

Papers	Data	Program
[18]	Digitized from true color orthophoto	ArcGIS 8.1 (ESRI); Fragstat
[39]	IKONOS images	ArcGIS 9.0; Fragstat

Papers	Data	Program
[45]	Topographic maps; Aerial photographs	GIS
[47]	Aerial photographs	GIS; Fragstat
[49]	Aerial photographs	GIS; Fragstat version 3.1
[50]	IKONOS	Fragstat version 3.3.
[54]	Aerial photography	Fragstat version 3.2
[55]	CORINE, Landsat MSS & TM, IRS-IC data, aerial photo; land & soil maps	ERDAS Imagine; Fragstat
[61]	Land use data is derived from map	Idrisi Kilimanjaro; Fragstat
[62]	Soil data is derived from Soil Map	Idrisi Kilimanjaro; Fragstat
[68]	Images of COFUNE landcover	Created program of ENVIIDL

3.2.4 Fractal Dimension Index Distribution (FRAC_X)–Class Metrics, Landscape Metrics

Fractal dimension is patch shape complexity measure that approaches 1 for simple shapes and 2 for complex shapes [50]. Indicators for change in landscape structure caused by urbanization provided information about specific aspects of landscape structure and thus were helpful to “guide” process of urbanization towards sustainability [64, 65].

Mean (FRAC_MN);

Weighted Mean (FRAC_AM);

Coefficient of Variation (FRAC_CV)

Papers	Data	Program
[54]	Aerial photography	Fragstat version 3.2
[69]	RS and map data	GIS
[67]	Cartographic data; Landsat 5 TM & 7 ETM; Digital vegetation photographs	GIS; Fragstat version 3.3
[51]	Data are derived from land-use map	ArcGIS; Fragstat version 3.3
[50]	IKONOS	Fragstat version 3.3

3.2.5 Related Circumscribing Circle Distribution (CIRCLE_X)–Class Metrics, Landscape Metrics

Related circumscribing circle is patch elongation measure; which is equal to 1 minus patch area divided by the area of the smallest circumscribing circle [50].

- Mean (CIRCLE_MN);
- Weighted Mean (CIRCLE_AM);
- Coefficient of Variation (CIRCLE_CV)

Papers	Data	Program
[18]	Digitized from true color orthophoto	ArcGIS 8.1 (ESRI); Fragstat
[50]	IKONOS	Fragstat version 3.3

3.2.6 Contiguity Index Distribution (CONTIG_X)–Class Metrics, Landscape Metrics

Contiguity index equals 0 for a one-pixel patch and approaches 1 as patch contiguity, or connectedness increases [50].

- Mean (CIRCLE_MN);
- Weighted Mean (CIRCLE_AM);
- Coefficient of Variation (CIRCLE_CV)

Papers	Data	Program
[18]	Digitized from true color orthophoto	ArcGIS 8.1 (ESRI); Fragstat
[50]	IKONOS	Fragstat version 3.3

3.2.7 Total Core Area (TCA)–Class Metrics, Landscape Metrics

TCA equals the sum of the core areas of each patch (m²) of the corresponding patch type, divided by 10,000 (to convert to hectares) [40].

Papers	Data	Program
[41]	Landsat 7 ETM+ and 5 TM; VHR RS images; HRSC; soil map; IKONOS	Tool extension (V-LATE) calculated within ArcGIS 8.x
[46]	Landsat TM; AVHRR; MODIS; TIGER DLG	GIS

3.2.8 Number of Disjunct Core Areas (NDCA)–Class Metrics, Landscape Metrics

Number of disjunct core areas equals the sum of the number of disjunct core areas contained within each patch of the corresponding patch type; that is, the number of disjunct core areas contained within the landscape [40].

Papers	Data	Program
[41]	Landsat 7 ETM+ and 5 TM; VHR RS images; HRSC; soil map; IKONOS	Tool extension (V-LATE) calculated within ArcGIS 8.x

3.2.9 Disjunct Core Area Density (DCAD)–Class Metrics, Landscape Metrics

DCAD equals the sum of number of disjunct core areas contained within each patch of the corresponding patch type, divided by total landscape area (m²), multiplied by 10,000 and 100 (to convert to 100 hectares) [40].

Papers	Data	Program
[54]	Aerial photography	Fragstat version 3.2

3.2.10 Core Area Distribution (CORE_X)–Class Metrics, Landscape Metrics

Core area is defined as the area within a patch beyond some specified edge distance or buffer width. Core area metrics reflect both landscape composition and landscape configuration [40].

- Mean (CORE_MN);
- Weighted Mean (CORE_AM);
- Coefficient of Variation (CORE_CV)

Papers	Data	Program
[54]	Aerial photography	Fragstat version 3.2

3.2.11 Disjunct Core Area (DCORE_X)–Class Metrics, Landscape Metrics

- Mean (DCORE_MN);
- Weighted Mean (DCORE_AM);
- Coefficient of Variation (DCORE_CV).

Papers	Data	Program
[54]	Aerial photography	Fragstat version 3.2

3.2.12 Core Area Index (CAI_X)–Class Metrics, Landscape Metrics

CAI equals the patch core area (m²) divided by total patch area (m²), multiplied by 100 (to convert to a percentage); in other words, CAI equals the percentage of a patch that is core area [40].

Mean (CAI_MN);

Weighted Mean (CAI_AM);

Coefficient of Variation (CAI_CV).

Papers	Data	Program
[54]	Aerial photography	Fragstat version 3.2

3.2.13 Core Area Percent of Land (PLAND)–Class Metrics, Landscape Metrics

PLAND equals the sum of the areas (m²) of all patches of the corresponding patch type, divided by total landscape area (m²), multiplied by 100 (to convert to a percentage); in other words, PLAND equals the percentage the landscape comprised of the corresponding patch type [40].

Papers	Data	Program
[41]	Landsat 7ETM+&5TM; VHRRS images; HRSC; soil map; IKONOS	(V-LATE) calculated within ArcGIS 8.x

3.3 Isolation Proximity

3.3.1 Proximity Index Distribution (PROX_X)–Class Metrics, Landscape Metrics

This index defines the spatial context of landscape patches in relation to their neighbors [36]. The proximity index combines spatial information on patch size and spacing, and will clearly distinguish a site with small patches distantly spaced from a site with large patches closely spaced. If these are perennial vegetation patches, intuitively, the latter site will more efficiently retain resources flowing or blowing about the landscape than the former. A site with larger and more closely packed vegetation patches will provide

more obstructions to trap wind-blown litter and soil particles, and any such particles flowing in run-off [70]. Thus, the proximity index may provide a useful indicator for the potential of a landscape to capture resources [10]. Proximity index considers size and proximity of all patches with the same land cover type inside a specified search radius [50]. Proximity is the degree of isolation of patches from nearby patches of the same class [54]. Proximity index equals the sum of patch area (m²) divided by the nearest edge-to-edge distance squared (m²) between the patch and the focal patch of all patches of the corresponding patch type whose edges are within a specified distance (m) of the focal patch [45].

Mean (PROX_MN);

Weighted Mean (PROX_AM);

Coefficient of Variation (PROX_CV).

Papers	Data	Program
[10]	Near-ground digital photography, aerial videography and high-resolution satellite imagery	Statistical Calculations
[18]	Digitized from true color orthophoto	ArcGIS 8.1 (ESRI); Fragstat
[45]	Topographic maps; Aerial photographs	GIS
[46]	Landsat TM; AVHRR; MODIS; TIGER DLG	GIS
[50]	IKONOS	Fragstat version 3.3.
[51]	Data are derived from land-use map	ArcGIS; Fragstat version 3.3
[54]	Aerial photography	Fragstat version 3.2
[60]	Landsat MSS; TM and ETM+	ERDAS Imagine 8.7; ARCGIS 9.0 (ESRI); Fragstat

3.3.2 Euclidean Nearest Neighborhood Distance (ENN_X)–Class Metrics, Landscape Metrics

Euclidean nearest neighborhood distance is the average distance between patches of same class,

representing patch isolation [49]. Euclidean nearest neighborhood distance is minimum edge-to-edge distance to the nearest neighbouring patch of the same type [50]. Euclidean nearest neighborhood distance is proximity of patches of the focal class, based on the average or area-weighted average distance between nearest neighbors [54]. Nearest neighborhood distance equals the nearest-neighbour distance from patch *j* to another patch *k* of the same type, based on shortest edge-to-edge distance [45]. A patch level the distance (*m*) to the nearest neighbouring patch of the same type, based on shortest edge-to-edge distance (2) is averaged over all patches in landscape:

$$ENN_MN = \frac{\sum_{i=1}^m \sum_{j=1}^n h_{ij}}{N} \quad (2)$$

where *h_{ij}* is distance from patch *ij* to nearest neighbouring patch of the same type (class), based on patch edge-to-edge distance, computed from cell centre to cell centre, and *N* is the total number of patches in the landscape (unit: m) [61]. “Greenways offer a promising planning strategy to address the challenge of making landscape planning sustainable” [71]. The spread of disturbances such as diseases and fire are greater when MNND is low and when PROXIM values are high [52]. Consensus is emerging: some form of ecological infrastructure is necessary to achieve a sustainable landscape condition [72].

Mean (ENN_MN);

Weighted Mean (ENN_AM);

Coefficient of Variation (ENN_CV).

Papers	Data	Program
[12]	Landsat ETM and MSS images	Imagine TM; ArcView TM; Fragstat; ATtILA
[18]	Digitized from true color orthophoto	ArcGIS 8.1 (ESRI); Fragstat
[45]	Topographic maps; Aerial photographs	GIS
[46]	Landsat TM; AVHRR; MODIS; TIGER DLG	GIS

Papers	Data	Program
[47]	Aerial photographs	GIS; Fragstat
[49]	Aerial photographs	GIS; Fragstat version 3.1
[50]	IKONOS	Fragstat version 3.3.
[51]	Data are derived from land-use map	ArcGIS; Fragstat version 3.3
[54]	Aerial photography	Fragstat version 3.2
[59]	Raster data layers	ARCGIS; Fragstat
[61]	Land use data is derived from Map	Idrisi Kilimanjaro; Fragstat
[73]	Aerial Photos	ArcView extension “patch 2.0”

3.4 Connectivity

3.4.1 Patch Cohesion Index (COHESION)–Class Metrics, Landscape Metrics

Patch cohesion index is measure of the physical connectedness of the focal land cover class [50]. COHESION equals 1 minus the sum of patch perimeter (in terms of number of cell surfaces) divided by the sum of patch perimeter times the square root of patch area (in terms of number of cells) for patches of the corresponding patch type, divided by 1 minus 1 over the square root of the total number of cells in the landscape, multiplied by 100 to convert to a percentage [40].

Papers	Data	Program
[50]	IKONOS	Fragstat version 3.3
[54]	Aerial photography	Fragstat version 3.2
[57]	Landsat TM and ETM	MiraMon Software; Fragstat

3.4.2 Connectance Index (CONNECT)–Class Metrics, Landscape Metrics

Connectance index is the percentage of patches which are joined, i.e. inside a specified threshold distance [50]. CONNECT equals the number of functional joining between all patches of the corresponding patch type (sum of *c_{ijk}* where *c_{ijk}* = 0 if patch *j* and *k* are not within the specified distance of

each other and $c_{ijk} = 1$ if patch j and k are within the specified distance), divided by the total number of possible joining between all patches of the corresponding patch type, multiplied by 100 to convert to a percentage [40].

Papers	Data	Program
[44]	Simulated data	3Q programme
[48]	Landsat TM	ArcView 3.2; Fragstat
[50]	IKONOS	Fragstat version 3.3.

3.5 Contagion Interspersion

3.5.1 Clumpiness (CLUMPY)–Class Metrics

CLUMPY equals the proportional deviation of the proportion of like adjacencies involving the corresponding class from that expected under a spatially random distribution. If the proportion of like adjacencies (G_i) is less than the proportion of the landscape comprised of the focal class (P_i) and $P_i < 0.5$, then CLUMPY equals G_i minus P_i , divided by P_i ; else, CLUMPY equals G_i minus P_i , divided by 1 minus P_i . Note, it can be shown that G_i equals 1 when the patch type is maximally clumped, but this requires adjustment for the perimeter of the class. If a_i is the area of class i (in terms of number of cells) and n is the side of a largest integer square smaller than a_i , and $m = a_i - n^2$, then the minimum perimeter of class i (i.e., when it is maximally clumped), $\min-e_i$, will take one of the three forms [74]: $\min-e_i = 4n$, when $m = 0$, or $\min-e_i = 4n + 2$, when $n^2 < a_i \leq n(1+n)$, or $\min-e_i = 4n + 4$, when $a_i > n(1+n)$.

Papers	Data	Program
[12]	Landsat ETM and MSS images	Imagine TM; ArcView TM; Fragstat; ATtILA
[54]	Aerial photography	Fragstat version 3.2

3.5.2 Proportion of Like Adjacencies (PLADJ)–Class Metrics, Landscape Metrics

Percentage of like adjacencies is percentage of neighbouring pixel, being the same land-cover class, based on double-count method [50].

Papers	Data	Program
[18]	Digitized from true color orthophoto	ArcGIS 8.1 (ESRI); Fragstat
[50]	IKONOS	Fragstat version 3.3.
[54]	Aerial photography	Fragstat version 3.2
[62]	Soil data is derived from Soil Map	Idrisi Kilimanjaro; Fragstat

3.5.3 Aggregation Index (AI)–Class Metrics, Landscape Metrics

Aggregation index is the percentage of neighbouring pixel, being the same land cover class, based on single-count method [50].

Papers	Data	Program
[18]	Digitized from true color orthophoto	ArcGIS 8.1 (ESRI); Fragstat
[50]	IKONOS	Fragstat version 3.3.
[54]	Aerial photography	Fragstat version 3.2

3.5.4 Interspersion Juxtaposition Index (IJI)–Class Metrics, Landscape Metrics

Interspersion juxtaposition index is the measure of evenness of patch adjacencies, equals 100 for even and approaches 0 for uneven adjacencies [50]. Interspersion juxtaposition index is degree of intermixing of patch types [54]. Indicators for change in landscape structure caused by urbanization provided information about specific aspects of landscape structure and thus were helpful to “guide” process of urbanization towards sustainability [64, 65].

Papers	Data	Program
[1]	Regional Technical Map	GIS
[18]	Digitized from true color orthophoto	ArcGIS 8.1 (ESRI); Fragstat
[50]	IKONOS	Fragstat version 3.3.
[51]	Data are derived from land-use map	ArcGIS; Fragstat version 3.3
[54]	Aerial photography	Fragstat version 3.2
[57]	Landsat TM and ETM	MiraMon Software; Fragstat

3.5.5 Landscape Division (DIVISION)–Class Metrics, Landscape Metrics

Landscape division equals the probability that 2 randomly chosen pixels in the landscape are not situated in the same patch [50].

Papers	Data	Program
[50]	IKONOS	Fragstat version 3.3
[54]	Aerial photography	Fragstat version 3.2

3.5.6 Splitting Index (SPLIT)–Class Metrics, Landscape Metrics

Splitting index equals the number of patches of a landscape divided into equal sizes keeping landscape division constant [50].

Papers	Data	Program
[50]	IKONOS	Fragstat version 3.3
[54]	Aerial photography	Fragstat version 3.2

3.5.7 Effective Mesh Size (MESH)–Class Metrics, Landscape Metrics

MESH equals the sum of patch area squared, summed across all patches of the corresponding patch type, divided by the total landscape area (m²), divided by 10,000 (to convert to hectares) [40].

Papers	Data	Program
[54]	Aerial photography	Fragstat version 3.2
[75]	Digital land-use & street, Vegetation, Municipality borders, Geological maps	Arc View

3.5.8 Contagion Index (CONTAG)–Landscape Metrics

Contagion index equals 0 for a one-pixel patch and approaches 1 as patch contiguity, or connectedness increases [50]. Contagion index (3) indicates the aggregation of patches.

$$CONTAG = \left[1 + \frac{\sum_{i=1}^m \sum_{k=1}^m \left[(P_i) \left(\frac{g_{ik}}{\sum_{k=1}^m g_{ik}} \right) \right] \ln \left(P_i \left(\frac{g_{ik}}{\sum_{k=1}^m g_{ik}} \right) \right)}{2 \ln(m)} \right] 100 \% \quad (3)$$

where P_i is the proportion of the landscape occupied by patch type i; g_{ik} is the number of adjacencies between pixels of patch types (classes) i and k based on the double-count method; and m is the number of patch types (classes) in the landscape [61]. The contagion-index specifies the degree of aggregation of the existing patches in the image. A patch is the smallest unit in the classified image and consists of pixels of the same class. The index therefore is used as a measure of dissection and fragmentation of the landscape. Changed values of the index point to the splitting of great homogeneous areas into little isolated areas as well as to the loss of corridors between habitats [68].

Papers	Data	Program
[18]	Digitized from true color orthophoto	ArcGIS 8.1 (ESRI); Fragstat
[50]	IKONOS	Fragstat version 3.3
[51]	Data are derived from land-use map	ArcGIS; Fragstat version 3.3
[61]	Land use data is derived from Map	Idrisi Kilimanjaro; Fragstat
[62]	Soil data is derived from Soil Map	Idrisi Kilimanjaro; Fragstat
[68]	Images of COFUNE landcover	Created program of ENVIIDL
[69]	RS and map data	GIS

3.6 Diversity

3.6.1 Patch Richness (PR)–Landscape Metrics

While ecosystems are evolving, the number of integrated species is regularly increasing steadily and also the abiotic features are becoming more and more complex. This development is accompanied by a rising degree of information, heterogeneity and complexity [76]. “The heterogeneity provided by patches and corridors in an area plays a key role in sustainability” [19]. PR equals the number of different patch types present within the landscape boundary [40].

Papers	Data	Program
[1]	Regional technical map	GIS
[18]	Digitized from true color orthophoto	ArcGIS 8.1 (ESRI); Fragstat
[51]	Data are derived from land-use map	ArcGIS; Fragstat version 3.3
[75]	Digital land-use & street, Vegetation, Municipality borders, Geological maps	Arc View
[77]	Species data	ADE software [78]; Canonical Correspondence Analysis (CCA) [79, 80]
[81]	IKONOS; Quickbird; CASI-2; SPOT; AVHRR; Landsat TM	Fragstats; Tassel Cap Transformation (TCT) [82]
[83]	AVHRR	Gap Analysis Program [84]

3.6.2 Patch Richness Diversity (PRD)–Landscape Metrics

Patch richness diversity equals the number of patch types (i.e. land cover categories) per 100 ha [50]. The units for the number of patch types per unit area are patches per 100 ha [61].

Papers	Data	Program
[18]	Digitized from true color orthophoto	ArcGIS 8.1 (ESRI); Fragstat
[50]	IKONOS	Fragstat version 3.3
[54]	Aerial photography	Fragstat version 3.2
[61]	Land use data is derived from Map	Idrisi Kilimanjaro; Fragstat
[75]	Digital land-use & street, Vegetation, Municipality borders, Geological maps	Arc View
[81]	IKONOS; Quickbird; CASI-2; SPOT; AVHRR; Landsat TM	Fragstats; TCT

3.6.3 Relative Patch Richness (RPR)–Landscape Metrics

Relative patch richness is the percentage of present patch types out of all categories [50]. RPR equals the number of different patch types present within the landscape boundary divided by the maximum potential number of patch types specified by the user, based on the particular patch type classification scheme, multiplied by 100 (to convert to percent) [40].

Papers	Data	Program
[18]	Digitized from true color orthophoto	ArcGIS 8.1 (ESRI); Fragstat
[50]	IKONOS	Fragstat version 3.3

3.6.4 Shannon Diversity Index (SHDI)–Landscape Metrics

Shannon diversity index (4) equals minus the sum of the proportional abundance of each patch type multiplied by the ln of that proportion [50]:

$$SHDI = -\sum_{k=1}^s P_k \ln P_k \tag{4}$$

where s is the number of habitat types, P_k is the proportion of area in habitat cover k [45].

Shannon diversity index (5), a measure which informs on the structural composition of the communities [85]:

$$H' = \sum p_i \log_2 p_i \tag{5}$$

where p_i is the relative frequency of species in a record [77].

Papers	Data	Program
[1]	Regional technical map	GIS
[18]	Digitized from true color orthophoto	ArcGIS 8.1 (ESRI); Fragstat
[43]	Aerial photographs	ArcViewTM (ESRI)
[44]	Simulated data	3Q programme
[45]	Topographic maps; Aerial photographs	GIS

Papers	Data	Program
[48]	Landsat TM	ArcView 3.2; Fragstat
[50]	IKONOS	Fragstat version 3.3
[57]	Landsat TM and ETM	MiraMon Software; Fragstat
[62]	Soil data is derived from soil map	Idrisi Kilimanjaro; Fragstat
[67]	Cartographic data; Landsat 5 TM & 7 ETM; Digital vegetation photographs	GIS; Fragstat version 3.3
[77]	Species data	ADE software; CCA
[86]	LANDSAT TM image	UNIX & PC Arc/Info [87, 88]; Erdas Imagine 8.5 [89]
[90]	Ecological data	Statistical analyses

3.6.5 Simpson Diversity Index (SIDI)–Landscape Metrics

Simpson diversity index is diversity measure, which equals 1 minus the sum of the squared proportional abundance of each patch type [50]. SIDI equals 1 minus the sum, across all patch types, of the proportional abundance of each patch type squared [40].

Papers	Data	Program
[18]	Digitized from true color orthophoto	ArcGIS 8.1 (ESRI); Fragstat
[54]	Aerial photography	Fragstat version 3.2
[50]	IKONOS	Fragstat version 3.3

3.6.6 Modified Simpson Diversity Index (MSIDI)–Landscape Metrics

Diversity measure equals minus the ln of the sum of the squared proportional abundance of each patch type [50]. MSIDI equals minus the logarithm of the sum, across all patch types, of the proportional abundance of each patch type squared [40].

Papers	Data	Program
[18]	Digitized from true color orthophoto	ArcGIS 8.1 (ESRI); Fragstat
[50]	IKONOS	Fragstat version 3.3

3.6.7 Shannon Evenness Index (SHEI)–Landscape Metrics

Diversity measure considers only evenness of patch sizes, not the number of patches [50]. SHEI equals minus the sum, across all patch types, of the proportional abundance of each patch type multiplied by that proportion, divided by the logarithm of the number of patch types. In other words, the observed Shannon’s diversity index is divided by the maximum Shannon’s diversity index for that number of patch types [40].

Papers	Data	Program
[18]	Digitized from true color orthophoto	ArcGIS 8.1 (ESRI); Fragstat
[48]	Landsat TM	ArcView 3.2; Fragstat
[50]	IKONOS	Fragstat version 3.3
[69]	RS and map data	GIS
[77]	Species data	ADE software; CCA

3.6.8 Simpson Evenness Index (SIEI)–Landscape Metrics

Simpson evenness index is diversity measure, which considers only evenness of patch sizes, not the number of patches [50]. SIEI equals 1 minus the sum, across all patch types, of the proportional abundance of each patch type squared, divided by 1 minus 1 divided by the number of patch types. In other words, the observed Simpson’s diversity index is divided by the maximum Simpson’s diversity index for that number of patch types [40].

Papers	Data	Program
[18]	Digitized from true color orthophoto	ArcGIS 8.1 (ESRI); Fragstat
[50]	IKONOS	Fragstat version 3.3
[86]	LANDSAT TM image	UNIX & PC Arc/Info; Erdas Imagine 8.5

3.6.9 Modified Simpson Evenness Index (MSIEI)–Landscape Metrics

Modified Simpson evenness index is diversity measure, which considers only evenness of patch sizes, not the number of patches [50]. MSIEI equals minus the logarithm of the sum, across all patch types, of the proportional abundance of each patch type squared, divided by the logarithm of the number of patch types. In other words, the observed modified Simpson's diversity index is divided by the maximum modified Simpson's diversity index for that number of patch types [40].

Papers	Data	Program
[18]	Digitized from true color orthophoto	ArcGIS 8.1 (ESRI); Fragstat
[50]	IKONOS	Fragstat version 3.3

4. Discussion and Conclusions

A great variety of different landscape metrics based on remote sensing data (RS), for monitoring ecosystems and also different programs for their calculation (fragstats, metrics, GIS) are considered in the current paper. The investigation identified subsets of metrics, enabled scientists to recognise main aspects of landscape pattern, facilitated the compilation of groups of landscapes with similar characteristics and indicated which metrics are frequently useful in landscape studies. The frequency of used papers per each metric has been taken into account. In the current paper, there are six main categories of metrics. The most used to the least used metrics have the following order:

- Area/Density/Edge (All types of RS data, 10 subcategories, 22 papers);
- Diversity (All types of RS data, 9 subcategories, 20 papers);
- Isolation Proximity (All types of RS data, 2 subcategories, 15 papers);
- Contagion Interspersion (VHR and HR RS data, 8 subcategories, 12 papers);
- Shape (VHR RS data, 13 subcategories, 17

papers);

- Connectivity (VHR and HR RS data, 2 subcategories, 5 papers).

It is observed from the aforementioned list that the three last categories of metrics use only VHR and/or HR remote sensing data. Particularly, only very high resolution (VHR) remote sensing data are used in the Shape Metric. This constraint can explain their limited use.

Furthermore, the frequency of used papers is divided into five groups. The frequency of used papers equals to the number of used papers per subcategory over the number of used papers per main category. It has been found that $\min = 1/17 = 0.059$ and $\max = 12/15 = 0.8$. The range from min to max has been divided into five equal pieces accordingly representing five groups, i.e. from Group A till Group E. To have a better idea of each group appearance per subcategory and main categories according to the frequency of used papers per each index, the first three-mentioned groups have the following order:

Group A:

- Euclidean Nearest Neighbourhood ($12/15=0.8$) from Isolation Proximity main category;
- Shannon Diversity Index ($13/20=0.65$) from Diversity main category;
- Shape Index ($11/17=0.647$) from Shape main category;
- Patch Density ($13/22=0.591$) from Area/Density/Edge main category (Exception).

Group B:

- Patch Cohesion Index ($3/5 = 0.6$) from Connectivity main category;
- Connectance Index ($3/5 = 0.6$) from Connectivity main category;
- Contagion Index ($7/12 = 0.583$) from Contagion Interspersion main category;
- Proximity Index Distribution ($8/15 = 0.533$) from Isolation Proximity main category;
- Number of Patches ($11/22 = 0.5$) from Area/Density/Edge main category;

- Interspersion Juxtaposition Index ($6/12 = 0.5$) from Contagion Interspersion main category.

Group C:

- Largest Patch Index ($9/22 = 0.409$) from Area/Density/Edge main category;
- Edge Density ($9/22 = 0.409$) from Area/Density/Edge main category;
- Class Area ($8/22 = 0.364$) from Area/Density/Edge main category;
- Patch Richness ($7/20 = 0.35$) from Diversity main category.

An explanation of the above results, regarding to the four indices of group A and two indices from the group B, leads to the following:

Euclidean Nearest Neighbourhood (ENN) distance is the proximity of patches to neighbors of the same class, based on the area-weighted average distance between nearest neighbors [54]. According to the results of Ref. [73], the number of patches increased while ENN between forest patches decreased. This illustrates that widespread forests were under fragmentation into smaller units. In other words, ENN underlies an assumption of habitat configuration [59]. ENN was also chosen by Lee et al. [47] because it was possible to measure a range of important changes in the spatial pattern of landscapes, without incurring significant inter-correlation between the indices. This index is one of chosen indices [49], which quantifies fundamental landscape characteristics and is found to be useful in several other landscape structural analyses. At last, Euclidean Nearest Neighborhood Distance is used by 12 authors out of 15, as the current index is chosen because it is possible to measure a range of important changes in the spatial pattern of landscapes.

As a global estimator of landscape structure, Shannon Diversity Index (SHDI), which gives more importance to the richness component and rare cover types, is calculated. In addition, SHDI does not only reflect the richness of habitats but also their relative importance in a given area [45]. According to The Ecological Society of America Committee on Land

Use [91], SHDI has greater sensitivity to rare cover types and it needs to be given greater importance during interpretation. SHDI might be useful to detect the area where rare and endangered species in focus [86]. In the end, Shannon Diversity Index is used by 13 authors out of 20 because it is relatively simple to use and to interpret [43].

Shape is a difficult parameter to quantify concisely in a metric. This shape index measures the complexity of patch shape compared to a standard shape [40]. According to Ref. [55], shapes of semi-natural patches are defined by the surrounding agricultural land use. This index is one of chosen indices [49], which quantifies fundamental landscape characteristics and is found to be useful in several other landscape structural analysis. Finally, despite Shape Index is used by 11 authors out of 17, the current index stays to be difficult parameter to quantify concisely in a metric.

Patch Density (PD) index identified as potential discriminator of landscape pattern has been observed to provide more information. Based on the results of Ref. [18] paper, they suggested the inclusion of PD and a landscape composition parameter for the study of landscape of low thematic resolution. According to Ref. [40], the density of patches in the entire landscape mosaic could serve as a good heterogeneity index because a landscape with greater patch density would have more spatial heterogeneity. Miyamoto et al. [49] may easily monitor future landscape condition using PD index. In their analysis, the increase of patch density for young coniferous plantations reflects the addition of many newly planted areas by extensive afforestation, whereas the increase of patch density for secondary forests reflects the dissection of patches by cutting across large areas of study. Finally, Patch Density index, which is an exception in Group A, is used by 13 authors out of 22, as this metric not only provides more information, but also may be easily monitored for landscape conditions.

Proximity index is dimensionless (has no units), and therefore the absolute value of the index has little

interpretive value; instead it is used as a comparative index [40]. According to results of Ref. [60], the value of proximity index for forest in all periods exceeded that of other patch types, but with an obvious decrease over time, suggesting a forest fragmentation process over this period. Proximity index was suggested by Bailey et al. [18] because although it has limitations, it has low correlations with other indices. However, due to the apparent sensitivity to the thematic resolution it has probably only suited for use in more complexly defined landscape. Finally, Proximity index is used by 8 authors out of 15 because the proximity index may provide a useful indicator for the potential of a landscape to capture resources [10].

Number of Patches (NP) index was chosen because it is commonly implemented in forms of landscape monitoring and is relatively simple to use and to interpret [43]. Furthermore, NP is probably most valuable, however, as the basis for computing other, more interpretable metrics [40]. The NP is a measure of fragmentation of a given class within a landscape since the landscape size is constant [39, 57]. According to the results of Ref. [12], the NP associated with each land cover class increased dramatically for the given period but thereafter fluctuated for bare areas and deciduous and mixed forest and continued to increase for pine and non-forested areas. In other words, NP underlies an assumption of habitat composition [59]. At the end, Number of Patches Index is used by 11 authors out of 22, as the current metric is not only probably most valuable but also relatively simple for the use and interpretations.

References

- [1] R.C. Venturelli, A. Galli, Integrated indicators in environmental planning: Methodological considerations and applications, *Ecological Indicators* 6 (2006) 228-237.
- [2] E.J. Miller, R.P. Brooks, M.J. Croonquist, Landscape ecology, in: *Effects of Landscape Patterns on Biotic Communities*, Kluwer Academic Publishers, 1997, pp. 137-153.
- [3] Rocky Mountain Institute, Indicators of opportunity workshop, in: *Proceeding of Meeting*, May 2/4/2001.
- [4] Urban Institute, National Neighbourhood Indicators Partnership, Washington DC, 2001.
- [5] Urban Quality Communication, Urban quality Indicators, Newsletter Ann Arbor, MI, 2001.
- [6] National Association of Environmental Professionals, Continuing Education Course Sustainability Indicators, Bowie MD, 2001.
- [7] P. Opdam, R. Foppen, C. Vos, Landscape ecology, in: *Bridging the Gap between Ecology and Spatial Planning in Landscape Ecology*, Kluwer Academic Publishers, 2002, pp. 767-779.
- [8] O. Bastian, U. Steinhardt, *Development and Perspectives of Landscape Ecology*, Kluwer Academic Publishers, Dordrecht Boston London, 2002.
- [9] D. Berry, Interagency Working Group of Sustainable Development Indicators, Council on Environmental Quality, Washington D.C., 2001.
- [10] J.N. Bastin, J.A. Ludwig, R.W. Eager, V.H. Chewings, A.C. Liedloff, Indicators of landscape function: Comparing patchiness metrics using remotely-sensed data from rangelands, *Ecological Indicators* 1 (2002) 247-260.
- [11] V. Tarzia, European common indicators: Towards a local sustainability profile, Final Project Report, Ambiente Italia Research Institute, Ancora Arti Grafiche, Milan, 2003.
- [12] L.M. Olsen, V.H. Dale, T. Foster, Landscape patterns as indicators of ecological change at Fort Benning, Georgia, USA, *Landscape and Urban Planning* 79 (2007) 137-149.
- [13] C.T. Hunsaker, D.E. Carpenter, *Environmental Monitoring and Assessment Program: Ecological Indicators*, Environmental Protection Agency, Research Triangle Park, NC, 1990.
- [14] J.R. Kelly, M.A. Harwell, Indicators of ecosystem recovery, *Environmental Management* 14 (1990) 527-545.
- [15] R.F. Noss, Indicators for monitoring biodiversity: A hierarchical approach, *Conservation Biology* 4 (1990) 355-364.
- [16] J. Cairns, P.V. McCormick, B.R. Niederlehner, A proposed framework for developing indicators of ecosystem health, *Hydrobiologia* 236 (1993) 1-44.
- [17] V.H. Dale, S.C. Beyeler, Challenges in the development and use of ecological indicators, *Ecological Indicators* 1 (2001) 3-10.
- [18] D. Bailey, F. Herzog, I. Augenstein, S. Aviron, R. Billeter, E. Szerencsits, et al., Thematic resolution matters: Indicators of landscape pattern for European agro-ecosystems, *Ecological Indicators* 7 (2007) 692-709.
- [19] R.T. Forman, *Land Mosaics: The Ecology of Landscapes and Regions*, Cambridge University Press, Cambridge, UK, 1995.
- [20] M.G. Turner, R.V. O'Neill, R.H. Gardner, B.T. Milne, Effects of changing spatial scale on the analysis of

- landscape pattern, *Landscape Ecology* 3 (1989) 153-162.
- [21] R.V. O'Neill, J.R. Krummel, R.H. Gardner, G. Sugihara, B. Jackson, D.L. DeAngelis, et al., Indices of landscape pattern, *Landscape Ecology* 1 (1988) 153-162.
- [22] K.H. Riitters, R.V. O'Neill, C.T. Hunsaker, J.D. Wickham, D.H. Yankee, S.P. Timmins, et al., A factor analysis of landscape pattern and structure metrics, *Landscape Ecology* 10 (1995) 23-39.
- [23] M.G. Turner, R.H. Gardner, R.V. O'Neill, *Landscape Ecology in Theory and Practice: Pattern and Process*, Springer-Verlag, New York, USA, 2001.
- [24] M. Burgi, A case study of forest change in the Swiss lowlands, *Landscape Ecology* 14 (1999) 567-575.
- [25] J.A. Griffith, S.V. Stehman, T.R. Loveland, Landscape trends in mid-Atlantic and southeastern U.S. ecoregions, *Environmental Management* 32 (2003) 572-588.
- [26] R.V. O'Neill, C.T. Hunsaker, K.B. Jones, K.H. Riitters, J.D. Wickham, P.M. Schwartz, et al., Monitoring environmental quality at the landscape scale, using landscape indicators to assess biotic diversity, watershed integrity, and landscape stability, *Bioscience* 47 (1997) 513-519.
- [27] A. Lausch, F. Herzog, Applicability of landscape metrics for the monitoring of landscape change: Issues of scale, resolution and interpretability, *Ecological Indicators* 2 (2002) 3-15.
- [28] C.D. Hargis, J.A. Bissonette, J.L. David, The behaviour of landscape metrics commonly used in the study of habitat fragmentation, *Landscape Ecology* 13 (1998) 167-186.
- [29] K.H. Riitters, J. Wickham, R. O'Neill, B. Jones, E. Smith, Global-scale patterns of forest fragmentation, *Conservation Ecology* 4 (2000) 27-56.
- [30] L. Fahrig, I. Jonsen, Effect of habitat patch characteristics on abundance and diversity of insects in an agricultural landscape, *Ecosystems* 1 (1998) 197-205.
- [31] M.J. Mazerolle, M.A. Villard, Patch characteristics and landscape context as predictors of species presence and abundance: A review, *Ecoscience* 6 (1999) 117-124.
- [32] L. Tischendorf, Can landscape indices predict ecological processes consistently?, *Landscape Ecology* 16 (2001) 235-254.
- [33] D.J. Bender, L. Tischendorf, L. Fahrig, Using patch isolation metrics to predict animal movement in binary landscapes, *Landscape Ecology* 18 (2003) 17-39.
- [34] M. Luck, J. Wu, A gradient analysis of urban landscape pattern: a case study from the Phoenix metropolitan region, Arizona, USA, *Landscape Ecology* 17 (2002) 327-339.
- [35] S. Saura, P. Carballal, Discrimination of native and exotic forest patterns through shape irregularity indices: An analysis in the landscapes of Galicia, Spain, *Landscape Ecology* 19 (2004) 647-662.
- [36] E.J. Gustafson, G.R. Parker, Using an index of habitat patch proximity for landscape design, *Landscape Urban Planning* 29 (1994) 117-130.
- [37] S.A.O. Cousins, O. Eriksson, The influence of management history and habitat on plant species richness in a rural hemiboreal landscape, Sweden, *Landscape Ecology* 17 (2002) 517-529.
- [38] S. Gachet, A. Leduc, Y. Bergeron, T. Nguyen-Xuan, F. Tremblay, Understory vegetation of boreal tree plantations: Differences in relation to previous land use and natural forests, *Forest Ecology Management* 242 (2007) 49-57.
- [39] F. Sivrikaya, G. Cakir, A.I. Kadiogullari, S. Kelles, E.Z. Baskent, S. Terzioglu, Evaluating land use/land cover changes and fragmentation in the Camili forest-planning unit of Northeastern Turkey from 1972 to 2005, *Land Degradation and Development* 18 (2007) 383-396.
- [40] K. McGarigal, B. Marks, FRAGSTATS: Spatial pattern analysis program for quantifying landscape structure, General Technical Report, PNW-GTR-351, U.S. Department of Agriculture, Forest Service, Pacific Northwest Research Station, Portland, 1995, available online at: <http://www.umass.edu/landeco/research/fragstats/fragstat.html>.
- [41] M. Bock, G. Rossner, M. Wissen, K. Remm, T. Langanke, S. Lang, et al., Spatial indicators for nature conservation from European to local scale, *Ecological Indicators* 5 (2005) 322-338.
- [42] S. Lang, D. Tiede, vLATE Extension for ArcGIS—vector basis, tool for quantitative landscape analysis, in: ESRI 18th European User Conference, Innsbruck, 2003.
- [43] W.E. Dramstad, M. Sundli Tveit, W.J. Fjellstad, G.L.A. Fry, Relationships between visual landscape preferences and map-based indicators of landscape structure, *Landscape and Urban Planning* 78 (2006) 465-474.
- [44] W.E. Dramstad, G. Fry, W.J. Fjellstad, B. Skar, W. Helliksen, M.-L.B. Sollund, et al., Integrating landscape-based values-Norwegian monitoring of agricultural landscapes, *Landscape and Urban Planning* 57 (2001) 257-268.
- [45] K.-H. Kim, S. Pauleit, Landscape character, biodiversity and land use planning: The case of Kwangju City Region, South Korea, *Land Use Policy* 24 (2007) 264-274.
- [46] J.A. Kupfer, National assessments of forest fragmentation in the US, *Global Environmental Change* 16 (2006) 73-82.
- [47] J.T. Lee, S. Thompson, Targeting sites for habitat creation: An investigation into alternative scenarios, *Landscape and Urban Planning* 71 (2005) 17-28.
- [48] L. Zhang, H. Wang, Planning an ecological network of Xiamen Island (China) using landscape metrics and network analysis, *Landscape and Urban Planning* 78 (2006) 449-456.
- [49] A. Miyamoto, M. Sano, The influence of forest

management on landscape structure in the cool-temperate forest region of central Japan, *Landscape and Urban Planning* 86 (2008) 248-256.

- [50] S. Schindler, K. Poirazidis, T. Wrbka, Towards a core set of landscape metrics for biodiversity assessments: A case study from Dadia National Park, Greece, *Ecological Indicators* 8 (2008) 502-514.
- [51] S.C. Ribeiro, A. Lovett, Associations between forest characteristics and socio-economic development: A case study from Portugal, *Journal of Environmental Management* 90 (2009) 2873-2881.
- [52] A. Botequilha Leitao, J. Ahern, Applying landscape ecological concepts and metrics in sustainable landscape planning, *Landscape and Urban Planning* 59 (2002) 65-93.
- [53] K. McGarigal, S.A. Cushman, M.C. Neel, E. Ene, FRAGSTATS: Spatial Pattern Analysis Program for Categorical Maps, Computer software program produced by the authors at the University of Massachusetts, Amherst, 2002, available online at: www.umass.edu/landeco/research/fragstats/fragstats.html.
- [54] S. Cushman, K. McGarigal, M. Neel, Parsimony in landscape metrics: Strength, universality, and consistency, *Ecological Indicators* 8 (2008) 691-703.
- [55] S. Weiers, M. Bock, M. Wissen, G. Rossner, Mapping and indicator approaches for the assessment of habitats at different scales using remote sensing and GIS methods, *Landscape and Urban Planning* 67 (2004) 43-65.
- [56] M.E. Gilpin, I. Hanski, *Metapopulation Dynamics: Empirical and Theoretical Investigations*, Academic Press, 1991, p. 336.
- [57] T. Lasanta, J.C. Gonzalez-Hidalgo, S.M. Vicente-Serrano, E. Sferi, Using landscape ecology to evaluate an alternative management scenario in abandoned Mediterranean mountain Areas, *Landscape and Urban Planning* 78 (2006) 101-114.
- [58] D. Ebert, T. Wade, J. Harrison, D. Yankee, Analytical Tools Interface for Landscape Assessments (ATtILA) User Guide, Version 2.9, DRAFT Environmental Protection Agency, Los Vegas, NE.
- [59] C.P. Quine, K. Watts, Successful de-fragmentation of woodland by planting in an agricultural landscape? An assessment based on landscape indicators, *Journal of Environmental Management* 90 (2009) 251-259.
- [60] Z. Wenguang, H. Yuanman, H. Jinchu, C. Yu, Z. Jing, L. Miao, Impacts of land-use change on mammal diversity in the upper reaches of Minjiang River, China: Implications for biodiversity conservation planning, *Landscape and Urban Planning* 85 (2008) 195-204.
- [61] E. Uuemaa, J. Roosaare, U. Mander, Scale dependence of landscape metrics and their indicatory value for nutrient and organic matter losses from catchments, *Ecological Indicators* 5 (2005) 350-369.
- [62] E. Uuemaa, J. Roosaare, A. Kanal, U. Mander, Spatial correlograms of soil cover as an indicator of landscape heterogeneity, *Ecological Indicators* 8 (2008) 783-794.
- [63] R. Eastman, *IDRISI Kilimanjaro: Guide to GIS and Image Processing*, Clark University, 2003.
- [64] J.N. DiBari, Evaluation of five landscape-level metrics for measuring the effects of urbanization on landscape structure: The case of Tucson, Arizona, USA, *Landscape and Urban Planning* 79 (2007) 308-313.
- [65] W. Ji, J. Ma, R. Twibell, K. Underhill, Characterizing urban sprawl using multi-stage remote sensing images and landscape metrics, *Computers, Environment and Urban Systems* 30 (2006) 861-879.
- [66] D.R. Patton, A diversity index for quantifying habitat "edge", *Wildlife Society Bulletin* 3 (1975) 171-173.
- [67] R. Pelorosso, A. Leone, A. Boccia, Land cover and land use change in the Italian central Apennines: A comparison of assessment methods, *Applied Geography* 29 (2009) 35-48.
- [68] P. Gasper, G. Menz, Landscape metrics as a tool for the analysis of spatial structures in classified satellite images, *IEEE* (1999) 137-139.
- [69] H. Li, J. Wu, Use and misuse of landscape indices, *Landscape Ecology* 19 (2004) 389-399.
- [70] D.J. Tongway, J.A. Ludwig, The conservation of water and nutrients within landscapes, in: J.A. Ludwig, D.T. Tongway, D. Freudenberger, J. Noble, K. Hodgkinson, (Eds.), *Landscape Ecology, Function and Management: Principles from Australia's Rangelands*, CSIRO, Melbourne, Australia, 1997, pp. 13-22.
- [71] J. Ahern, Greenways as a planning strategy, *Landscape and Urban Planning* 33 (1995) 131-155.
- [72] A. Rescia, E. Astrada, J. Bono, C. Blasco, P. Meli, J. Adamoli, Environmental analysis in selection of alternative corridors in a long-distance linear project: A methodological proposal, *Journal of Environmental Management* 80 (2006) 266-278.
- [73] A. Bar, J. Löffler, Ecological process indicators used for nature protection scenarios in agricultural landscapes of SW Norway, *Ecological Indicators* 7 (2007) 396-411.
- [74] B.T. Milne, Lessons from applying fractal models to landscape patterns, in: M.G. Turner, R.H. Gardner (Eds.), *Quantitative Methods in Landscape Ecology*, Springer-Verlag, New York, 1991, pp. 199-235.
- [75] E. Tasser, E. Sternbach, U. Tappeiner, Biodiversity indicators for sustainability monitoring at municipality level: An example of implementation in an alpine region, *Ecological Indicators* 8 (2008) 204-223.

- [76] F. Muller, Indicating ecosystem and landscape organisation, *Ecological Indicators* 5 (2005) 280-294.
- [77] M. Aubert, D. Alard, F. Bureau, Diversity of plant assemblages in managed temperate forests: A case study in Normandy (France), *Forest Ecology and Management* 175 (2003) 321-337.
- [78] J. Thioulouse, D. Chessel, S. Doledec, J.M. Olivier, ADE-4: A multivariate analysis and graphical display software, *Statistical Computing* 7 (1997) 75-83.
- [79] C.J.F. Ter Braak, The analysis of vegetation-environment relationships by canonical correspondence analysis, *Vegetation* 69 (1987) 69-77.
- [80] C.J.F. Ter Braak, I.C. Prentice, A theory of gradient analysis, *Advance Ecological Resources* 18 (1988) 93-138.
- [81] D.C. Duro, N.C. Coops, M.A. Wulder, T. Han, Development of a large area biodiversity monitoring system driven by remote sensing, *Progress in Physical Geography* 31 (2007) 235-260.
- [82] S.P. Healy, W.B. Cohen, Y. Zhiqiang, O.N. Krankina, Comparison of tasseled capbased Landsat data structures for use in forest disturbance detection, *Remote Sensing of Environment* 97 (2005) 301-310.
- [83] T. Ricketts, M. Imhoff, Biodiversity, urban areas, and agriculture: locating priority ecoregions for conservation, *Conservation Ecology* 8 (2003) 1.
- [84] J.M. Scott, F. Davis, B. Csuti, R. Noss, B. Butterfield, C. Groves, et al., Gap analysis: A geographic approach to protection of biological diversity, *Wildlife Monographs* 123 (1993) 1-41.
- [85] E.C. Pielou, *Ecological Diversity*, Wiley, New York, 1975.
- [86] H.M. Dogan, M. Dogan, A new approach to diversity indices-modelling and mapping plant biodiversity of Nallihan (A3-Ankara/Turkey) forest ecosystem in frame of geographic information systems, *Biodiversity and Conservation* 15 (2006) 855-878.
- [87] ESRI, *PC Arc/Info*, Command References, Redlands, CA, 1994.
- [88] ESRI, *Understanding GIS, The Arc/Info Method*, Version 7.1 for Unix and Windows NT, John Wiley & Sons Inc., New York, 1997.
- [89] ERDAS, *ERDAS Field Guide*, 4th ed., ERDAS Inc., Atlanta, Georgia, 1997.
- [90] J. Storkey, D.A. Bohan, A.J. Haughton, G.T. Champion, J.N. Perry, G.M. Poppy, et al., Providing the evidence base for environmental risk assessments of novel farm management practices, *Environmental Science & Policy* 11 (2008) 579-587.
- [91] V.H. Dale, S. Brown, R.A. Haeuber, N.T. Hobbs, N. Huntly, R.J. Naiman, et al., Ecological principles and guidelines for managing the use of land, *Ecological Application* 10 (2000) 639-670.



Journal of Environmental Science and Engineering
Volume 5, Number 11, November 2011

David Publishing Company
1840 Industrial Drive, Suite 160, Libertyville, IL 60048
Tel: 1-847-281-9862; Fax: 1-847-281-9855
<http://www.davidpublishing.com>
environmental@davidpublishing.com

